Risk Hedging Strategies in New Energy Markets

SHUYING LAI

Ph.D. (Engineering)

Supervisor: Dr. Jeremy (Jing) Qiu

Associate Supervisor: Dr. Dong Yuan

A thesis submitted in
fulfillment of the
requirements for the
degree of Doctor of
Philosophy

School of Electrical and Information Engineering

Faculty of Engineering

The University of Sydney
Australia

21 December 2022

DECLARATION

This thesis contains no material which has been accepted for the award of any other degree or diploma in any university or other tertiary institution and, to the best of my knowledge and belief, contains no material previously published or written by another person, except where due reference has been made in the text. I give consent to this copy of my thesis, when deposited in the University Library, being made available for loan and photocopying subject to the provisions of the Copyright Act 1968.

I hereby certify that the work embodied in this thesis contains published chapters/scholarly work of which I am a joint author. I have included as part of the thesis a written statement, endorsed by my supervisor, attesting to my contribution to the joint publications/scholarly work.

Chapter 3 of this thesis is published as [S. Lai, J. Qiu, Y. Tao, and J. Zhao, "Risk hedging for gas power generation considering power-to-gas energy storage in three different electricity markets," Applied Energy, vol. 291, p. 116822, 2021]. I designed the model, analyzed the data, and wrote the drafts.

Chapter 4 of this thesis is published as [S. Lai, J. Qiu, Y. Tao, and Y. Liu, "Risk hedging strategies for electricity retailers using insurance and strangle weather derivatives," International Journal of Electrical Power & Energy Systems, vol. 134, p. 107372, 2022]. I designed the study, analyzed the data, and wrote the drafts.

Chapter 6 of this thesis is published as [S. Lai, J. Qiu, Y. Tao, and X. Sun, "Demand response aggregation with operating envelope based on data-driven state estimation and sensitivity function signals," *IEEE Transactions on Smart Grid,* vol. 13, no. 3, pp. 2011-2025, 2022]. I designed the study, analyzed the data, and wrote the drafts.

Chapter 7 of this thesis is published as [S. Lai, J. Qiu, Y. Tao, and J. Zhao, "Pricing for electric vehicle charging stations based on the responsiveness of demand," IEEE Transactions on Smart Grid, 2022]. I designed the study, analyzed the data, and wrote the drafts.

Chapter 8 of this thesis is published as [S. Lai, J. Qiu, Y. Tao, and J. Zhao, "Individualized pricing of energy storage sharing based on discount sensitivity," IEEE Transactions on Industrial Informatics, vol. 18, no. 7, pp. 4642-4653, 2021, doi: 10.1109/TII.2021.3119953]. I designed the study, analyzed the data, and wrote the drafts.

Chapter 9 of this thesis is published as [S. Lai, J. Qiu, and Y. Tao, "Credit-based pricing and planning strategies for hydrogen and electricity energy storage sharing," IEEE Transactions on Sustainable Energy, vol. 13, no. 1, pp. 67-80, 2021]. I designed the study, analyzed the data, and wrote the drafts.

Author:

Shuying Lai
December 2022

Approved by Principal Supervisor:

Dr. Jing Qiu
December 2022

ACKNOWLEDGEMENTS

My Ph.D. research experience in Australia was amazing and memorable, during which period I was supported by several people, including my supervisors, my husband, my parents, my research colleagues, and my two bunnies. This thesis has become an important milestone in my life, marking the completion of my Ph.D. studying and the new start of my academic career. I would like to take this precious chance to express my greatest gratitude to those who helped and supported me during my research period.

Firstly, I am truly grateful to my principal supervisor, Dr. Jing Qiu. It is the luckiest thing to work under his supervision. His character, wisdom, leadership, and hard-working have positively influenced other research fellows and me. With continuous and timely support and guidance from Dr. Qiu, I can effectively conduct research and write research papers productively. Meanwhile, I also deeply thank my co-supervisor, Dr. Dong Yuan, who has helped and taught me a lot in my research with his vast experience in both research and engineering practices.

Secondly, I also appreciate my husband, Yuechuan Tao, who has supported me a lot in both my studying and living. Luckily, he also conducts research under the supervision of Dr. Qiu. During research studying, we often discuss timely-interesting ideas, mathematical models, programming, and even the design of the figures. At other times, we often hang out together to explore the spectacular natural beauty and delicious cuisine of Australia.

Thirdly, I express many thanks to my family, especially my parents. Their love and support are a solid base when I am pursuing my dream. The sacrifice and support of my parents are the strongest motives for me to strive for goals.

Last but not least, I give my gratitude to my two bunnies, i.e., doggy and nature, for their accompanying me during my research period.

LIST OF PUBLICATIONS

The following eight publications are the major Ph.D. research results of this candidate, as well as two manuscripts that are currently under review and are included as part of this thesis (**P**: published; **AR**: under review.

[P1]S. Lai, J. Qiu, Y. Tao, and J. Zhao, "Pricing for Electric Vehicle Charging Stations based on the Responsiveness of Demand," IEEE Transactions on Smart Grid, 2022

[P2]S. Lai, J. Qiu, Y. Tao, and X. Sun, "Demand Response Aggregation with Operating Envelope Based on Data-driven State Estimation and Sensitivity Function Signals," *IEEE Transactions on Smart Grid,* 2022.

[P3]S. Lai, J. Qiu, Y. Tao, and Y. Liu, "Risk hedging strategies for electricity retailers using insurance and strangle weather derivatives," *International Journal of Electrical Power & Energy Systems*, vol. 134, p. 107372, 2022.

[P4]S. Lai, J. Qiu, and Y. Tao, "Credit-Based Pricing and Planning Strategies for Hydrogen and Electricity Energy Storage Sharing," *IEEE Transactions on Sustainable Energy,* vol. 13, no. 1, pp. 67-80, 2021.

[P5]S. Lai, J. Qiu, Y. Tao, and J. Zhao, "Individualized Pricing of Energy Storage Sharing Based on Discount Sensitivity," *IEEE Transactions on Industrial Informatics,* vol. 18, no. 7, pp. 4642-4653, 2021.

[P6]S. Lai, J. Qiu, Y. Tao, and J. Zhao, "Risk hedging for gas power generation considering power-to-gas energy storage in three different electricity markets," *Applied Energy*, vol. 291, p. 116822, 2021.

[P7]S. Lai, J. Qiu, Y. Tao, and J. Zhao, "Pricing Strategy for Energy Supplement Services of Hybrid Electric Vehicles Considering Bounded-Rationality and Energy Substitution Effect," *IEEE Transactions on Smart Grid,* 2022.

[P8]S. Lai, J. Qiu, Y. Tao, and J. Zhao, "Pricing for Electric Vehicle Charging Stations based on the Responsiveness of Demand," *IEEE Transactions on Smart Grid,* 2022.

[AR1]S. Lai, J. Qiu, Y. Tao, and J. Zhao, " Demand Response of Electrical Vehicle Aggregator Using Financial Hedges: Options," *IEEE Transactions on Transportation Electrification*, under review.

[AR2]S. Lai, J. Qiu, Y. Tao, and J. Zhao, "Customized Pricing Strategy for Households based on Occupancy-aided Load Disaggregation," *IEEE Transactions on Energy Markets, Policy and Regulation*, under review.

[AR3]S. Lai, J. Qiu, and Y. Tao, " Charging/Refueling Navigation Strategies for Plug-in Hybrid Hydrogen and Electric Vehicles with Irrationalities and Energy Substitution," *IEEE Transactions on Industrial Informatics,* under review.

Apart from the manuscripts in this thesis, the candidate has other papers published and under review. These papers are listed below.

[P9]S. Lai, J. Qiu, and Y. Tao, "Option-based portfolio risk hedging strategy for gas generator based on mean-variance utility model," *Energy Conversion and Economics*, 2021.

[P10]S. Lai, Y. Tao, J. Qiu, J. Zhao, and H. Zhao, "Gas Generation Portfolio Management Strategy Based on Financial Derivatives: Options," in *2019 9th International Conference on Power and Energy Systems (ICPES)*, 2019: IEEE, pp. 1-6.

[P11]Y. Zheng, J. Yang, J. Yin, K. Hu, **S. Lai***, and J. Qiu, "Portfolio management strategy for power-to-gas storage-driven natural gas power generation," *International Transactions on Electrical Energy Systems*, vol. 31, no. 4, p. e12761, 2021.

[P12]Y. Tao, J. Qiu, **S. Lai**, X. Sun, and J. Zhao, "Adaptive Integrated Planning of Electricity Networks and Fast Charging Stations Under Electric Vehicle Diffusion," *IEEE Transactions on Power Systems,* 2022.

[P13]J. Qiu, Y. Tao, **S. Lai**, and J. Zhao, "Pricing Strategy of Cold Ironing Services for All-electric Ships Based on Carbon Integrated Electricity Price," *IEEE Transactions on Sustainable Energy,* 2022.

[P14]X. Zhao, L. Li, Y. Tao, **S. Lai**, X. Zhou, and J. Qiu, "Aggregated operation of heterogeneous small-capacity distributed energy resources in peer-to-peer energy trading," *International Journal of Electrical Power & Energy Systems,* vol. 141, p. 108162, 2022.

[P15]Y. Tao, J. Qiu, **S. Lai**, X Sun, and J. Zhao, B Zhou, and L Cheng, "Data-driven on-demand energy supplement planning for electric vehicles considering multi-charging/swapping services," *Applied Energy,* vol. 311, p. 118632, 2022.

[P16]Y. Tao, J. Qiu, **S. Lai**, and J. Zhao, "Renewable energy certificates and electricity trading models: Bi-level game approach," *International Journal of Electrical Power & Energy Systems,* vol. 130, p. 106940, 2021.

[P17]C. Si, Y. Tao*, J. Qiu, **S. Lai**, and J. Zhao, "Deep reinforcement learning based home energy management system with devices operational dependencies," *International Journal of Machine Learning and Cybernetics,* pp. 1-17, 2021.

[P18]G. Liu, Y. Tao*, L. Xu, Z. Chen, J. Qiu, and **S. Lai**, "Coordinated management of aggregated electric vehicles and thermostatically controlled loads in hierarchical energy systems," *International Journal of Electrical Power & Energy Systems,* vol. 131, p. 107090, 2021.

[P19]T. Wan, Y. Tao, J. Qiu, and **S. Lai**, "Data-driven Hierarchical Optimal Allocation of Battery Energy Storage System," *IEEE Transactions on Sustainable Energy*, 2021.

[P20]Y. Tao, J. Qiu, and **S. Lai**, "A supervised-learning Assisted Computation Method for Power System Planning," *IEEE Transactions on Artificial Intelligence,* vol. 1, no. 01, pp. 1-1, 2021.

[P21]Y. Tao, J. Qiu, and **S. Lai**, "A hybrid cloud and edge control strategy for demand responses using deep reinforcement learning and transfer learning," *IEEE Transactions on Cloud Computing,* 2021.

[P22]Y. Tao, J. Qiu, and **S. Lai**, "Deep Reinforcement Learning Based Bidding Strategy for EVAs in Local Energy Market Considering Information Asymmetry," *IEEE Transactions on Industrial Informatics,* 2021.

[P23]Y. Tao, J. Qiu, **S. Lai**, Y. Wang, and X. Sun, "Energy Management Strategy of Micro-grids in Joint Energy, Reserve and Regulation Markets based on Non-intrusive Load Monitoring," in *2021 IEEE International Power and Renewable Energy Conference (IPRECON)*, 2021: IEEE, pp. 1-6.

[P24]Y. Tao, J. Qiu, **S. Lai**, X. Zhang, Y. Wang, and G. Wang, "A Human-machine Reinforcement Learning Method for Cooperative Energy Management," *IEEE Transactions on Industrial Informatics,* 2021.

[P25]Y. Tao, J. Qiu, and **S. Lai**, "A Data-driven Management Strategy of Electric Vehicles and Thermostatically Controlled loads Based on Modified Generative Adversarial Network," *IEEE Transactions on Transportation Electrification,* 2021.

[P26]Y. Tao, J. Qiu, **S. Lai**, and J. Zhao, "Integrated electricity and hydrogen energy sharing in coupled energy systems," *IEEE Transactions on Smart Grid,* vol. 12, no. 2, pp. 1149-1162, 2020.

[P27]Y. Tao, J. Qiu, **S. Lai**, J. Zhao, and Y. Xue, "Carbon-oriented electricity network planning and transformation," *IEEE Transactions on Power Systems,* vol. 36, no. 2, pp. 1034-1048, 2020.

[P28]Y. Tao, J. Qiu, **S. Lai**, X. Zhang, and G. Wang, "Collaborative Planning for Electricity Distribution Network and Transportation System Considering Hydrogen Fuel Cell Vehicles," *IEEE Transactions on Transportation Electrification,* vol. 6, no. 3, pp. 1211 - 1225, 2020.

[P29]G. Liu, **S. Lai**, J. Qiu, Y. Tao, and J. Zhao, "An Internet of Things Framework for the Credit-Based Peer-to-Peer Energy Sharing Mechanism Under the Distributed Negotiation," *Available at SSRN 4054437.*

[P30]Y Tao, G Wang, X Zhang, **S Lai**, Y Wang, H Liu, J Qiu, "Two-layer Scheduling of Aggregated Electric Vehicles and Thermostatically Controlled Loads in Micro-grid," in *2019 9th International Conference on Power and Energy Systems (ICPES)*, 2019: IEEE, pp. 1-6.

[P31]Y. Tao, J. Qiu, **S. Lai**, Y. Wang, and X. Sun, "Reserve Evaluation and Energy Management of Micro-grids in Joint Electricity Markets based on Non-intrusive Load Monitoring," *IEEE Transactions on Industry Applications,* 2022.

[P32]G. Liu, **S. Lai**, J. Qiu, Y. Tao, and J. Zhao, "Credit-based Peer-to-Peer energy sharing mechanism under the distributed negotiation framework," *International Journal of Electrical Power & Energy Systems,* vol. 144, p. 108598, 2023.

[P33]Y. Tao, J. Qiu, **S. Lai**, X. Sun, and J. Zhao, "Flexible Voyage Scheduling and Coordinated Energy Management Strategy of All-Electric Ships and Seaport Microgrid," *IEEE Transactions on Intelligent Transportation Systems,* 2022.

I warrant that I have obtained, where necessary, permission from the copyright owners to use any third-party copyright material reproduced in the thesis or to use any of my own published work (e.g., journal chapters) in which the copyright is held by another party (e.g., publisher, co-authors).

ABSTRACT

In recent years, two typical developments have been witnessed in the energy market. On the one hand, the penetration of renewable generations has gradually replaced parts of the traditional ways to generate energy, such as fossil fuel generation. Although renewable generation has merits in terms of environmental protection and energy cost saving, the intermittent and unstable nature of renewable generation can lead to energy supply uncertainty, which might exacerbate the imbalance between energy supply and demand. As a result, the problem of energy price risks might occur.

On the other hand, with the introduction of distributed energy resources (DERs), new categories of markets besides traditional wholesale and retail markets are emerging. These new markets include the energy sharing market, energy storage sharing market, renewable energy trading market, peer-to-peer (P2P) trading, trading at the local and community levels, etc. The main benefits of the penetration of DERs are threefold. First, DERs can increase power system reliability. Second, the cost of transmission can be reduced. Third, end users can directly participate in some of these new types of markets according to their energy demand, excess energy, and cost function without third-party intervention. However, energy market participants might encounter various types of uncertainties, including DER supply uncertainty, end-user behavior uncertainty, wholesale market price uncertainty, etc. Therefore, it is necessary to develop proper risk hedging strategies for different energy market participants in emerging new markets.

Thus, we propose risk hedging strategies that can be used to guide various market participants to hedge risks and enhance utilities in the new energy market. These participants can be categorized into the supply side and demand side. To be specific, for participants from the supply side, generators, retailers, ESS coordinators, EVCSs, etc., are considered. For participants from the demand side, consumers, prosumers, EV users, EV aggregators, etc., are investigated. Regarding the wide range of hedging tools analyzed in this thesis, four main types of hedging strategies are developed, including the application of ESS, financial tools, DR management, and pricing strategy.

Several benchmark test systems have been applied to demonstrate the effectiveness of the proposed risk hedging strategies. Comparative studies of existing risk hedging approaches in the literature, where applicable, have also been conducted. The real applicability of the proposed approach has been verified by simulation results.

TABLE OF CONTENTS

GLOSSARY

Abbreviations

AEMO	Australian energy market operator
BESS	Battery energy storage system
CDD	Cooling degree day
CVaR	Conditional value at risk
CHP	Combined heat and power
DERs	Distributed energy resources
DGs	Distributed generations
DLMP	Distribution locational marginal pricing
DNO	Distributed network operator
DR	Demand response
EE	Extreme events
ESS	Energy storage system
EV	Electric vehicle
EVA	Electric vehicle aggregator
EVCS	Electric vehicle charging station
FCEV	Fuel cell electric vehicle
GV	Gasoline vehicle
GN	Gas network
HVAC	Heating, ventilation, and air conditioning
HDD	Heating degree day
IEHS	Integrated electricity charging and hydrogen refueling stations
ISO	Independent system operator
OPF	Optimal power flow
P2G	Power-to-gas
P2P	Peer to peer
PDN	Power distribution network
PEV	Plug-in electric vehicle
PH2EV	Plug-in hybrid hydrogen and electric vehicles
PV	Photovoltaics
QoS	Quality of service
SOC	State of charge
SSR	Self-sufficiency ratio
TN	Transportation network
TOU	Time-of-use
VaR	Value at risk
V2G	Vehicle to grid
WTP	Willingness-to-participate

LIST OF FIGURES

LIST OF TABLES

1. INTRODUCTION

In a traditional energy market, energy suppliers offer to sell the energy that they generate for a particular bid price in the wholesale market, while load-serving entities (the demand side) bid for that energy to meet their customers' energy demand in the retail market. In recent years, the energy market has developed with uttermost rapidity in terms of two aspects. First, the penetration of renewable generations has gradually replaced parts of the traditional ways to generate energy, such as fossil fuel generation. However, the intermittent and unstable nature of renewable generation can lead to energy supply uncertainty, which might exacerbate the imbalance between energy supply and demand. Second, with the introduction of DERs, new categories of markets besides traditional wholesale and retail markets are emerging, including the energy sharing market, renewable energy trading market, P2P trading, etc. However, market participants might encounter various types of uncertainties, including DER supply uncertainty, end-user behavior uncertainty, wholesale market price uncertainty, etc. Hence, we propose risk hedging strategies that can be used to guide various market participants in new categories of markets to hedge risks and enhance utilities. Four main types of hedging strategies are developed, including the application of ESS, financial tools, DR management, and pricing strategy. This chapter introduces basic concepts related to the structure and market participants of both traditional and new energy markets. Moreover, various types of risks in the new energy markets are discussed.

1.1 Traditional Energy Market

Traditional energy markets, including both wholesale and retail markets, are commodity markets that deal specifically with the trading of energy [1]. In the wholesale market, energy suppliers offer to sell the energy generated at a particular bidding price, while load-serving entities (retailers) bid for that energy to meet the energy demand of end users. In many jurisdictions, a two-settlement structure is witnessed, namely, a day-ahead market for bulk energy trading and a real-time market for energy supply-demand balancing [1]. The wholesale trading of the national electricity market (NEM) is transported via high voltage transmission lines from generators to large industrial energy users and to local electricity distributors in each region. In addition, the output from all generators is aggregated and scheduled at five-minute intervals to meet demand [2].

In the retail market, the interface between retailers and end users is provided to sell electricity, gas, and energy services to residential and business end users, who are allowed to select among competitive

retailers and choose the retailer that can best serve their home or business. For example, the Australia Energy Market Commission (AEMC) makes the rules that facilitate the provision of electricity and gas services to end users, including [3]: *'*

i. *End user connections*
ii. *Retail competition that allows end users to choose between competing retailers and to switch their retailer*
iii. *Energy-specific end user protections*
iv. *Basic terms and conditions contained in standard and market retail contracts'*

1.2 Energy Market in a New Environment

In recent years, the energy transition has been firmly underway, and three main trends can be concluded. First, the application of renewable energy accelerates. There was an estimated $303.5 billion invested in renewable energy capacity in 2020, according to Bloomberg New Energy Finance (BNEF)'s latest figures [4]. Second, the utilization of fossil fuels is reducing. In 2020, Carbon Tracker research suggested that 46% of coal-fired power plants would be unprofitable, rising to 53% by 2030 [4]. Third, global energy demand is continuously increasing. According to the US Energy Information Administration, global energy demand will continue to rise through 2050, with oil remaining the largest energy source [4]. Hence, it is necessary to analyze the impact of these main trends on the structure and operation of the energy market in the new environment, as well as potential risks the market participants might encounter. Two main developments in the energy market caused by the emerging trends will be discussed in the following parts.

1.2.1 Development One of Energy Market at Transmission Level

For the first development of the energy market in the new environment at the transmission level, renewable energy generations are developing rapidly to gradually replace the traditional ways of generations, such as fossil fuel generation. Renewable energy often referred to as clean energy, comes from natural sources or processes that are constantly replenished. For example, solar, wind, hydro, tidal energy, geothermal, and biomass energy [5].

For solar energy, it is a kind of renewable energy that is obtained from the electromagnetic radiation of the sun. It generates electricity and heat in a manner that is sustainable [6]. This energy can be used to generate electricity or be stored in batteries or thermal storage. Normally, there are three types of solar

energy, i.e., photovoltaic solar energy, solar thermal energy, and passive solar energy. For solar PV, the installed PV panels can transform the light and heat of the sun into electric energy [6]. For solar thermal energy, it provides heat using mirrors so that rays of the sun can be concentrated into a receptor and reach temperatures of up to 1000°C. The heat is then used to warm up a liquid which generates vapor and moves a turbine to generate electricity [6]. For passive solar energy, no mechanism is used to collect and use the energy of the sun. Instead, it is the oldest method to take advantage of solar radiation. For example, the utilization of bioclimatic architecture to keep the building warm during the night times [6]. The benefits of utilizing solar energy are that it will not bring about greenhouse gas emissions, and it is pollution-free. In addition, solar energy is renewable and replenishable energy that can reduce the dependency on fossil fuels. Furthermore, the maintenance cost of solar panels is affordable with new technology being readily available. However, the efficiency of the solar system drops on cloudy and rainy days, and it cannot generate electricity at night times. Additionally, to store surplus energy, an energy storage system is required, which is quite expensive. Moreover, even the most advanced solar panels still only convert around 20-25% of the energy of the sun into power. Thus, the energy conversion rate is quite low. In Australia, solar energy Solar accounted for 9.9% (or 22.5 TWh) of Australia's total electrical energy production in 2020, and it is the fastest growing generation type [7].

For wind energy, it describes the process of utilizing wind to generate mechanical power or electricity. This mechanical power can be used for specific tasks, such as grinding grain or pumping water, or a generator can convert this mechanical power into electricity [8]. A wind turbine is an important device that can convert wind energy into electrical energy. There are two basic types of wind turbines, namely, horizontal-axis turbine and vertical-axis turbine [8]. There are several benefits to using wind power. First, the generation process is emission-free. Second, turbines are available in a wide variety of sizes, which is adaptable to different locations. Third, wind energy is replenishable. However, wind energy is intermittent and unpredictable, which can increase volatility in the solar energy supply [8]. In Australia, wind supplies 35.9% of the country's clean energy and 9.9% of Australia's overall electricity in 2020 [7].

For hydroelectric power, it harnesses the power of fast-moving water in a large river or rapidly descending water from a high point to convert the force of that water into electricity by spinning the turbine blades [9]. To be specific, the turbine converts the kinetic energy of the water into mechanical energy, and a generator converts the mechanical energy from the turbine into electrical energy. The merits

of using hydro power are that the source of hydro power is renewable, and it can be paired well with other renewables. In addition, it is emission-free since the generation of hydroelectricity releases no emissions into the atmosphere. Moreover, hydro power is more reliable than solar and wind energy because water usually has a constant and steady flow. Furthermore, hydro plants can adjust the flow of water to produce more energy or less energy according to the electricity demand. However, there is a limited place for hydro plant construction, and the initial construction fees are expensive. Additionally, although the generation process produces no emission, the reservoirs, such as plants at the bottom, can decompose and release a large amount of carbon and methane. Furthermore, the performance of hydro can be influenced by climate change, such as drought [9]. In Australia, more than 100 operating hydroelectric power stations with a total installed capacity of about 7800 megawatts (MW) are operating, which are located mostly in New South Wales (55%) and Tasmania (29%) [10].

For tidal energy, it is produced by the natural surge of ocean waters during the rise and fall of tides caused by the gravitational interaction between Earth, the sun, and the moon [11]. To be specific, tidal energy works via a turbine that is connected to a gearbox, which can turn a generator to generate electricity. There are several merits to using tidal energy. First, compared with solar and wind energy, tides can be easily predicted because tides occur at expected times. Second, the efficiency of tidal energy is 80%, which is much higher than solar or wind energy generators. Third, it produces no greenhouse gas or other waste. However, the initial construction cost is very expensive, and the sites for constructing barrages are limited. Moreover, tidal stations can only produce energy for certain periods of a day when the tide is moving in and out [11]. In Australia, the tidal energy system is considered to have the highest technical maturity, which can produce approximately 2004 TWh per year of tidal energy [12].

For geothermal energy, it is a type of renewable energy source that comes from the heat generated during the original formation of the planet and the radioactive decay of materials, which can be used to generate electricity and heat buildings, etc. [13]. This type of renewable energy is not only environmental-friendly but also more reliable and sustainable than solar and wind energy. However, during the exploitation and digging process, gasses stored under the surface of the earth might be released into the atmosphere. In Australia, although geothermal energy source is considerable, the development of geothermal energy is not financially viable because it is difficult to discover suitable geothermal resources, and the flow of hot fluid from the geothermal reservoirs is at a high rate [14].

For biomass energy, it is energy generated or produced by living or once-living organisms [15]. And the generated energy can be used to create heat or converted into electricity. There are five main types of biomass energy, including agricultural residues, animal waste, forest residues, industrial waste, and sewage. The detailed mechanism of biomass energy to generate electricity is that biomass is burned in a boiler to produce high-pressure steam, which flows over a series of turbine blades. As a result, the rotation of the turbine drives a generator to produce electricity. Apart from the benefits of being carbon-neutral and renewable, the utilization of biomass energy can reduce the dumped garbage in landfills. Moreover, it is less expensive than fossil fuels. However, biomass energy is not as efficient as fossil fuel energy. Furthermore, the merit of biomass energy being carbon-neutral is questionable because the use of animal and human waste can escalate the number of methane gases, which can be damaging to the environment [15]. According to Clean Energy Council, biomass energy generated approximately 3164 GWh of electricity in Australia in 2020, which equals 1.4% of total electricity generation, and 5.0% of total clean energy generation [16].

1.2.2 Development Two of Energy Market at Distribution Level

For the second development of the energy market at the distribution level, DERs are becoming more prominent in recent years. It can be defined as the renewable energy units or systems located in houses, residential buildings, or businesses to offer them power [17]. On account of the fact that electricity is generated or managed behind the electricity meter in houses, residential buildings, or businesses, DER is also called “behind the meter” [18]. Compared with the traditional way of generating electricity at big and centralized power stations, it is more decentralized and starting to come from many places, including millions of homes and businesses. Examples of DERs include roof-top solar PV units, wind generating units, battery storage, the battery of EVs to export power back to the grid (V2G), fuel cells, combined heat and power units, etc. [17].

For roof-top solar PV unit, it is a PV system that has installed electricity-generating solar panels on the rooftop of a residential or commercial building or structure [19]. The benefits of roof-top PV include low electricity bills, low carbon footprint, low maintenance costs, etc. However, there are certain disadvantages to using solar PVs. First, the initial cost to purchase the solar system is expensive, including payments for solar panels, inverters, batteries, wiring, and installation. Second, the efficiency of roof-top PV is weather dependent. In Australia, the per-capita rooftop solar installation rates are the

highest in the world, with rooftop and utility-scale solar already meeting over 100% of demand in South Australia. In addition, it is expected to have five times more rooftop solar capacity by 2050 [20].

For wind generating units, wind turbines are connected at the distribution level of an electricity delivery system to support the operation of local electricity distribution networks [17]. Distributed wind generating units are commonly installed at residential, agricultural, commercial, industrial, and community sites [17]. There are certainly advantages of distributed wind generation. First, small-scale wind power generation can save space for wind generating unit construction and transportation fees of wind turbines. Second, the pressure on the electrical grid can be reduced by introducing distributed wind generating units. Third, a wind turbine operates whenever it is windy. However, the energy generated is intermittent, and noises can be produced by the wind turbine blades. In NSW, Australia, small wind turbines sized to suit domestic properties, farms, or small businesses are becoming increasingly popular [17].

For battery energy storage, it is an electrochemical device that charges energy from the grid or a power plant and then discharges that energy later to provide electricity to end-users or other grid services when needed [21]. The benefits of battery storage have been well recognized in terms of generation backup, transmission alleviation, voltage control, frequency regulation, peak shaving, load shifting, etc. [18]. In recent years, the battery of EVs to export power back to the grid has been under dramatic development, i.e., V2G. For V2G, it describes a system in which EVs, such as PEV or PHEV, communicate with the power grid to sell demand response services by either discharging electricity from the battery of the EV to the grid or by throttling their charging rate [22]. The benefit of the V2G technique is that the imbalance between electricity demand and supply can be mitigated, and EVs can save costs on building unnecessary electricity systems [22].

For fuel cell, it is an electrochemical cell that converts the chemical energy from a fuel into electricity via an electrochemical reaction of hydrogen fuel with oxygen or another oxidizing agent. It composes of three adjacent segments, namely, the anode, the electrolyte, and the cathode [23]. Fuel cells are categorized primarily by the type of electrolyte employed, such as polymer electrolyte membrane (PEM) fuel cells, direct methanol fuel cells, alkaline fuel cells (AFCs), phosphoric acid fuel cells (PAFCs), molten carbonate fuel cells (MCFCs), and solid oxide fuel cells (SOFCs), etc. [23]. Compared with the battery, fuel cells require a continuous source of fuel and oxygen to sustain the reaction [23]. There are

several advantages of using fuel cells. First, it is of high efficiency reaching over 80%. Second, it is reliable as the power offered does not degrade over time. Third, it is environmentally friendly. However, the cost of manufacturing is high due to the high cost of platinum. In addition, it lacks the infrastructure to distribute hydrogen. Moreover, hydrogen is expensive to produce [23].

For CHP, it is a technology that produces electricity and thermal energy at high efficiencies using a range of technologies and fuels, which is also known as cogeneration [24]. The benefits of the CHP are numerous, including increased fuel efficiency, reduced energy wastage, reduced energy costs, reduced greenhouse gas emissions, reduced reliance on the grid, etc. However, there are certain disadvantages of using CHP. For example, the installation cost of the CHP is costly, and if a system is using diesel or other fossil fuels as its fuel source, then they are not an eco-friendly choice [24]. There are numerous companies offering cogeneration services in Australia, such as The Evo Group and the Inoplex, etc.

With the introduction of DERs, the energy market is diversified into a variety of ranges, including the energy sharing market, energy storage sharing market, renewable energy trading market, P2P trading, trading at the local and community levels, etc.

For energy sharing market, it aims to meet the energy needs of end-users through excess energy trading within a sharing community when households have excess energy. In such a sharing market, prosumers can save energy purchasing costs and become more self-sufficient [25]. For the energy storage sharing market, end-users will borrow the capacity of the shared ESS managed by the ESS coordinator. In the renewable energy trading market, renewable energy will be traded. '*The global renewable energy market was valued at $881.7 billion in 2020 and is projected to reach $1,977.6 billion by 2030, growing at a compound annual growth rate of 8.4% from 2021 to 2030*' [26]. For peer-to-peer trading, it describes a trading process where energy buyers and energy sellers trade directly with each other without a third party. For trading at local or community levels, it is designed to provide local economic and social benefits, such as reduced energy costs and energy autonomy [27].

1.3 Risks in the New Energy Market

Although renewable energy generation and DERs are reliable and environmentally friendly, there are certain risks associated with the two developments in the energy market. Before discussing the risks mentioned, the main market participants in the new energy market will be explained first. Note that this thesis focuses on the risk hedging strategy of the energy market. Hence, only the participants related to

the energy market will be mentioned. The market participants, i.e., the stakeholders, can be categorized into two broad types, namely, the supply side and the demand side. For the supply side, generators, retailers, ESS coordinators, EVCSs, etc., are common research targets. For the demand side, consumers, prosumers, EV users, etc., are mainly focused.

1.3.1 Risks for the Supply Side

First, the risks that occurred for the supply side in the new energy market will be elaborated. The use of natural gas to generate electricity has become pervasive due to the fast response ability of natural gas generators [28-32]. In some countries such as China and Australia, coal power generation serves the baseload (i.e., customers), while natural gas generators are used primarily for peak hours when electricity prices are high or fast response regulation is required. However, this operation process incurs high risks because gas generators generate electricity only when electricity prices are high. Therefore, as a type of thermal power generation (i.e., power generation process in which heat energy is converted into electricity), natural-gas-fired power generation requires a relatively high Levelized cost of energy (LCOE) compared to coal-fired power generation. LCOE is defined as the average price per unit output required for a plant to break even over its operating lifetime [33]. Hence, in the bid-to-sell process, gas generators will bid at prices higher than their LCOEs, making them much more likely to fail in bidding compared to coal-fired generators. As a result, gas generators cannot sell sufficient electricity, and significant risks are incurred.

Although gas generators incur the risk of being unable to succeed in the bid, they still have a promising future. This is because natural-gas-fired power generation plays a critical role in converting gas back into electricity and selling energy in electricity markets. Based on emerging P2G technology, renewable energy could be stored economically on a large scale in the form of natural gas [34]. However, it will still encounter high risks, and the profits will be influenced by the fluctuation of electricity prices. Because gas generators play an important role in power systems, it is necessary to implement certain hedging tools to reduce the risks associated with these generators.

As for energy retailers, they will encounter risks of demand-supply imbalance. With the penetration of DERs, greenhouse gas emission has been substantially reduced [35]. However, the incorporation of DERs will lead to a large-scale demand fluctuation. As a result, an imbalance of demand and supply might occur [36]. Although this type of risk will not cause tremendous losses for the electricity retailer,

it happens more frequently. Furthermore, the increase of EEs caused by climate change will further augment the demand-supply imbalance. EEs like bushfires and ice storms can lead to huge damage to power transmission lines and towers, which will make the retailers unable to satisfy the demand requirements [36-38]. Although the occurrence of this type of risk is rare, the damages are tremendous.

As for ESS coordinators, they will bear the risks of energy price volatility. With the increasing penetration of renewable resources, such as rooftop PV generation [39], greenhouse gas emissions can be reduced. However, renewable resources are difficult to operate reliably due to their intermittent and unstable features [40]. Thus, the ESS is employed to smooth the spatial and temporal imbalance between the energy demand and renewable energy generation. Nevertheless, the investment costs of ESS are substantial, and the costs are entirely borne by the end-users. Furthermore, because of the random usage patterns of different residents, the utilization of the residential ESS is inefficient. To this end, the concept of energy storage sharing is introduced where the centrally controlled ESS by the ESS coordinator can provide storage services to the end-users as if they were using the behind-the-meter ESS. However, the ESS coordinator will bear the risk of price fluctuation that the prosumers would otherwise have encountered if they were using the self-built ESS.

As for EVCSs, they might incur losses from selling at too high a price that is unattractive to the EV users or selling at too low a price, which results in losing profits for the EVCSs that EVs would otherwise have been willing to pay. Moreover, the low charging price set by EVCSs has a side effect, i.e., potential long queueing length, which might increase the risks of PDN and TN congestion. To be specific, EVs are believed to have the promising potential to reduce greenhouse gas emissions and urban air pollution if EVs are charged with renewable energy [41, 42]. As a result, EVs are burgeoning to gradually replace GVs [43]. Under this context, the synergistic effect of PDNs and TNs has become an emerging topic to discuss [44, 45]. To be specific, the growth of EVs will increase the EV traffic flow in TN. Then, the increasing EV traffic flow will increase the charging demand at the EVCSs, and the increased charging demand at EVCSs will further affect the operation of PDN. To this end, the increasing penetration of EVs can pose a potential impact on the security and stability of the PDN [44]. Additionally, the substitution of GVs with EVs might induce two types of potential risks for TN [45]. First, EVCSs are usually constructed on prosperous roads to obtain more traffic capture, but the attraction of the additional EV flow will worsen the traffic condition. Second, the charging behavior of EV users might cause long

queueing lengths within certain EVCSs. Hence, the EVCS plays an important role in guiding EV users' charging selection decisions through pricing strategy to mitigate the above-mentioned issues.

1.3.2 Risks for the Demand Side

Next, the risks that occurred on the demand side in the new energy market will be explained. As for consumers, they might incur financial risks and physical risks. For financial risks, consumers might encounter high energy prices when there are energy shortages or high demand for energy. As a result, the energy costs of consumers are increased, and the utility of consumers will reduce. As for physical risks, consumers might incur insufficient energy supply in the energy market when there is high energy demand, or there is a power outage. Consequently, curtailment of energy consumption might occur, which is also detrimental to the level of satisfaction of consumers with energy consumption.

As for prosumers, they will incur risks of expensive initial costs of DERs during the sharing process, with consumers being the 'free-riders' if the sharing process is modeled as a trading process. For example, [46, 47] modeled energy sharing as an energy trading process. In such a trading process, the pure consumers could participate and benefit from the sharing economy by purchasing electricity at a relatively low price [48]. However, they made less contribution toward energy sharing. It would result in the end-users being less incentivized to invest in DERs. As a result, prosumers will bear the risks of high investment costs on DERs themselves. Consequently, the development of the DERs could be hindered. Moreover, prosumers will encounter high risks due to the fluctuating sharing price if they directly participate in the sharing market in which the pricing mechanism is either non-cooperative game clearing or auction-based clearing. This is because prosumers normally lack the expertise of risk-hedging.

As for EV users, they will encounter financial risks, time risks, and physical risks. For financial risks, EV users might incur high charging costs when the price of the selected EVCS is high on average or when the charging demand for EVs is high. As for time risks, EV users might encounter risks of long traveling time on the road, long waiting time, and charging time at EVCSs due to the increasing penetration of EVs. Regards physical risks, two sub-categories of risks are discussed, i.e., the risk of insufficient SOC to arrive at the selected EVCS and the risks of EV battery degradation, etc. Thus, it is necessary to develop proper strategies to guide the charging/refueling of EV users to hedge those mentioned risks of EV users and increase EV user satisfaction.

1.4 State-of-art Hedging Strategies

To date, the state-of-art risk hedging methods for the energy market can be mainly categorized into four types:

- Financial tools: The first is financial tools, which are defined as the hedging tools that can increase the chances for market participants to either receive more net profits under certain risks or incur fewer risks under certain net profits [49]. Those financial tools include bilateral contracts, forward, swap, future, option contracts, etc. [50-53]. Take the bilateral contract as an example, the risks of demand fluctuation caused by the penetration of DERs normally happen at the distribution level. Although this type of risk will not cause tremendous losses for the electricity retailer, it happens more frequently. Normally, to hedge this type of risk, retailers can firstly sign bilateral contracts with the generation companies (GENCOs) to stabilize the electricity prices and cover the majority of the estimated demand [37]. Then, when overconsumption occurs, the retailer will compensate for the demand gap from the spot market at the real-time electricity price [36].
- ESSs: As for ESS, i.e., physical tools, energy storage like P2G and battery can be used to smooth the energy usage [54]. The benefits of the BESS have been well recognized in terms of generation backup, transmission alleviation voltage control, frequency regulation, etc. Apart from BESS, the P2G is also a promising ESS technology since the process of electricity-hydrogen conversion is carbon-free if electricity is from renewable energy [55, 56]. P2G devices can convert excess electricity into hydrogen through water electrolysis, and the energy is stored in the form of gas. Then, the gas can be converted back to electricity by the installed gas generators and fuel cells when needed [34]. Therefore, applying the P2G as an additional ESS can increase the flexibility of the integrated multi-carrier energy system and provide the customer with reliable services.
- Demand response: It is defined as a change in the energy consumption of end-users to better match the energy demand with the supply [57]. There are mainly two types of DR strategies, namely, price-based DR and incentive-based DR. For price-based DR, it is a type of DR strategy to incentivize the end-users to alter their load patterns according to the time-varying prices [58-61], such as time-of-use rates, critical peak pricing, and real-time pricing. For incentive-based DR, it aims to maximize the benefits of retailers, which will increase by triggering an incentive price to influence end-user behaviors to change their demand consumption, such as [62-65]. For example, include direct load control, interruptible/curtailable rates, emergency DR programs, capacity market

programs, and demand bidding programs.

- Pricing strategy: The pricing strategy can be utilized to incentivize end-users to alter their energy consumption patterns to ensure power system stability, including energy consumption amount and energy consumption location (charging station or retailer selection choice) [66]. As for developing pricing mechanisms, there are mainly two types of pricing strategies. The first type is based on the clearing scheme. In the existing literature, there are two commonly used clearing schemes. The first type of clearing is based on the noncooperative game, such as [67]. The second type of clearing is based on the auction, such as [68]. The second type of pricing strategy is that the retailer, ESS coordinator, or EVCS is responsible for formulating the price to realize the insulation between the end-users and the energy market [69-72]. For example, value-based pricing, competitive pricing, skimming pricing, cost-plus pricing, penetration pricing, dynamic pricing, etc.

1.5 Research Problems

However, existing literature that utilized financial tools, ESS, DR, or pricing strategies to hedge the risks of market participants in the new energy market remained several research problems to be addressed.

As for literature that utilized financial tools, the application of only one type of financial tool relies heavily on the estimation of demand and prices. Based on the increasing penetration of DERs, demand and price variation will increase, which will cause greater difficulty in demand and price estimation. Therefore, a more estimation-invariant hedging tool is required.

As for literature that utilized the ESS to hedge risks of demand and supply imbalance, the capital costs of the ESS are still expensive at this stage. To reduce the investment costs, the concept of energy storage sharing has been put forward. As a result, it is more economical for a group of prosumers to share the ESS invested and managed by the coordinator rather than investing in the self-built ESS [73, 74]. Thus, to adapt to the increasing trend of sharing economy, proper sharing mechanisms and relevant pricing strategies in an integrated energy system need to be developed to enhance the comprehensiveness of the sharing model.

As for literature that utilized more than one financial tool or a combination of financial tools and ESS, the budget constraints on investment must be involved in the decision-making process. Since the budgets for investments are limited, efficient allocation of resources like financial tools and physical tools is necessary.

As for literature that used DR, when the DR aggregation becomes large, an improper DR strategy may cause infeasibilities in the system operation, such as voltage violation and thermal overloading problems, which jeopardize the security of the electricity services [75]. Therefore, it is improper to neglect the network constraints like [76, 77].

As for the pricing strategy proposed by some existing literature, they utilized the same sharing price for all end-users. It neglected that different end-users had different energy consumption profiles. Consequently, using the same price could not incentivize individual end-user. For example, in [28, 69, 78], the same sharing price was formulated for all the prosumers, which was derived via the optimization process. Without applying a customized pricing strategy, end-users would not be willing to participate in the energy trading or sharing process. Moreover, most of them formulated the end-user decision-making strategy according to the expected utility of end-users, such as EV users, under the assumption that end users are rational, such as [79-81]. However, this assumption deviated from real-life decision-making due to the subjectivities of end-users. Hence, it is necessary to consider the irrationalities of end-users in formulating decision-making strategies.

Furthermore, with the penetration of weather-related EEs, such as bushfires and ice storms, the supply shortage risks caused by the EEs at the transmission level are happening, which can cause huge losses to the retailer. However, references are lacking on risk-hedging strategies toward the risks caused by the EEs at the transmission level. To fully consider both supply shortage and demand fluctuation risks, more comprehensive risk-hedging strategies are needed for the retailer.

Moreover, as one form of energy, hydrogen offers an opportunity for sector coupling between the electricity, gas, and transport sectors. According to [82], hydrogen is a versatile energy carrier that can be served as an input into a range of industrial processes. The application of hydrogen can enable deep decarbonization across the energy and industrial sectors. Hydrogen can also facilitate the transition to high penetration of intermittent renewable generation in the electricity network. However, the energy substitution effect between electricity demand and hydrogen demand is not well studied. Take the energy demand of EV users as an example, there exists an energy substitution between electricity and hydrogen for PH2EV, which is not investigated in existing charging/refueling navigation literature [83, 84]. Here, PH2EV that consumes either electricity or hydrogen can be served as a new promising type of EV to balance energy supplement duration and energy cost. In addition, PH2EVs can increase the flexibility

and alternatives of energy. It is important to incorporate the impact of energy substitution in energy purchasing strategy formulation so that the balance between energy cost and energy supplement duration can be obtained by purchasing the right amount of electricity and hydrogen.

1.6 Contributions of this Thesis

The increasing penetration of renewable energy generation and DERs has brought benefits to the new energy market. For example, it is environmentally friendly and cost-saving for end-users. However, due to the unstable and intermittent nature of renewable energy, such as solar and wind power, as well as the increasing energy demand, certain risks will occur, which is detrimental to the energy market participants. Hence, it is necessary to propose a relevant risk hedging strategy to hedge risks and ensure the utility of the market participants, which is the purpose of our thesis. In general, our model: 1) develops more estimation-invariant financial hedging tools to hedge the risk of increasing demand fluctuation caused by the penetration of DERs. 2) considers the budget constraint when utilizing a combination of financial tools and physical tools to hedge risks. 3) takes the subjectivity and bounded rationality of end-users into consideration when making the pricing strategy to better incentivize end-users to participate in the energy trading or sharing process. 4) incorporate new emerging trends like the burgeoning of extreme events and the increasing application of hydrogen into the model formulation.

To be specific, the contribution of this research consists of developing a series of effective risk hedging tools and strategies for market participants in the new energy market, which are summarized as follows:

- **The applications of financial tools and physical tools (in chapters 3 and 4)**.
    a) By formulating the hedging tools consisting of a combination of financial tools and physical tools, the reliance on the prediction of the prices is avoided.
    b) Portfolio theory is applied, considering the budget limitations of the gas generator and the retailer, to determine the optimal weight of financial tools and physical tools to invest.
- **The implementation of the DR strategy (in chapters 5 and 6)**
    a) A rigorous incentive-based DR mechanism based on both call and put options is implemented to shift the charging/discharging profile (consumption pattern) of the EV aggregator (EVA), who manages the EVs (chapter 5).
    b) The proposed price-based DR strategy of the DR aggregator, i.e., a single entity that manages the aggregation of the controllable residential loads, can fully consider operational

constraints of the power systems without obtaining full information on the electricity network (chapter 6).

- **The pricing strategy in the electricity market (in chapters 7 and 8)**
  a) A dynamic pricing strategy, considering the competition relationship between EVCSs, is proposed based on a coupled PDN and TN to maximize the net charging profit of the EVCS. Under this pricing strategy, more charging demand can be attracted. Additionally, the proposed pricing strategy can achieve spatial load shifting by incentivizing EV users to alter their station-selection decision to avoid congestion of the electricity network (chapter 7).
  b) A two-stage pricing model for energy storage sharing has been presented based on the clustering of different load patterns. In the proposed model, the price structure and the price level for capacity sharing are jointly optimized. Moreover, novel concepts of bulk capacity borrowing and discount sensitivity are introduced to model individualized pricing for the first time (chapter 8).
- **The pricing strategy in the hybrid energy market (in chapters 9 and 10)**
  a) Two pricing strategies have been proposed to increase the total net profits of the coordinator and the willingness of the prosumers to participate in the capacity and energy sharing process. In addition, a novel business model of credit-based sharing has been proposed to integrate both capacity sharing and energy sharing (chapter 9).
  b) A tri-level pricing strategy for IEHSs is formulated considering the integration among EVs, IEHSs, and both the PDN and GN. In this pricing strategy, the temporal shift of EVs within one IEHS and the spatial shift of EVs among multiple IEHSs are modeled. To ensure the effectiveness of the pricing strategy in guiding EV behaviors, the bounded rationality of EVs in station selection is rigorously modeled based on the cognitive hierarchy (CH) theory (chapter 10).

1.7 Thesis Outlines

The thesis is divided into twelve chapters. The first chapter is the introduction, which introduces the basic concepts and preliminaries of this research. Chapter 2 is the literature review part. Chapter 3 focuses on the application of financial tools and physical tools within three types of markets, i.e., the financial market, the ancillary market, and the spot market. Chapter 4 focuses on the application of financial tools

and physical tools under the circumstance where increasing penetration of EEs caused by climate change will further augment the demand-supply imbalance. Chapter 5 focuses on an option-based DR strategy to mitigate the demand-supply imbalance and save energy costs for both retailers and the aggregator who manages EVs. Chapter 6 focuses on utilizing price-based DR aggregation with the operating envelope framework based on the representative signals produced by the DNO in the context of the big data era. Chapter 7 focuses on proposing a dynamic pricing strategy for EVCSs to facilitate EVCSs to earn higher profits while alleviating the potential negative impacts on both PDN and TN, considering the responsiveness of aggregated demand towards charging price. Chapter 8 focuses on proposing an individualized pricing strategy that can facilitate the coordinator to capture the most considerable possible net profits through price discrimination based on discount sensitivity in the electricity market. Chapter 9 focuses on proposing a credit-based pricing strategy for hydrogen and electricity energy storage sharing in a hybrid energy market. Chapter 10 focuses on proposing a tri-level dynamic pricing strategy for IEHSs to guide the charging/refueling decisions of EVs and ensure the operation of IEHSs, PDN, and GN in a hybrid energy market, considering the bounded rationality of EV users.

- **Chapter 2- Literature review**

  This chapter introduces the definition related to risks occurred in the energy market. Next, research works relating to risk hedging strategies applied to hedge risks like demand-supply imbalance, operational risks, energy price fluctuation, etc., are categorized into four main types, namely, the application of financial tools, physical tools, DR, and pricing strategies.

- **Chapter 3- Risk hedging for gas power generation considering power-to-gas energy storage in three different electricity markets**

  This chapter proposes a portfolio strategy for gas generators to earn profits and hedge risks in three different electricity markets, namely, the spot, the ancillary, and the financial markets. The presented approach is to apply energy storage and financial derivatives to hedge the market risks of gas generators, including short put option and short call option, and the option value deduction process is also involved. To be specific, the concept of the binomial tree has been brought up to deduct the option value. The purpose is to calculate the premium of the option in the financial markets.

- **Chapter 4- Risk hedging strategies for electricity retailers using insurance and strangle**

weather derivatives

This chapter proposes a hedging strategy, besides the normal bilateral contract, including insurance, the strangle weather derivatives, and the energy storage system, to hedge the risks at both the transmission and distribution levels. To be specific, at the transmission level, a rigorous risk-hedging model based on insurance is proposed for the retailer to hedge the risks. In this chapter, an economic adjusting index is introduced to represent the different risk aversion levels of the retailer toward the low probability but high loss events, i.e., the EEs. At the distribution level, a risk management strategy based on the strangle weather derivatives and ESS is designed for the retailer to hedge the risks. Moreover, the proposed model offers a guide for choosing diverse forms of hedging portfolios (a set of hedging tools) for retailers under different budget constraints.

- **Chapter 5- Demand response of electrical vehicle aggregator using financial hedges: options**

  This chapter proposes an option-based DR strategy to mitigate the demand-supply imbalance and save energy costs for both retailers and the aggregator who manages the EVs. To incentivize the EV owners to participate in DR programs, a clustering-based Nucleolus method is proposed to obtain the optimal cost saving allocation among end-users and ensure the satisfaction of the end users. Furthermore, the time to find the nucleoli can be shortened via the clustering technique and the nested linear program.

- **Chapter 6- Demand response aggregation with operating envelope based on data-driven state estimation and sensitivity function signals**

  This chapter proposes a price-based DR aggregation with the operating envelope framework based on the representative signals produced by the DNO in the context of the big data era. The DNO provides representative signals, including real-time state estimation and sensitivity functions, to the DR aggregators based on the proposed Semi-supervised Coupled Generative Adversarial Imputation Network (SC-GAIN) and big data analysis. The DR aggregators can realize the secure and efficient real-time dispatch of the controllable loads based on the received signals.

- **Chapter 7- Pricing for electric vehicle charging stations based on the responsiveness of demand**

This chapter proposes a dynamic pricing strategy for EVCSs to facilitate EVCSs to earn higher profits while alleviating the potential negative impacts on both PDN and TN. First, a pricing strategy, considering the competition effect established based on the TN, is formulated to facilitate the EVCS to attract the defined competitive charging demand. Second, a two-step approach is proposed to mathematically formulate the responsiveness of demand towards the charging price. Third, EV user behaviors are incorporated based on both an admission control scheme and a queueing model to further adjust the charging demand.

- **Chapter 8- Individualized pricing of energy storage sharing based on discount sensitivity**

  This chapter proposes a two-stage pricing mechanism between the coordinator who operates the shared energy storage and the prosumers who are borrowing the shared capacity from the coordinator. Individualized pricing is derived via the two-stage pricing process. It is a pricing strategy that can facilitate the coordinator to capture the most considerable possible net profits through price discrimination. First, prosumers are clustered into different groups using the data-driven approach. Then, novel concepts of bulk capacity borrowing and discount sensitivity are introduced to model the individualized pricing for the first time. As a result, the price structures and the price levels can be jointly optimized.

- **Chapter 9-Credit-based pricing and planning strategies for hydrogen and electricity energy storage sharing**

  This chapter proposes a two-stage credit-based sharing model between the coordinator who manages the shared ESS and the prosumers who borrow the capacity and energy from the coordinator. Both capacity and energy sharing are integrated via the proposed credit-based sharing model. As for energy sharing, two forms of energy are considered: electricity and hydrogen. In addition, both cost-based and demand-based pricing strategies are introduced to customize the sharing prices so that the coordinator can obtain larger net profits and the prosumers can reduce their energy purchase costs.

- **Chapter 10-Pricing strategy for energy supplement services of hybrid electric vehicles considering bounded-rationality and energy substitution effect**

  This chapter proposes a dynamic pricing strategy for IEHSs to guide the charging/refueling decisions of EVs and ensure the operation of IEHSs, PDN, and GN. First, a tri-level dynamic

pricing strategy is proposed considering the interactions among EVs, IEHSs, and both PDN and GN. Second, the bounded rationality of EVs in station selection is modeled based on the cognitive theory. Third, energy substitution for PH2EVs between electricity charging and hydrogen refueling is analyzed.

- **Chapter 11-Conclusion and future works**

  The concluding remarks and future works are given in this chapter

2. LITERATURE REVIEW

The market participants, such as the generator, the retailer, the end-users, etc., will encounter various risks in the energy market. Those risks include energy demand-supply imbalance, energy price fluctuation, the uncertainty of end-user behavior, unexpected weather-related extreme events, etc. With the penetration of renewable energy generation and the DERs, the energy demand-supply imbalance is more severe. Consequentially, risks of energy price volatility will be exacerbated. As a result, it is necessary to come up with effective and proper risk hedging strategies to hedge the risks of market participants and ensure their utility. A thorough literature review has been undertaken to understand the existing academic research works and industrial practices and to better identify potential research gaps.

2.1 Risk Hedging Strategy for Energy Suppliers in the Wholesale Market

Based on an increased focus on the reduction of greenhouse gases and detrimental gas emissions, as well as on the fast response ability of natural gas generators, the use of natural gas to generate electricity has become pervasive [28-32]. Hence, research on the gas generator has been focused. In some countries such as China and Australia, coal power generation serves the baseload, while natural gas generators are used primarily for peak hours when electricity prices are high or fast response regulation is required.

2.1.1 Risks Encountered by the Energy Generator

However, the operation process of the gas generator incurs high risks because gas generators generate electricity only when electricity prices are high. Therefore, as a type of thermal power generation (i.e., power generation process in which heat energy is converted into electricity), natural-gas-fired power generation requires a relatively high Levelized cost of energy (LCOE) compared to coal-fired power generation. LCOE is defined as the average price per unit output required for a plant to break even over its operating lifetime [33]. Therefore, in the bid-to-sell process, gas generators will bid at prices higher than their LCOEs, making them much more likely to fail in bidding compared to coal-fired generators. As a result, gas generators cannot sell sufficient electricity, and significant risks are incurred. Although gas generators incur the risk of being unable to succeed in the bid, they still have a promising future. This is because natural-gas-fired power generation plays a critical role in converting gas back into electricity and selling energy in electricity markets. Based on emerging P2G technology, renewable energy could be stored economically on a large scale in the form of natural gas [34]. Because gas generators play an important role in power systems, it is necessary to implement certain hedging tools to reduce the risks

associated with these generators.

2.1.2 Risk Hedging Strategy for the Energy Generator

In the literature, to maximize profits and hedge risks, financial derivatives were used by gas generators in [50]. These derivatives comprise forward contracts, futures, swaps, options, etc. [51]. It is common for the gas generator to use a bilateral contract or the future and forward contract to hedge risks [85]. Ref. [52] described a method to measure and manage the market risks by utilizing the future contract, and it also proposes the stochastic optimization techniques to price the derivatives. Ref. [86] studied the relationship between energy and stock prices in Asia. As a result, the discovered relation can hedge energy risks. Ref. [53] utilized real options to highlight the flexibility value of the demand response under both operational and planning uncertainties. Simulation results showed that both the short-run and long-run risks had been hedged. However, they only utilize financial tools to hedge risks. As for Ref. [87], both physical and financial tools were used to hedge risks arising from the profit variation and the spot price uncertainty in bilateral markets, and the risk assessment methods are evaluated in detail.

Physical tools like P2G will have a promising future due to the following two aspects of reasons. First, the energy storage costs of the P2G is relatively low compared to other energy storage device like the battery. And it is suitable for the gas generator to use the P2G device to store energy. Second, the use of P2G can increase the flexibility and alternatives of energy. Ref. [88] examined the economic feasibility of pipe storage, and it also considered the study of the cost-effectiveness of P2G to store the H_2 and renewable methane. In [89], P2G was utilized to convert waste energy to natural gas. In this literature, day-ahead scheduling and gas load management have been examined to minimize the consumption costs of the users. Ref. [90] emphasized the benefits of using a P2G device. By using the P2G, the load curtailment can be reduced, and the use of renewable energies can be increased. Simulation results have shown that the wind and solar capacity can be reduced by around 23%, and the load curtailment can be reduced by 87%. In [34], quantitative studies have been added to evaluate the economically operational aspects of P2G. In addition, the case of the Great Britain system has been analyzed to indicate the benefits of using P2G. As for [91], the concept of a combined P2G and gas-fired power plant (GFPP) system was proposed to achieve CO_2 emission reduction and the utilization of renewable energy. Simulation results showed that the proposed system could increase the utilization of surplus renewable energy to 30% and reduce more emissions of CO_2 than the traditional operation system. Ref. [92] proposed a coordinated

bidding strategy for wind farms and P2G facilities. Simulation results indicated that profits of both the wind farm and the P2G facilities could be increased by using the proposed bidding strategy. In [93], a scenario-based stochastic decision-making model was proposed to facilitate the operation of both the natural gas generating unit (NGG) and P2G conversion facilities. The effectiveness of the proposed model was verified based on case studies in the Pennsylvania, New Jersey, and Maryland markets. Ref. [94] proposed a maximum production point tracking (MPPT) strategy to enhance the performance of HT-P2G. Simulation results indicated that the proposed strategy can improve the conversion efficiency and the loading capacity which is beneficial for the HT-P2G in the long term.

Due to the limitation of the investment budgets, the gas generator should determine the optimal proportion of the different financial tools or physical tools to invest in. In [95], the portfolio theory was used to find out the optimal energy storage management. The optimal portfolio is where the utility curve tangents to the efficient frontier, which is the set of optimal portfolios that provide the highest expected return for a given level of risk or the lowest risk for a given level of expected return. In [96], the mean-variance theory was also used to decide the optimal weight for energy and ancillary markets. Ref. [97] proposed an adapted power portfolio strategy to optimize the profit per unit of risk of the aggregator. Simulation results showed that financial risk had been reduced while the robustness to uncertainties has been increased. Ref. [98] proposed a combined economic-degradation model to enhance the profits of the distributed energy storage plants by considering the multi-service portfolio of energy storage. Case studies showed that the long-run revenues can be guaranteed due to lengthier storage life span.

2.1.3 Research Gaps

There are still three issues that remain unaddressed. The research gaps could be summarized in three aspects. First, the risk hedging strategy for gas generators lacks a careful consideration of the energy market and the financial market. For the energy market, the spot market and the ancillary market should be examined as well. Ref. [99] investigated the risk hedging of the hydropower plants. Model efficiency on risk hedging has been tested via simulation in the Brazilian market. However, the model only considered the spot market in the traditional power system. Similar to [99], Ref. [100] proposed a decentralized and interdependent risk hedging model that includes both the coordination optimization model and the risk-aware optimal power flow model. However, only the traditional power system modeling is considered, whereas the energy market operation analysis is lacking.

Second, both financial and physical tools need to be combined with hedging risks and ensuring the profits of the gas generator. Financial tools like forward, options, and swaps are common financial derivatives to hedge risks. As for physical tools, energy storage like P2G and battery can be used to smooth the energy usage. Ref. [101] used the forward contract to hedge the risks of end-users on fuels and electricity purchasing. A forward contract has been used to determine the energy amount and price in a future transaction. For [102], it utilized exotic options to hedge both the price and quantity risks of the power generator. It is an option that includes a variety of options and other financial derivatives. However, physical tools are lacking, which will limit the application of the derivatives. This is because options like short put and short call require the energy storage to make a price difference gain. In [103], mean-variance portfolio theory has been used to allocate the proportion of the energy storage into each market, whereas only physical tools are used to hedge risks.

Third, budget constraints on investment have to be involved in the decision-making process. Since the budgets for investments are limited, efficient allocation of resources like financial tools and physical tools is necessary. Regarding [102], the proposed exotic option included an infinite collection of derivatives, which is unrealistic and not applicable to the real-world case. To test the model efficiency, constraints like budget limitation should be considered. Thus, proper models and theories have to be used to determine the optimal proportion of the tools. All three types of markets need to be examined to provide a more comprehensive analysis of the effectiveness of the financial and physical tools used by the gas generator. In addition, the bidding process should be considered in both the energy spot market and the ancillary market [104].

2.2 Risk Hedging Strategy for the Energy Retailer in the Retail Market

2.2.1 Risks Encountered by the Energy Retailer

With the penetration of DERs, greenhouse gas emission has been substantially reduced [35]. However, the incorporation of DERs will lead to a large-scale demand fluctuation. As a result, an imbalance of demand and supply might occur [36]. The risks of demand fluctuation caused by the penetration of DERs normally happen at the distribution level. Although this type of risk will not cause tremendous losses for the electricity retailer, it happens more frequently. Normally, to hedge this type of risk, retailers can first sign bilateral contracts with generation companies (GENCOs) to stabilize the electricity prices and cover majority of the estimated demand [37]. Then, when overconsumption occurs, the retailer will compensate

for the demand gap from the spot market at the real-time electricity price [36]. Furthermore, the increase of EEs caused by climate change will further augment the demand-supply imbalance. EEs like bushfires and ice storms can lead to huge damage to power transmission lines and towers, which will make the retailers unable to satisfy the demand requirements [36, 38]. The risks caused by EEs normally occur at the transmission level. Although the occurrence of this type of risk is rare, the damages are tremendous. Studies on the risk hedging strategy of this type of risk from the perspective of energy retailers are lacking. It can be found that energy retailers incur risks at both the transmission and distribution levels. Therefore, more appropriate risk hedging strategies should be developed for retailers to hedge both types of risks. Additionally, the impact of DERs and EEs should be incorporated as well.

2.2.2 Risk Hedging Strategy for the Energy Retailer

In the literature, risk hedging strategies relating to both the *transmission level* and the *distribution level* are discussed. For the *risks of the transmission level*, most of the existing literature hedged the risks from the perspectives of the system planner, the power generators, and the electricity retailers. For literature from the perspective of the system planner, system stability and security problems were focused on. For example, ref. [105] proposed a data-based robust optimization model for the system planner to enhance the electric-gas systems against sequential extreme weather events. The system state was adjusted immediately after each occurrence of extreme weather events to minimize the costs of the system. Ref. [106] established a rare association rule learning system for the system planner for the long-term prediction of the weather-related EEs to identify the spatial and temporal distribution of the system security weakness. An ensemble system was formulated to assess continuous and discrete environmental-input features separately. From the viewpoint of the power generators, literature studied the methodology to hedge the financial risks of demand volatility and price fluctuation. For example, ref. [107] proposed a methodology for the power generator to forecast the density of the long-term peak electricity demand under the impact of extreme weather. A semi-parametric additive model was used to estimate the relationship between the electricity demand and the driver variables, including temperature and economic variables, etc. Simulation results showed that the financial risks of demand volatility could be evaluated and hedged. Ref. [102] designed a power option for the power generator to hedge price-quantity risk in a competitive electricity market. Results showed that the proposed option could address the problem of lacking liquidity in the current bilateral electricity trading scheme. For literature focusing on risk-hedging

strategies for the electricity retailer, ref. [108] proposed a deviation mutual insurance mechanism to reduce the energy deviation settlement costs of the retailer through contract transfer. Simulation results indicated that the deviation between energy consumption and energy contracts could be reduced. However, references that focus on the transmission risk-hedging strategy from the perspective of the retailer are rare.

For the *risks of the distribution level*, most of the existing literature hedged the risks from the perspective of the end-users and electricity retailers. From the perspective of the end-users, references mainly studied the method to reduce energy costs. For example, ref. [109] proposed a real-time price-based demand response management model for heat and power consumers to hedge real-time price risks. The price uncertainty was considered via robust optimization to minimize worst-case heat and electricity purchase costs. Numerical results showed that the energy costs of the end-users could be minimized considering the uncertainty of the electricity prices. Ref. [110] formulated a two-stage stochastic decision-making methodology that enables end-users to decide the optimal energy procurement under the uncertainty of electricity price and renewable supply to reduce energy purchasing costs. Ref. [111] constructed a grand energy coalition for the end-users based on cooperative game theory to optimize the ESS operation. Case studies showed that the energy coalition could reduce the variability of the load profile and energy purchase costs. In addition, the allocation of the cost savings from cooperative energy storage operations could incentivize the end-users to stay in the grand coalition. From the perspective of the retailers, most references focused on the risk-hedging strategies for mitigating demand and price fluctuation. For example, ref. [112] designed an optimal demand response call option for the retailer to hedge the risks of demand-supply imbalance caused by renewable resources. The retailer could exercise the call option to conduct load curtailment when there was a high chance of peak load. Results showed that optimal social welfare could be obtained. Ref. [113] proposed an integrated model to estimate the profitability of retailers with responsive end-users. The model was designed to identify the demand responsiveness impact of the end-users on the spot prices based on their price elasticity. It provided insights to quantify the effect of demand response and risk reduction of the retailers. Ref. [114] proposed three new designs of demand response programs based on the robust optimization approach to minimize the energy procurement costs of the retailer. Ref. [115] modeled the financial risks of market price uncertainty using expected downside risks to configure the forward contract portfolio and determine the

selling price. Ref. [116] ensured a risk-constrained payoff for the retailer based on varied bilateral quantities and associated prices. Risks are quantified via the risk-adjusted recovery on capital. Simulation results showed that the proposed method could ensure a risk-constrained payoff for the retailer.

2.2.3 Research Gaps

However, there are still four aspects of issues that remain unaddressed by the existing literature. First, the current risk-hedging strategy for the retailer is incomplete. First, most of the references studied the risk-hedging strategies for retailers at the distribution level to mitigate demand fluctuation, such as [112, 113]. With the penetration of weather-related EEs, the supply shortage risks caused by the EEs at the transmission level is happening, which can cause huge losses to the retailer. However, references are lacking on risk-hedging strategies toward the risks caused by the EEs at the transmission level. To fully consider both supply shortage and demand fluctuation risks, more comprehensive risk-hedging strategies are needed for the retailer.

Second, since the EEs are of extremely low probability but tremendous damages, the total loss value predicted would be smaller, such as [117]. As a result, the retailer would pay a smaller amount of insurance premium to cover the total loss value predicted. However, a lower amount of insurance premium would lead to a higher amount of insurance excess. Consequently, the retailer was unable to claim monetary compensation back even when there were damages caused by the EEs. To enhance the hedging effectiveness of the insurance, a proper risk valuation method must be developed to incorporate the risk preference of the retailer and facilitate the retailer to predict the total loss value and pay the right amount of insurance premium for the right insurance contract.

Third, the existing risk-hedging methods rely heavily on the prediction of the electricity price, such as [36, 37, 118]. As a result, when the predictions of the electricity price are inaccurate, the effectiveness of the hedging tools is compromised. Hence, a more price-irrelevant financial tool is needed to reduce the reliance of the retailer on the prediction of the price level.

Fourth, the retailer has a limited capital investment for risk-hedging strategies in real practice. However, the existing literature failed to consider the investment budget constraints of the retailer, such as [108, 112, 113], neglect of which will lead to impractical hedging tool portfolio decisions. Thus, it is necessary to incorporate the influence of budget restrictions.

2.3 Risk Hedging Strategy for the EVCS in the Retail Market

2.3.1 Risks Encountered by the EVCS

EVs are believed to have the promising potential to reduce greenhouse gas emissions and urban air pollution if EVs are charged with renewable energy [41, 42]. As a result, EVs are burgeoning to gradually replace GVs [43]. Under this context, the synergistic effect of PDNs and TNs has become an emerging topic to discuss [44, 45]. To be specific, the growth of EVs will increase the EV traffic flow in TN. Then, the increasing EV traffic flow will increase the charging demand at EVCSs, and the increased charging demand at EVCSs will further affect the operation of PDN. To this end, the increasing penetration of EVs can pose a potential impact on the security and stability of the PDN [44]. Additionally, the substitution of GVs with EVs might induce two types of potential risks for TN [45]. First, EVCSs are usually constructed on prosperous roads to obtain more traffic capture, but the attraction of the additional EV flow will worsen the traffic condition. Second, the charging behavior of EV users might cause long queueing lengths within certain EVCSs. Hence, the EVCS plays an important role in guiding EV users' charging selection decisions through pricing strategy to mitigate the above-mentioned issues.

2.3.2 Risk Hedging Strategy for the EVCS

The pricing strategy of the EVCS is investigated in the literature. However, in some of the existing references [119, 120], EVCSs simply applied the DLMP as the charging price. Although DLMP has the advantage of stimulating EV loads to maintain the voltage, current, and power flow within acceptable limits and alleviate the congestion of PDN, using the DLMP can only cover the marginal costs of EVCSs. Thus, it fails to facilitate the EVCSs to gain higher profits. In practice, EVCSs are self-interested [121]. Hence, EVCSs can formulate their own pricing strategies to not only cover the cost of EVCSs but also gain higher profits. For example, in [122], a dynamic pricing strategy for EVCSs was proposed to maximize their charging profit under a realistic environment where various types of EVs were considered. An algorithm based on the price elasticity of EVs was developed to find the parameters required for charging management, including information like EV arrival, renewable energy output, price of electricity, etc. Simulation results proved that the proposed pricing strategy could achieve close-to-optimal performance for EVCSs. In [123], a combinatorial online pricing strategy was presented via a reward-based model to increase the charging profit and prevent power outages. In such a strategy, EVCSs were incentivized by the utility on their contribution to charging load shifting. Results showed that the charging profit of the EVCS was enhanced. In [121], an optimal charging price strategy was proposed

considering the interdependent operation of both PDN and TN to maximize the charging profit of the EVCS. To incorporate the circumstance of increasing competition among EVCSs, an optimal pricing strategy for the EVCS was proposed in [124] to maximize the charging profit in both monopoly and duopoly markets, in which the charging service was offered by one EVCS and two EVCSs, respectively. Similarly, in [125], the competition between EVCSs was considered to maximize the charging profit. In [125], the pricing strategy was proposed based on a multileader-multifollower Stackelberg game model. In this model, the EVCS optimized the charging price according to the prediction of the EVCS selection decision of EV users and the pricing decision of other EVCSs. Some references not only aimed to maximize charging profit but also aimed to enhance customer satisfaction or PDN stability via pricing strategy. For example, in [126], a stochastic dynamic pricing and energy management policy for the EVCS was proposed to balance the competing objectives of profitability enhancement, customer satisfaction assurance, and PDN security. In [127], an online pricing scheme for the EVCS was formulated, considering both the EV driver behaviors in EVCS selection and the EVCS behavior in charging service management. Results showed that both customer satisfaction and EVCS profitability could be enhanced.

Apart from increasing charging profit, in some references, the pricing strategy could enhance the QoS at the EVCS. In [128], an optimal pricing scheme was designed to reduce the service dropping rate of the EVCS based on the queueing network that had multiple services and heterogeneous service rates. The relationship between the dropping rate and the station-selection decision of EV users was formulated to minimize the number of EVs leaving the EVCS. In [129], a scheduled flat-rate pricing policy was formulated considering different battery sizes and the charging services EV users choose (i.e., DC or AC) to reduce the waiting time of the EV users in the queue. In this policy, EV users were deterred from charging more than an energy threshold, hence reducing the load and waiting time at the EVCS. In [130], a coordinated dynamic pricing model was proposed to minimize the waiting time of EV users at the EVCS via inspiring the temporal EV load shifting during evening peak load hours. A heuristic solution was introduced to minimize the overlap between EV users and residential peak load periods. As an improvement, [131] not only ensured the QoS at the EVCS via the proposed pricing strategy but also preserved the smart grid stability. In [131], peak load management (PLM) was presented to schedule EV charging or discharging processes based on the available information acquired via smart communication

technology and equipment, such as roadside units. As a result, the system stability in terms of peak load reduction and the EV satisfaction in terms of power requested with reduced waiting time was ensured.

2.3.3 Research Gaps

However, there are still three issues that remain unaddressed in the existing literature. First, although [124, 125] analyzed the competition among EVCSs based on a Stackelberg game model, the relationship between the TN and the price competition is ignored. In practice, the competition among EVCSs is established based on the TN. For example, when the EVCSs are close to each other, the competition between them might become intense. On the contrary, when the EVCSs are far from each other, the competition between them might become less intense. If two EVCSs are not related to each other in TN through traffic flow, they do not have a competitive relationship. Hence, the competition model in the literature, such as [124, 125], may overestimate the competition degree.

Second, in some of the existing literature [120, 132, 133], the pricing strategy of the EVCS is formulated based on the demand responsiveness of individual EV users towards the charging price. For example, in [132], the pricing strategy is formulated by solving each EV decision problem based on travel time and charge cost minimization. Similarly, the pricing strategy of [133] utilized a congestion game to model the route-selection and station-selection behavior of each EV to minimize the travel duration and energy consumption costs. However, this type of pricing strategy formulated from the microscopic view of individual EV users showing the response of EVs towards the charging price is problematic in two aspects. First, the computational complexity of the pricing optimization of these references will increase significantly as the number of EVs increases. Despite using the clustering method, it might still be computational complex to optimize the detailed EV charging behavior of each cluster. Second, it is almost impossible for EVCSs to have access to real-time or future data related to traffic flow conditions, SOC of individual EVs, and the traveling plan of individual EVs. Hence, the pricing strategy of [120, 132, 133] can only be applied to day-ahead pricing or long-term pricing where the energy price is pre-determined using historical data. As a result, it is more computationally efficient to formulate a pricing strategy for the EVCS from a more macroscopic view by considering the total demand responsiveness towards the charging price. There are research articles modeling the pricing strategy of EVCSs from an aggregated viewpoint by considering the aggregated charging demand, such as [121]. However, it is assumed in [121] that the total charging demand was inelastic to the charging

price, which is obviously inappropriate. As an improvement, in [43], price elasticity was utilized to analyze the relationship between the charging price and the total charging demand. However, it should be noted that the queueing length at the EVCSs can also influence demand responsiveness. Therefore, the balance between charging price, total charging demand, and queueing length needs to be further investigated.

Third, the impact of the queueing length on EV users' charging behaviors is not investigated [134]. EVs normally will need to queue before connecting to a plug during peak charging periods. However, the EV may leave the queue due to impatience when the queueing length is too long, which will reduce the QoS of the charging station and EV satisfaction. Hence, to increase the effectiveness of the formulated pricing strategy, it is necessary to investigate the behaviors of EVs towards the queueing length.

Table 2.1 is added to summarize the pricing strategies in the literature as well as the proposed pricing strategy from five main aspects, namely, the modeling of PDN, the modeling of TN, the competition between EVCSs, the modeling of EV behaviors in station selection, routing, or charging process, and the charging demand responsiveness towards the charging price. Noted that demand responsiveness towards price means that the pricing strategy of EVCSs is formulated considering the demand responsiveness, which is further classified into four sub-aspects, i.e., the aggregated demand response, the individual demand response, the inelastic demand response, and the elastic demand response.

TABLE 2.1. METHODS SUMMATION REGARDING THE PRICING STRATEGY

	PDN	**TN**	**Competition between EVCSs**	**EV behaviors**	**Demand responsiveness towards charging price**			
					Aggregated response	**Individual response**	**Inelastic response**	**Elastic response**
[3]	-	-	-	-	√	-	-	√
[6]	√	√	-	-	-	-	-	-
[7]	√	√	-	-	-	-	-	-
[8]	-	-	-	-	√	-	√	-
[10]	√	-	-	-	-	-	-	-
[11]	-	-	√	-	-	-	-	-
[12]	-	-	√	-	√	-	-	√
[13]	√	-	-	-	√	-	-	√
[14]	√	-	-	√	-	-	-	-
[19]	√	√	-	-	-	√	-	√
[20]	√	√	-	√	-	√	-	-

Proposed	√	√	√	√	√	-	-	√

2.4 Risk Hedging Strategy for the Shared ESS Coordinator in the Energy Sharing or Energy Storage Sharing Market

The installation of DERs, such as rooftop PVs, is promising in reducing greenhouse gas emissions [39]. However, the power generated by the DERs is intermittent, which will cause system stability and security issues [40]. Thus, the ESS is implemented to smooth the power generation. The benefits of the BESS have been well recognized in terms of generation backup, transmission alleviation, voltage control, frequency regulation, etc. Apart from BESS, the P2G is also a promising ESS technology since the process of electricity-hydrogen conversion is carbon-free if electricity is from renewable energy [55, 56]. P2G devices can convert excess electricity into hydrogen through water electrolysis, and the energy is stored in the form of gas. Then, the gas can be converted back to electricity by the installed gas generators and fuel cells when needed [34]. Therefore, applying the P2G as an additional ESS can increase the flexibility of the integrated multi-carrier energy system and provide the customer with reliable services.

As one form of energy, hydrogen offers an opportunity for sector coupling between the electricity, gas, and transport sectors. According to [82], hydrogen is a versatile energy carrier that can be served as an input into a range of industrial processes. The application of hydrogen can enable deep decarbonization across the energy and industrial sectors. Hydrogen can also facilitate the transition to high penetration of intermittent renewable generation in the electricity network. Moreover, governments are putting more emphasis on the application of hydrogen. The Australian government formulates a series of development strategies for the hydrogen industry [82]. The National Hydrogen Roadmap report of the *Commonwealth Scientific and Industrial Research Organization (CSIRO), Australia,* states that the most significant near-term opportunity is blending hydrogen into the existing natural gas network for heating systems in buildings [82]. With the advancement of the P2G technology in the future, excess renewable energy could be economically stored on a large scale in the form of gas (natural gas or hydrogen).

However, the capital costs of the ESS are still expensive at this stage. To reduce the investment costs, the concept of energy storage sharing has been put forward. As a result, it is more economical for a group of prosumers to share the ESS invested and managed by the coordinator rather than investing in the self-built ESS [73, 74].

2.4.1 Risks Encountered by the Shared ESS Coordinator

With the burgeoning of DERs, the energy demand-supply imbalance is becoming more server, which

might be detrimental to the sharing profit of the ESS coordinator. As a result, proper sharing mechanisms and relevant risk hedging strategies in an integrated energy system need to be developed to enhance the comprehensiveness of the sharing model and the utility of the ESS coordinator.

2.4.2 Risk Hedging Strategy for the Shared ESS Coordinator

In the literature, some references focused on the operation strategy in an energy-sharing market. For example, ref. [46] proposed a fair peer-to-peer energy sharing framework among the buildings within a community. A cost reduction ratio distribution model had been proposed to ensure the fairness of the sharing payments. Results showed that the energy costs of the buildings could be reduced, and the net demand profiles of the buildings were smoother and smaller. Ref. [135] developed a risk aversion energy sharing model based on a devised local energy market. Results showed that not only the energy costs of the prosumers could be reduced, but also the information security of the energy sharing process could be ensured via blockchain technology. Ref. [136] proposed a bi-level game-theoretic energy sharing model to determine the optimal sizing of the PV panels. Numerical results showed that the economic benefits of the PV prosumers could be improved. Ref. [137] constructed a grand energy coalition for energy sharing based on cooperative game theory, in which the financial incentives from energy sharing were fairly allocated among the prosumers via the Nucleolus method. Simulation results showed that the cooperative energy management had been scaled up from 15 players to 100 players.

Apart from the operation strategy, some references investigated the pricing strategy in the energy sharing market. For example, ref. [138] proposed a pricing strategy for energy sharing in community microgrids based on the supply-demand ratio. Simulation results indicated that the electricity bill of the consumers was reduced by 12.4%, and the annual income of the prosumers was increased by £57. Ref. [72] proposed an optimal DERs sharing allocation and pricing strategy based on the welfare maximization model and game-theoretical model. Results showed that the welfare of both prosumers and consumers could be maximized in both models. Ref. [139] proposed an energy sharing and pricing strategy to deal with the market bidding problem of virtual energy stations in the multi-carrier energy system. Results showed that a win-win situation for all inner energy cells could be achieved.

For literature focused on the operation strategy of capacity sharing, ref. [47] proposed the capacity sharing and operation game. Each agent determined two actions: the capacity trading and the day-ahead charging/discharging decision. It was found that by using the proposed model, both the energy costs and

the peak-to-average ratio could be decreased. Ref. [69] proposed a two-stage capacity sharing model between the coordinator and the prosumers. Numerical simulation indicated that the proposed two-stage model could reduce the costs of the users by 34.7% and the capacity invested by 54.3%. Ref. [140] proposed the combinatorial auction for resource sharing of energy storage. Resource like the capacity, energy, and charging/discharging power was purchased from the energy storage operator via the auction. The operator would determine the winner of the auction and the related payments. Simulation results showed that both the social welfare and computational efficiency could be enhanced.

Except for operational strategy, some literature studied the pricing strategy for capacity sharing. For example, ref. [70] proposed a data-driven pricing method for PV generation and energy storage sharing in residential building clusters. Ref. [68] proposed an auction pricing model on joint energy storage ownership sharing between the sharing facility controller and the residential community. Ref. [69] developed a novel business model to optimize virtual energy storage sharing among users based on two capacity pricing strategies. Results showed that the costs of end-users could be reduced by 34.7% via the proposed pricing strategies. However, research that focuses on the pricing strategy of capacity sharing is still rare.

2.4.3 Research Gaps

There are still three issues that remain unaddressed in the existing literature. As for the first issue, most of the references did not reveal the essence of the sharing economy. For example, refs [46, 47] modeled energy sharing as an energy trading process. In such a trading process, the pure consumers could participate and benefit from the sharing economy by purchasing electricity at a relatively low price [48]. However, they made less contribution toward energy sharing. It would result in the end-users being less incentivized to invest in DERs. As for the prosumers, they were also less incentivized to participate in energy sharing. Furthermore, the current literature lacked the link between capacity and energy sharing. It is expected to formulate a method that can integrate both sharing services.

For the second factor, the existing literature on energy sharing utilized the same sharing price for all end-users. It neglected that different end-users had different energy consumption profiles. Consequently, using the same sharing price could not incentivize individual end-user, for example, in [28, 69, 78], the same sharing price was formulated for all the prosumers, which was derived via the optimization process. Without applying a customized pricing strategy, the prosumers would not be willing to participate in the

sharing process. Furthermore, the pricing strategy of these references did not make use of the dynamic demand-supply information, such as [69, 72]. Such a pricing strategy would reduce the profit of the coordinator [141].

For the third factor, most of the references only considered the virtual layer of the sharing process, i.e., the pricing strategy, the operation management, the incentivizing mechanism, etc., whereas the physical layer of the sharing process was ignored. For example, [69, 138, 139] neglected the voltage and capacity constraints and network power loss. Thus, these references cannot ensure the security of the power system in the sharing process.

2.5 Risk Hedging Strategy for the End-user in the Retail Market

EVs have the promising potential to be effective in mitigating greenhouse gas emissions in the transportation sector. EVs outweigh GVs in terms of energy saving, carbon reduction, and environmental protection [128]. Hence, the penetration of EVs in some countries has experienced steady growth. In this thesis, EV users are mainly focused. In practice, PEV is a common type of EV powered by electricity that is undergoing dramatic development. However, the burgeoning of PEVs can bring new challenges to charging management. Especially when massive EVs simultaneously gather at stations, long queueing lengths and long waiting times might happen, which will reduce the comfort and utility of EVs. In recent years, hydrogen has become a versatile energy carrier that can be served as an input into a range of industrial processes, including the EV industry [78]. Thus, FCEV has become another type of EV that is powered by hydrogen, which has the advantages of high reliability and high efficiency [142]. Compared FCEV with PEV, the energy service time is significantly reduced via hydrogen refueling. Thus, the problem of long waiting times can be mitigated. However, the energy costs of hydrogen refueling are higher than electricity charging. As a result, PH2EV, which consumes either electricity or hydrogen, can be served as a new promising type of EV to balance energy supplement duration and energy cost. In addition, PH2EVs can increase the flexibility and alternatives of energy. Although PH2EV is still in the prototype stage, it can reach mass commercialization once some technical and financial issues are overcome in the future.

2.5.1 Risks Encountered by the EV User

However, the uncontrolled and random charging pattern of EVs can cause reliability and security issues to the grid [44]. In addition, the comfort and utility of EV users might be compromised. Thus, to

ensure the practicability of the EV industry, it is necessary to develop proper charging/refueling navigation strategies for all EVs.

2.5.2 Risk Hedging Strategy for the EV User

In the existing literature, these strategies can be categorized into three types, i.e., station selection, routing, and energy purchasing strategies. For literature that investigated the ***station selection*** strategy of EV users, ref. [143] proposed a station selection guidance for EV users based on the virtual service range to save energy costs for EV users. Additionally, a charging priority index was formulated to evaluate the utility of EV users gained from the station selection decision. The higher the index is, the better off EV users will be. Differently, ref. [144] provided a user-oriented EV control scheme based on an efficient assignment of EVs to charging stations that could minimize the mean travel time of EVs. Moreover, ref. [79] formulated multiple evolutionary games to guide EVs to choose fast-charging stations based on the energy price that could minimize the traveling time and waiting time. However, privacy leakage of EV users might occur during the information communication process. Hence, to avoid privacy threats, ref. [145] proposed a blockchain-based efficient station selection protocol for EV users to minimize both charging time and waiting time. This protocol could facilitate EVs to select stations without sharing private information to stations.

For literature that considered the ***navigation*** strategy of EV users, ref. [146] formulated a route scheduling for EVs based on the online EV system and microwave power transfer system to maximize the total residual energy so that all EVs could arrive at their destinations. Similarly, the energy consumption of a trip was optimized in [80] via model-based strategies that considered specific EV parameters, the topology of TN, and real-time traffic conditions. For reference that aimed to minimize the traveling time when making routing decisions, ref. [147] introduced an intention-aware routing system to minimize the expected journey time of EVs. Simulation results showed that the proposed system could reduce the overall journey time by 50%. Furthermore, ref. [148] not only developed a navigation algorithm that could reduce traveling time, but energy efficiency could be achieved as well. In addition, the battery longevity of EVs could be improved.

For literature that studied the ***energy purchasing*** strategy of EV users, ref. [149] proposed a delay-optimal charging scheduling to minimize the mean waiting time of EVs at the station. Apart from minimizing waiting time, some references aimed at reducing charging bills. In [83], a real-time energy

management algorithm was proposed to reduce the charging bills of EVs and achieve peak load shaving. Similarly, in [150], an offline and online scheduling algorithm for EVs was proposed to reduce charging costs. There is literature that modeled not only the energy purchasing decisions but also the navigation decisions. For example, ref. [81] developed an intelligent vehicle-to-vehicle charging navigation strategy for traveling route selection, as well as the best charging-discharging EV pair matching. Ref. [84] also proposed an optimal routing and charging framework for EVs to increase the welfare of EVs and reduce fuel and charging costs.

2.5.3 Research Gaps

However, there are still two issues that remain unaddressed. First, most of the existing literature formulated EV decision-making strategies according to the expected utility of EVs under the assumption that EV users are rational, such as [79-81]. However, this assumption deviated from real-life decision-making due to the subjectivities of EVs. Hence, it is necessary to consider the irrationalities of EV users in formulating decision-making strategies. Second, besides normal charging/refueling navigation problems, there exists an energy substitution between electricity and hydrogen for PH2EV, which is not investigated in existing charging/refueling navigation literature [83, 84]. It is important to incorporate the impact of energy substitution in energy purchasing strategy formulation so that the balance between energy cost and energy supplement duration can be obtained by purchasing the right amount of electricity and hydrogen.

2.6 Conclusion

This chapter provides a thorough literature review relating to the risks encountered by both the energy supply side and the energy demand side in the energy wholesale market, retail market, and the energy sharing/energy storage sharing market. Moreover, the relevant risk hedging strategy, as well as the related research gaps, are logically elaborated. The summarized efforts done in the literature can help to 1) understand the fundamental concept of the energy market and risk hedging strategies for the various market participants; 2) identify potential gaps between research and practice. To sum up, this chapter forms the basis for risk hedging studies in the subsequent chapters.

3. RISK HEDGING FOR GAS POWER GENERATION CONSIDERING POWER-TO-GAS ENERGY STORAGE IN THREE DIFFERENT ELECTRICITY MARKETS

The increasing penetration of intermittent renewable energy has introduced great risks to energy systems and markets. As a result, extensive research on ESS has been undertaken to address the risks caused by renewable energy. Among different types of ESSs, the P2G storage devices are of great potential. Thus, P2G has been used in this chapter as a storage device to provide gas fuel for gas power generators. The aim of this chapter is to investigate a portfolio strategy for gas generators to earn profits and hedge risks in three different electricity markets, namely, the spot, the ancillary, and the financial markets. The presented approach is to apply energy storage and financial derivatives to hedge the market risks of gas generators, including short put option and short call option, and the option value deduction process is also involved. Simulations are carried out based on the real historical data from 2016 to 2018 in the Australian electricity markets. Three cases are presented, namely, the traditional model, the individual market case, and the proposed portfolio model. Based on the comparison of the three cases, simulation results show that the proposed portfolio model will help gas generators to earn a return of 1.0429 and hedge risks down to 0.0018. It has been found that the returns of the proposed model from 2016 to 2018 are 26.3% higher, whereas the risks are 88.1% lower on average compared with the traditional model and the individual market case.

3.1 Introduction

The emerging P2G technology has attracted significant attention. First, the energy storage costs of the P2G are relatively low compared to other energy storage devices. And it is suitable for the gas generator to use the P2G device to store energy. Second, the use of P2G can increase the flexibility and alternatives of energy. Although the model in this chapter can be applied to other types of storage devices like the battery, P2G will be the focus due to the reasons mentioned above. The operation mechanism of P2G is to convert surplus renewable energy to natural gas via electrolysis, while natural gas can be economically stored on a large scale. When needed, gas-fired power generation can be used to convert natural gas back to electricity. Therefore, P2G can be deemed a promising ESS. Meanwhile, gas power generation plays an important role in converting stored clean natural gas to electricity and will account for an increasing

share in electricity markets if more P2G is deployed. This is the reason that this chapter will focus on the risk hedging strategies for gas power generation considering its gas fuel supply coming from P2G.

The operation of gas power generators is in alignment with the current attention on reducing greenhouse gases [1]. Although the application of gas generation will facilitate renewable energy integration during an emergency due to its fast-response capability, the penetration of intermittent renewable energy will make the demand more unpredictable and hence more price volatility in electricity markets [2]. With the emerging P2G technology, gas power generation can improve its fast-response capability to store the surplus renewable energy and smooth the electricity price fluctuation [3]. Hence, it is suggested to use ESS to smooth the fluctuations in electricity prices. As a kind of energy storage device, P2G can be used in the spot, the ancillary, and the financial markets to store energy and earn profits in this chapter. The operation process of the gas generator with the P2G devices may smooth the fluctuation to some extent. However, it will still encounter high risks, and the profits will be influenced by the fluctuation of electricity prices. Thus, more comprehensive approaches are required.

In the literature, to maximize profits and hedge risks, financial derivatives were used by gas generators in [4]. These derivatives comprise forward contracts, futures, swaps, options, etc. [5]. It is common for the gas generator to use a bilateral contract or the future and forward contract to hedge risks [6]. However, they only utilize financial tools to hedge risks. As for [10], both physical and financial tools were used to hedge risks arising from the profit variation and the spot price uncertainty in bilateral markets, and the risk assessment methods are evaluated in detail. Physical tools like P2G will have a promising future due to the following two aspects of reasons. First, the energy storage costs of the P2G are relatively low compared to other energy storage devices like the battery. And it is suitable for the gas generator to use the P2G device to store energy. Second, the use of P2G can increase the flexibility and alternatives of energy [34, 88-91].

However, there are still three issues that remain unaddressed. The research gaps could be summarized in three aspects. First, the risk hedging strategy for gas generators lacks a careful consideration of the energy market and the financial market. For the energy market, the spot market and the ancillary market should be examined as well. Ref. [99] investigated the risk hedging of the hydropower plants. Model efficiency on risk hedging has been tested via simulation in the Brazilian market. However, the model only considered the spot market in the traditional power system. Similar to [99], ref. [100] proposed a

decentralized and interdependent risk hedging model that includes both the coordination optimization model and the risk-aware optimal power flow model. However, only the traditional power system modeling is considered, whereas the energy market operation analysis is lacking. Second, both financial and physical tools need to be combined with hedging risks and ensuring the profits of the gas generator. Financial tools like forward, options, and swaps are common financial derivatives to hedge risks. As for physical tools, energy storage like P2G and battery can be used to smooth the energy usage. Ref. [101] used the forward contract to hedge the risks of end-users on fuels and electricity purchasing. A forward contract has been used to determine the energy amount and price in future transactions. For [102], it utilized exotic options to hedge both the price and quantity risks of the power generator. It is an option that includes a variety of options and other financial derivatives. However, physical tools are lacking, which will limit the application of the derivatives. This is because options like short put and short call require the energy storage to make a price difference gain. In [103], mean-variance portfolio theory has been used to allocate the proportion of the energy storage into each market, whereas only physical tools are used to hedge risks. Third, budget constraints on investment have to be involved in the decision-making process. Since the budgets for investments are limited, efficient allocation of resources like financial tools and physical tools is necessary. Regarding [102], the proposed exotic option included an infinite collection of derivatives, which is unrealistic and not applicable to the real-world case. To test the model efficiency, constraints like budget limitation should be considered. Thus, proper models and theories have to be used to determine the optimal proportion of the tools. All three types of markets need to be examined to provide a more comprehensive analysis of the effectiveness of the financial and physical tool used by the gas generator. In addition, the bidding process should be considered in both the energy spot market and the ancillary market [104].

In this chapter, a hedging method relating to the options will be used, namely the short put and the short call option. However, these two options can only be implemented when there are energy storage devices because the application of energy storage will make the gas generator possible to purchase energy at a lower price and sell the energy later at a higher price, which is the operation mechanism of the two options. With the help of P2G devices, these two types of options can be implemented. Therefore, the P2G and the financial derivatives will be jointly considered in the portfolio model to hedge the risks of gas generators. We consider using the short put (sell put) and the short call (sell call) to hedge the risk

for certain periods. Because the operation mechanism of the two options is more suitable for the electricity market, it offers a channel of additional payments and a risk-smoothing tool for the original operation.

Technical terms of the financial options will be given. The term '*short'* or '*long'* is irrelevant to the time scale but simply the behavior to buy or sell an option. Options refer to the right of the option buyer to sell or to buy an asset at the exercise price on or before a specified date, whereas the seller has no right but the obligation to that deal [151]. For call options, the buyer has the right to buy the assets. On the other side, the seller of the call has no right but an obligation to that particular call option. For put options, the buyer has the right to sell the assets [151]. On the other side, the seller of the put has no right but an obligation to that particular put option. The specified date in the contract is the maturity date (or expiration date), and the specified price is called the exercise price or the strike price. In this chapter, the American options will be used so that the options can be exercised at any time up to the maturity date, whereas the European option can only be exercised at the predetermined date. To gain the right of the options, the buyer of the options should pay the premium to the seller, and the seller will receive the premium as revenues ("*a price (premium) is paid or received for purchasing or selling options"*) [151]. The main contributions of this chapter are as follows:

- First, the rigorous mathematical models of profits in three types of markets are presented, namely, the spot market, the ancillary market, and the financial market. In this model, the revenues and costs have been calculated to derive the relative investment weights among the three markets. Within the financial market, two types of options are utilized and accommodated to the operation mechanism of the gas generator. Both the financial and physical tools have to be considered to hedge the risks of the gas generator. As for the physical tools, P2G has been chosen due to its promising future application. Within both the ancillary market and the spot market, a comprehensive bidding process is also examined. Within the bidding process, the probability of succeeding in a bid is figured out via a data-driven method that enables deep learning of the previous bidding strategies.
- Second, the concept of the binomial tree has been brought up to deduct the option value. The purpose is to calculate the premium of the option in the financial markets. This is also a novelty of the chapter since no previous work on using options to hedge risks has derived the value of the options. Additionally, the DerivaGem has been introduced as a shortcut to calculate the premium,

and it is software that will shorten the calculation times for deriving option values. Moreover, the 10-step tree has been displayed to illustrate the operation of the DerivaGem.

- Third, a novel investment decision strategy among the three markets based on the portfolio model has been proposed. By considering the budget limitations of the gas generator, portfolio theory has to be applied to determine the optimal weight of the three markets and the optimal weight of short put and short call options within the financial market. By plotting the minimum variance frontier, the efficient frontier can be found [151]. Then the utility curve will be used to tangent the efficient frontier. It can serve as a reliable method for asset management for the gas generator that participates in the spot, the ancillary, and the financial market.

3.2 Framework

This chapter will involve three different markets that are interacted with each other, namely, the spot, the ancillary, and the financial markets. By the application of the mean-variance theory and utility maximization, the optimal investment weight can be determined for each market under certain budgets restriction.

Fig. 3-1 shows the proposed framework and the time axis that is used to calculate the revenues and the costs. In Fig. 3-1, n time slots are equal to one year and N periods are equal to N years. The revenues and costs every 30 minutes will be aggregated to calculate the annual revenues and the costs of the three markets. Then the annual return and risk will be calculated to derive the expected return and risks for N years. In this framework, the bidding strategy is modeled for both the spot and the ancillary markets. However, they are different. For the spot market, the bidding process will occur in both the day-ahead and real-time markets. For the ancillary market, the bidding process includes the strategy to provide upward/downward-enabled energy and capacity. As for the financial market, the short put and short call options are utilized to form a portfolio. It is the first application of the portfolio strategy. After that, the mean-variance portfolio theory will be used again to calculate the optimal weight of investment in the three markets, which is the second application of the portfolio strategy.

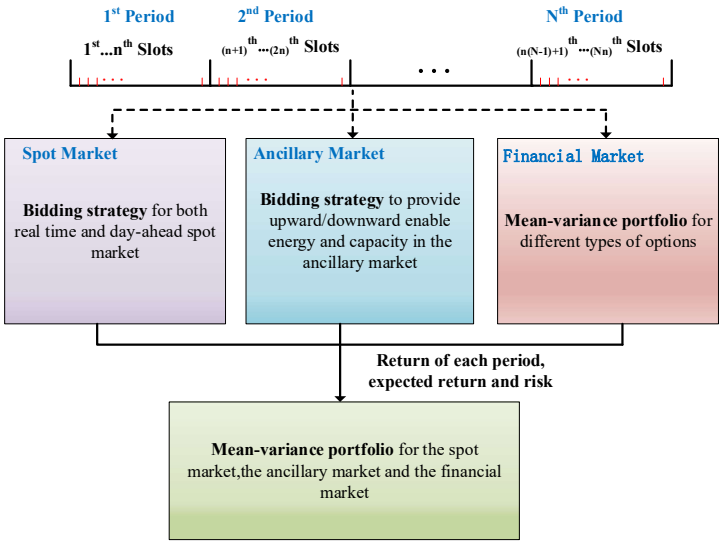

Fig. 3-1. The proposed framework of the mechanism within the three markets.

3.3 Models for Spot Market Bidding

In the spot market, the market-clearing includes both day-ahead and real-time adjustments. The day-ahead scheduling power and the real-time power adjustment will be the bidding targets. Since it is based on the historical data obtained from the ISO, a probability distribution has been used to model the day-ahead and real-time energy prices. Thus, the net profits of the gas generator in the spot market can be derived as [1]:

$$\max . NP^{S} = \sum_{t=n(T-1)+1}^{nT} R^{S}(t) - \sum_{t=n(T-1)+1}^{nT} C^{S}(t) - \sum_{t=n(T-1)+1}^{nT} C_{oper}(t) - \sum_{T=1}^{nT} C_{annual} \tag{3.1}$$

where $R^{S}(t)$, $C^{S}(t)$, $C_{oper}(t)$ and C_{annual} are the bid-to-sell revenues, bid-to-buy costs, operation costs of the P2G storage device at time *t,* and the annualized capital costs of the P2G device.

The revenues of the gas generator in the spot market include the bid-to-sell revenues earned in both the day-ahead and real-time markets. As for the costs of the gas generator, the bid-to-buy costs incurred in both the day-ahead and real-time markets should be considered. A penalty could occur when the real-time adjusted power exceeds the limitation of the tolerance level. Other costs like operational costs and annualized capital costs will be considered as well. It is assumed that the operational costs are equal to a fixed proportion of the annualized capital costs [1]. The expected revenue function containing both day-ahead and real-time can be derived as:

$$R^{S}(t) = X_{sell}(t) \times \begin{Bmatrix} \mathbb{E}\left[\lambda^{D}_{sell}(t)\, p^{D}_{sell}(t) + \lambda^{R}_{sell}(t)\, \Delta p^{R}_{sell}(t)\right] \\ -\overline{w}_{sell}(t) - \underline{w}_{sell}(t) \end{Bmatrix} \tag{3.2}$$

$$\Delta P_{sell}^{R}(t)=\begin{cases}-\Delta P_{sell}^{RD}(t), & \lambda_{sell}^{R}(t)\le\lambda_{sell}^{B}(t)\\ \Delta P_{sell}^{RI}(t), & \lambda_{sell}^{R}(t)>\lambda_{sell}^{B}(t)\end{cases} \tag{3.3}$$

$$\overline{w}_{sell}(t)=\begin{cases}\lambda_{sell}^{P}(t)\times\left(\Delta P_{sell}^{RI}(t)-\xi P_{sell}^{D}(t)\right), & \lambda_{sell}^{R}(t)>\lambda_{sell}^{B}(t)\,\&\\ & \Delta P_{sell}^{RI}(t)>\xi P_{sell}^{D}(t)\\ 0, & Otherwise\end{cases} \tag{3.4}$$

$$\underline{w}_{sell}(t)=\begin{cases}\lambda_{sell}^{P}(t)\times\left(\Delta P_{sell}^{RD}(t)-\xi P_{sell}^{D}(t)\right), & \lambda_{sell}^{R}(t)\le\lambda_{sell}^{B}(t)\,\&\\ & \Delta P_{sell}^{RD}(t)>\xi P_{sell}^{D}(t)\\ 0, & Otherwise\end{cases} \tag{3.5}$$

where $\lambda_{sell}^{D}(t)$, $\lambda_{sell}^{R}(t)$ and $\lambda_{sell}^{B}(t)$ are the day-ahead electricity price, the real-time electricity price and the adjusted bidding price to sell electricity at time *t*, respectively; $p_{sell}^{D}(t)$ and $\Delta p_{sell}^{R}(t)$ are the bid-to-sell day-ahead scheduling power and the real-time power adjustment at time *t*; In equation (3.3), $\Delta P_{sell}^{RI}(t)$ and $\Delta P_{sell}^{RD}(t)$ are the bid-to-sell real-time adjusted power either increasing or decreasing; In equation (3.2), $\overline{w}_{sell}(t)$ and $\underline{w}_{sell}(t)$ are the penalty costs for the bid-to-sell stage when the real-time adjusted power exceeds the limitation of the tolerance level (ξ is the percentage limit of day-ahead scheduling power). If the limitation level is exceeded, penalty costs will be put on the exceeded part; otherwise, there will be no penalty costs; $\lambda_{sell}^{P}(t)$ is the penalty price for the adjusted power in the bid-to-sell spot market. The expected costs involving both day-ahead and real-time can be derived as:

$$C^{S}(t)=X_{buy}(t)\times\left\{\begin{array}{l}\mathbb{E}\left[\lambda_{buy}^{D}(t)\,p_{buy}^{D}(t)+\lambda_{buy}^{R}(t)\,\Delta p_{buy}^{R}(t)\right]\\ +\overline{w}_{buy}(t)+\underline{w}_{buy}(t)\end{array}\right\} \tag{3.6}$$

$$\Delta P_{buy}^{R}(t)=\begin{cases}\Delta P_{buy}^{RI}(t), & \lambda_{buy}^{R}(t)\le\lambda_{buy}^{B}(t)\\ -\Delta P_{buy}^{RD}(t), & \lambda_{buy}^{R}(t)>\lambda_{buy}^{B}(t)\end{cases} \tag{3.7}$$

$$\overline{w}_{buy}(t)=\begin{cases}\lambda_{buy}^{P}(t)\times\left(\Delta P_{buy}^{RI}(t)-\xi P_{buy}^{D}(t)\right), & \lambda_{buy}^{R}(t)\le\lambda_{buy}^{B}(t)\,\&\\ & \Delta P_{buy}^{RI}(t)>\xi P_{buy}^{D}(t)\\ 0, & Otherwise\end{cases} \tag{3.8}$$

$$\underline{w}_{buy}(t)=\begin{cases}\lambda_{buy}^{P}(t)\times\left(\Delta P_{buy}^{RI}(t)-\xi P_{buy}^{D}(t)\right), & \lambda_{buy}^{R}(t)>\lambda_{buy}^{B}(t)\,\&\\ & \Delta P_{buy}^{RD}(t)>\xi P_{buy}^{D}(t)\\ 0, & Otherwise\end{cases} \tag{3.9}$$

where $p_{buy}^{D}(t)$ and $\Delta p_{buy}^{R}(t)$ are the bid-to-buy day-ahead scheduling power and the real-time power adjustment at time *t*; $\overline{w}_{buy}(t)$ and $\underline{w}_{buy}(t)$ are the penalty costs when the real-time adjusted power

exceeds the limitation of the tolerance level; $\Delta P_{buy}^{RI}(t)$ and $\Delta P_{buy}^{RD}(t)$ are the bid-to-buy real-time adjusted power either increasing or decreasing; $\lambda_{buy}^{B}(t)$ is the adjusted bidding price to buy electricity at time *t*; $\lambda_{buy}^{R}(t)$ is the penalty price for the adjusted power in the bid-to-buy spot market; $\lambda_{buy}^{P}(t)$ is the penalty price for the adjusted power in the bid-to-buy spot market. As for the annualized costs, it can be derived as:

$$\begin{aligned} C_{oper}(t) &= m \times \varepsilon \times IC_{P2G} \times CRF \\ &= m \times \varepsilon \times IC_{P2G} \times \frac{i(1+i)^{y}}{(1+i)^{y}-1} \\ &= m \times \varepsilon \times C_{annual} \end{aligned} \tag{3.10}$$

where m is the percentage of the maintenance costs in the spot market; ε is the half-hour discount factor; IC_{P2G} is the initial investment costs of the P2G device; *CRF* is the capital recovery factor; *i* is the effective annual rate; y is the operation life cycle of the P2G device measured in years; $IC_{P2G} \times CRF$ is the annualized investment costs.

s.t.

$$X_{sell}(t) + X_{buy}(t) \le 1 \tag{3.11}$$

$$X_{sell}(t), X_{buy}(t) \in \{0,1\} \tag{3.12}$$

$$\rho_{store}^{S}(t+1) = \rho_{store}^{S}(t) + \frac{RT_{M}}{V_{CapA} \times Mol} \times \begin{pmatrix} X_{buy}(t) \times \dfrac{\eta_{cha}\left(P_{buy}^{D}(t) + \Delta P_{buy}^{R}(t)\right)}{LHV} \times \Delta tMol \\ -X_{sell}(t) \times \dfrac{\left(P_{sell}^{D}(t) + \Delta P_{sell}^{R}(t)\right)}{\eta_{dis} \times LHV} \times \Delta tMol + Q_{P}(t) - Q_{S}(t) \end{pmatrix} \tag{3.13}$$

where $X_{sell}(t)$ and $X_{buy}(t)$ are the binomial variables representing bid-to-sell and bid-to-buy, the constraints indicate that bid-to-buy and bid-to-sell cannot coexist; $\rho_{store}^{S}(t+1)$ is the pressure of the P2G gas tank measured in *Pa* at time *t+1*; $\rho_{store}^{S}(t)$ is the pressure of the P2G gas tank in the spot market measured in *Pa* at time *t*; R is the gas constant measured in $J \bullet mol^{-1} \bullet K^{-1}$; T_M is the mean temperature inside the gas tank measured in *K*; V_{CapA} is the capacity of the gas tank measured in m^3; Mol is the molar mass of the gas measured in $kg \bullet mol^{-1}$; η_{cha} is the charging efficiency of the P2G; η_{dis} is the discharging efficiency of the P2G; LHV is the lower heat value of the gas (*MWh/kg*); Δt

is the time resolution of 30 minutes; $Q_P(t)$ is the purchased gas measured in *kg* at time *t*; $Q_S(t)$ is the sold gas measured in *kg* at time *t*.

3.4 Models for Ancillary Market Bidding

Within the ancillary market, we will mainly focus on frequency regulation. P2G will be used to participate in the upward and downward regulation bidding process. The optimization of the P2G storage capacity and the enabled energy will be the bidding targets. The purpose of the gas generator in the ancillary market is to maximize net profits. Therefore, the objective function in the ancillary market can be derived as [152]:

$$\max . NP^A = \sum_{t=n(T-1)+1}^{nT} R^A(t) - \sum_{t=n(T-1)+1}^{nT} C^A(t) - \sum_{t=n(T-1)+1}^{nT} C_{oper}(t) \tag{3.14}$$

where $R^A(t)$ and $C^A(t)$ are the revenues and costs of the secondary reserve market at time *t*.

The revenues involving both the gain on capacity and the enabled energy, and both upward and downward regulation, should be examined. To compare the revenues for the capacity and the enabled energy, the upward regulation will result in an increase in revenues for the gas generator, whereas the downward regulation will increase the revenues of the gas generator on capacity but decrease the revenues on the enabled energy. For the costs, the bid-to-buy costs and the penalty costs for the upward and downward secondary reserve-enabled energy at time *t* are considered [152]. Equations relating to the revenues are shown below:

$$R^A(t) = R^A_{CA}(t) + R^A_{EN}(t) \tag{3.15}$$

$$R^A_{CA}(t) = \lambda^{UP}_{CA}(t) \times P^{UP}_{CA}(t) + \lambda^{DW}_{CA}(t) \times P^{DW}_{CA}(t) \tag{3.16}$$

$$R^A_{EN}(t) = X_{OUT}(t) \times \left\{ \lambda^{UP}_{EN}(t) \times P^{UP}_{EN}(t) \right\} - X_{IN}(t) \times \left\{ \lambda^{DW}_{EN}(t) \times P^{DW}_{EN}(t) \right\} \tag{3.17}$$

where $R^A_{CA}(t)$ and $R^A_{EN}(t)$ are the revenues for the capacity and the enabled energy of the ancillary market; $\lambda^{UP}_{CA}(t)$ and $\lambda^{DW}_{CA}(t)$ are the prices for the upward and downward secondary reserve capacity at time *t*; $P^{UP}_{CA}(t)$ and $P^{DW}_{CA}(t)$ are the power for the upward and downward secondary reserve capacity at time *t*; $\lambda^{UP}_{EN}(t)$ and $\lambda^{DW}_{EN}(t)$ are the price for the upward and downward secondary reserve energy at time *t*; $P^{UP}_{EN}(t)$ and $P^{DW}_{EN}(t)$ are the power for the upward and downward secondary reserve

enabled energy at time *t*. The costs function, including the enabled energy and purchased energy, can be shown as follows:

$$C^{A}(t) = X_{IN}(t) \times \left\{ \lambda_{buy}^{A}(t) \times P_{buy}^{A}(t) \right\} + \beta_{EN}^{UP}(t) + \beta_{EN}^{DW}(t) \tag{3.18}$$

$$\beta_{EN}^{UP}(t) = \begin{cases} 0, & X_{OUT}(t) \bullet P_{EN}^{UP}(t) = P_{EN}^{MS,UP}(t) \\ \lambda_{UP}^{P}(t)\left(P_{EN}^{MS,UP}(t) - X_{OUT}(t) P_{EN}^{UP}(t) \right), & X_{OUT}(t) \bullet P_{EN}^{UP}(t) < P_{EN}^{MS,UP}(t) \end{cases} \tag{3.19}$$

$$\beta_{EN}^{DW}(t) = \begin{cases} 0, & X_{IN}(t) \bullet P_{EN}^{DW}(t) = P_{EN}^{MS,DW}(t) \\ \lambda_{DW}^{P}(t)\left(P_{EN}^{MS,DW}(t) - X_{IN}(t) P_{EN}^{DW}(t) \right), & X_{IN}(t) \bullet P_{EN}^{DW}(t) < P_{EN}^{MS,DW}(t) \end{cases} \tag{3.20}$$

where in equation (3.18), $\beta_{EN}^{UP}(t)$ and $\beta_{EN}^{DW}(t)$ are the penalty costs for the upward and downward secondary reserve enabled energy at time *t*. If the market signal cannot be reached in the upward or downward regulation process, penalty costs will be set on the part that equals the difference between the market signal and the actual enabled power; $\lambda_{UP}^{P}(t)$ and $\lambda_{DW}^{P}(t)$ are the penalty price for the increased and decreased power in the ancillary market; $P_{EN}^{MS,UP}(t)$ and $P_{EN}^{MS,DW}(t)$ are the market signal of energy quantity to regulate upward and downward; $\lambda_{buy}^{A}(t)$ and $P_{buy}^{A}(t)$ are the purchase price and energy at time *t*.

s.t.

$$X_{IN}(t) + X_{OUT}(t) \le 1 \tag{3.21}$$

$$X_{IN}(t), X_{OUT}(t) \in \{0,1\} \tag{3.22}$$

$$X_{OUT}(t) \bullet P_{EN}^{UP} \le P_{CA}^{UP}(t) \tag{3.23}$$

$$P_{CA}^{UP}(t) \le E_{store}^{A}(t) \tag{3.24}$$

$$X_{IN}(t) \bullet P_{EN}^{DW}(t) \le P_{CA}^{DW}(t) \tag{3.25}$$

$$P_{CA}^{DW}(t) \le E_{\max} - E_{store}^{A}(t) \tag{3.26}$$

$$0 \le E_{store}^{A}(t) \le E_{\max} \tag{3.27}$$

$$\rho_{store}^{A}(t+1) = \rho_{store}^{A}(t) + \frac{RT_M}{V_{CapA} \times Mol} \times \begin{pmatrix} X_{IN}(t) \times \dfrac{\eta_{cha}\left(P_{buy}^{A}(t) + P_{EN}^{DW}(t) \right)}{LHV} \times \Delta tMol \\ -X_{OUT}(t) \times \dfrac{\left(P_{EN}^{UP}(t) \right)}{\eta_{dis} \times LHV} \times \Delta tMol + Q_P(t) - Q_S(t) \end{pmatrix} \tag{3.28}$$

where $X_{IN}(t)$ and $X_{OUT}(t)$ are the market signals indicating whether the gas generator involves in downward regulation or upward regulation. Moreover, upward energy regulation and downward energy regulation cannot coexist; $\rho_{store}^{A}(t+1)$ is the pressure of the P2G gas tank measured in *Pa* at time *t+1*; $\rho_{store}^{A}(t)$ is the pressure of the P2G gas tank in the ancillary market measured in *Pa* at time *t*; $E_{\max}$ is the maximum energy storage capacity of the gas generator.

3.5 Models for Financial Market Option Pricing

To figure out the premium of that specific option, the option value, that is, the option price, must be calculated first. The option price includes both the intrinsic and the extrinsic value, which is the time value [151].

Option premium=intrinsic value + extrinsic value

If the option is in-the-money (ITM), the above equation satisfies. If the option is out-the-money (OTM), the intrinsic value is zero. For the call option, ITM means the spot price is higher than the strike price, whereas it is the opposite for the ITM put option.

As for OTM, it means the option cannot be exercised [151]. Here we utilize the binomial-tree method to calculate the option value [151]. It uses an iterative procedure to measure option value.

The option value calculation by using the binomial-tree method will be derived in the following sections [151]:

Theorem 1: *The delta value is the ratio of the option price change to the stock price change, and it is the amount to form a risk-free portfolio if we sell (short) one option and buy (long) delta shares.*

Proof: *First, we form a portfolio that includes* Δ *long stocks and one short call. If the share price increases, then at the maturity date, the value of the portfolio will be*:

$$S_0 \times u \times \Delta - f_u \tag{3.29}$$

If it is decreasing, the value will be:

$$S_0 \times d \times \Delta - f_d \tag{3.30}$$

where S_0 is the current share price; u is the increasing coefficient; d id the decreasing coefficient; Δ is the number of shares to be held; f_u is the related option price if the stock price increases to $S_0 \times u$; f_d is the related option price if the stock price decreases to $S_0 \times d$.

To figure out the Δ that will make the portfolio riskless, the two equations above will be equal.

$$S_0 \times u \times \Delta - f_u = S_0 \times d \times \Delta - f_d \tag{3.31}$$

Then Δ can be calculated:

$$\Delta=\frac{f_u-f_d}{S_0\times u-S_0\times d} \tag{3.32}$$

Theorem 2*: In the risk-free world, the parameter P can be treated as the probability that the stock will increase, whereas (1-P) is the probability that the stock will decrease. Thus, the value of the option can be calculated.*

Proof: If the risk-free rate is *r*, then we discount the value to the present value using the continuous discount method:

$$\left(S_0\times u\times\Delta-f_u\right)\times e^{-rT} \tag{3.33}$$

Since the original costs are:

$$S_0\times\Delta-f \tag{3.34}$$

Then let the discounted value equals the original costs:

$$\left(S_0\times u\times\Delta-f_u\right)e^{-rT}=S_0\times\Delta-f \tag{3.35}$$

So, the option value *f* can be derived as:

$$f=S_0\times\Delta\times\left(1-u\times e^{-rT}\right)+f_u\times e^{-rT} \tag{3.36}$$

Plug in equation (3.32), and we can derive:

$$f=S_0\times\left(\frac{fu-fd}{S0\times u-S0\times d}\right)\times\left(1-u\times e^{-rT}\right)+f_u\times e^{-rT} \tag{3.37}$$

$$f=\left(\frac{f_u\times\left(1-d\times e^{-rT}\right)+f_d\times\left(u\times e^{-rT}-1\right)}{u-d}\right) \tag{3.38}$$

Since the above equation is complex, we simplify it into:

$$f=e^{-rT}\times\left(f_u\times\left(\frac{e^{rT}-d}{u-d}\right)+f_d\times\left(\frac{u-e^{rT}}{u-d}\right)\right) \tag{3.39}$$

Thus, we can replace $\frac{e^{rT}-d}{u-d}$ with parameter *p* and $\frac{u-e^{rT}}{u-d}$ with (1-*p*). Therefore, we have:

$$f=e^{-rT}\times\left[p\times f_u+(1-p)\times f_d\right] \tag{3.40}$$

$$p=\frac{e^{rT}-d}{u-d} \tag{3.41}$$

Theorem 3: *The parameter u and d can be related to the volatility of the share price.*

Proof: In the real world, the required rate of return might be different from the risk-free rate *r*.

Therefore, r will be replaced by u ; We define $\sigma\sqrt{\Delta t}$ as the standard deviation of the return of a particular stock during a short period Δt .

$$p\times S_0\times u+(1-p)\times S_0\times d=S_0\times e^{\mu\Delta t}\sigma^2\times\Delta t=e^{\mu\Delta t}\times(u+d)-u\times d-e^{2\mu\Delta t} \tag{3.42}$$

$$p=\frac{e^{\mu\Delta t}-d}{u-d} \tag{3.43}$$

By using the equation $Cov=E(x)^2-\left[E(x)\right]^2$:

$$\sigma^2\times\Delta t=p\times u^2+(1-p)\times d^2-\left[p\times u+(1-p)\times d\right]^2 \tag{3.44}$$

$$\sigma^2\times\Delta t=e^{\mu\Delta t}\times(u+d)-u\times d-e^{2\mu\Delta t} \tag{3.45}$$

$$u=e^{\sigma\sqrt{\Delta t}} \tag{3.46}$$

$$d=e^{-\sigma\sqrt{\Delta t}} \tag{3.47}$$

For simplicity, the DerivaGem will be used to calculate the option value, which is the same as the binomial-tree method [153]. The diagram below displays the operation of the binomial tree by using the DerivaGem.

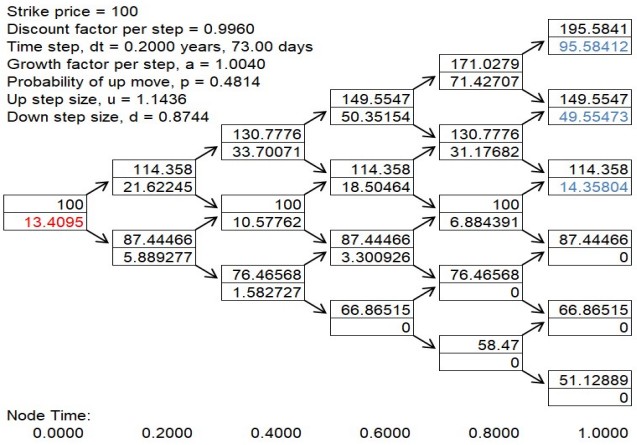

Fig. 3-2. Five-step binomial tree display

Fig. 3-2 shows an example of the operation of the binomial tree. It is similar to a random walk. The original asset has a price of 100, it will either increase by u or decrease by d in the following five steps, and each step equals approximately 0.2 years or 73 days. In the diagram, every box has two values, the upper value is the underlying asset price, and the lower value is the option price. The value in blue is a result of early exercise, whereas the value in red is the American option price at present. By using the DerivaGem tool, *p, u, d,* and the option value can be calculated automatically.

3.6 Models for Financial Market

As the penetration of renewable resources become more pervasive, the fluctuation of the demand will increase dramatically. As a result, it is more difficult to forecast the demand correctly. By merely utilizing the energy storage devices and the conventional bilateral contract between the gas generator and the energy retailer, the risks could only be hedged to a limited extent [36]. Therefore, it is necessary to encompass the financial derivatives to hedge the price risks. For the financial derivatives, the short put and short call will be used for the following two reasons. First, the gas generator will gain extra profits from the two types of options, that is, the premiums. Second, it will be more attractive to offer ownership to other participants in the energy market because whoever purchases the call or put will have the right to exercise or not to exercise. In contrast, the long call and the long put will be less attractive for the option buyers. Thus, in this chapter, the financial derivative, including the short put and short call, will be discussed, respectively. Previously, the thermal generator will also use financial derivatives, such as swaps or the future contract, but as the development of P2G is not mature, the short put and short call option will not be applicable. Since the nature of the short put and the short call require the application of the energy storage devices to store the energy and make price-difference gains. In this chapter, due to the rapid development of the energy storage devices, the short put and short call, together with the P2G devices, will be used to hedge the risks in the three markets mentioned above.

3.6.1 Short Put

For short put, the gas generator is the seller of the put options in this chapter. When the spot price is lower than the strike price, the buyer of the put will execute the options because it will make more profit at the exercise price. Therefore, the gas generator will be forced to buy electricity at a predetermined amount at the exercise price. When the market price is higher than the exercise price, no put will be executed [151]. If P2G is used, this amount of energy will be stored in the form of gas and later re-transformed into electricity when the spot price of electricity is higher than the exercise price. Fig. 3-3 will illustrate the mechanism mentioned above:

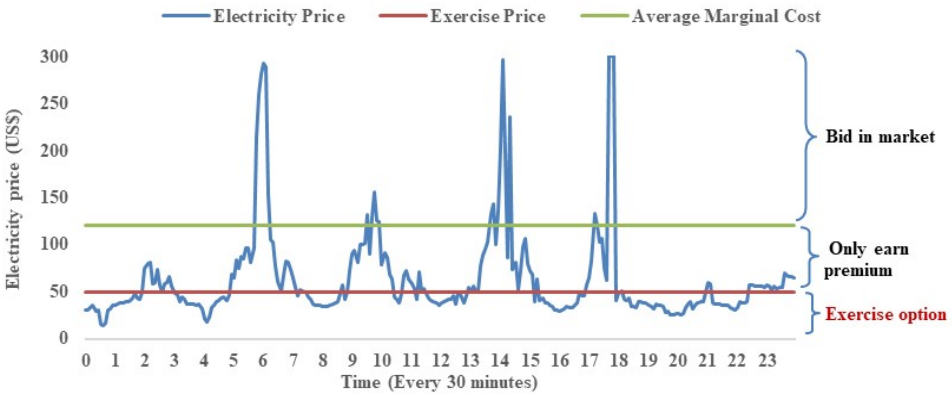

Fig. 3-3. The operation mechanism of the short put option every 30 minutes.

It is assumed that the premium has been discounted every half hour for calculation simplicity. Thus, the gas generator will always earn a premium regardless of the price change. In addition to the premium earned, the gas generator will also gain profits in the bid-to-sell stage. Although the gas generator will be forced to purchase energy at the exercise price when the spot price is lower than the exercise price, the price difference gain when the price of the sold energy is much higher than the marginal costs will ensure the profits of the gas generator when the bid-to-sell is completed [151]. The revenues and costs can be derived as:

$$\begin{cases} R_{sp}(t) = \psi_{sp} + Pr_{bid}(S) \times Pr_{hp}(S) \times S(t) \times P_{sell}^{sp}(t) \\ C_{sp}(t) = 0 \end{cases}, S(t) \geq \partial E_{sp} \tag{3.48}$$

$$\partial > 1 \tag{3.49}$$

$$\begin{cases} R_{sp}(t) = \psi_{sp} \\ C_{sp}(t) = 0 \end{cases}, E_{sp} < S(t) < \partial E_{sp} \tag{3.50}$$

$$\begin{cases} R_{sp}(t) = \psi_{sp} \\ C_{sp}(t) = E_{sp} \times P_{buy}^{sp}(t) \end{cases}, S(t) \leq E_{sp} \tag{3.51}$$

where $R_{sp}(t)$ and $C_{sp}(t)$ represent the revenues and costs for short put with P2G device at time t; $S(t)$ is the market price of the electricity; ψ_{sp} is the premium of the put option; E_{sp} is the exercise price of the short put. When the price is higher than the marginal cost, the gas generator will participate in bidding in the spot market; $Pr_{bid}(S)$ is the probability to succeed in a bid; $Pr_{hp}(S)$ is the probability of high price; $P_{buy}^{sp}(t)$ is the amount of electricity that the gas generator is forced to buy due to short put; ∂ is the coefficient determined by the gas generator, the value may be varied on the degree of risk aversion

3.6.2 Short Call

The gas generators are the seller of the call option. Different from the short put option, once the gas generator has the short call, it will receive a premium, and it will have an obligation to sell a certain amount of electricity at the exercise price when the spot price is higher than the exercise price. Thus, the gas generator will buy the electricity at a lower price in the form of gas in the bidding market and be forced to sell the stored electricity in the market if the spot price is higher than the exercise price and the option is exercised at the strike price [151]. Fig. 3-4 will illustrate the mechanism mentioned above:

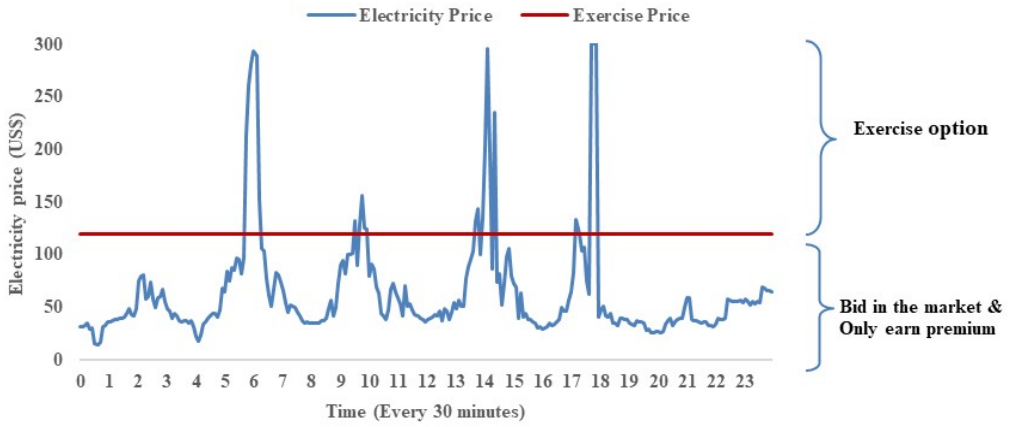

Fig. 3-4. The operation mechanism of the short call option every 30 minutes.

Similar to the operation mechanism of the short put option, besides the premium earned, the gas generator will also gain profits in the bid-to-sell stage. Although the gas generator will be forced to sell energy at the exercise price when the spot price is higher than the exercise price, the price difference gain when the costs of the sold energy are much lower than the marginal costs will ensure the profits of the gas generator when the bid-to-sell is completed [151]. The revenues and costs can be described as:

$$\begin{cases} R_{sc}(t) = \psi_{sc} + E_{sc} \times P_{sell}^{sc}(t) \\ C_{sc}(t) = 0 \end{cases}, S(t) \geq E_{sc} \tag{3.52}$$

$$\begin{cases} R_{sc}(t) = \psi_{sc} \\ C_{sc}(t) = 0 \end{cases}, \omega E_{sc} < S(t) < E_{sc} \tag{3.53}$$

$$0 \leq \omega \leq 1 \tag{3.54}$$

$$\begin{cases} R_{sc}(t) = \psi_{sc} \\ C_{sc}(t) = Pr_{bid}(S) \times Pr_{lp}(S) \times S(t) \times P_{buy}^{sc}(t) \end{cases}, S(t) \leq \omega E_{sc} \tag{3.55}$$

where $R_{sc}(t)$ and $C_{sc}(t)$ represent the revenues and costs for the short call with P2G device at time t; ψ_{sc} is the premium of the call option; E_{sc} is the exercise price of call option; $Pr_{lp}(S)$ is the

probability of low price; $P_{buy}^{sc}(t)$ is the amount of electricity that the gas generator will buy if the call option has been exercised; ω is the coefficient determined by the gas generator, the value may be varied on the degree of risk aversion.

The energy balance equation is as follows:

$$\rho_{store}^{F}(t+1)=\rho_{store}^{F}(t)+\frac{RT_M}{V_{CapA}\times Mol}\times\begin{pmatrix}\dfrac{\eta_{cha}\left(P_{buy}^{sp}(t)+P_{buy}^{sc}(t)\right)}{LHV}\times\Delta tMol\\ -\dfrac{\left(P_{sell}^{sp}(t)+P_{sell}^{sc}(t)\right)}{\eta_{dis}\times LHV}\times\Delta tMol+Q_P(t)-Q_S(t)\end{pmatrix} \tag{3.56}$$

where $\rho_{store}^{F}(t+1)$ is the pressure of the P2G gas tank measured in *Pa* at time *t+1*; $\rho_{store}^{F}(t)$ is the pressure of the P2G gas tank in the financial market measured in *Pa* at time *t*.

3.6.3 Prediction of the Probability to Succeed in a Bid

The probability of succeeding in a bid, $Pr_{bid}(S)$, is an important parameter in equations (3.48) and (3.55). It is unreasonable to assume that the gas generator can win the bid for sure. Thus, in this chapter, we consider a probabilistic model for the operation strategies of the gas generators in the financial market. The probability of succeeding in a bid is figured out through a data-driven method that enables deep learning of the previous bidding strategies. A deconvolution and convolution combination network is utilized to extract the features of the historical data shown in Fig. 3-5. The input parameter is a 48*3 matrix, which can be expressed as $\left[S(t)_{(1\to48)}, D(t)_{(1\to48)}, Temp(t)_{(1\to48)}\right]$, where $S(t)$ is the electricity price, $D(t)$ is the total demand, $Temp(t)$ is the ambient temperature. The output is a vector with two elements $\left[Pr_{bid\_succeed}, Pr_{bid\_fail},\right]^T$, where $Pr_{bid\_succeed}$ is the predicted probability of succeeding in a bid and Pr_{bid_fail} is the predicted failed bidding probability [154]. The cross-entropy is used as the loss function. To obtain the output, the input matrix will pass through the proposed network, and the layer information of the proposed network is shown in Table 3-1.

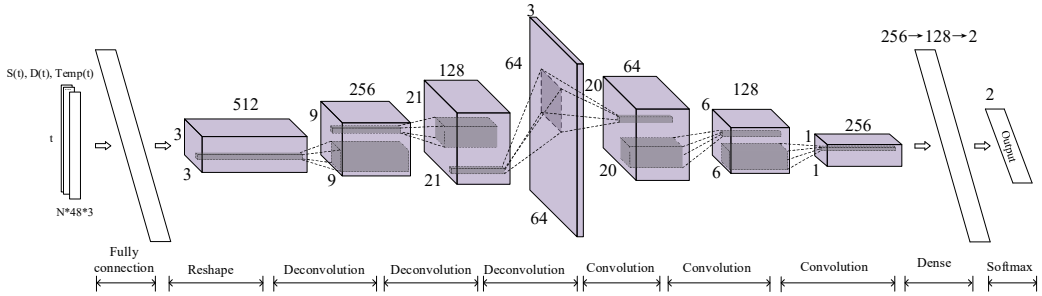

Fig. 3-5. Proposed combined deconvolution architecture

TABLE 3-1. LAYER CONFIGURATION OF THE PROPOSED ARCHITECTURE.

Layer Index	Layer	Parameter	Layer Index	Layer	Parameter
1	Input	48*3	7	Convolution	5*5*3, 128, ReLu
2	Dense	512, Linear	8	Convolution	5*5*3, 256, ReLu
3	Deconvolution	3*3*3,256, ReLu	9	Dense	256, Linear
4	Deconvolution	5*5*2,128, ReLu	10	Dense	128, Linear
5	Deconvolution	4*4*3,3, ReLu	11	Dense	2, Linear
6	Convolution	5*5*3,64, ReLu	12	Output	Softmax

The input data will first pass a dense layer to increase the number of features to 512. Then the data will pass three deconvolution layers with filters 3*3*3, 5*5*2 and 4*4*3 respectively and followed by three convolution layers to increase the number of feature maps to 256 with filters 5*5*3. The procedure can be described as:

$$\mathbf{y}_j^l = f\left(\sum_{i \in M_j} \mathbf{x}_i^{l-1} \otimes \mathbf{k}_{ij}^l + b_j^l\right) \tag{3.57}$$

where $\mathbf{y}_j^l$ is the output of the j^{th} map in l^{th} layer; $\mathbf{x}_i^{l-1}$ is the input of the i^{th} map in layer l-1; M_j is the set of the input maps; $\otimes$ denotes the convolutional operation; $\mathbf{k}_{ij}^l$ represents the weight of the filter of the corresponding convolutional layer and b_j^l is the bias respectively.

The ReLu function is utilized as an activation function, shown as:

$$ReLU\left(x\right) = \max\left(0, x\right) \tag{3.58}$$

After the convolution layer, the extracted features will pass through three dense layers to reduce the number of features gradually. At the output layer, SoftMax, shown as equation (3.59), is applied to project the output value to (0,1) and guarantee that the summation of the output equals 1, which can represent probability.

$$Softmax(i) = \frac{e^i}{\sum_j e^j} \tag{3.59}$$

where $Softmax(i)$ is the SoftMax value of i^{th} output, and j represents the index of the output.

3.7 The Return, Expected Return, and the Variance of the Three Markets

Then the return of the P2G devices in the spot, ancillary, and the financial market at time t can be derived as:

$$r^{mt}(T)=\frac{\sum_{t=n(T-1)+1}^{nT}R^{mt}(t)-\sum_{t=n(T-1)+1}^{nT}C^{mt}(t)-\sum_{t=n(T-1)+1}^{nT}C_{oper}(t)-\sum_{T=1}^{nT}C_{annual}}{\sum_{t=n(T-1)+1}^{nT}C^{mt}(t)+\sum_{t=n(T-1)+1}^{nT}C_{oper}(t)} \tag{3.60}$$

where $r^{mt}(T)$ is the rate of return at the T^{th} period. The revenue and costs are aggregated by n time slots to calculate $r^{mt}(T)$.

Then the average return and risk for N periods can be deducted as:

$$\mathbb{E}\left(r^{mt}(T)\right)=\left[\prod_{T=1,mt\in(S,A,sp,sc)}^{N}\left(1+r^{mt}(T)\right)\right]^{1/N}-1 \tag{3.61}$$

$$\sigma\left(r^{mt}(T)\right)^2=\frac{\sum_{T=1,mt\in(S,A,sp,sc)}^{N}\left[r^{mt}(T)-\mathbb{E}\left(r^{mt}(T)\right)\right]^2}{N} \tag{3.62}$$

where $\mathbb{E}\left(r^{mt}(T)\right)$ is the average rate of return for total N periods; $\sigma\left(r^{mt}(T)\right)^2$ is the variance of the rate of return. By using the geometric average [155], $\mathbb{E}\left(r^{mt}(T)\right)$ for N periods is calculated in equation (3.61). Then $\sigma\left(r^{mt}(T)\right)^2$ is utilized to measure the risk in equation (3.62); *mt* means market types, namely, the spot market, the ancillary market, and the financial market, which includes the short put market and short call market

3.8 Mean-variance Portfolio Theory Application on the Two Options

According to the definition of the market portfolio in [156]. it is a set of assets including both risky and risk-free assets to either maximize the return or minimize the risk. Therefore, by applying this concept to the electricity market, the optimal portfolio can be found by maximizing the utility, which is shown in equation (3.63).

$$Max.U=\mathbb{E}\left(r_{sp\ \&\ sc}(T)\right)-\frac{1}{2}A\sigma\left(r_{sp\ \&\ sc}(T)\right)^2 \tag{3.63}$$

s.t.

$$\mathbb{E}\left(r^{F}(T)\right)=\mathbb{E}\left(r_{sp\ \&\ sc}(T)\right)=W_{sp}\times\mathbb{E}\left(r_{sp}(T)\right)+W_{sc}\times\mathbb{E}\left(r_{sc}(T)\right)\geq E_{MP} \tag{3.64}$$

where U is the utility function [157], the level of risk aversion will be chosen according to the utility theory in [158]. A is the risk aversion coefficient for the gas generator. We can attribute numbers 1 to 5 for A that represent different levels of risk aversion. The larger the number is, the more risk-averse the investor is. It is positive in this chapter because most investors are risk-averse, which means the gas generator is also risk-averse. In [158], the risk aversion function might change. If it is negative, the

investor is risk-loving, which means he or she prefers risks. If A equals zero, the investor is risk-neutral, which indicates that the utility of the investor will not change with the level of risk aversion index.

$$\begin{aligned}\sigma\left(r^{F}(T)\right)^{2} &= \sigma\left(r_{sp\ \&\ sc}(T)\right)^{2} \\ &= W_{sp}{}^{2}\times\sigma\left(r_{sp}(T)\right)^{2}+W_{sc}{}^{2}\times\sigma\left(r_{sc}(T)\right)^{2}+ \\ &\quad \sum_{i,j\in(sp,sc)} 2\times W_{i}\times W_{j}\times\rho_{i,j}\times\sigma\left(r_{i}(T)\right)\times\sigma\left(r_{j}(T)\right), \\ &\forall i,j\in\Omega_{options},i\neq j\end{aligned} \tag{3.65}$$

$$\rho_{i,j}=\frac{COV_{i,j}}{\sigma\left(r_{i}(T)\right)\times\sigma\left(r_{j}(T)\right)},\forall i,j\in\Omega_{options},i\neq j \tag{3.66}$$

$$COV_{i,j}=\sum_{T=1}^{N}\left(r_{i}(T)\times r_{j}(T)\right)\Big/N-\mathbb{E}\left(r_{i}(T)\right)\times\mathbb{E}\left(r_{j}(T)\right),\quad \forall i,j\in\Omega_{options},i\neq j \tag{3.67}$$

$$\Omega_{options}=\{sp,sc\} \tag{3.68}$$

$$W_{sp}+W_{sc}=1 \tag{3.69}$$

$$0\leq W_{sp}\leq 1 \tag{3.70}$$

$$0\leq W_{sc}\leq 1 \tag{3.71}$$

where $\mathbb{E}\left(r_{sp\ \&\ sc}(T)\right)$ is the average rate of return of short put and short call for total time slots N; $\sigma\left(r_{sp\ \&\ sc}(T)\right)^{2}$ is the variance of the short put and short call for total time slots N; $\sigma\left(r_{i}(T)\right)$ and $\sigma\left(r_{j}(T)\right)$ are the standard deviations of the option i and j, where $i\neq j$, i and j $\in$ $\Omega_{options}$ (sets of options), namely, short put and short call; $\rho_{i,j}$ and $COV_{i,j}$ are the correlation coefficient and the covariance for short put and short call [159]; W_{sp} and W_{sc} are the weights of investment on short put and short call; E_{MP} is the target return.

3.9 Mean-variance Portfolio Theory Application on the Three Markets

After the determination of the optimal portfolio weights of the two options, we use the determined weight to calculate the return, average return, and risk of the portfolio containing the two options. Then the mean-variance portfolio theory will be used again to calculate the optimal investment weights for the three markets, namely, the spot market, the ancillary market, and the financial market.

$$Max.U=\mathbb{E}\left(r^{S,A\&F}(T)\right)-\frac{1}{2}A\sigma\left(r^{S,A\&F}(T)\right)^{2} \tag{3.72}$$

s.t.

$$\mathbb{E}\left(r^{S,A\&F}(T)\right)=W_{S}\times\mathbb{E}\left(r^{S}(T)\right)+W_{A}\times\mathbb{E}\left(r^{A}(T)\right)+W_{F}\times\mathbb{E}\left(r^{F}(T)\right)\geq E_{MP} \tag{3.73}$$

$$\begin{aligned}\sigma\left(r^{S,A\&F}(T)\right)^{2} &= W_{S}{}^{2}\times\sigma\left(r^{S}(T)\right)^{2}+W_{A}{}^{2}\times\sigma\left(r^{A}(T)\right)^{2}+W_{F}{}^{2}\times\sigma\left(r^{F}(T)\right)^{2} \\ &\quad +\sum_{p,q\in(S,A\&F)}\left[2\times W_{p}\times W_{q}\times\rho_{p,q}\times\sigma\left(r_{p}(T)\right)\times\sigma\left(r_{q}(T)\right)\right]\end{aligned} \tag{3.74}$$

$$\rho_{p,q}=\frac{COV_{p,q}}{\sigma\left(r_p(T)\right)\times\sigma\left(r_q(T)\right)},\quad \forall p,q\in\Omega_{markets,\,p\neq q} \tag{3.75}$$

$$COV_{p,q}=\sum_{T=1}^{N}\left(r_p(T)\times r_q(T)\right)\Big/N-\mathbb{E}\left(r_p(T)\right)\times\mathbb{E}\left(r_q(T)\right),\quad \forall p,q\in\Omega_{markets,\,p\neq q} \tag{3.76}$$

$$\Omega_{markets}=\left\{S,A,F\right\} \tag{3.77}$$

$$W_S+W_A+W_F=1 \tag{3.78}$$

$$0\le W_S\le 1 \tag{3.79}$$

$$0\le W_A\le 1 \tag{3.80}$$

$$0\le W_F\le 1 \tag{3.81}$$

where $\mathbb{E}\left(r^{S,A\&F}(T)\right)$ is the average rate of return of spot, ancillary and financial markets for total time slots N; $\sigma\left(r^{S,A\&F}(T)\right)^2$ is the variance of spot, ancillary and financial markets for total time slots N; $\sigma\left(r_p(T)\right)$ and $\sigma\left(r_q(T)\right)$ are the standard deviation of the option p and q, where $p\neq q$, p and q $\in$ $\Omega_{markets}$ (sets of markets), namely, the spot, the ancillary and the financial market; $\rho_{p,q}$ and $COV_{p,q}$ are the correlation coefficient and the covariance for the three markets [159]; W_S , W_A , and W_F are the weights of investment on the three markets

3.10 Case Study

3.10.1 Parameter Setting

TABLE 3-2. PARAMETER VALUES RELATED TO THE OPTIONS WITHIN THE CHAPTER

Parameters	Value	Parameters	Value
A	1~5	ψ_{sp}	3.85US$
E_{MP}	15%~20%	ψ_{sc}	9.23US$
E_{sp}	38.46US$	∂	$\in(1,\infty)$
E_{sc}	92.31US$	ω	$\in(0,1)$

TABLE 3-3. PARAMETER VALUES RELATED TO THE P2G WITHIN THE CHAPTER

Parameters	Value	Parameters	Value
C_{annual}	1,114,615US$	T_M	-213.15~-183.15K
IC_{P2G}	16,719,231US$	y	15 years
R	$8.3145 J\bullet mol^{-1}\bullet K^{-1}$	η_{P2G}^{ch}, η_{P2G}^{dis}	70%~80%

In Table 3-2, the parameters relating to the options are explained. These parameters include the risk-aversion index, the premium value, and the exercise prices of both types of options, etc.

For Table 3-3, the parameters of P2G are given. These parameters include the annualized capital costs of the P2G, the gas constant measured in $J \bullet mol^{-1} \bullet K^{-1}$, the mean temperature inside the gas tank measured in K, the life cycle of the P2G device, and the charging/discharging efficiency of the P2G device.

3.10.2 Input Data Analysis

In this chapter, the data relating to electricity prices every 30 minutes from 2016 to 2018 are obtained from the AEMO [160]. The common currency unit of US$ will be used in this chapter with the exchange rate of 1.3 AU$ to 1 US$ on 25th January 2021. The electricity price distributions for the spot market and the market signal for both upward/downward regulation of the ancillary market are shown in Figs. 3-6 and 3-7. In Fig. 3-6, the historical data of the spot market price is shown in a frequency histogram. Via the estimated density, it can be found that the distribution has a mean electricity price of 78.9 US$/MWh. A general overview of the simulated input data can be gained via the histogram. For Fig. 3-7, the market signal to regulate upward or downward will be presented. It has been found that the upward regulation has a mean volume of 127.6 MW, which is higher than that of the downward regulation (106.8 MW). Moreover, the electricity price range for the upward regulation lies mostly from about 15.4 US$/MWh to 53.8 US$/MWh, whereas for the downward regulation, most of the dots range from about 11.5 US$/MWh to 34.6US$/MWh.

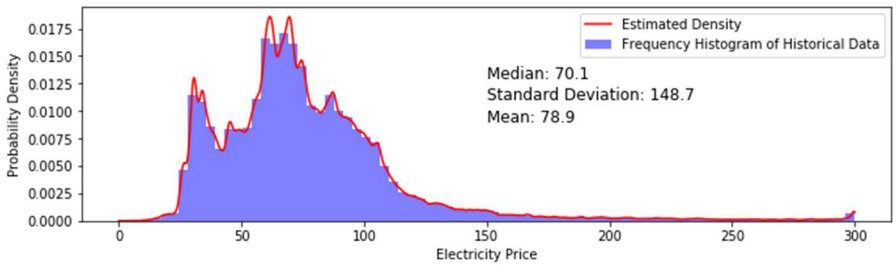

Fig. 3-6. Distribution of the electricity price in the spot market from 2016 to 2018

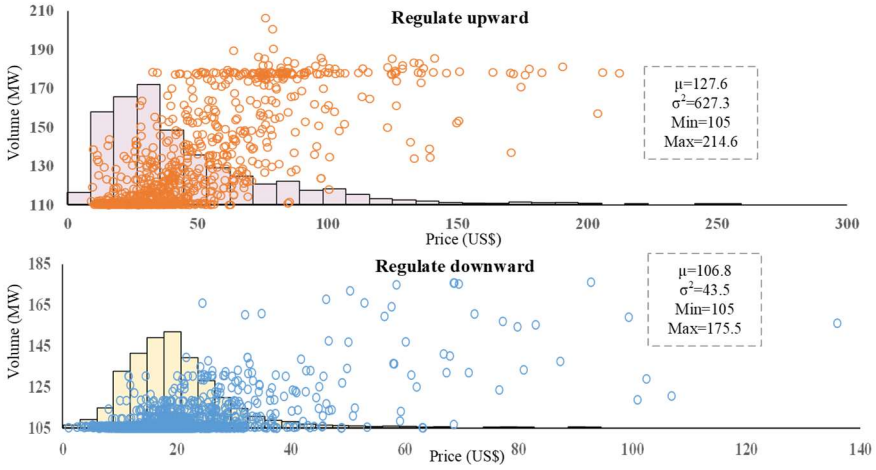

Fig. 3-7. Scatter plots and histograms of the amount of energy that is regulated upward/downward in the ancillary market.

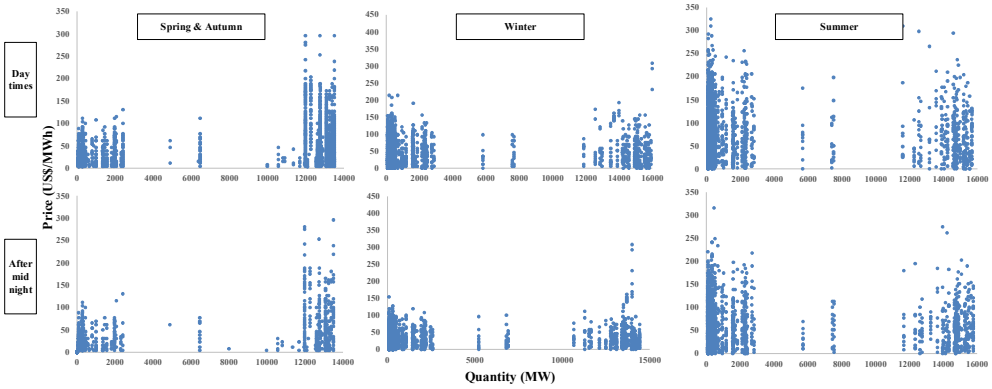

Fig. 3-8. Scatter plots of bidding price and related quantity with different time horizons.

Fig. 3-8 illustrates the scatter plots of the bidding price and the related quantity of bidding for all three years. The time horizon has been divided into three parts, i.e., spring and autumn, winter, and summer. Within each part, the daytime bidding process and after midnight bidding process have been compared. It can be found that the gas generator will bid a larger amount at a high price to sell the energy during summer times compared with the other seasons. And the amount of bidding will be the least for the gas generator in spring and autumn. Additionally, within each season, the bidding process of the daytime and the after-midnight period have been compared. It indicates that although the price will not change, the amount of bidding processes is much more in the daytime. In other words, the bidding process is more active in the daytime. In contrast, the bidding process is less active at the night-time, which is in accordance with the normal operation time of the gas generator.

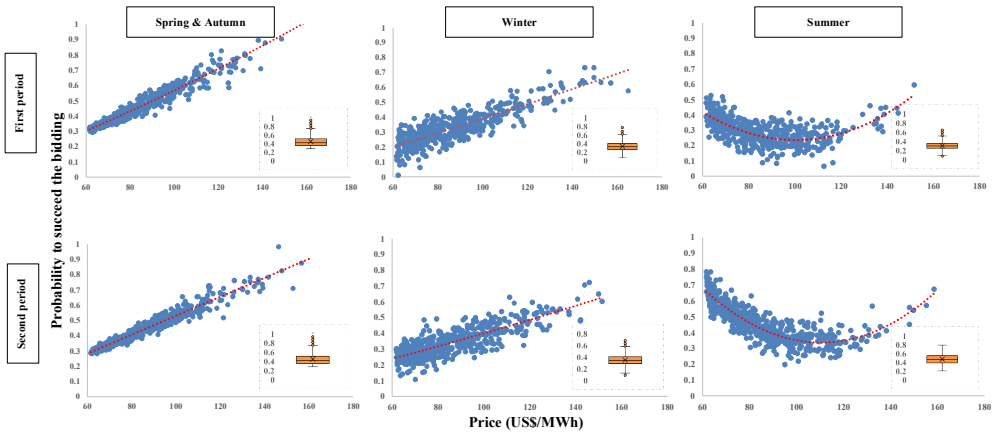

Fig. 3-9. Scatter plots of the predicted probability of succeeding in the bidding with different time horizons.

Fig. 3-9 shows the scatter plots of the predicted probability to succeed the bidding at different seasons of the three years or different periods but within the same season. The probability of succeeding in a bid is figured out via a data-driven method that enables deep learning of the previous bidding strategies. In the figure, it can be found that as the electricity bidding price increases within a reasonable range, the probability of succeeding the bid will increase as well, which is applicable to each season. However, the medium is different, as shown by the boxplot. A Box plot is presented to show the distribution situation of the probability of success in the bidding. The medium of distribution in spring and autumn is approximately 0.6, about 0.5 for winter, and it is around 0.4 for summer. This could be explained by the risk-return theory, i.e., the higher return, the higher risk. In other words, although the probability of succeeding in the bidding in summer and winter is higher than that of other seasons, the fluctuation of the probability distribution is also more volatile.

3.10.3 Numerical Analysis of the Profits and Costs of the Three Markets

A numerical analysis is carried out. The profits and costs of the three markets have been calculated and compared. Additionally, the energy storage state of charge condition has been analyzed under the three different markets. In this section, Table 3-4 compared the returns and variance of the three cases, namely, the traditional model, the individual market case, and the proposed model.

Fig. 3-10 illustrates the operation process of the spot market, including both the day-ahead and real-time buy/sell mechanism. The real-time purchasing quantity will change with the relative relationship between the real-time electricity price and the day-ahead bidding price. When the electricity prices are low, both the day-ahead purchase and the real-time purchase amount will increase, while the selling quantity of both day-ahead and real-time will increase when the electricity price is high. In addition, the

energy storage represented by the yellow area will increase when the gas generator is purchasing energy while decreasing when selling energy. The results are in alignment with the operation mechanism of the gas generator, with which the price difference gain can be made.

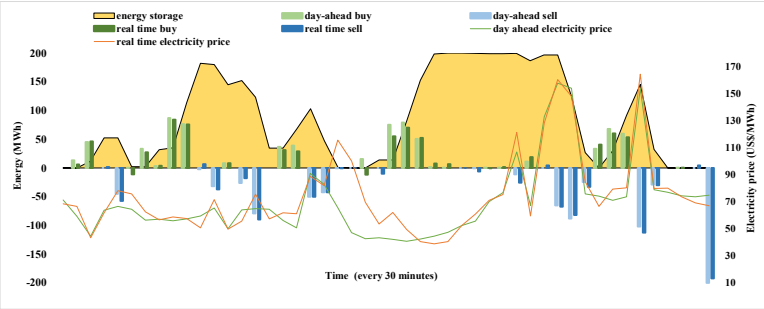

Fig. 3-10 Revenues and costs of the spot market every 30 minutes

Fig. 3-11 illustrates the revenues and costs of the ancillary market. The orange and dark blue colors represent revenues of upward regulation of the enabled energy (Renup) and the costs of downward regulation of the enabled energy (Cendw), respectively. The dark green bars represent the revenues of upward regulation of the capacity (Rcaup) and the light green bars are the revenues of downward regulation of the capacity (Rcadw). Cbuy is the purchasing costs in the ancillary market. The movements of the Renup and Cendw are following the change of the market signal measured in the grey dash line. It can be found that the market signal will only affect the enabled energy, not the capacity. Moreover, after every upward regulation, the storage of P2G will decrease, whereas the storage would increase if the downward regulation occurred, which could be approved by the yellow areas representing the storage state.

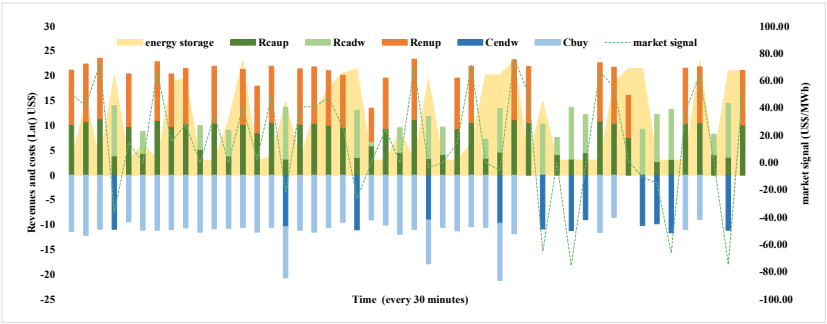

Fig. 3-11. Revenues and costs of the ancillary market every 30 minutes

Fig. 3-12 shows the net profits of short put for every 30 minutes measured in green color. When the price is lower than the exercise price, the option will be exercised by the put owner, and the gas generator will be forced to purchase the energy at the exercise price, and the energy storage represented by the yellow area will increase, which means the gas generator will store the purchased energy into the P2G

device; when the price is in between the exercise price and the high price threshold, the gas generator will merely earn the premiums; when the price is higher than the high price threshold, the gas generator will bid and sell the energy. Once the bid is successful, the energy will be sold. Thus, the energy storage will decrease, and the price difference gain will be made. Although there are negative profits, the overall average profits are positive.

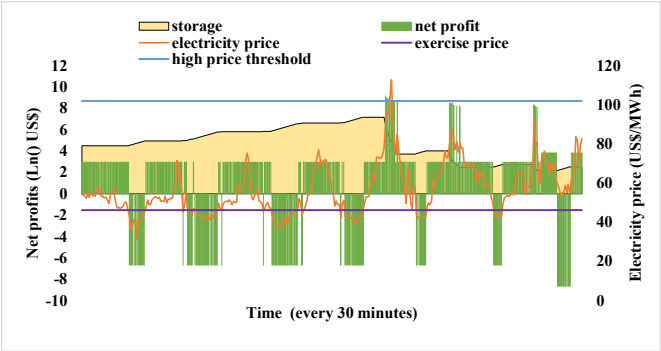

Fig. 3-12 Net profits of short put every 30 minutes.

Fig. 3-13 shows the net profits of short call for every 30 minutes measured in green color. The net profits, including both the premium and the gain from selling the electricity. When the price is lower than the low price cap, the gas generator will bid to purchase electricity from the spot market and store that energy in the P2G device; when the price is higher than the low price cap but lower than the exercise price, the gas generator will merely earn premiums; when the price is higher than the strike price, the stored energy will be compulsorily sold to the call owner at the exercise price which is lower than the spot price. Worth noticing, that the exercise price of the short call will be much higher than the exercise price of the short put option because the call option buyer will only be attracted when the option can be used to hedge the high purchasing costs when the electricity price is high. Additionally, the exercise price will be slightly lower than the electricity price when the price is high for the short call, and slightly higher than the electricity price when the price is low for the short put.

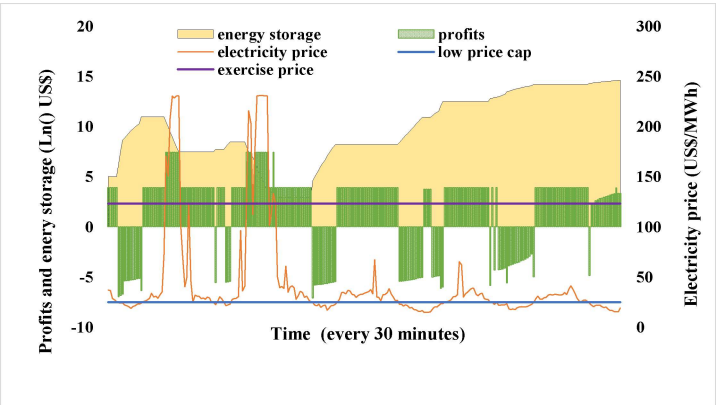

Fig. 3-13. Net profits of short call every 30 minutes.

Table 3-4 shows the returns, the expected returns, and risks in 2016, 2017, and 2018. Consider the short put, it has the largest return for all three years compared to the short call. Although the short call has the smallest return for three years, the short call has the smallest variance, which means it has the least risk. To compare the three markets, the optimal weight of the two types of options has to be determined. After the simulation, it has been found that the optimal weight of the portfolio for short put and short call, which is subject to utility maximization, is 27.6% and 72.4%. Then plugging those weights, we obtain the expected return and risk for the portfolio of the two types of options, which are 1.0433 and 0.0042, respectively. After the portfolio of the three markets, it can be calculated that the expected return is 1.0429, and the variance is 0.0018. Although the return has reduced slightly, the benefits outweighed, as the risk has decreased significantly. It has been found that the returns of the proposed model from 2016 to 2018 are 26.3% higher, whereas the risks are 88.1% lower on average compared with the traditional model and the individual market case.

TABLE 3-4. SIMULATION RESULTS OF RETURNS AND RISKS FOR THREE YEARS (RETURN=NET PROFITS/COSTS).

		Traditional model	**Financial market**			**Spot market**	**Ancillary market**
			Short put	Short call	Portfolio		
2016	Return	0.6157	1.3388	0.8075	0.9541	1.298	0.9404
2017	Return	0.8148	1.8987	0.7986	1.1022	0.8188	0.9086
2018	Return	0.7943	1.9465	0.7451	1.0767	0.9823	0.8039
Expected return		0.7416	1.7133	0.7835	1.0433	1.0235	0.8834
Variance		0.0079	0.0763	0.0008	0.0042	0.0397	0.0034

3.10.4 Case Analysis of Risk Aversion Index

The case analysis on different risk aversion indexes has been conducted to offer optimal investment alternatives in different markets and different types of options when the level of risk aversion of the investor varies. It has been found that the more risk-averse the investor is, the more likely the ancillary market will be invested. By comparison, less investment will occur in the spot market.

In Fig. 3-14, the proportion of short put and short call according to different risk aversion index will be illustrated in the mean-variance diagram. The blue dots on the red line is the efficient portfolios, and the red line is the efficient frontier. To find the optimal portfolio, the utility curve has been drawn to tangent the efficient frontier. According to the degree of risk aversion (1-4), four utility curves have been drawn to provide more alternatives for the investors [158]. From purple to brown, brown to orange, and

orange to the green line, the investor becomes more risk-averse. The four utility curves are related to A (the degree of risk aversion), ranging from 1 to 4 [158]. The tangent points are the optimal portfolio weight of each type of option to invest. It can be found that the more risk-averse the investor is, the less expected return will be pursued. As most people are risk-averse, more dots will locate on the lower left side of the graph.

In Fig. 3-15, green, orange, and blue colors represent the spot, the ancillary, and the financial market, respectively. Within the financial market, grey and yellow refer to short call and short put. A is the degree of risk aversion. From 1 to 4, the investor becomes more risk averse [158]. Since the variance is 0.0397 for the spot market, which is the highest among the other markets when the risks increase, the more risk-averse the investor is, the less likely the investor will invest in the spot market. In other words, the more risk-averse the investor is, the more likely the ancillary market will be invested because it has the lowest standard deviation referring to Table 3-4. Additionally, within the financial market, the short call option is more preferred than the short put option. This might be due to the reason that most investors are risk-averse, the short call option will have a variance of merely 0.0008 in this chapter. The optimal portfolio is varied when the levels of risk aversion are different.

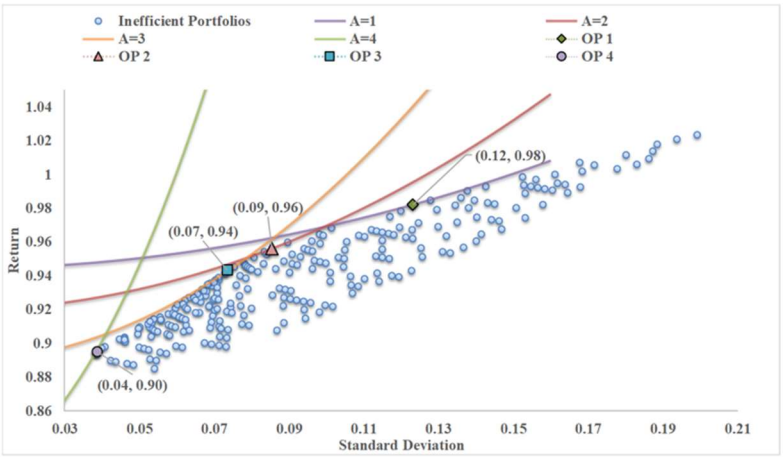

Fig. 3-14. Mean-variance diagram relating to the optimal weight of short put and short call with changes of risk aversion index

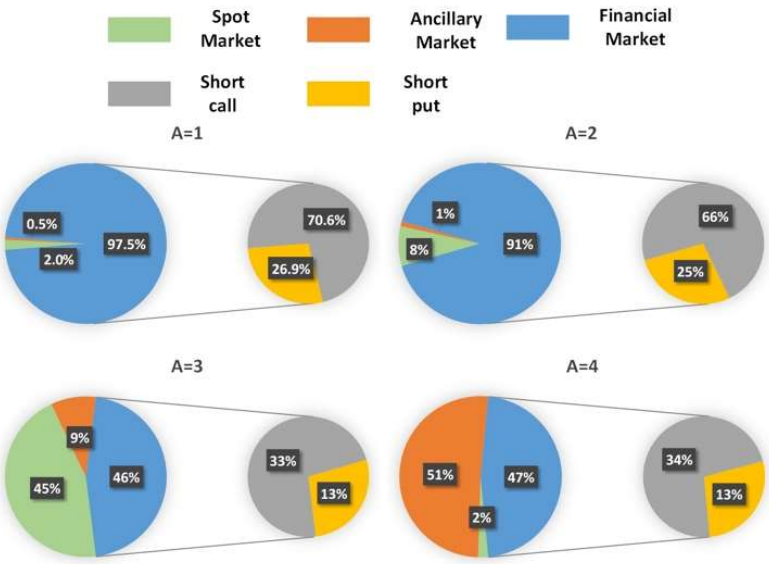

Fig. 3-15. Optimal portfolio weight among the three types of markets with changes in risk aversion index

3.11 Conclusion

In this chapter, first, the conventional operation mechanism of gas generators in the spot and ancillary market has been discussed. Then the binomial model was used to deduct the value of the American option. Next, the short put and short call have been evaluated in the financial market. Lastly, the mean-variance portfolio theory has been utilized to figure out the optimal weight of the three types of markets. According to the simulation results, the optimal portfolio will vary if the investor has different degrees of risk aversion. The main finding of this chapter is that the more risk-averse the investor is more likely to invest in the ancillary market. By comparison, less investment will occur in the spot market. After comparing the results of the individual market and the portfolio, it can be found that the utilization of financial derivatives and mean-variance portfolio theory can facilitate the gas generators to earn more profits and hedge risks in electricity markets compared with the traditional operation mechanism. The proposed option-based risk-hedging mechanism is transferable because it can be applied to other market participants, such as energy retailers and prosumers, etc. In the future, several inviting research areas are worth examining, including the effectiveness of different option combinations to reduce profits variation and the effective profits allocation or the cost assignment on a coalition of market participants.

4. RISK HEDGING STRATEGY FOR ELECTRICITY RETAILERS USING INSURANCE AND STRANGLE WEATHER DERIVATIVES

With the increase in extreme weather events and the penetration of distributed energy resources, electricity retailers will encounter more risks at both transmission and distribution levels during the business operation process. For risks at the transmission level, huge damages to the transmission lines and towers caused by extreme events, like bushfires, ice storms, and flooding, will lead to power shortages. For risks at the distribution level, demand variations in accordance with temperature change will result in energy procurement difficulty for the retailers. In this chapter, besides the normal bilateral contract, the insurance, the strangle weather derivatives, and the energy storage system are implemented to hedge the risks at both the transmission and distribution levels. Simulation results show that the proposed model ensures higher profits for the retailers in summer and winter compared to the conventional model when there are no extreme events occurring. When there are extreme events in both summer and winter, the proposed model incurs a lower reduction in profits than that of the conventional model. In brief, the overall profits of the retailer using the proposed hedging model are higher than the conventional model, and the overall profit variation of the conventional model is about 26% higher than the proposed model. Furthermore, when the budget of the retailer is sufficient, all three hedging tools can be invested. Whereas when the budget of the retailer is limited, the investment order should be insurance the first, strangle weather derivatives the second, and energy storage system the third.

4.1 Introduction

With the penetration of DERs, greenhouse gas emission has been substantially reduced [35]. However, the incorporation of DERs will lead to a large-scale demand fluctuation. As a result, an imbalance of demand and supply might occur [36]. The risks of demand fluctuation caused by the penetration of DERs normally happen at the distribution level. Although this type of risk will not cause tremendous losses for the electricity retailer, it happens more frequently. Normally, to hedge this type of risk, retailers can first sign bilateral contracts with generation companies (GENCOs) to stabilize the electricity prices and cover majority of the estimated demand [37]. Then, when overconsumption occurs, the retailer will compensate for the demand gap from the spot market at the real-time electricity price [36]. Furthermore, the increase of EEs caused by climate change will further augment the demand-supply imbalance. EEs like bushfires and ice storms can lead to huge damage to power transmission lines and towers, which will make the

retailers unable to satisfy the demand requirements [36, 38]. The risks caused by EEs normally occur at the transmission level. Although the occurrence of this type of risk is rare, the damages are tremendous. Studies on the risk hedging strategy of this type of risk from the perspective of energy retailers are lacking. It can be found that energy retailers incur risks at both the transmission and distribution levels. Therefore, more appropriate risk hedging strategies should be developed for retailers to hedge both types of risks. Additionally, the impact of DERs and EEs should be incorporated as well.

In the literature, risk hedging strategies relating to both the *transmission level* and the *distribution level* are discussed. For the *risks of the transmission level*, most of the existing literature hedged the risks from the perspectives of the system planner, the power generators, and the electricity retailers [105-107]. However, references that focus on the transmission risk-hedging strategy from the perspective of the retailer are rare. For the *risks of the distribution level*, most of the existing literature hedged the risks from the perspective of the end-users and electricity retailers [109-112].

However, there are still four aspects of issues that remain unaddressed by the existing literature. First, the current risk-hedging strategy for the retailer is incomplete. First, most of the references studied the risk-hedging strategies for retailers at the distribution level to mitigate demand fluctuation, such as [112, 113]. With the penetration of weather-related EEs, the supply shortage risks caused by the EEs at the transmission level is happening, which can cause huge losses to the retailer. However, references are lacking on risk-hedging strategies toward the risks caused by the EEs at the transmission level. To fully consider both supply shortage and demand fluctuation risks, more comprehensive risk-hedging strategies are needed for the retailer. Second, since the EEs are of extremely low probability but tremendous damages, the total loss value predicted would be smaller, such as [117]. As a result, the retailer would pay a smaller amount of insurance premium to cover the total loss value predicted. However, a lower amount of insurance premium would lead to a higher amount of insurance excess. Consequently, the retailer was unable to claim monetary compensation back even when there were damages caused by the EEs. To enhance the hedging effectiveness of the insurance, a proper risk valuation method must be developed to incorporate the risk preference of the retailer and facilitate the retailer to predict the total loss value and pay the right amount of insurance premium for the right insurance contract. Third, the existing risk-hedging methods rely heavily on the prediction of the electricity price, such as [36, 37, 118]. As a result, when the predictions of the electricity price are inaccurate, the effectiveness of the hedging

tools is compromised. Hence, a more price-irrelevant financial tool is needed to reduce the reliance of the retailer on the prediction of the price level. Fourth, the retailer has a limited capital investment for risk-hedging strategies in real practice. However, the existing literature failed to consider the investment budget constraints of the retailer, such as [108, 112, 113], neglect of which will lead to impractical hedging tool portfolio decisions. Thus, it is necessary to incorporate the influence of budget restrictions.

Hence, we proposed a novel management strategy to hedge the risks of electricity retailers at both transmission and distribution levels and to ensure a positive income for the retailers. The main contributions of this chapter are as follows:

- First, a rigorous risk-hedging model based on insurance is proposed for the retailer to hedge the risks at the transmission level. The conventional risk hedging insurance lacked the consideration of the risk preference of the retailer on the total loss value caused by EEs [117]. As a result, the insurance purchased will be ineffective and undesirable for the retailer. By contrast, in this chapter, an economic adjusting index is introduced to represent the different risk aversion levels of the retailer toward the low probability but high loss events, i.e., the EEs. The larger the adjusting index is, the more risk-averse the retailer is. As a result, the larger the loss value caused by the EEs is. Therefore, the retailer is more willing to pay for the insurance premium to get a higher chance of receiving monetary compensation from the insurance, and vice versa.
- Second, a risk management strategy based on the strangle weather derivatives and ESS is designed for the retailer to hedge the risks at the distribution level. The traditional risk hedging tools like options and forward contracts relied heavily on the forecast of the electricity prices, such as [36, 37, 118]. However, the increasing penetration of DERs will further amplify the fluctuation of demands and prices, which will increase the forecast difficulty. By using the proposed strangle weather derivative and the ESS, the reliance on the prediction of the prices is avoided.
- Third, the proposed model offers a guide for choosing diverse forms of hedging portfolios (a set of hedging tools) for retailers under different budget constraints. The conventional risk hedging model ignored the impact of the budget constraints on the choice of the hedging tools, such as [108, 112, 113], which can lead to ineffective risk-hedging portfolios. In our model, different budget constraints of the retailer are simulated in the case study to provide a suggestion for the retailers on the appropriate combination of the hedging tools to invest in, namely, the proper quantity of

insurance contracts and strangle weather derivative contracts to sign with and the appropriate capacity of the ESS to invest in.

4.2 The Framework and Wholesale Methodology of the Proposed Hedging Strategy

In this chapter, the proposed risk hedging strategy covers the risks at both the transmission and distribution levels. As for the objective of the chapter, it aims to minimize the costs of the retailers at both the transmission and distribution levels. Additionally, the retailer will decide the proper amount of insurance contracts, strangle weather derivatives to sign with, and the capacity of the ESS to invest in. The framework of the hedging strategy is shown in Fig. 4-1.

At the transmission level, the retailer utilizes the insurance contract based on the adjusted risk valuation method to hedge the encountered power shortage risks caused by EEs, such as the damages caused by bushfires and ice storms. The adjusted risk value can reflect the risk preference of the retailer toward the EEs, which can increase the effectiveness of the insurance contract.

At the distribution level, the retailer uses the proposed strangle weather derivatives to hedge the risks of demand fluctuation caused by normal changes in temperatures and the increasing penetration of the DERs. The proposed strangle weather derivatives encompass two parts: the HDD (CDD) put and the HDD (CDD) call. Worth noticing that the strangle weather derivatives used in this chapter is a novel strategy that is different from the traditional financial strangle [161]. In addition, the ESS is used to smooth the demand and facilitate the operation of the strangle weather derivatives.

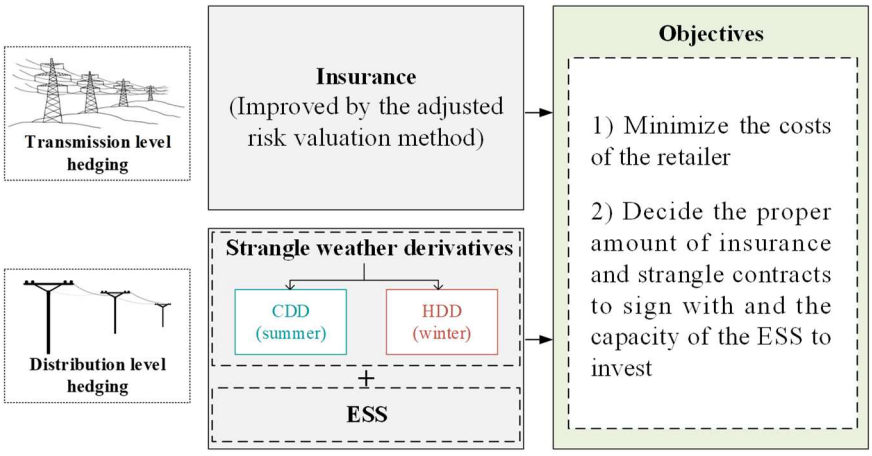

Fig. 4-1. The framework of the proposed hedging strategy for the retailer.

The wholesale methodology flowchart of the proposed model is shown in Fig. 4-2. The processes within the solid black squares and the dotted black squares are the conventional wholesale methodology, in which electricity retailer signs bilateral contracts with both the power generator and the end-users to

satisfy the electricity demand. If the demand is still unsatisfied, the retailer will purchase extra electricity in the spot market. However, the procurement costs in the spot market are high. Thus, a novel hedging strategy is proposed in this chapter to reduce energy procurement in the spot market. Apart from signing bilateral contracts with both the power generator and the end-users, the processes within both the red squares and the solid black squares are the wholesale methodology of our hedging method. Here, the processes within the red squares are the contributions of our model. To hedge power outage risks caused by the EEs, insurance contracts based on the adjusted risk valuation method are introduced. For risk-hedging on the demand fluctuation, when the electricity demand is higher than the supply (D1>S1) and the condition of exercising the call is satisfied, the retailer will exercise the HDD (CDD) call signed with the power generator to satisfy the load demand. In other words, the energy supply is increased, i.e., S=S1+S2. If the demand is still higher than the supply (D1>S1+S2), the retailer will purchase extra electricity in the spot market. On the contrary, when the demand is lower than the supply(D1<S1) and the condition of exercising the put is satisfied, the retailer will exercise the HDD (CDD) put signed with the end-users to increase the load demand. Thus, the demand is increased to D=D1+S3.

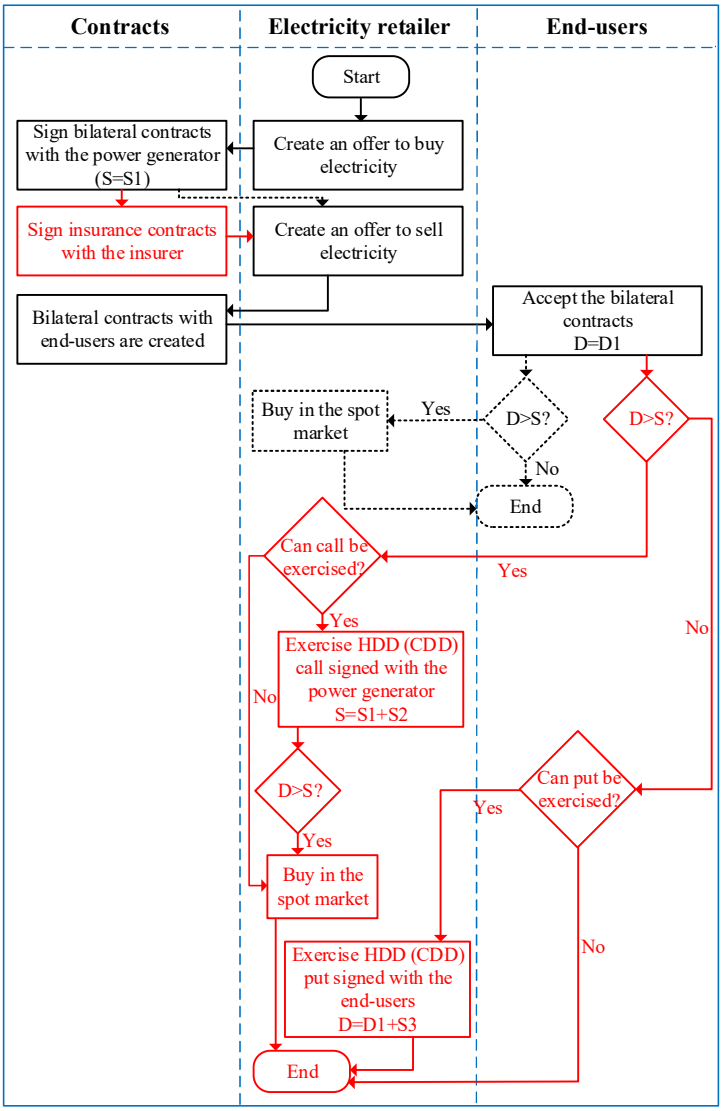

Fig. 4-2. The wholesale methodology flowchart.

4.3 The Conventional Hedging Strategy for the Retailer

4.3.1 Conventional Model

Traditionally, electricity retailers sign bilateral forward contracts with power generators to purchase a certain amount of energy at the contract price. Additionally, the retailers also sign bilateral contracts with the end-users to sell a certain amount of energy at the contract price. When the load demand is higher than the energy purchased from the power generator, retailers will incur additional costs to purchase the energy in the spot market. Thus, the forecast of electricity price and demand is critical for the retailers. Besides the bilateral contracts, ESS is also used to facilitate the retailer in risk-hedging. Details of ESS constraints and models can be referred to [36]. The objective function of the conventional model is shown as follows:

$$\max . \pi_{ret}^{Con} = \sum_{t=1}^{T} \left[\lambda_{RL} \times P_L^{Con}(t) - \lambda_{RG} \times P_{RG}(t) - \lambda(t) \times P_S(t) - a\% \times \lambda_{RL} \times P_L^{Con}(t) \right] + R_{ESS} - C_{ESS} \quad (4.1)$$

s.t. $$P_L^{Con}(t) = P_{RG}(t) + P_S(t) + P_{ESS}^{sell}(t) \quad (4.2)$$

where $\pi_{ret}^{Con}(t)$ is the conventional profits of the retailer; λ_{RL} is the contract price between the retailer and the end-users; R_{ESS} is the revenue of operating the ESS; C_{ESS} is the costs of the ESS, including the fixed costs and the operational costs of the ESS; $P_{ESS}^{sell}(t)$ is the energy from the ESS that is sold to the end-users; λ_{RG} is the contract price between the retailer and the generator; $\lambda(t)$ is the real-time energy price at time *t*; $a\%$ is the fixed payment percentage of the transmission and distribution networks; $P_{RG}(t)$ is the energy procurement amount between retailers and generators at time *t*; $P_S(t)$ is the extra amount of energy purchased by the retailers at the real-time price to satisfy the demand; $P_L^{Con}(t)$ is the total load demand under the conventional model which involves three parts: the energy from the generators, the energy from the ESS, and the energy from the spot market.

4.3.2 Brief Comparison

In this chapter, the proposed risk hedging model improves the conventional mechanism from the following three aspects. First, as EEs have become an emerging phenomenon over the past decades, the adjusted risk valuation model has been proposed to incorporate the risk preference of the retailer toward the EEs. Second, strangle weather derivatives are proposed to hedge demand variation risks at the distribution level. Third, budget constraints have been considered to facilitate the retailer in determining the proper number of risk-hedging tools to invest in. Detailed models of the proposed hedging strategies are presented in section 4.5 and section 4.6, respectively.

4.4 Risk Valuation Method

Normally, risk assessment involves three steps: 1) identify the risks, 2) determine the probability of the risks that have caused damage, 3) and quantify the risks [162]. For step 1, the risks identified at the transmission level are the risks of transmission system breakdown and power outages caused by the EEs. Insurance can be used to hedge these types of risks. In this chapter, a novel method to estimate the total loss value, i.e., the target of step 3, will be proposed to enhance the effectiveness of the insurance contract. Additionally, two components should be derived first. They are the adjusted risk value proposed in section 4.4.2 and the probability mentioned in step 2 that the EEs, such as bushfires and ice storms, have

caused breakdowns in the energy transmission process. The derivation of step 2 can be referred to [163].

4.4.1 Conventional Calculation of Expected Risk Value

Traditionally, the total loss value can be calculated by multiplying the loss value with the related probability of occurrence. Thus, the expected value of losses can be presented as [162]:

$$L = \int_{0}^{+\infty} yPr(y)\,dy \tag{4.3}$$

where L is the total loss value; y is the value of the loss; $Pr(y)$ is the probability density function (PDF) of the loss.

4.4.2 Adjusted Risk Valuation Method

Before introducing the detailed risk hedging model, certain concepts would be explained first. The main elements within insurance include *the insurer* (i.e., an insurance company), *the insured party* (i.e., the retailer in this case, which is the same as the beneficiary), *the premium* (i.e., the price paid to the insurance company by the retailer), *the claims* (i.e., the monetary compensation that can be made to the retailer for the loss events), and the *insurance excess* which is an insurance excess necessary to block claims for losses of high frequency but low severity [164].

The adjusted risk valuation method is closely related to the CVaR [165]. Because the adjusted risk valuation method is inspired by the concept of CVaR that is losses exceeding the value-at-risks should be assessed. However, the adjusted risk valuation method is an extension of the CVaR method. The reasons we choose the adjusted risk valuation method rather than the CVaR are twofold. First, compared with CVaR, the proposed risk valuation method incorporates the increasing impact of EEs, like bushfires and ice storms, by giving the mathematical formulation to represent the probability that the EEs will occur. Second, different from CVaR, the proposed method introduces an economic adjustment index to measure the risk preference of the retailer toward the damages caused by the EEs. Thus, the adjusted risk valuation method is more suitable.

As mentioned before, the damages caused by the EEs are tremendous, while the probability of occurrence is low. When using equation (4.3) to calculate the total loss value, a high loss value y multiplies extremely low loss probability $Pr(y)$ will result in a low total loss value L. Thus, the estimation of the total loss value is extremely small. To ensure that the predicted total loss value is not always smaller than the insurance excess, we proposed a novel adjusted risk valuation method based on

the economic adjusting index that can incorporate the risk preference of the retailer toward the EEs.

In this model, the standard deviation $\tau\sigma$ represents the loss threshold of the retailer. Two probabilities will be introduced, the risk area probability $Pr\left(y(t)>\tau\sigma\right)$ and the health area probability $Pr\left(y(t)\le\tau\sigma\right)$. For the risk area under EEs, it refers to the unacceptable level of costs incurred during the system breakdown, and those costs are higher than the loss threshold of the retailer. Whereas the health area under EEs refers to the acceptable level of costs incurred during the system breakdown, and the costs are lower than the loss threshold of the retailer. In this chapter, we also introduce the economic adjusting index τ to involve the impact of the risk attitudes of the retailers toward the EEs. The larger the τ is, the more concerned the retailer is about the network vulnerability under EEs [162]. In the model, the reciprocal format of the PDF of τ, i.e. $f_\tau(\tau)$, is designed to describe and match the catastrophic consequences of the EEs. The PDF of the economic adjustment index τ can be referred to [162] as follows:

$$1-Pr\left(y(t)\le\tau\sigma\right)=Pr\left(y(t)>\tau\sigma\right)=\int_{(\tau\sigma)^+}^{+\infty}Pr\left(y(t)\right)dy(t) \tag{4.4}$$

$$f_\tau(\tau)=\begin{cases}exp\left(-\tau\sigma/\mu\right) & if \quad \tau>0\\ 0 & else\end{cases} \tag{4.5}$$

where $\tau\sigma$ is the loss threshold for the retailer; τ is the economic adjustment index ($\forall\tau\ge0$); $f_\tau(\tau)$ is the PDF of the economic adjustment index τ. By applying the proposed adjusted risk valuation method, the adjusted risk value under EEs can be derived as follow:

$$L_\tau(t)=\frac{L(t)}{f_\tau(\tau)}=\frac{\int_{(\tau\sigma)^+}^{+\infty}y(t)Pr\left(y(t)\right)dy(t)}{exp\left(-\tau\sigma/\mu\right)U(\tau)} \tag{4.6}$$

where $U(\tau)$ is the staircase function that can be used to ensure $\forall\tau\ge0$; σ and μ are the standard deviation and expected value of loss due to uncertainties; $L_\tau(t)$ is the adjusted risk value under the EEs.

4.5 Hedging Strategy for the Retailer at the Transmission Level

For the hedging risks at the transmission level, insurance based on the adjusted risk valuation method is used because it is a financial tool designed for mitigating losses of low frequency but catastrophic

damages. For equation (4.9), $Pr_{EED}\left(L_{\tau}(t)\right)$ is the probability of system breakdowns to the energy transmission network caused by the EEs. Thus, it is not an extremely low probability as $Pr\left(y(t)\right)$. As for equations (4.7)-(4.9), they did not adopt the conventional method to decide the number of insurances. Instead, the proposed adjusted risk valuation method is utilized, which can be referred to section 4.4.2. Thus, the adjusted risk value $L_{\tau}(t)$ is adjusted according to the risk preference of the retailer toward the EEs. As a result, the total loss value caused by the EEs C_{EE} is not necessarily lower than the insurance excess exc_{Ins}. Thus, the claim can be obtained by the retailer when the total loss value is higher than the excess of the insurance to cover part of the damages caused by the EEs. The mathematical formula of the $Pr_{EED}\left(L_{\tau}(t)\right)$ can be referred to [163]. The revenues and costs of the retailers by using the insurance to hedge the risks can be shown as follows [162]:

$$R_{Ins} = W_{Ins} \times X_{Ins} \times \left(C_{EE} - exc_{Ins}\right) \tag{4.7}$$

$$C_{Ins} = X_{Ins} \times \lambda_{Ins} \tag{4.8}$$

$$C_{EE} = \sum_{t=1}^{EEP}\left(L_{\tau}(t) \times Pr_{EED}\left(L_{\tau}(t)\right)\right) \tag{4.9}$$

where R_{Ins} and C_{Ins} are the revenues (claim payments) and costs of the insurance for the whole year; $Pr_{EED}\left(L_{\tau}(t)\right)$ is the probability that the EEs, such as bushfire and ice storm, that have caused breakdowns to the energy transmission network; exc_{Ins} is the insurance excess that must be exceeded by the total loss caused by the EEs C_{EE} during the extreme event period to acquire the claim payments; X_{Ins} is the number of insurance purchased for hedging the risks at the transmission level under the EEs; W_{Ins} is the binary parameter, if the total loss value is larger than the excess, W_{Ins} will be 1, else, 0; λ_{Ins} is the premium of the insurance; EEP is the extreme event period, such as the duration of bushfire or ice storm.

According to [117], a low insurance premium will lead to a high insurance excess. When the predicted total loss value is larger than the excess of the insurance, the claims calculated by total loss value minus excess will be paid to the retailer to cover part of the risks at the transmission level. Thus, the insurance premium paid by the retailer can influence whether the claim of the insurance will be paid by the insurer.

In other words, the insurance premium paid by the retailer can affect the effectiveness of the insurance. Additionally, the insurance premium is closely related to the net written premium surplus ratio ψ_{Ins} defined in equation (4.11), which can refer to [117]. Hence, the premium is calculated as the predicted claims multiply $(1+\psi_{Ins})$. Thus, the insurance premium can be derived via equation (4.10) as:

$$\lambda_{Ins}=E\left[W_{Ins}\times\left(\sum_{t=1}^{EEP}\left(L_{\tau}(t)\times Pr_{EED}\left(L_{\tau}(t)\right)\right)-exc_{Ins}\right)\right]\times\left(1+\psi_{Ins}\right) \tag{4.10}$$

where

$$\psi_{Ins}=\frac{\sigma\left[\left(\sum_{t=1}^{EEP}\left(L_{\tau}(t)\times Pr_{EED}\left(L_{\tau}(t)\right)\right)-exc_{Ins}\right)\right]}{E\left[\left(\sum_{t=1}^{EEP}\left(L_{\tau}(t)\times Pr_{EED}\left(L_{\tau}(t)\right)\right)-exc_{Ins}\right)\right]} \tag{4.11}$$

where ψ_{Ins} is the net written premium surplus ratio of its standard deviation against the expected claim payments.

4.6 Hedging Strategy for the Retailer at the Distribution Level

The retailers mainly hedge risks arising from cold winters, warm winters, hot summers, and cool summers. When the temperature is cold in winter or hot in summer, end-users will need more electricity either for heating or cooling. As a result, retailers might incur a loss for purchasing extra energy at the spot price. On the contrary, for the warm winter and cool summer, the end-users will reduce their demand for electricity compared to cold winter and hot summer, which will bring profit reduction to the retailers.

Before explaining the detailed model, technical terms relating to the weather derivatives are explained. Weather derivatives can be defined as financial instruments used by companies or individuals to hedge risks of weather-related losses [166]. Ref. [161] defined HDD (CDD) as *the number of degrees that a daily average temperature is below (above) 65^{o} Fahrenheit (18^{o} Celsius). To long (short) a call/put means to buy (sell) the call/put options.*

In this chapter, an HDD call and a CDD call can be bought by the retailers from the seller of the call, i.e., the power generator, when the temperature is cold in winter and hot in summer. When the HDD (CDD) calls are exercised, the retailer can purchase energy from the seller of the call at the strike price and store energy for later usage. And when the demand for electricity is higher than the amount of energy in the bilateral contract between the retailer and the end-users, the retailer can sell the stored energy to the end-users at the contract price to satisfy the extra load demand. If the demand is still unsatisfied, the

retailer will purchase energy in the spot market. On the other hand, it is advised for the retailer to buy an HDD put and a CDD put from the end-users if the temperature is warm in winter or cool in summer. By purchasing the HDD put and CDD put, the retailer can exercise the strangle weather derivative to sell electricity to the end-users at the strike price to increase profits. In our model, the HDD call and the HDD put can form the HDD strangle for winter, whereas the CDD call and the CDD put can be combined to form the CDD strangle for summer. The HDD strangle and the CDD strangle are called the strangle weather derivatives. A detailed model of the strangle weather derivatives is explained as follows.

4.6.1 Proposed Strangle Weather Derivatives

4.6.1.1 HDD strangle

In this chapter, the HDD strangle covers the winter in Australia (June to August). It is a contract between the retailer and the strangle seller, i.e., the power generator and the end-users, in which the retailer is the buyer of the HDD strangle. The HDD strangle includes the HDD call and the HDD put. For the HDD put, when the strike value of the HDD put K_{HDD}^{put} is higher than the $HDD(n)$, which is the heating degree day for cd periods, referred to equation (4.13), the put will be exercised. Whereas the call is out of the money, that means the call will not be exercised [33]. In this case, it is normally in a warm winter, where the demand for electricity is reduced compared to the cold winter. The retailer can purchase electricity from the spot market at a low price and exercise the put option to sell the purchased electricity to the end-users at a higher price (the strike price $K_{HDD}^{put} \times TS_{HDD}^{put}$). For the HDD call, when the $HDD(n)$ is higher than the strike value K_{HDD}^{call} of the HDD call, the call will be exercised. In this case, it is normally in a cold winter, where demand for electricity is relatively high, the retailer will exercise the HDD call by purchasing electricity from the power generators at the determined HDD call strike price $K_{HDD}^{call} \times TS_{HDD}^{call}$ and selling that energy to satisfy the extra demand. The revenues and costs of the retailer using the HDD strangle are shown as follows [167, 168]:

$$\begin{aligned} R_{HDD} &= X_{HDD} \times P_{HDD} \\ &\times \sum_{n=d-cd}^{d} \left[W_{HDD}^{put}(n) \times \left(K_{HDD}^{put} - HDD(n) \right) \times TS_{HDD}^{put} + W_{HDD}^{call}(n) \times \left(HDD(n) - K_{HDD}^{call} \right) \times TS_{HDD}^{call} \right] \end{aligned} \tag{4.12}$$

$$HDD(n) = \left(18 - \overline{T}(n) \right) \tag{4.13}$$

$$C_{HDD} = X_{HDD} \times \left(\lambda_{HDD}^{put} + \lambda_{HDD}^{call} \right) \tag{4.14}$$

where R_{HDD} and C_{HDD} are the revenues and costs of the HDD strangle for winter, and each strangle contract covers cd days; n is the start day of the HDD; d is the end day of the HDD; P_{HDD} is the amount of energy covered by each HDD strangle contract; K_{HDD}^{put} and K_{HDD}^{call} are the strike value of the HDD put and HDD call; $HDD(n)$ is the heating degree day for cd periods; $W_{HDD}^{put}(n)$ and $W_{HDD}^{call}(n)$ are the binary parameters. If the strike value of HDD put K_{HDD}^{put} is larger than the $HDD(n)$, the put option will be exercised and $W_{HDD}^{put}(n)$ equals one, otherwise 0; If the $HDD(n)$ is larger than the strike value of HDD call K_{HDD}^{call}, the call option will be exercised and $W_{HDD}^{call}(n)$ equals one, otherwise 0; TS_{HDD}^{put} and TS_{HDD}^{call} are the tick sizes of the HDD put and HDD call; *18* is the reference temperature; $\overline{T}(n)$ is the daily average temperature; X_{HDD} is the number of HDD strangle contract that covers cd periods; λ_{HDD}^{put} and λ_{HDD}^{call} are the premiums of the HDD put and the HDD call.

4.6.1.2 CDD strangle

The CDD strangle covers the summer of Australia (December to February) in this chapter. The mechanism is similar to that of an HDD strangle. However, the CDD strangle is a strategy for summer. Thus, the strike value and the tick size are different from that of the HDD strangle. Additionally, the cooling degree day $CDD(n)$ is calculated differently from the $HDD(n)$, which is presented as equation (4.16). The revenues and costs of the retailer using the CDD strangle are shown as below [24]:

$$R_{CDD} = X_{CDD} \times P_{CDD} \times \sum_{n=d-cd}^{d} \left[W_{CDD}^{put}(n) \times \left(K_{CDD}^{put} - CDD(n) \right) \times TS_{CDD}^{put} + W_{CDD}^{call}(n) \times \left(CDD(n) - K_{CDD}^{call} \right) \times TS_{CDD}^{call} \right] \quad (4.15)$$

$$CDD(n) = \left(\overline{T}(n) - 18 \right) \quad (4.16)$$

$$C_{CDD} = X_{CDD} \times \left(\lambda_{CDD}^{put} + \lambda_{CDD}^{call} \right) \quad (4.17)$$

where R_{CDD} and C_{CDD} are the revenues and costs of the CDD strangle for summer, and each strangle contract covers cd days; n is the start day of the CDD; d is the end day of the CDD; P_{CDD} is the amount of energy covered by each CDD strangle contract; K_{CDD}^{put} and K_{CDD}^{call} are the strike value of the *CDD* strangle; $CDD(n)$ is the cooling degree day for cd periods; $W_{CDD}^{put}(n)$ and $W_{CDD}^{call}(n)$ are the

binary parameters. If the strike value of CDD put K_{CDD}^{put} is larger than the $CDD(n)$, the put option will be exercised and $W_{CDD}^{put}(n)$ equals one, otherwise 0; If the $CDD(n)$ is larger than the strike value of CDD call K_{CDD}^{call}, the call option will be exercised and $W_{CDD}^{call}(n)$ equals one; otherwise 0; TS_{CDD}^{put} and TS_{CDD}^{call} are the tick sizes of the CDD put and CDD call; X_{CDD} is the number of *CDD* strangle contracts; λ_{CDD}^{put} and λ_{CDD}^{call} are the premiums of the CDD put and the CDD call.

4.6.2 Energy Storage System Model

The energy storage devices can be used to smooth the fluctuation of the electricity price by charging or discharging power. Ref. [117] indicated that ESS is suitable for balancing small but frequent contract imbalances. Thus, it will be used to hedge demand variation risks. In current markets, there are a variety of energy storage devices. Compared with other ESSs, the BESS is the most cost-effective storage device. Therefore, in this chapter, the battery is utilized by the retailer to hedge risks. The revenues and costs formulae are shown as follows [36]:

$$R_{ESS} = \sum_{t=1}^{T}\left(\lambda_{RL} \times P_{ESS}^{sell}(t) - \lambda(t) \times P_{ESS}^{buy}(t)\right) \tag{4.18}$$

$$C_{ESS} = X_{Bat}^{fix} \times C_{Bat}^{fix} + \sum_{t=1}^{T} C_{Bat}^{oper}(t) \tag{4.19}$$

$$C_{Bat}^{oper}(t) = m \times X_{Bat}^{fix} \times C_{Bat}^{fix} \tag{4.20}$$

$$C_{Bat}^{fix} = IC_{Bat} \times \frac{r}{1 - 1/(1+r)^{y}} \tag{4.21}$$

$$\begin{aligned} E_{store}(t+1) = E_{store}(t) + \eta_{cha} \times \left(P_{ESS}^{buy}(t) + \left(\frac{W_{HDD}^{call}(n) \times P_{HDD} + W_{CDD}^{call}(n) \times P_{CDD}}{24} \right) \right) \times \Delta t \\ - \left(P_{ESS}^{sell}(t) + \frac{W_{HDD}^{put}(n) \times P_{HDD} + W_{CDD}^{put}(n) \times P_{CDD}}{24} \right) \times \Delta t \Big/ \eta_{dis} \end{aligned} \tag{4.22}$$

where R_{ESS} and C_{ESS} are the revenues and costs of the energy storage devices of the proposed model for the whole year; $P_{ESS}^{sell}(t)$ is the electricity sold to the end-users from the spot market; $P_{ESS}^{buy}(t)$ is the electricity purchased by the retailer in the spot market and is stored in the ESS; X_{Bat}^{fix} is the number of battery needed to store the energy; C_{Bat}^{fix} is the annualized fixed cost per battery device; $C_{Bat}^{oper}(t)$ is the operation costs of the battery of the proposed model at time *t*; m is the maintenance rate of the

battery; IC_{Bat} is the initial costs of the battery; $E_{store}(t)$ is the energy storage state of the proposed model at time *t*.

4.7 The Objective Function of the Proposed Hedging Strategy

The aim of the proposed model is to minimize the costs during the risk-hedging process of the retailer at both transmission and distribution levels. The components of the gains include the revenue from the insurance contract R_{Ins}, the revenue from the strangle weather derivatives $R_{HDD}+R_{CDD}$, and the net profits from normal operation using bilateral contracts π_{ret}^{Con}. For the costs components, the premium paid to obtain the insurance C_{Ins}, loss caused by EEs C_{EE} estimated in section 4.5, and the premium paid to obtain the strangle weather derivatives $C_{HDD}+C_{CDD}$ are all considered. In addition, the budget constraint has been considered in equation (4.25) which is determined by the budget limit of the retailer that will impact the investment decision of the retailer on the hedging tool portfolio. The objective function for the whole year can be shown as follows:

$$min\left(C_{retail}^{Total}-R_{retail}^{Total}\right)=C_{Ins}+C_{HDD}+C_{CDD}+C_{EE}-R_{Ins}-R_{HDD}-R_{CDD}-\pi_{ret}^{Con} \tag{4.23}$$

s.t.
$$P_L^{prop}(t)=P_L^{Con}(t)+\frac{\sum_{n=d-cd}^{d}\left(W_{HDD}^{call}(n)\times P_{HDD}+W_{HDD}^{put}(n)\times P_{HDD}\right)}{24}+\frac{\sum_{n=d-cd}^{d}\left(W_{CDD}^{call}(n)\times P_{CDD}+W_{CDD}^{put}(n)\times P_{CDD}\right)}{24} \tag{4.24}$$

$$\begin{bmatrix} X_{Bat}^{fix}\times\lambda_{Bat}^{fix}+X_{HDD}\times\lambda_{HDD}^{put}+X_{HDD}\times\lambda_{HDD}^{call} \\ +X_{CDD}\times\lambda_{CDD}^{put}+X_{CDD}\times\lambda_{CDD}^{call}+X_{Ins}\times\lambda_{Ins} \end{bmatrix}\leq Budget \tag{4.25}$$

where R_{retail}^{Total} and C_{retail}^{Total} are the total retailer revenues and costs for the whole year; π_{ret}^{Con} is the conventional annual profits of the retailers by using the bilateral contracts, which can be referred to equation (4.1); $P_L^{prop}(t)$ is the total load demand of the end-users under the proposed model which involves three parts: the energy from the generators and the spot market, the energy from the battery, and the energy from the strangle weather derivatives.

4.8 Case Study

4.8.1 Experiment Setting

In this chapter, all the data relating to energy price and demand are obtained from the AEMO [160].

Other data like daily average temperature for the months of January, February, June to August, and December of the simulated years can be found in [169]. The proposed model is compared with the reference using the bilateral contracts in Table 4-2 and the reference using the options in Table 4-3. Moreover, a discussion of the proposed model with references using the bilateral contract, insurance, and options is further conducted in Figs. 4-4 to 4-9. Since our model is a mixed-integer linear program problem, it can be solved via the CPLEX solver.

The uncertainties considered include the electricity demand and price. Monte Carlo simulation is utilized to address uncertainty problems by modeling their probability density functions.

TABLE 4-1. PARAMETER VALUES WITHIN THE CHAPTER.

Parameter	Value	Parameter	Value
exc_{Ins}	36,000 AU$	r	5%
IC_{Bat}	50,000 AU$	y	20 years
P_{HDD} , P_{CDD}	1 MWh	η_{cha} , η_{dis}	90%

In Table 4-1, the parameter values relating to the insurance, the strangle weather derivatives, and the ESS are given. For the insurance, the insurance excess exc_{Ins} is given. For the strangle, the coverage amount per HDD/CDD contract P_{HDD} / P_{CDD} is given. For the ESS, the initial costs of the ESS IC_{Bat}, the discount rate r, the ESS lifetime y, and the charging/discharging efficiency η_{cha} and η_{dis} are included.

4.8.2 Simulation Results Analysis

Fig. 4-3 shows the compositions of the total load demand (PL) of the end-users for a year. Conventionally, the total demand includes the energy from the contract signed between the retailer and the generator if the contract coverage amount (PG_contract) is enough to satisfy the loads. If it is not adequate, the retailer will purchase extra energy (P_spot) from the spot market at the spot price, which is higher than the contract selling price between the retailer and the end-users. By contrast, in the proposed model, when the load demand is higher than the energy supply, the retailers will exercise the HDD/CDD call to buy electricity from the power generator to satisfy the extra load demand. On the contrary, when the demand is lower than the supply, the retailer will exercise the HDD/CDD put into selling the electricity at the strike price to the end-users to enhance the sales. Here, P_strangle is the

electricity purchased via the strangle weather derivatives to satisfy the demand. In addition, the retailer can discharge electric power from the BESS to satisfy the load, which is PESS_sell. By using the HDD/CDD call and the HDD/CDD put, the energy procurement in the spot market has been reduced and replaced by the energy from the ESS and the strangle weather derivatives, which is cost-saving for the retailer.

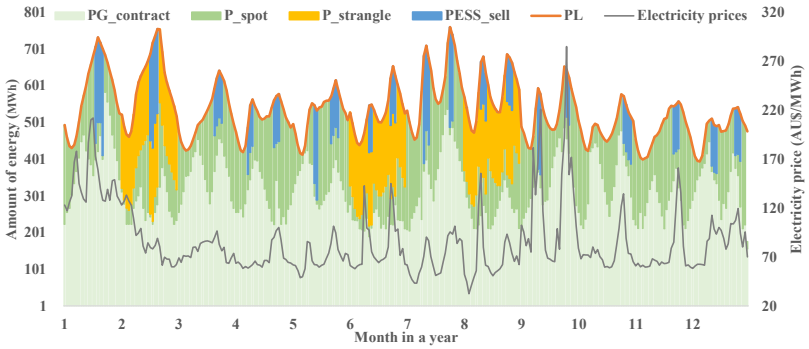

Fig. 4-3. The composition of the total load demand.

Fig. 4-4 illustrates the execution of the strangle weather derivatives in both summer and winter. For the summer period, the CDD strangle covers three months, and those are January, February, and December. The blue bars show the amount of accumulated $CDD(n)$ for a week. In this chapter, the contract period of each strangle covers one week, and the strike value of the CDD call is higher than the CDD put. In brief, the CDD strangle is exercised when the $CDD(n)$ is higher than the strike value of CDD call or smaller than the strike value of CDD put. To be specific, the CDD call represented by the yellow dots is exercised when the $CDD(n)$ is higher than the CDD call strike value, whereas if the $CDD(n)$ is lower, the CDD put represented by the purple diamond is exercised. For the winter period, the HDD strangle also includes three months, i.e., June, July, and August. The red bars are the weekly accumulated $HDD(n)$. The identical methodology is applied to decide the execution of the HDD call (blue triangle) and the HDD put (green square). Not all the strangles in these six months are exercised because temperature changes within certain ranges in both summer and winter are acceptable. When the temperature variation exceeds the acceptable range, strangle is exercised.

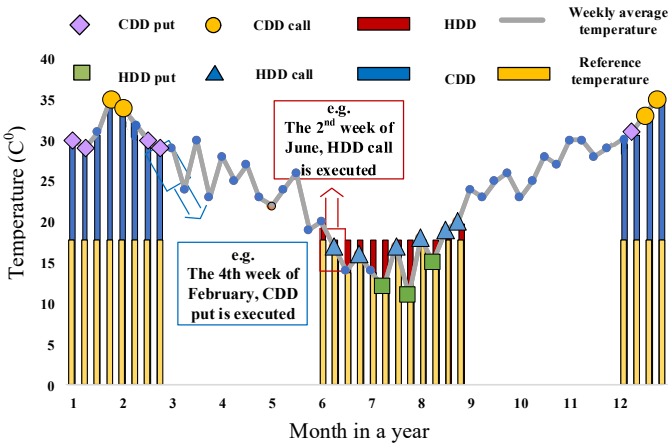

Fig. 4-4. The execution date for the HDD strangle and the CDD strangle.

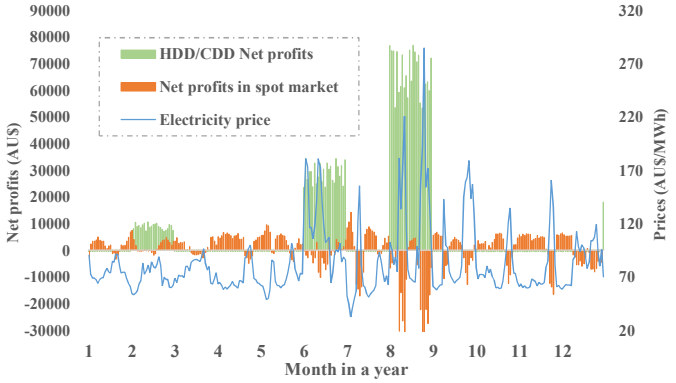

Fig. 4-5. The profits from the strangle and the normal operation.

Fig. 4-5 shows the net profits for the HDD and CDD strangles, which are positively correlated with the spot prices. The orange areas show the net profits of the retailer under the conventional model, which are negatively correlated with the spot price. Due to the opposite relationship between the net profits under the proposed model and the conventional model, the HDD and CDD strangles can be utilized to offset the losses when the electricity price is high (or when the net profits under the conventional model are negative). Although the strangle incurs costs, that is, the premium of the strangle, the retailer will make more profits with fewer risks on average.

In Table 4-2, we compare the profits of the conventional models with the profits of the proposed model under circumstances where there are EEs, and there are no EEs during the simulated periods. For circumstance that no EEs occurs, it can be found that the profits of the proposed model (18,777,003 AU$ in summer and 21,569,735 AU$ in winter, respectively) are higher than the conventional model (12,771,094 AU$ in summer and 12,851,821 AU$ in winter, respectively). This is because the strangle weather derivatives are used in the proposed model to hedge the risks of demand variation in both winter

and summer. When there are EEs in both summer and winter, the profits of the conventional model decrease by around 35% in summer and 31% in winter compared to the profits in summer and winter, where no EEs have occurred. Although the profits under the proposed model are also reduced to some extent, it reduced by 24% in summer and 22% in winter. This can be explained by the use of insurance to offset the losses. As for other times besides winter and summer, the conventional model is more profitable and gains 40,881,709AU$ under no EEs. Whereas for the proposed model, besides the ESS, the insurance is also purchased. And the investment costs of the proposed model are higher than the conventional ones. Thus, the net profits are lower under the proposed model, which is 33,357,132AU$. However, the insurance takes effect when there are EEs because the profit reduction of the proposed model under EEs is lower than that of the conventional model. In other words, the utilization of insurance has reduced the profit fluctuation, and the risks have been hedged. On average, the profits of the proposed model are higher than the conventional model under either EEs or non-EEs, and the overall profit variation of the conventional model is about 26% higher than the proposed model.

TABLE 4-2. COMPARISON OF THE NET PROFITS BETWEEN THE CONVENTIONAL MODEL AND THE PROPOSED MODEL UNDER EES AND NON-EES.

	Profits of the conventional model (AU$)		**Profits of the proposed model (AU$)**	
	EEs	**no EEs**	**EEs**	**no EEs**
Summer	8,264,758	12,771,094	14,212,836	18,777,003
Winter	8,894,736	12,851,821	16,757,272	21,569,735
Other times	28,685,633	40,881,709	27,516,059	33,357,132
Overall Profits	45,845,127	66,504,625	58,486,167	73,703,871

TABLE 4-3. COMPARISON BETWEEN THE STATE-OF-ART MODEL AND THE PROPOSED MODEL.

	Using option	**Proposed model**
Total costs	**26,167,123**	**21,354,203**
average profits	**29,281,453**	**46,095,019**
ROR	**1.12**	**2.16**
ESS efficiency	**52%**	**68%**

In Table 4-3, the comparison between the state-of-art model using options and the proposed model is illustrated [112]. Four types of performance indices are utilized. The first index is the costs of the retailer, and it can be found that the total costs of the retailer using the proposed model are smaller than that of using the options. The second index is the profits of the retailer. It can be found that the profits of the

retailer under the proposed model are 46,095,019 AU$, which is higher than the model using the options. The third performance indicator, rate of return (ROR), is utilized to measure the gain of the retailer [170]. It is calculated by dividing the profits of the retailer by the total costs of the retailer. It can be found that the ROR of the retailer using the option is 1.12, which is lower than that of using the proposed model. Furthermore, for the fourth index, the ESS efficiency is compared. It can be found that the ESS usage efficiency of the proposed model is 16% higher than that the model using the option.

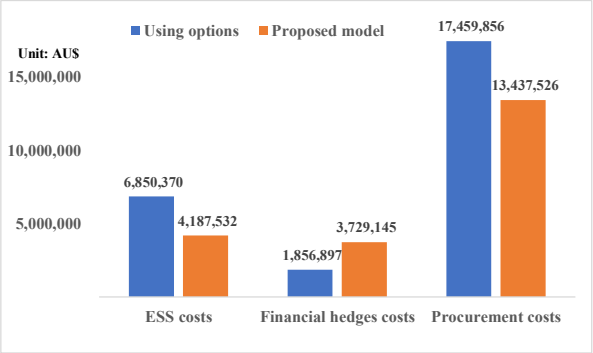

Fig. 4-6. The cost comparison of the retailer between the proposed model and the model using options.

In Fig. 4-6, the costs of the retailer include three types of costs, i.e., the ESS costs, the financial hedges costs, and the energy procurement costs. It can be found that the ESS costs (investment plus operational costs) and the procurement costs of the retailer are significantly reduced using the proposed model. However, the financial hedges costs of the proposed model are more than doubled compared to the model using the options. This is because the retailer purchases both the strangle weather derivatives and the insurance under the proposed model, whereas the state-of-art model only utilizes the options.

In Fig. 4-7, the distribution of the total loss value is represented by the blue bars. There are four methods used in this chapter, and they are the bilateral forward contract, the ESS, the strangle weather derivatives and the insurance. According to the simulations, the bilateral forward contract can cover loss value (negative net profits) of a relatively small amount compared to the other three hedging methods. For most of the time, the ESS and the strangle weather derivatives are utilized to hedge risks of intermediate damages with relatively high frequencies. For risks under EEs, insurance is used, which is of fewer frequencies but tremendous damages.

In Fig. 4-8, the number of each type of hedging tool used depends on the budget limit of the retailers. Three hedging tools are compared, the ESS, insurance and the strangle weather derivatives, which include both the HDD strangle and the CDD strangle. For low budgets, the utilization of all the hedging

tools is reduced. The insurance and the ESS will not be used in this situation. As the budget increases, the usage of all the hedging tools is increasing. When the budget reaches 8,000k AU$, the number of insurance contracts remains the same while more HDD strangle and CDD strangle are purchased compared to the 6,000k AU$ budget scenario. For ESS, the number of batteries increases rapidly under the 8,000k AU$ budget. In brief, the demand for insurance is the most inelastic one. This could be explained by the feature of the insurance that it will merely be used when there are tremendous losses caused by the EEs. Therefore, it is unlikely for retailers to purchase plenty of insurance contracts. By contrast, the demand for the battery is quite elastic. The elasticity of the strangle weather derivatives lies in the middle. Thus, when the budget of the retailer is sufficient, all three hedging tools can be invested. Whereas when the budget of the retailer is limited, the investment order should be insurance the first, strangle weather derivatives the second, and ESS the third.

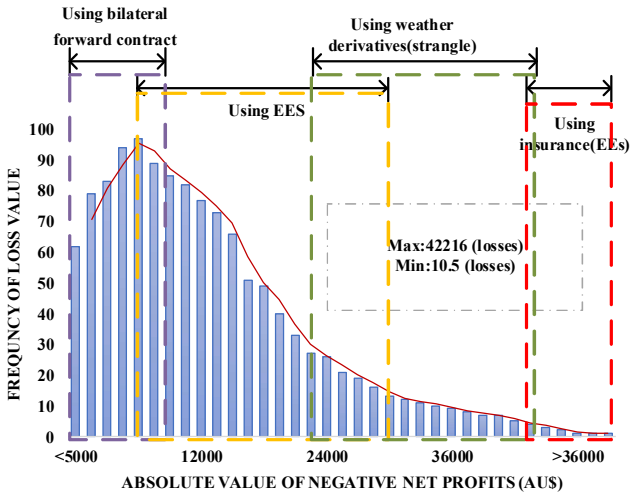

Fig. 4-7. The frequency distribution of the negative net profits.

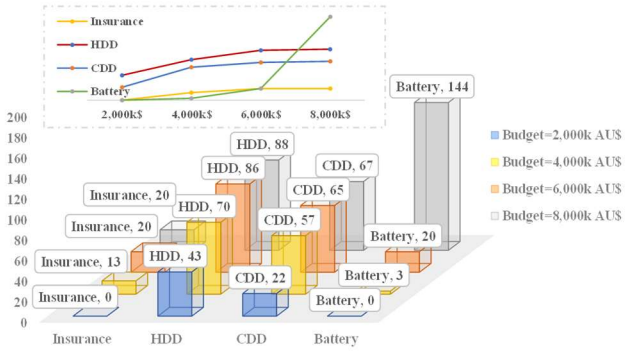

Fig. 4-8. The investment options under different budgets.

4.9 Discussion with Other Works

In Fig. 4-9, the risk-hedging methods of the existing works are applied based on the data simulated in our model. Thus, the results of using the existing works can be compared with our model. four performance indices are illustrated, namely, the average profits, the total costs of the retailer, the ESS efficiency, and the payback period. For average profits and total costs, it can be found that only using the bilateral contracts of [36] to hedge risks results in the smallest profits for the retailer at 25,427,301 AU$, whereas the total costs are the highest at 29,175,439 AU$. This is because the bilateral contracts can only be served as basic risk hedging contracts for the retailer to pre-determine the amount of electricity to buy from the power generator at a fixed purchase price and the amount of electricity to sell to the end-users at a fixed selling price. However, bilateral contracts are unable to hedge the risks caused by EEs or the risks of demand fluctuation. When using the hedging strategy of [108, 117] to hedge the risks of the retailer, the profits are higher than the model using the bilateral contracts but lower than that of the proposed model. Whereas the total costs are lower than the model using the bilateral contracts but higher than that of the proposed model. When using the hedging strategy of [112], the results are similar to the results of using the hedging strategies of [108, 117]. However, [108, 112, 117] merely consider the risk hedging strategies at either the transmission or the distribution levels. More comprehensive hedging strategies for the retailer are needed. Compared with all the other hedging strategies, our model can ensure the highest profits at 46,095,019 AU$ and the lowest total costs at 13,437,526 AU$. This is because in our model, besides the bilateral contracts and ESS, the insurance is purchased by the retailer to hedge the risks of power shortage caused by the EEs at the transmission level. Additionally, the strangle weather derivatives are proposed to hedge the risks of demand fluctuation at the distribution level.

For ESS efficiency and payback period, the results of these two performance indices using the strategies of [36, 108, 117] are quite similar. It can be found that using the strategies of [112] results in slightly higher ESS efficiency. This is because the option utilized can reduce the peak load of end-users by forcing them to sell a certain amount of load to the retailer. Then the electric power will be stored in the ESS managed by the retailer. Hence, the SOC of the ESS is increased. By comparison, the proposed model can ensure the highest ESS usage efficiency. This is because the SOC of the ESS is enhanced via the strangle weather derivatives, in which the SOC is increased via both the HDD (CDD) call and HDD (CDD) put. Thus, the ESS usage efficiency is increased accordingly. Additionally, the payback period

of ESS based on the proposed model is shortened compared with using the strategies of the other three references. This is because the average profits of the retailer using the proposed model are the highest.

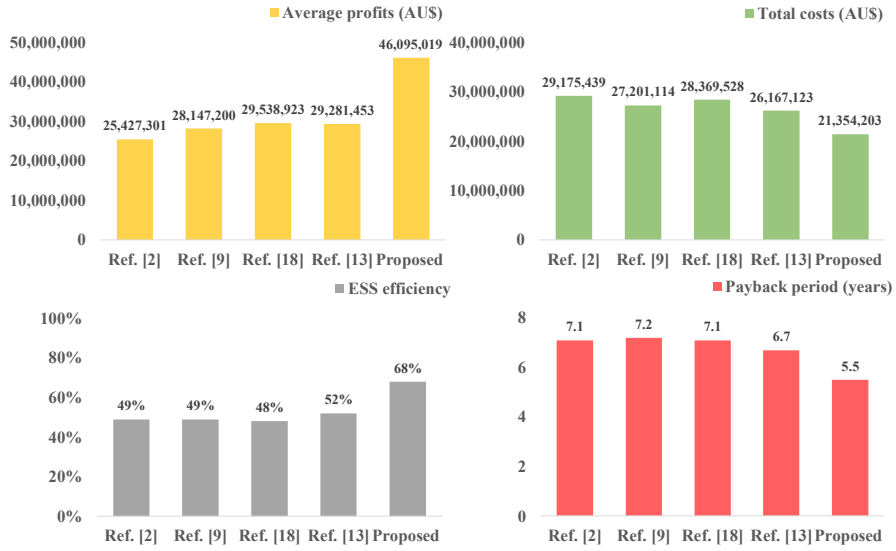

Fig. 4-9. Discussion among the existing references and the proposed model.

4.10 Conclusion

In this chapter, besides the utilization of the bilateral contract and the energy storage system, two more tools have been proposed to hedge the risks of the retailers at both transmission and distribution levels. They are the insurance and the strangle weather derivatives. For risks at the transmission level, it might occur when there are extreme events, this type of risk causes huge damage to the transmission network, but the risks are of relatively low frequency. Thus, insurance based on the adjusted risk valuation method is used to hedge the power shortage risks. For risks at the distribution level, the retailers mainly deal with the problem of demand fluctuation caused by the distributed energy resources and climate change, which is much less severe but more frequent than the damages caused by extreme events. Hence, the strangle weather derivatives and the energy storage system is chosen to hedge this type of risk. Simulation results indicate that the proposed model ensures higher profits for the retailers in summer (about 6 million AU$ higher) and winter (about 9 million AU$ higher) compared to the conventional model when there are no extreme events occur. On average, the profits of the proposed model are higher than the conventional model.

5. OPTION-BASED DEMAND RESPONSE MANAGEMENT FOR ELECTRIC VEHICLE AGGREGATOR

Renewable energy resources, such as wind power, can serve as alternative energy sources to fossil fuels to reduce carbon emissions. However, the intermittent feature of wind power generation can lead to an imbalance between the energy demand and supply. Thus, in this chapter, an option-based DR strategy is proposed to mitigate the demand-supply imbalance and save energy costs for both the retailer and the EVA that manages the EVs. In the first part, option-based DR is conducted by the retailer to incentivize EVA to either charge or discharge electricity (DR decisions). Additionally, a robust optimization method is formulated to model the wind power uncertainty impact on the DR decisions. To tackle computational complexity of the robust optimization, a dual approximation approach is applied. In the second part, a clustering-based Nucleolus method is formulated to allocate the cost saving of the EVA resulting from the DR decisions among EV users and ensure their satisfaction. The time on finding the nucleoli (the optimal cost saving allocation) can be shortened via the clustering technique and nested linear program. According to the simulation results, the proposed DR strategy can save energy costs for the retailer and the EVA at 26.2% and 6% compared with using the price-based DR strategy. For the cost saving allocation, the formulated clustering-based Nucleolus allocation method can ensure the willingness of the EV users to participate in the DR strategy.

5.1 Introduction

To cope with the climate change and energy crisis, the utilization of renewable resources, such as wind power, is growing rapidly around the globe [110]. Although wind power is a kind of alternative energy source of fossil fuel to reduce carbon emission, the intermittent feature and limited predictability of wind power generation can lead to the imbalance of energy demand and supply, which is challenging to both the power systems and the electricity market participants. To this end, DR strategies can be designed to encourage energy users to adjust their energy consumption patterns to mitigate the demand and supply imbalance problem. DR mainly considers the shiftable loads, lighting, and HVAC [171]. On the other hand, EVs are considered an effective tool to reach a low-carbon economy. In the near future, EVs have the potential to become one of the major electricity-consuming appliances [172]. Additionally, the inherent flexibility of the EVs makes them promising DR resources. However, when EV users directly participate in the energy market, they will encounter risks of energy price uncertainty. As a result, EVAs

act as a mediator between the retailer and EV owners and should be introduced to realize the insulation between EV users and the electricity market. Insulation means that EV users do not directly participate in the electricity market. Thus, the DR strategy of the retailer for the EV aggregator that can reduce energy demand and supply imbalance should be focused on.

In the literature, there are mainly two types of DR strategies, namely, price-based DR and incentive-based DR. For ***price-based DR***, it is a type of DR strategy to incentivize the end-users to alter their load patterns according to the time-varying prices [58], such as time-of-use rates, critical peak pricing, and real-time pricing. In existing research articles, the DR strategy could be formulated from the perspectives of the EV owners, the charging stations, and the electricity retailer [58-61]. However, price-based DR has two main drawbacks. First, the DR income of EVs to compensate for providing load flexibility cannot be ensured due to the volatility of the price. Second, price-based DR is conducted under organized infrastructure and regulatory approval, which is expensive. For ***incentive-based DR***, it aims to maximize the benefits of retailers, which will increase by triggering an incentive price to influence end-user behaviors to change their demand consumption. For example, direct load control, interruptible/curtailable rates, emergency DR programs, capacity market programs, and demand bidding programs [62-65]. However, literature relating to incentivizing EVA to yield load flexibility using incentive-based DR by the retailer is not investigated yet.

Thus, in this chapter, we propose a novel option-based DR strategy (incentive-based DR) to incentivize EVA to charge or discharge electricity to mitigate the demand-supply imbalance considering the uncertainty of wind generation. In such a strategy, the retailer is the option buyer who is responsible for exercising the call and the put options to conduct option-based DR. For the EVA, it is the option seller who manages the EV users to either increase or decrease charging demand in response to the option-based DR strategy. Three contributions are listed as follows:

- First, a rigorous option-based DR mechanism based on both call and put options are implemented to shift the consumption patterns of the EV users managed by the EVA to mitigate demand-supply imbalance. For the call option, it is designed for the retailer to reduce peak demand when the energy supply is smaller than demand by compelling the EVA to discharge a certain amount of electricity. For the put option, it is designed for the retailer to increase demand when the energy supply is higher than the demand by compelling the EVA to charge a certain amount of electricity.

- Second, based on robust counterpart theory, a robust optimization method is formulated to model the wind power uncertainty impact on the DR decisions. The model avoids the excessive conservativism of the conventional robust model by introducing a parameter to adjust the robustness of the proposed method against the level of conservativism of the solution. Furthermore, an equivalent linear formulation of the robust optimization method is derived via dual approximation.
- Third, a clustering-based Nucleolus allocation method is formulated to optimally allocate the cost saving of EVA among the EV users by ensuring their satisfaction with the allocation. The clustering technique is applied to improve the computation efficiency of finding the nucleoli (the optimal cost saving allocation) by reducing the set of coalitions. Moreover, a nested linear program is applied to further enhance the computational efficiency of finding out the nucleoli.

5.2 The Framework of the Proposed Model

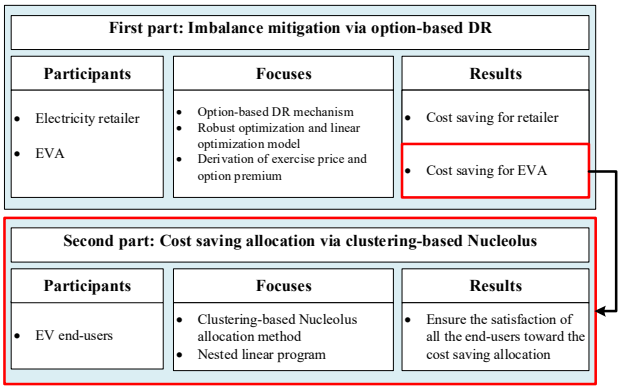

Fig. 5-1. The framework of the proposed model

The framework of the proposed model encompasses two parts, as shown in Fig. 5-1. In **the first part**, the option-based DR, including both call and put options, is first proposed to mitigate the imbalance between the energy demand and supply by incentivizing EVA to charge/discharge a certain amount of energy. Additionally, a robust optimization model is formulated to model the wind uncertainty impact on the DR decisions. Furthermore, based on the objective to minimize total cost, the optimal exercise price and option premium of both call and put options are derived. In **the second part**, the clustering-based Nucleolus allocation method is developed to optimally allocate the cost saving of EVA among the EV users to ensure the willingness of all the EV users toward the allocation. Clustering techniques and nested linear programs are used to reduce computation complexity.

5.3 Proposed Option-based DR Strategy

5.3.1 Objective Function and Constraints

In this chapter, we aim to minimize social costs, including the financial cost of the retailer and the EVA, as well as the cost of operational risks caused by wind power fluctuation, shown as (5.1). Equation (5.2) is the demand-supply balance constraint. In (5.2), the total load demand equals $l_t + \widetilde{P_t^{ch}}$. For the energy supply, the electricity can be purchased in the day-ahead and real-time markets by the retailer. Besides, the retailer is assumed to have wind farms to partially substitute energy procurement. The option-based DR is proposed to shift the EV charging profile $\widetilde{P_t^{ch}}$ to balance the demand and supply. The detailed mechanism of the option-based DR can refer to in **Propositions 1** and **2** in section 5.3.

$$\min C^{total} = C^{ret} + C^{agg} + C^{wind} \tag{5.1}$$

$$s.t. \quad l_t + \widetilde{P_t^{ch}} - y_t \times P^{call} + z_t \times P^{put} = P_t^{da} + P_t^{rt} + \widetilde{w_t} \tag{5.2}$$

where C^{total} is the total costs occurred during the electricity trading process; C^{ret} is the cost of the retailer; C^{agg} is the costs of the EVA; C^{wind} is the cost of operational risks caused by wind power fluctuation; l_t is the load of the end-users other than the charging demand of EVs; $\widetilde{P_t^{ch}}$ is the aggregated EV charging profile at time *t*; y_t and z_t are the amount of call and put options exercised at time *t*; P^{call} and P^{put} are the electricity coverage amount per call and put options; P_t^{da} and P_t^{rt} are the amount of electricity purchased in the day-ahead and real-time markets; $\widetilde{w_t}$ is the actual wind power.

5.3.1.1 The mechanism of option-based DR

In this chapter, it is assumed that the retailer purchases both call and put options from the EVA to conduct DR. As a result, the retailer has the right to exercise the options, whereas the EVA has an obligation to comply with the option execution decision made by the retailer in return for option premiums (payments) [33]. The mechanism of the option-based DR is:

Proposition 1. *For the call option, it is designed for the retailer to hedge the risks of increasing demand when supply<demand. And it is exercised when the real-time electricity price* λ_t^{rt} *is higher than the call option exercise price* λ_{EP}^{call}.

Explanation: By exercising the call option, the retailer can reduce the demand of the EVs by $y_t \times P^{call}$

amount at time *t*, shown as (5.2). As a result, the retailer must pay a payment of $\lambda_{EP}^{call} \times y_t \times P^{call}$ to the EVA at time *t*.

Proposition 2. *For the put option, it is designed to enhance the revenues of the retailer under the case of decreasing demand when supply>demand. And it is exercised when the put option exercise price* λ_{EP}^{put} *is higher than the real-time price* λ_t^{rt} .

<u>*Explanation:*</u> By exercising the put option, the retailer can increase the demand of the EVs by $z_t \times P^{put}$ amount at time *t*, shown as (5.2). As a result, the retailer receives a payment of $\lambda_{EP}^{put} \times z_t \times P^{put}$ from the EVA at time *t*.

5.3.1.2 Costs of the retailer

The costs of the electricity retailer include the premium costs C^{op}, the energy purchase costs in both the day-ahead C^{da} and the real-time markets C^{rt}, and the DR costs C^{dr}. Additionally, the profit of selling electricity to EVA π^0 is considered a negative cost, shown as (5.3). Note that the trading is scheduled in an intraday market.

$$C^{ret} = C^{op}\left(Y,Z\right) + C^{da}\left(\mathbf{P^{da}}\right) + C^{dr}\left(\mathbf{y},\mathbf{z}\right) + C^{rt}\left(\mathbf{P^{rt}}\right) - \pi^0 \tag{5.3}$$

The option premium costs of the call and put options paid by the retailer to the EVA can be formulated as equation (5.4).

$$C^{op}\left(Y,Z\right) = \lambda^{call} \times Y + \lambda^{put} \times Z \tag{5.4}$$

where λ^{call} and λ^{put} are the premium of the call and put options; Y ($Y = \sum_{t \in T} y_t$) and Z ($Z = \sum_{t \in T} z_t$) are the total amount of the call and put option contracts.

The day-ahead and real-time energy purchase costs are formulated as equations (5.5) and (5.6). The decisions of the real-time purchasing are based on the expectation of the wind information state s [63].

$$C^{da}\left(\mathbf{P^{da}}\right) = \sum_{t=1}^{T}\left(\lambda_t^{da} \times P_t^{da}\right) \times \Delta t \tag{5.5}$$

$$C^{rt}\left(\mathbf{P^{rt}}\right) = \mathbb{E}_s\left[\sum_{t=1}^{T}\left(\lambda_t^{rt} \times P_t^{rt}\right) \times \Delta t\right] \tag{5.6}$$

where λ_t^{da} and λ_t^{rt} are the day-ahead and real-time price.

The DR cost is shown in equation (5.7). The DR decisions are also based on the expectation of wind state s [63].

$$C^{dr}\left(\mathbf{y},\mathbf{z}\right)=\mathbb{E}_{s}\begin{bmatrix}\sum_{t=1}^{T}\left(\lambda_{EP}^{call}\times y_{t}\times P^{call}\right)\times\Delta t\\-\sum_{t=1}^{T}\left(\lambda_{EP}^{put}\times z_{t}\times P^{put}\right)\times\Delta t\end{bmatrix} \tag{5.7}$$

5.3.1.3 Costs of the EVA

The costs of the EVA include energy trading costs π^{0}, disutility cost Φ_{t} caused by DR, and the degradation costs $C_{SOC,t}^{EV}$ of the battery [63]. Additionally, the premium from selling the options C^{op} and the DR income C^{dr} are treated as negative costs, shown as (5.8).

$$C^{agg}=\sum_{t=1}^{T}\Phi_{t}-C^{op}\left(Y,Z\right)-C^{dr}\left(\mathbf{y},\mathbf{z}\right)+\sum_{t=1}^{T}C_{SOC,t}^{EV}+\pi^{0} \tag{5.8}$$

The disutility cost is formulated in a quadric form as (5.9) [63].

$$\Phi_{t}=a\left(y_{t}\times P^{call}+z_{t}\times P^{put}\right)^{2}+b\left(y_{t}\times P^{call}+z_{t}\times P^{put}\right) \tag{5.9}$$

When the call option is exercised, the EVA will reduce electricity consumption by $y_{t}\times P^{call}$ amount in return of $\lambda_{EP}^{call}\times y_{t}\times P^{call}$ amount of payments from the retailer; when the put option is exercised, the EVA will increase electricity consumption by $z_{t}\times P^{put}$ amount by paying $\lambda_{EP}^{put}\times z_{t}\times P^{put}$ amount of payments to the retailer. In addition, the EVA receives premium payments $C^{op}\left(Y,Z\right)$ from the retailer.

The degradation cost of EVs is formulated as (5.10) [173].

$$C_{SOC,t}^{EV}=\varphi\times P_{t}^{ch}\times\Delta t+\varphi\times SOC_{t}^{EV}\times E^{EV}\times\eta^{l}\times\Delta t \tag{5.10}$$

where

$$P_{t}^{ch}=\widetilde{P_{t}^{ch}}+z_{t}\times P^{put}-y_{t}\times P^{call} \tag{5.11}$$

where $C_{SOC,t}^{EV}$ is the SOC-related degradation costs; φ is the cost coefficient of the lifetime depression of the EV battery; P_{t}^{ch} is the power charging at time t that is derived based on adjusting planned power charging $\widetilde{P_{t}^{ch}}$ via the option-based DR; SOC_{t}^{EV} is the aggregated SOC of all the EVs at time t; E^{EV} is the total rated energy capacity of the EV battery; η^{l} is the leakage loss factor of the EV battery.

In order to characterize EV usage, information such as driving distance and driving duration is collected [174]. Then, the SOC balance constraint of EVs is shown in equation (5.12).

$$SOC_{t+1}^{EV} = SOC_t^{EV} + P_t^{ch} \times \eta^{ch} \times \Delta t / E^{EV} - \sum_{i \in I} \left(E_i^{EV} \times \frac{dr_{i,t}}{dr_i^{total}} \times pr_{i,t}^{dr} / \eta^{dis} \right) \times \Delta t / E^{EV} \quad (5.12)$$

$$P^{\min} \le P_t^{ch} \le P^{\max} \quad (5.13)$$

where $dr_{i,t}$ is the driving distance of EV i; $pr_{i,t}^{dr}$ is the probability corresponding to $dr_{i,t}$; E_i^{EV} is the rated energy capacity of the EV owned by EV i; dr_i^{total} is the total driving distance the EV owner i can drive with a fully charged battery; η^{ch} / η^{dis} is the charging/discharging efficiency; $P^{\min}$ and $P^{\max}$ are the minimum and maximum charging power.

5.3.1.4 Costs of operational risks caused by wind power fluctuation

It is assumed the retailer can partially substitute the procurement in the electricity market with self-generated wind power to save energy costs and reduce carbon emissions. If the wind generation $\widetilde{w_t}$ is within the admissible region of wind power (ARWP) range $\left[w^{low}, w^{up} \right]$, the wind power can be accommodated by the system without causing operational risks. On the contrary, if the $\widetilde{w_t}$ is outside the range, operational risks will occur. Thus, in this chapter, C^{wind} is used as a risk indicator to measure the risks caused by wind power fluctuation under a given confidence level [175]. Here, the ARWP range is the given confidence level, and it is influenced by the reserves provided by the EVs. By allocating more flexible capacity for EVs, the ARWP range can be broadened, and the risks of excess wind power and power shortage can be reduced. The wind power costs can be formulated as (5.14).

$$C^{wind} = \lambda^{WPC} \times P^{WPC} \times \Delta t + \lambda^{PS} \times P^{PS} \times \Delta t \quad (5.14)$$

where C^{wind} is the costs caused by wind power fluctuation; C^{WPC} is the cost caused by excess wind power; C^{PS} is the cost caused by power shortage; λ^{WPC} and λ^{PS} are the coefficients of excess wind power and power shortage, respectively; P^{WPC} and P^{PS} are the excess wind power and shortage of wind power.

Axiom 1. $\widetilde{w_t} > w^{up}$, excess wind power occurs, which can be expressed as equation (5.15).

$$\begin{aligned} P^{WPC} &= \mathbb{E}\left[f^{up}\left(w^{up}, \widetilde{w_t}\right) \middle| 0 < f^{up}\left(w^{up}, \widetilde{w_t}\right) < w^{\max} - w^{up} \right] \\ &= \int_{0 \le \widetilde{w_t} - w^{up} \le w^{\max} - w^{up}} \left(\widetilde{w_t} - w^{up}\right) pr_v\left(\widetilde{w_t}\right) dw_t \end{aligned} \quad (5.15)$$

$$f^{up}\left(w^{up}, \widetilde{w_t}\right) = \max\left(0, \widetilde{w_t} - w^{up}\right) \quad (5.16)$$

Axiom 2. On the contrary, $\widetilde{w_t} < w^{low}$, power shortage occurs, which can be expressed as equation (5.17).

$$\begin{aligned} P^{PS} &= \mathbb{E}\left[f^{low}\left(w^{low}, \widetilde{w_t}\right) \middle| 0 < f^{low}\left(w^{low}, \widetilde{w_t}\right) < w^{low} \right] \\ &= \int_{0 \le w^{low} - \widetilde{w_t} \le w^{low}} \left(w^{low} - \widetilde{w_t}\right) pr_v\left(\widetilde{w_t}\right) dw_t \end{aligned} \tag{5.17}$$

$$f^{low}\left(w^{low}, \widetilde{w_t}\right) = \max\left(0, w^{low} - \widetilde{w_t}\right) \tag{5.18}$$

where P^{WPC} and P^{PS} are the total excess wind power and power shortage power, respectively; $f^{up}\left(w^{up}, \widetilde{w_t}\right)$ and $f^{low}\left(w^{low}, \widetilde{w_t}\right)$ are the excess wind power and power shortage power at time t, respectively; $w^{\max}$ is the maximum capacity of the wind generation; w^{up} is the upper boundary of wind generation, above which excess wind power should be curtailed; w^{low} is the lower boundary of wind generation, below which power shortage will occur; $pr_v\left(\widetilde{w_t}\right)$ is the occurrence probability of wind power at time t under different wind speeds, which can be derived via equation (5.19) [176].

$$pr_v\left(\widetilde{w_t}\right) = \int_{\underline{v}}^{\overline{v}} f_{\widetilde{w_t}}(v) dv \tag{5.19}$$

s.t.

$$f_{\widetilde{w_t}}(v) = 2v \Big/ \left(v^*\right)^2 \cdot \exp\left[-\left(v / v^*\right)^2 \right] \tag{5.20}$$

$$v^* = 2v^{mean} / \sqrt{\pi} \tag{5.21}$$

where $f_{\widetilde{w_t}}(v)$ is the Rayleigh PDF of the wind speed v; v^{mean} is the mean wind speed; $\underline{v}$ and $\overline{v}$ are the lower and upper bound of the wind speed.

5.3.2 Robust Optimization for Wind Power Uncertainty

Data uncertainty can impact the quality and feasibility of the model. Thus, we formulate a robust optimization method to model the impact of wind generation uncertainty on the DR decision by avoiding the conservatism of the solution [177, 178].

5.3.2.1 Uncertainty set

First, the uncertainty set needs to be defined. The uncertainty of the DR model considered is the actual wind power generation $\widetilde{w_t}$. Let $\delta w_t \left| \gamma_t \right| = \widehat{w_t}$, where $\widehat{w_t}$ is the wind power prediction error and w_t is the predicted values of wind power generation can be obtained via the time series forecasting method [177, 178]. Thus, the uncertainty set Ξ for wind generation $\widetilde{w_t}$ is:

$$\Xi\left(\varphi_t,\widetilde{w_t}\right):=\left\{\begin{array}{l}\widetilde{w_t}:\exists\gamma_t\in\mathbb{R}^T s.t.\widetilde{w_t}\in\left[\begin{array}{l}w_t-\delta w_t\left|\gamma_t\right|,\\ w_t+\delta w_t\left|\gamma_t\right|\end{array}\right],\\ \left|\gamma_t\right|\le 1,\frac{1}{T}\sum_{t\in T}\left|\gamma_t\right|\le\varphi_t\end{array}\right\} \tag{5.22}$$

where φ_t is the uncertainty level of the uncertainty set Ξ; δ and γ_t are the volatility coefficients.

Axiom 3. When $\varphi_t=0$, the uncertainty set Ξ is a nominal deterministic case w_t; when φ_t increases, the range of the uncertainty set Ξ enlarges; when φ_t reaches the maximum amount, the worst-case uncertainty is presented.

5.3.2.2 Robust optimization model

Then, we formulate a robust approach via the robust counterpart theory to model the wind power uncertainty impact on the DR decisions. Denote the vector of decision variables as $\mathbf{x}$, including $\mathbf{P^{da}}$, $\mathbf{P^{rt}}$, $\mathbf{y}$, and $\mathbf{z}$. The robust counterpart is formulated as (5.23)-(5.25).

$$\min C^{total}\left(\mathbf{x},\widetilde{w_t}\right) \tag{5.23}$$

s.t.
$$\sum_m \Psi_{m,t}+\xi\left(\Gamma_t\right)\le -l_t-\widetilde{P_t^{ch}},\forall t \tag{5.24}$$

$$\Psi_{m,t}=-P_{m,t}^{da}-P_{m,t}^{rt}-w_{m,t}-y_{m,t}\times P^{call}+z_{m,t}\times P^{put} \tag{5.25}$$

where $\xi\left(\Gamma_t\right)$ is the protection function of the t^{th} constraint.

In the robust optimization model, a parameter Γ_t is introduced to adjust the robustness of the model against the conservatism of the solution, where $\Gamma_t\in\left[0,\left|J_t\right|\right]$ and $\left|J_t\right|$ measures the total number of parameters that are uncertain. The protection function can be formulated as (5.26):

$$\xi\left(\Gamma_t\right)=\max_{\left\{M_t\cup\{j_t\}\middle|\substack{M_t\subseteq J_t,\\ |M_t|=\lfloor\Gamma_t\rfloor,j_t\in J_t\setminus M_t}\right\}}\left\{\sum_{m\in M_t}\Psi_{m,t}^{*}+\left(\Gamma_t-\lfloor\Gamma_t\rfloor\right)\Psi_{j_t,t}^{*}\right\} \tag{5.26}$$

where
$$\Psi_{m,t}^{*}=-P_{m,t}^{da}-P_{m,t}^{rt}-\hat{w}_{m,t}-y_{m,t}\times P^{call}+z_{m,t}\times P^{put} \tag{5.27}$$

Axiom 4. When $\Gamma_t=0$, $\xi\left(\Gamma_t\right)=0$, then constraint (5.24) is equivalent to the nominal problem; when $\Gamma_t=\left|J_t\right|$, the problem is similar to Soyster's method.

5.3.2.3 Linear optimization model

As equation (5.26) is non-linear, we should find the equivalent linear formulation to the robust optimization model.

Proposition 3. The linearized protection function $\xi(\Gamma_t)$ is:

$$\xi(\Gamma_t) = \max \sum_{m \in J_t} \Psi^*_{m,t} \mu_{m,t} \tag{5.28}$$

$$s.t. \sum_{m \in J_t} \mu_{m,t} \le \Gamma_t \tag{5.29}$$

$$0 \le \mu_{m,t} \le 1, \forall m \in J_t \tag{5.30}$$

Proof: The optimal solution value of equations (5.28)-(5.30) consists of $\lfloor \Gamma_t \rfloor$ uncertain parameters at 1 and one uncertain parameter at $\Gamma_t - \lfloor \Gamma_t \rfloor$. This is equivalent to the selection of a subset $\left\{ M_t \cup \{j_t\} \middle| M_t \subseteq J_t, |M_t| = \lfloor \Gamma_t \rfloor, j_t \in J_t \setminus M_t \right\}$ with a corresponding function $\sum_{m \in M_t} \Psi^*_{m,t} + \left(\Gamma_t - \lfloor \Gamma_t \rfloor\right) \Psi^*_{j_t,t}$.

Proposition 4. The robust optimization model can be reformulated as the linear optimization model as follows:

$$\min C^{total}\left(\mathbf{x}, \widetilde{w_t}\right) \tag{5.31}$$

s.t.

$$\sum_m \Psi_{m,t} + \mu_t \Gamma_t + \sum_{m \in J_t} \rho_{m,t} \le -l_t - \widetilde{P_t^{ch}}, \forall t \tag{5.32}$$

$$\mu_t + \rho_{m,t} \ge \Psi^*_{m,t}, \forall t, m \in J_t \tag{5.33}$$

$$\mu_t \ge 0, \forall t \tag{5.34}$$

$$\rho_{m,t} \ge 0, \forall t, m \in J_t \tag{5.35}$$

Proof: The dual of proposition 3 is as follows:

$$\min \sum_{m \in J_t} \rho_{m,t} + \mu_t \Gamma_t \tag{5.36}$$

s.t. equations (5.33)-(5.35)

where $\mu_{m,t}$ and $\rho_{m,t}$ are the dual variables.

Since equation (5.36) is the dual problem to proposition 3, and proposition 3 is feasible and bounded for all $\Gamma_t \in \left[0, \left|J_t\right|\right]$, then equation (5.36) is also feasible and bounded. Additionally, $\xi(\Gamma_t)$ is equal to the objective function value of equation (5.36). Replacing it to equation (5.26), we found that the linear optimization of equation (5.26) is shown as proposition 4.

5.4 Derivation of Exercise Price and Option Premium

5.4.1 Option Exercise Price

First, the optimal exercise price can be derived as follows:

Theorem 1. The optimal call option exercise price λ_{EP}^{call*} and optimal put option exercise price λ_{EP}^{put*} that can ensure $C^{total}\left(\lambda_{EP}^{call*},\lambda_{EP}^{put*}\right)\le C^{total}\left(\lambda_{EP}^{call},\lambda_{EP}^{put}\right)$ are shown as equations (5.37) and (5.40).

5.4.1.1 Call option

$$\lambda_{EP}^{call*}=\int_{s_1}^{s_2}\Phi^{'}\left(y_t\right)\beta\left(s\right)ds\Big/\int_{s_1}^{s_2}\beta\left(s\right)ds \tag{5.37}$$

$$\beta\left(s\right)=\alpha\left(s\right)\Big/\lambda_t^{rt}\,pr_v\left(l_t-P_t^{da}-y_t\times P^{call}\right) \tag{5.38}$$

where $\alpha\left(s\right)$ is the prior probability density function of the wind information state s, where, $s\in\left[s_1,s_2\right]$; $\Pr\left(\bullet\right)$ is the wind power cumulative probability distribution function [63].

Proof: By taking the partial derivative of the total costs C^{total} in (5.31) to the exercise price λ_{EP}^{call} of the call option, we have:

$$\begin{aligned}\frac{\partial C^{total}}{\partial\lambda_{EP}^{call}}&=\int_{s_1}^{s_2}\frac{1}{\lambda_t^{rt}}\left(\Pr^{-1}\right)^{'}\frac{\lambda_{EP}^{call}}{\lambda_t^{rt}}\left[\lambda_{EP}^{call}-\Phi^{'}\left(y_t\right)\right]\alpha\left(s\right)ds\\&=\int_{s_1}^{s_2}\frac{\left[\lambda_{EP}^{call}-\Phi^{'}\left(y_t\right)\right]}{\lambda_t^{rt}\,pr_v\left(l_t-P_t^{da}-y_t\times P^{call}\right)}\alpha\left(s\right)ds\end{aligned} \tag{5.39}$$

5.4.1.2 Put option

$$\lambda_{EP}^{put*}=\int_{s_1}^{s_2}\Phi^{'}\left(z_t\right)\beta^{*}\left(s\right)ds\Big/\int_{s_1}^{s_2}\beta^{*}\left(s\right)ds \tag{5.40}$$

$$\beta^{*}\left(s\right)=\alpha\left(s\right)\Big/\lambda_t^{rt}\,pr_v\left(l_t-P_t^{da}+z_t\times P^{put}\right) \tag{5.41}$$

Proof: By taking the partial derivative of the total costs C^{total} in (5.31) to the exercise price λ_{EP}^{put} of the put option, we have:

$$\begin{aligned}\frac{\partial C^{total}}{\partial\lambda_{EP}^{put}}&=\int_{s_1}^{s_2}\frac{1}{\lambda_t^{rt}}\left(\Pr^{-1}\right)^{'}\frac{\lambda_{EP}^{put}}{\lambda_t^{rt}}\left[\lambda_{EP}^{put}-\Phi^{'}\left(z_t\right)\right]\alpha\left(s\right)ds\\&=\int_{s_1}^{s_2}\frac{\left[\lambda_{EP}^{put}-\Phi^{'}\left(z_t\right)\right]}{\lambda_t^{rt}\,pr_v\left(l_t-P_t^{da}+z_t\times P^{put}\right)}\alpha\left(s\right)ds\end{aligned} \tag{5.42}$$

5.4.2 Option Premium

Then, based on the optimal exercise prices of both the call and put options, the option premiums can

be derived.

Theorem 2. The option premium $\lambda^{call/put}$ is the larger value of the binomial value $\lambda_{BV}^{call/put}$ and the intrinsic value $\lambda_{IV}^{call/put}$ of the option [54], which satisfies equation (5.43):

$$\lambda^{call/put} = \max\left(\lambda_{BV}^{call/put}, \lambda_{IV}^{call/put}\right) \tag{5.43}$$

$$\lambda_{BV}^{call/put} = e^{-rT^*} \times \left(\lambda_u^{call/put} \times \frac{e^{rt} - d}{u - d} + \lambda_d^{call/put} \times \frac{u - e^{rt}}{u - d}\right) \tag{5.44}$$

$$u = e^{\sigma\sqrt{t}} \quad , \quad d = e^{-\sigma\sqrt{t}} \tag{5.45}$$

$$\lambda_{IV}^{call} = \max\left[\left(\lambda_t^{rt} - \lambda_{EP}^{call}, 0\right)\right] \tag{5.46}$$

$$\lambda_{IV}^{put} = \max\left[\left(\lambda_{EP}^{put} - \lambda_t^{rt}, 0\right)\right] \tag{5.47}$$

where e^{-rT^*} is the continuous discount rate; r is the required rate of return of the retailer; T^* is the total duration of the options, which is the same for call and put options; u is the increasing coefficient; d is the decreasing coefficient; $\lambda_u^{call/put}$ ($\lambda_d^{call/put}$) is the related option price if the electricity price has an increasing (decreasing) potential [54].

5.5 Cost saving Allocation among EVs using Nucleolus

After conducting option-based DR, the cost savings of the EVA gained from the DR are allocated among the EV owners based on the formulated clustering-based Nucleolus allocation method. The meaning of cost saving is the costs of each EV user can be reduced by cooperatively participating in the option-based DR. [111].

Compared with the other allocation methods, like the Shapley value, Nucleolus can ensure the stability of the grand coalition by ensuring the satisfaction of the end-users toward the allocation [111]. This is because the Nucleolus not only satisfies the efficiency and individual rationality principles mentioned in the following section, it also guarantees that the allocation is within the core defined in equation (5.50). Here, a grand coalition is a coalition that encompasses all the EV owners [111].

5.5.1 Preliminaries of Nucleolus

Before introducing the formulated clustering-based Nucleolus allocation method, the preliminaries of Nucleolus should be explained first.

The optimized decision variables can be plugged into the cost function of the EVA, i.e., equation (5.8),

and the minimized cost of EVA C^{agg} can be derived. Then, we define $C^{agg}(\mathcal{T})$ as the minimized coalitional energy costs by having the EV users cooperatively trade in a coalition $\mathcal{T}$ with the retailer. For the coalition, we have $\mathcal{T} \subseteq \mathcal{N}$, where $\mathcal{N}$ is the grand coalition.

First, the definition of cost saving is mathematically defined in **Definition 1**.

Definition 1. If the value of the coalition is positive, i.e., $V(\mathcal{T}) > 0$, it is more cost-saving for EV owners to cooperatively participate in the coalition managed by the EVA, which can be expressed as (5.48), according to [111]:

$$V(\mathcal{T}) = \sum_{i \in \mathcal{T}} C_i - C^{agg}(\mathcal{T}) \times (1+\varsigma) \tag{5.48}$$

where C_i is the costs of EV *i* individually trading with the retailer, and no DR is involved; $\mathcal{T}$ is the coalition of the EV users; ς is the management fee charged by the EVA, which decreases the cost saving allocated to the EV users.

Second, the cost saving is allocated among the EV users according to **Principles 1** and **2**.

Additionally, the allocation of the cost saving satisfies the imputation (5.49), which includes both efficiency (the first term) and individual rationality (the second term) principles [111]:

$$\mathcal{I} = \left\{ \chi \in \mathbb{R}^{\mathcal{N}} \middle| \sum_{i \in \mathcal{N}} \chi_i = V(\mathcal{N}), \chi_i \geq V(\{i\}), \forall i \in \mathcal{N} \right\} \tag{5.49}$$

Principle 1. *Efficiency*: $\sum_{i \in \mathcal{N}} \chi_i = V(\mathcal{N})$, where χ_i is the cost saving allocation to EV *i* under the grand coalition.

Explanation: The efficiency principle requires that all the cost savings resulting from the option-based DR should be allocated to the EV users.

Principle 2. *Individual rationality*: $\chi_i \geq V(\{i\}), \forall i \in \mathcal{N}$, where $V(\{i\})$ is the cost saving if EV *i* individually trading with the retailer without DR.

Explanation: The individual rationality principle ensures that all EV users are better off when participating cooperatively in the option-based DR.

Third, the stability of the cost saving allocation should be verified, which is explained in Definition 2.

Definition 2. Given a cost saving allocation χ_i, it is said to be stabilizing and within the core if the excess $\varepsilon(\chi, \mathcal{T}) \leq 0$. The excess measures the level of the dissatisfaction of the EV users toward the cost

saving allocation. Therefore, the core and the excess can be expressed as:

$$\mathcal{C}=\left\{\chi\in\mathcal{I}\left|\varepsilon\left(\chi,\mathcal{T}\right)\le 0,\forall\mathcal{T}\in 2^{\mathcal{N}}\right.\right\} \tag{5.50}$$

$$\varepsilon\left(\chi,\mathcal{T}\right)=V\left(\mathcal{T}\right)-\sum\nolimits_{i\in\mathcal{T}}\chi_i \tag{5.51}$$

5.5.2 Computation of Nucleolus based on clustering

However, the calculation of the Nucleolus follows the iterative process of lexicographically minimizing the excesses of $2^{\mathcal{N}}$ set of coalitions, which is NP-hard [179]. Hence, to reduce the calculation complexity, a clustering-based Nucleolus allocation method is proposed.

The aim of clustering is to reduce the set of the coalition. Density-Based Spatial Clustering of Applications with Noise (DBSCAN) clustering technique is used to cluster EVs. Currently, there are many clustering algorithms, such as K-Means, Affinity propagation, Ward hierarchical clustering, Birch, etc. In this chapter, we applied the DBSCAN algorithm based on the clustering feature of the energy consumption profile of EVs. The reason to apply this particular clustering technique is that there is no need to decide the number of clustering categories in advance [180], and it can effectively deal with noise points [181].

After clustering, the grand coalition $\mathcal{N}$ is changed into a new grand coalition $\mathcal{N}^*$, where $\mathcal{N}^*<\mathcal{N}$, and the set of the coalitions is reduced significantly to $2^{\mathcal{N}^*}$, where $2^{\mathcal{N}^*}\ll 2^{\mathcal{N}}$. To further improve the calculation efficiency, a nested linear program (LP) is applied. The problem of finding the nucleolus can be linearized based on the nested linear program as follows:

$$LP_1=\min_{\chi\in\mathcal{I},\varepsilon_1}\left\{\varepsilon_1\left|\varepsilon_1+\chi\left(\mathcal{T}^*\right)\ge V\left(\mathcal{T}^*\right),\forall\mathcal{T}^*\subset\mathcal{N}^*\right.\right\} \tag{5.52}$$

$$LP_2=\min_{\chi\in\mathcal{I},\varepsilon_2}\left\{\varepsilon_2\left|\begin{array}{l}\varepsilon_1^*+\chi\left(\mathcal{T}^*\right)=V\left(\mathcal{T}^*\right),\forall\mathcal{T}^*\in\mathcal{S}_1^*,\\ \varepsilon_2+\chi\left(\mathcal{T}^*\right)\ge V\left(\mathcal{T}^*\right),\forall\mathcal{T}^*\in 2^{\mathcal{N}^*}\setminus\mathcal{S}_1^*\end{array}\right.\right\} \tag{5.53}$$

$$LP_{k+1}=\min_{\chi\in\mathcal{I},\varepsilon_{k+1}}\left\{\varepsilon_{k+1}\left|\begin{array}{l}\varepsilon_r^*+\chi\left(\mathcal{T}^*\right)=V\left(\mathcal{T}^*\right),\forall\mathcal{T}^*\in\mathcal{S}_r^*,\\ \forall r\in\{1,\ldots k\}\\ \varepsilon_{k+1}+\chi\left(\mathcal{T}^*\right)\ge V\left(\mathcal{T}^*\right),\forall\mathcal{T}^*\in 2^{\mathcal{N}^*}\setminus\mathcal{H}_k^*\end{array}\right.\right\} \tag{5.54}$$

$$\mathcal{H}_k^*=\cup r\in\{1,\ldots k\}\,\mathcal{S}_r^* \tag{5.55}$$

where $\left(\chi_1,\varepsilon_1^*\right)$, $\left(\chi_2,\varepsilon_2^*\right)$, and $\left(\chi_{k+1},\varepsilon_{k+1}^*\right)$ are the optimal solutions to the LP_1, LP_2, and LP_{k+1}; $\mathcal{S}_1^*$ and $\mathcal{S}_r^*$ are the tight sets of the LP_2 and LP_{k+1} problems; $\mathcal{H}_k^*$ is the collection of the tight set

$\mathcal{S}_r^*$.

The nested LP consists of two sets of constraints, the first set of constraints $\varepsilon_r^* + \chi\left(\mathcal{T}^*\right) = V\left(\mathcal{T}^*\right), \forall \mathcal{T}^* \in \mathcal{S}_r^*, \forall r \in \{1,...k\}$ ensures that only the candidate imputations of the previous LP with the worst excess value equal to ε_r^* are considered. The second set of constraints $\varepsilon_{k+1} + \chi\left(\mathcal{T}^*\right) \geq V\left(\mathcal{T}^*\right), \forall \mathcal{T}^* \in 2^{\mathcal{N}^*} \setminus \mathcal{H}_k^*$ aims to minimize the worst excess values among all the remaining coalitions.

5.6 Case Study

5.6.1 Simulation Setting

In this chapter, the data relating to electricity prices in January of 2021 are obtained from the AEMO [160]. Three case studies are carried out to verify the effectiveness of the proposed model, which are:

Case1 No DR

Case 2 Contingent price-based DR where only demand reduction is considered [182]

Case 3 Proposed option-based DR where both demand reduction and demand enhancement are rigorously modeled.

5.6.2 Simulation Results

5.6.2.1 Results on DR strategy

Table 5-1 shows the case comparisons on costs and DR amount of the three cases mentioned above. For cost comparison, it can be found that case 1 has the highest total costs (11407 AU$). By comparison, case 3 has the lowest total costs. To be specific, the costs of the retailer and the costs of the EVA of case 3 are the lowest among the other two cases. In addition, both case 2 and case 3 incur wind uncertainty costs of 560 AU$ and 410 AU$, respectively. For DR amount comparison, case 2 only has a demand reduction amount of 842 kW, which is lower than that of case 3 (951 kW). Compared with case 2, except for demand reduction, demand enhancement of an amount of 1239 kW is also conducted in case 3.

TABLE 5-1. CASE RESULT COMPARISON OF COSTS AND DR AMOUNT

		Case 1	Case 2	Case 3
Costs (AU$)	Retailer	3248	2531	1869
	EVA	8159	6749	6347
	Social costs	11407	9280	8216
	Wind uncertainty costs	0	560	410
	Total costs	11407	9840	8606

Demand response amount (kW)	Demand reduction	0	842	951
	Demand enhancement	0	0	1239

Figs. 5-2 to 5-4 show the EV load profile components of cases 1-3. In Fig. 5-2 (case 1), no DR is considered. To balance demand-supply and satisfy the load under the uncertainty of wind power, the retailer in case 1 can only buy energy in the spot market.

Compared with case 1, case 2 in Fig. 5-3 conducts demand reduction based on contingency price to balance demand and supply under wind uncertainty [182]. As a result, the original load demand is modified into the adjusted load demand in Fig. 5-3. Additionally, the peak load of the adjusted load demand is flattened when the electricity price is high. For example, demand reduction occurs during 1:00-5:00 in the morning and 22:00-24:00 in the evening.

For case 3 in Fig. 5-4, the demand reduction amount is slightly higher than in case 2, which means the peak load is further flattened when the price is high via the exercise of the call option. Except for demand reduction, demand enhancement is also involved, such as 7:00-9:00 in the morning and 19:00-21:00 in the evening. When the electricity price and the demand are low, put options are exercised by the retailer to enhance the electricity demand of the EVA.

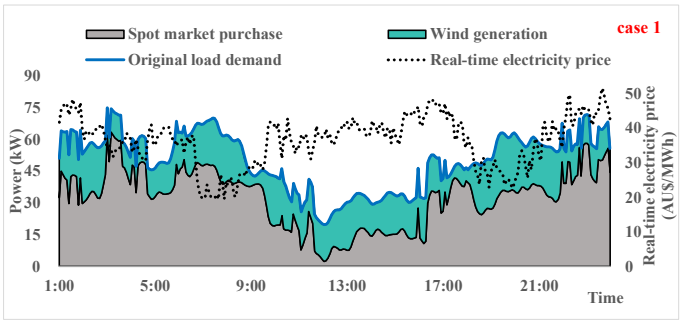

Fig. 5-2. The load profile components of case 1.

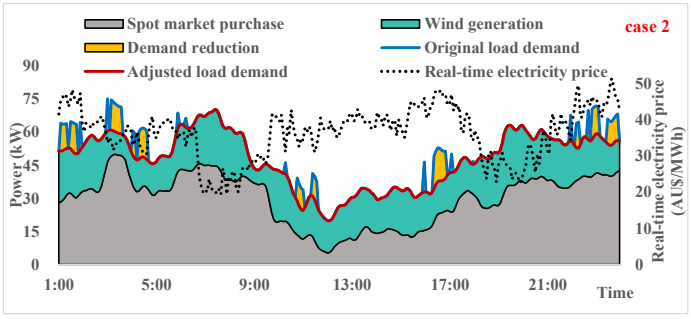

Fig. 5-3. The load profile components of case 2.

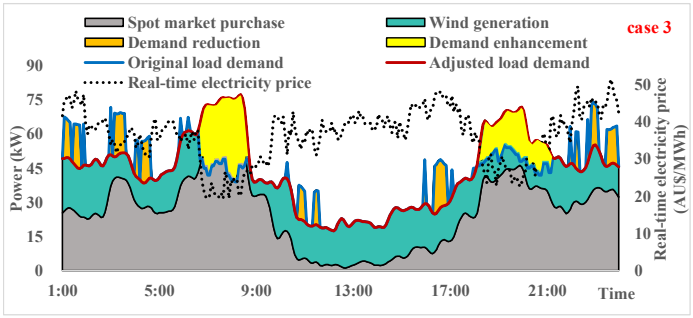

Fig. 5-4. The load profile components of case 3.

The demand reduction and demand enhancement under the proposed model in Fig. 5-4 are further decomposed into three clusters according to consumption features, which can refer to in Figs. 5-5 to 5-7.

For cluster 1 in Fig. 5-5, the EV users mainly consume energy in the morning from 6:00 to 9:00 and in the evening from 18:00 to 21:00 when the electricity price is low. It can be found that no demand enhancement is conducted. This is because, during those periods, the actual wind generation is higher than the predicted wind generation. Thus, the demand and supply are balanced. However, in the early morning, the late evening, and certain periods around 17:00, demand reduction is conducted. This is because the actual wind generation is lower than the predicted wind generation.

On the contrary, EV users of cluster 2 in Fig. 5-6 mainly consume energy in the early morning from 4:00 to 7:00, and EVs of cluster 3 in Fig. 5-7 mainly consume energy in the late evening from 21:00 to 24:00. These two clusters have two common features that are a) when the real-time price is higher than the call option exercise price, the energy demand is higher than supply, b) when the real-time price is lower than the put option exercise price, the demand is lower than the supply. As a result, both demand reduction and demand enhancement are conducted. The differences are that the total demand enhancement of cluster 2 in Fig. 5-6 is lower than that of cluster 3 in Fig. 5-7, whereas the total demand reduction of cluster 2 is slightly higher than that of cluster 3.

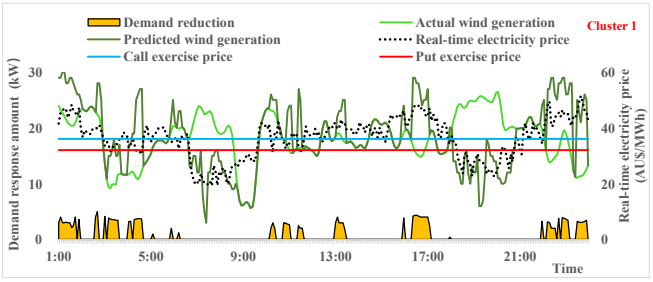

Fig. 5-5. The DR decision for cluster 1.

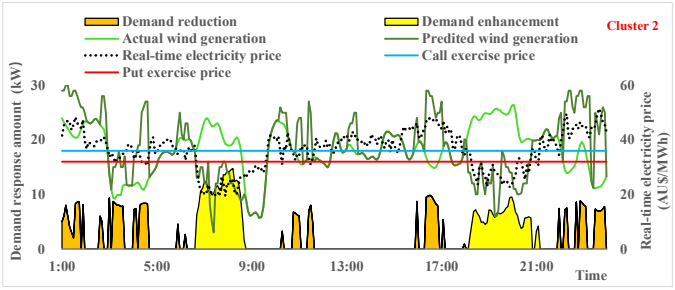

Fig. 5-6. The DR decision for cluster 2.

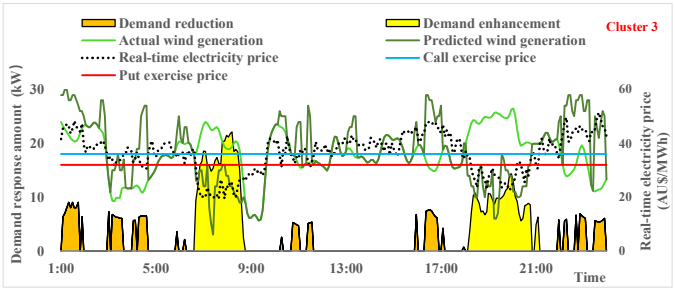

Fig. 5-7. The DR decision for cluster 3.

5.6.2.2 Results on cost saving allocation

In the following section, the cost savings from option-based DR are allocated via both the Shapley method and the proposed clustering-based Nucleolus allocation. Note that using the traditional Nucleolus allocation method will get quite similar allocation results as using the clustering-based Nucleolus method. The only difference is that the proposed method is more computationally efficient. Hence, the traditional Nucleolus is not analyzed.

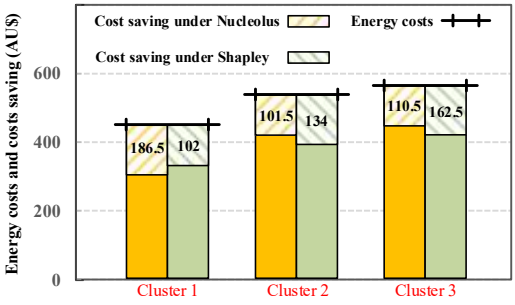

Fig. 5-8. The energy costs and cost saving allocation of the three clusters under both Shapley and the clustering-based Nucleolus allocation.

In Fig. 5-8, the energy costs and costs saving allocation of the three clusters under both Shapley and Nucleolus allocation methods are illustrated. For energy costs, the three clusters are different, in which cluster 3 has the largest energy costs, while cluster 1 has the smallest energy costs. This is because the EVs in cluster 3 participate more in DR (larger total DR amount), which can be proven via Fig. 5-7. By contrast, EVs in cluster 1 are less engaged in the DR. For cost saving, the total cost saving (398.5 AU$) of the three clusters under either allocation method is the same. However, the allocation within each

cluster is varied. For Shapley, the mechanism is to allocate more cost saving to EVs that have contributed more to the DR, i.e., cluster 3. Hence, cluster 3 has the highest cost saving allocation of 162.5 AU$ under the Shapley method. By comparison, the mechanism of the clustering-based Nucleolus allocation method is to ensure the least engaged EV users participate in the DR process. Thus, cluster 1 has the most cost saving of 186.5 AU$.

Fig. 5-9 shows the largest excess averaged over 30 runs under different numbers of EVs in the grand coalition. It is found that the excess value of Shapley is always positive, which means the allocation under the Shapley method is unstable, i.e., (5.50) is not satisfied. On the contrary, the excess under the Nucleolus method is non-positive, which indicates that the allocation under clustering-based Nucleolus is stable.

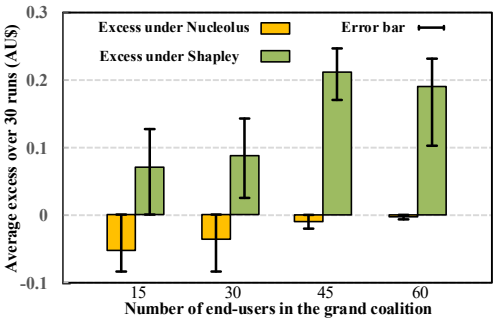

Fig. 5-9. The largest excess averaged over 30 runs.

Fig. 5-10 illustrates the linearization of the allocation process under the proposed clustering-based Nucleolus allocation method. The largest tetrahedron represents the imputation defined in section 5.5.1. The green tetrahedron is the core in equation (5.50), and it is also the LP1 (linear program) process. Within the core, it satisfies X1+X2<V(1,2), X1+X3<V(1,3), and X2+X3<V(2,3). For the LP2 process, it is illustrated as a thick black line. Lastly, in the LP3 process, the nucleoli of the three clusters under the clustering-based Nucleolus method are found shown as the red dot (X1=186.5, X2=101.5, X3=110.5).

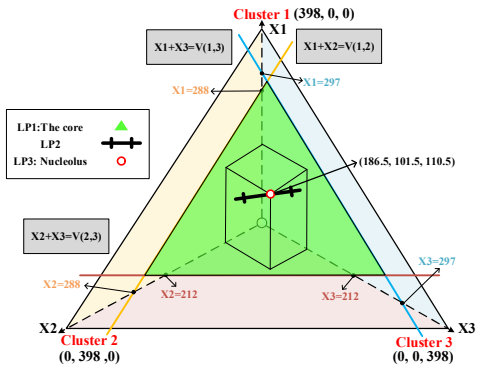

Fig. 5-10. The LPs process under the proposed clustering-based Nucleolus.

TABLE 5-2 BRIEF COMPARISON OF THE TWO ALLOCATION METHODS

No. of EVs:60	**Cost saving allocation (AU$)**	**Stability**
Shapley	X1=102, X2=203, X3=215	0.18
Clustering-based Nucleolus	X1=186.5, X2=101.5, X3=110.5	0

Table 5-2 briefly compares the simulation results of the two allocation methods from two aspects. As for cost saving allocation, detailed explanations can be referred to in Fig. 5-8. From the perspective of stability, the proposed Nucleolus is more stable than the Shapley allocation method, which indicates the satisfaction of the EVs toward the cost saving allocation is ensured using the proposed allocation method.

5.7 Conclusion

In this chapter, option-based DR is proposed to mitigate the imbalance of demand and supply caused by the intermittent feature of wind power generation. First, the EVA is incentivized to alter the energy consumption pattern via the option-based DR conducted by the retailer. Then, the cost saving of the EVA obtained from the option-based DR is allocated among the EV users via the proposed clustering-based Nucleolus allocation method. Results indicate that the proposed option-based DR can save costs for both the retailer and the EVA compared with the price-based DR strategy at 26.2% and 6%, respectively. Furthermore, the proposed allocation method is more stable compared with the Shapley method, and it can ensure the satisfaction level of the EV owners toward the allocation.

6. DEMAND RESPONSE AGGREGATION WITH OPERATING ENVELOPE BASED ON DATA-DRIVEN STATE ESTIMATION AND SENSITIVITY FUNCTION SIGNALS

With the increasing penetration of renewable energy sources (RES), the value of the demand response (DR) draws wide attention. In order to realize the coordinated dispatch of widely spread resources, the aggregation of the controllable residential loads is managed by a single entity, namely the DR aggregator. Under price-based DR programs, the DR aggregators actively respond to market signals to reach maximum welfare. To avoid the quality of electricity services being jeopardized, the operational constraints of the network should be considered by the DR aggregators. However, DR aggregators are not expected to have access to the monitoring equipment and have limited knowledge of the network states. Hence, in this chapter, we proposed a DR aggregation with the operating envelope framework based on the representative signals produced by the distributed network operator (DNO) in the context of big data era. The DNO provides representative signals, including real-time state estimation and sensitivity functions, to the DR aggregators based on the proposed Semi-supervised Coupled Generative Adversarial Imputation Network (SC-GAIN) and big data analysis. The DR aggregators can realize the secure and efficient real-time dispatch of the controllable loads based on the received signals. The proposed framework was verified on the IEEE 33-bus and 123-bus systems. The case studies show that the proposed SC-GAIN algorithm can better deal with the missing data, and the learned sensitivity functions can effectively avoid the overestimation of the true DR potential

6.1 Introduction

Motivated by the growth in the share of RES, the distribution network faces significant changes. Although RES provides substantial contributions to the sustainability of the power grids, the intermittent renewable energy outputs can arouse severe security problems to the network assets. In order to make the future grids more active and flexible, DR is considered as a promising approach.

The DR can be categorized into incentive-based DR programs and price-based DR programs. In the incentive-based DR programs, the end-users are provided with financial incentives, and they are obliged to respond to the DR signals [183]. The incentive-based DR programs can be further classified into direct load control and load curtailment. Direct load control allows the system operators to directly manage the

end-users' appliances via remote control technologies [184-187]. Different from direct load control, the load curtailment programs only authorize the system operator to cut down the end-users' supply during a contingency [188, 189]. However, even though the incentive-based DR is an effective approach to save the network operation costs and solve stability issues, it will obviously result in privacy and comfort problems for the end-users.

Compared with incentive-based DR programs, price-based DR programs are more flexible. The electricity usage profiles are stimulated by different electricity price signals, such as TOU price [190], real-time price (RTP) [191], and critical peak price (CPP) [192]. The end-users schedule the controllable loads to earn maximum welfare by responding to the price signals actively [193]. In order to integrate widely spread controllable resources, different prosumers are aggregated to form collusion to earn the largest benefits [76, 77, 194, 195].

Nevertheless, when the DR aggregation becomes large, an improper DR strategy may cause infeasibilities in the system operation, such as voltage violation and thermal overloading problems, which jeopardize the security of the electricity services [75]. Therefore, it is improper to neglect the network constraints like [76, 77]. In a price-based DR strategy, the DNO does not directly control the controllable loads but takes responsibility for formulating DR prices to stimulate customers [196, 197]. The customers are expected to respond to the DR prices. However, in real applications, it is difficult for DNO to obtain the detailed demand elasticities, cost functions, and utility functions of all the customers. Hence, the true DR potential may be overestimated [75], which will result in the abovementioned problems in power systems. DNO cannot always both meet the DR requirements and satisfy the grid safety constraints merely through price stimulations. Then, to ensure the network security and quality of the electricity services, DNO has to block parts of the DR requests in real-time if the DR of the customers arouses the violation of the network constraints [198]. However, this operation behavior of DNO will cause disutility to the customers. Ref. [15] presented an extended multi-perspective model for residential thermal DR in energy and capacity markets. To consider the network constraints, the power flow model was considered at the lower level in the market clearing. Ref. [20] proposed a tri-layer integrated DR model where the physical constraints of the different networks were strictly considered. To address the nonlinear and nonconvex problems in the distribution network, the mixed-integer second-order cone programming method and the piecewise linearization process were used. Ref. [199] pointed out that the reliable and

cost-effective integration of DR requires accounting for their physical properties from the system perspective. Therefore, in their proposed model, the Markov decision model for thermostatically controlled loads was integrated with a chance-constrained optimal power flow that accounts for the uncertainty of photovoltaic resources. Ref. [200] proposed a model-based predictive control method for the utilization of flexible resources effectively to provide DR in low-voltage distribution networks with solar photovoltaic, taking into account system states. In the proposed method, a linear power flow method based on the relaxation of branch power losses applicable to radial distribution networks was formulated. In [201], the DR further considered the network constraints and operational constraints of three-phase unbalanced distribution systems. In these references, although the network constraints were considered in the optimization problem of the DR aggregator, they ignore that the load scheduling and power dispatch are the tasks performed by different agents in a price-based DR program. In other words, the prosumers or DR aggregators are not authorized to access the information of network variables, and they do not have the capability to solve the OPF problem on their own knowledge. To fully address the aforementioned problem, a novel DR aggregation with the operating envelope framework is proposed in this chapter. The main contributions can be summarized as follows:

- First, in the proposed framework, the DR strategy of the aggregator can fully consider the operational constraints of the power systems without obtaining full information about the electricity network. In the existing literature, such as [199], the DR aggregator is assumed to master all the system information, including network parameters and variables, to consider network constraints in the optimization problem. Different from the existing references, in the proposed framework, DNO and the DR aggregator belong to different agents that can cooperate to realize the real-time DR with an operating envelope via limited exchanges of representative information. Therefore, the DR aggregator can choose a preferable usage profile within the operating envelope, which provides more initiatives to the DR aggregator. The improvement of the DR scheduling structure to coordinate the DR aggregator and DNO is of great practical significance. With the proposed framework, the DR aggregator is not required to obtain unauthorized data at a higher level, and less communication burden will be brought to the cyber-physical network. Since less information exchange is required, data security problems will be unlikely to occur.
- Second, to provide accurate representative information to the DR aggregator, DNO realizes the real-

time state estimation based on the weighted total least squares (WTLS) estimator [202]. However, in real applications, missing data occur regularly due to various reasons, such as sampling failure, communication delay, or loss of phasor measurement units (PMUs). To deal with the missing data, a Semi-supervised Coupled Generative Adversarial Imputation Network (SC-GAIN) is proposed to impute the missing value. Compared with the conventional Generative Adversarial Network (GAN)-based learning structure, the algorithm is extended to better solve the imputation problem in an electrical context. The coupling learning structure is proposed to learn the joint distribution of multi-domain electric states in power systems by enforcing a weight-sharing constraint. Besides, the conventional GAN is further extended to the semi-supervised context by forcing the discriminator to predict class labels so that a more data-efficient discriminator can be trained to help GAN impute the missing data with high quality. The proposed learning structure is verified in case studies. Simulation results show that the proposed methodology has lower estimation errors and can better deal with missing data compared with state-of-the-art methods [202-204].

- Third, the sensitivity function is regarded as the representative information delivered by DNO to the DR aggregator. The sensitivity function is learned by the DNO based on big data analysis. The sensitivity function is a set of independent linear and quadratic equations obtained by aggregators based on the state estimation of DNO, which characterize the magnitude of the network variables, including power flows and voltage, and current, as a function of the DR allocation. Based on the received sensitivity function, the DR aggregator can estimate the operating envelope accurately. By using the proposed sensitivity function, the true flexibility that DR brings to the power systems can be studied. Compared with the sensitivity factor used in [75], the proposed methodology can better estimate DR capacity to ensure that the network constraints are not violated.

6.2 Conventional Price-based Demand Response Scheduling

6.2.1 Objective Function

In this section, we present a conventional price-based DR scheduling model based on [191] and [199]. We further extend the mathematical model in reference to more types of controllable resources and reactive power DR.

In the price-based DR scheduling, the DR aggregators actively respond to two signals λ_t^P and λ_t^Q, representing suitably accurate prediction of system requirements on active and reactive power,

respectively, i.e., predicted day-ahead electricity price. The objective function is to minimize the total energy consumption cost in equation (6.1).

$$\min \sum_{t} \left(\lambda_t^P P_{j,t}^{Tot} \Delta t + \lambda_t^Q Q_{j,t}^{Tot} \Delta t \right) \tag{6.1}$$

where $P_{j,t}^{Tot}$ and $Q_{j,t}^{Tot}$ are the total active and reactive power consumption of the controllable load at bus *j*; λ_t^P and λ_t^Q are the weights for each time step *t* of the scheduling horizon.

The total active and reactive power consumption of the controllable load can be further decomposed as equations:

$$P_{j,t}^{Tot} = P_{j,t}^{SL} + P_{j,t}^{ESS,CH} - P_{j,t}^{ESS,DS} + P_{j,t}^{HVAC} - P_{j,t}^{PV} \tag{6.2}$$

$$Q_{j,t}^{Tot} = Q_{j,t}^{SL} - Q_{j,t}^{ESS} + Q_{j,t}^{HVAC} - Q_{j,t}^{PV} \tag{6.3}$$

where $P_{j,t}^{SL}$ and $Q_{j,t}^{SL}$ are the active and reactive power consumption of the shiftable load; $P_{j,t}^{ESS,CH}$ and $P_{j,t}^{ESS,DS}$ are the charging and discharging power of the BESS; $P_{j,t}^{HVAC}$ and $Q_{j,t}^{HVAC}$ are the active and reactive power consumption of the HVAC; $P_{j,t}^{PV}$ is the active power generation of the DGs; $Q_{j,t}^{ESS}$ is the reactive power generation of the BESS from smart inverter; $Q_{j,t}^{PV}$ is the reactive power generation of the photovoltaics (PVs) from smart inverters.

6.2.2 Device Operating Constraints

The operating constraints of the controllable devices are modeled mainly based on [191]. These constraints include the upward and downward power limits of the controllable devices, the energy balance equation of the BESS, and the thermodynamic behavior of the HVAC. Detailed models can be referred to in the Appendix.

6.2.3 Operating Envelope Constraints

In the conventional model, the DR aggregator is assumed to master all the system information [199]. To ensure that the scheduling of the DR aggregators is feasible, the following network constraints should be met:

$$P_{ij,t}^{B} - \sum_{k \in \Omega_j^+} P_{jk,t}^{B} - P_{j,t}^{ST} + P_{j,t}^{Tot} = r_{ij} \left(\left(P_{ij,t}^{B} \right)^2 + \left(Q_{ij,t}^{B} \right)^2 \right) \Big/ V_{j,t}^2 \tag{6.4}$$

$$Q_{ij.t}^{B}-\sum_{k\in\Omega_{j}^{+}}Q_{jk.t}^{B}-Q_{j,t}^{ST}+Q_{j,t}^{Tot}=x_{ij}\left(\left(P_{ij,t}^{B}\right)^{2}+\left(Q_{ij,t}^{B}\right)^{2}\right)\Big/V_{j,t}^{2} \tag{6.5}$$

$$V_{i,t}^{2}-V_{j,t}^{2}=2\left(r_{ij}P_{ij,t}^{B}+x_{ij}Q_{ij,t}^{B}\right)-\left(r_{ij}^{2}+x_{ij}^{2}\right)\frac{\left(P_{ij,t}^{B}\right)^{2}+\left(Q_{ij,t}^{B}\right)^{2}}{V_{i,t}^{2}} \tag{6.6}$$

$$\left(I_{ij,t}\right)^{2}=\frac{\left(P_{ij,t}^{B}\right)^{2}+\left(Q_{ij,t}^{B}\right)^{2}}{V_{i,t}^{2}} \tag{6.7}$$

$$\underline{V_{i}}\le V_{i,t}\le\overline{V_{i}},\left(I_{ij,t}\right)^{2}\le\left(I_{ij}^{\max}\right)^{2} \tag{6.8}$$

$$-P_{ij}^{B,\max}\le P_{ij,t}^{B}\le P_{ij}^{B,\max},-Q_{ij}^{B,\max}\le Q_{ij,t}^{B}\le Q_{ij}^{B,\max} \tag{6.9}$$

$$\left(P_{ij,t}^{B}\right)^{2}+\left(Q_{ij,t}^{B}\right)^{2}\le\left(S_{ij}^{B,\max}\right)^{2} \tag{6.10}$$

where Ω_{j}^{+} is the set of electric buses connecting to bus *j*; $P_{ij,t}^{B}$ and $Q_{ij.t}^{B}$ are the active and reactive power flow; $P_{j,t}^{ST}$ and $Q_{j,t}^{ST}$ are the active power and reactive power from the sub-station; r_{ij} and x_{ij} are the resistance and reactance; $V_{i,t}$ is the nodal voltage; $I_{ij,t}$ is the branch current; $I_{ij}^{\max}$ is the maximum current magnitude; $P_{ij}^{B,\max}$ and $Q_{ij}^{B,\max}$ are the maximum active and reactive power flow; $S_{ij}^{B,\max}$ is the maximum apparent power flow.

Equations (6.4)-(6.7) are the DistFlow equations [199, 205]. Equation (6.8) is the limits of the voltage and current magnitude. Equation (6.9) is the active and reactive power flow limits. Equation (6.10) is the limit of the apparent power.

6.3 Proposed DR Aggregation Framework based on Representative Signals Produced by DNO

While the previous references highlight the importance of network physical constraints in DR programs, the effective coordination between the DNO and the customers has not been discussed. Usually, the residential DR is operated by a DR aggregator on behalf of the interest of the participated customers but is less concerned about the physical network constraints. The responsibility of the DNO is to monitor the system state and ensure that electricity services are not jeopardized with the monitoring and control infrastructures. Note that DNO does not care about end-user interests. Thus, DR and power dispatch are tasks that belong to different agents and lack coordination. In the existing references like [199-201, 206], the network physical constraints are integrated into the optimization problem of the DR

aggregator. It indicates that the DR aggregator needs to access the full information of the electricity network. However, in applications, the DR aggregators are not expected to access the monitoring equipment. It is impractical for the DR aggregator who operates the devices at the behind-meter level to be authorized to access the information at a higher level (distribution level) from the DNO. Although it seems trivial that the DR aggregator cannot obtain full information about the electricity network, hidden critical problems, including communication burden and data security, may exist. Therefore, the DR aggregator has limited knowledge of the network states, and they do not have the capability to solve the optimization problem with the operating envelope constraints (6.4)-(6.10) embedded. In this chapter, we proposed a DR aggregation framework, shown in Fig. 6-1, where the DR aggregators can dispatch the controllable resources with the operating envelope based on the representative signals produced by the DNO. Based on the proposed method, the DR aggregator does not require complete information of the system states. DNO and DR aggregators belonging to different agents can cooperate to realize the real-time DR with the operating envelope via limited exchanges of representative information.

In the proposed framework, the DNO first predicts the network variables, such as demand, and produces the sensitivity functions in the day ahead. In the sensitivity function, the magnitude change of the electric states in power systems (including voltage magnitude, current magnitude, active power flow, and reactive power flow) is a function of DR allocation (such as an increase in active and reactive power). Then DNO sends the representative signals to the DR aggregators. The representative signals are the system variables and the sensitivity functions related to the point of the connection of the DR aggregators. The DR aggregators solve the day-ahead DR scheduling formulated in section 6.5.1 based on these representative signals. In the real-time control, the DNO conducts the real-time state estimation introduced in section 6.4.1 and produces the sensitivity functions introduced in section 6.4.3. The real-time state estimation and sensitivity functions are supported by data-driven methodologies. Based on the received representative signals, the DR aggregators realize the real-time dispatch of the aggregated controllable resources with the operating envelope formulated in section 6.5.2. The individual dispatch behind the coordination is out of the scope of our chapter.

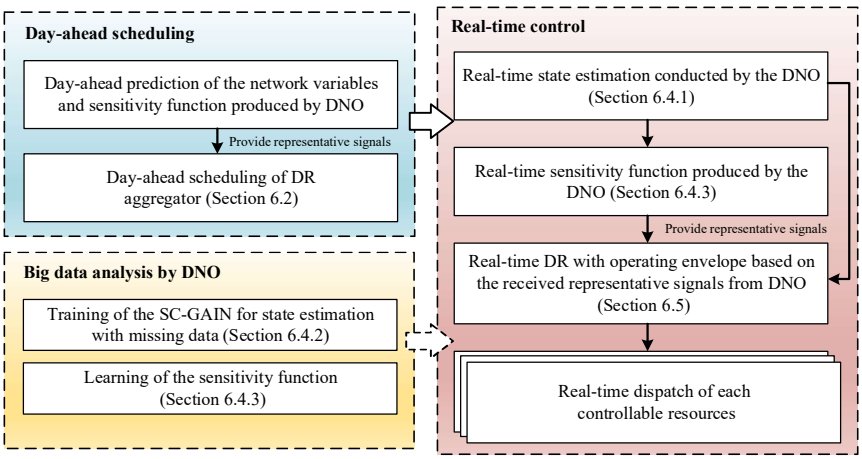

Fig. 6-1. Proposed DR aggregation framework.

6.4 State Estimation and Sensitivity Analysis of DNO Based on Data-Driven Methodology

6.4.1 State Estimation based on PMU Measurement

The measurements of the system states include the actual measurements and the pseudo-measurements. The actual measurements are based on PMUs, which are capable of measuring time-synchronized phase-angles, voltage amplitudes, and branch current phasor.

The phase-angle at bus *i* can be formulated by the first-order Taylor series approximation of $e^{j\delta_i}$:

$$e^{j\delta_i} \approx e^{j\delta_i^{MS}} + je^{j\delta_i^{MS}} \varsigma_{\delta_i} \tag{6.11}$$

where δ_i and δ_i^{MS} are the true and measured phase angle at bus *i*; ς_{δ_i} is the measurement error of the phase angle.

The phase measurement of the voltage at the i^{th} bus is:

$$\widehat{V}_i = \widehat{V}_i^{MS} + \varsigma_{\widehat{V}_i} \tag{6.12}$$

where $\widehat{(\bullet)}$ represents the complex value; $\widehat{V}_i$ and $\widehat{V}_i^{MS}$ are the true and measured voltage; $\varsigma_{\widehat{V}_i}$ is the complex voltage phasor measurement error, which can be further expressed as:

$$\varsigma_{\widehat{V}_i} = e^{j\delta_i}\left(\varsigma_{V_i} + j\varsigma_{\delta_i} V_i\right) \tag{6.13}$$

PMUs can directly measure the branch current phasor:

$$\hat{I}_{ij}^{MS} + \varsigma_{\hat{I}_{ij}} = \left(\left(Y_{ij}/2\right) + \left(1/Z_{ij}\right)\right)V_i + \left(-\left(1/Z_{ij}\right)\right)\widehat{V}_j \tag{6.14}$$

where $\hat{I}_{ij}^{MS}$ is the measured current; Y_{ij} and Z_{ij} are the admittance and impedance of feeders; $\varsigma_{\hat{I}_{ij}}$ is the complex current phasor measurement error, which can be further expressed as:

$$\varsigma_{\hat{I}_{ij}} = e^{j\theta_{ij}} \left(\varsigma_{I_{ij}} + j\varsigma_{\theta_{ij}} I_{ij} \right) \tag{6.15}$$

where I_{ij} and θ_{ij} are the current magnitude and phasor angle.

Even though there is an increased monitoring capability in the distribution system, widespread monitoring is not available in the short term. In this case, DNO will generate pseudo-measurements of the active and reactive power injection from the actual measurements. The pseudo-measurements are generated from the actual measurements of voltage magnitude and voltage angle based on big data analysis of the system states through regressing the linear relationship between $[\boldsymbol{P}, \boldsymbol{Q}]$ and $[\boldsymbol{V}, \boldsymbol{\delta}]$, shown as (6.16).

$$\begin{bmatrix} \boldsymbol{P} \\ \boldsymbol{Q} \end{bmatrix} = \begin{bmatrix} \mathbb{A}_{11} & \mathbb{A}_{12} \\ \mathbb{A}_{21} & \mathbb{A}_{22} \end{bmatrix} \begin{bmatrix} \boldsymbol{V} \\ \boldsymbol{\delta} \end{bmatrix} + \begin{bmatrix} \mathbb{C}_1 \\ \mathbb{C}_2 \end{bmatrix} \tag{6.16}$$

where $\mathbb{A}$ and $\mathbb{C}$ are the regression matrix and bias vector.

First, the historical and generated load profiles for the targeted network are entered into the simulation platform to calculate the power flow and nodal voltage. With numerous times of simulations, a specific electricity network operation library can be built. Then, Bayesian regression is utilized to regress the relationship between $[\boldsymbol{P}, \boldsymbol{Q}]$ and $[\boldsymbol{V}, \boldsymbol{\delta}]$. The detailed model can be referred to [207].

In the real-time estimation, when the actual measurements of voltage magnitude and voltage angle are obtained, the pseudo-measurements can be calculated according to equation (6.16). After obtaining the actual and pseudo-measurements, DNO will figure out the state estimation by correcting the value of the actual and the pseudo-measurements based on the weighted total least squares (WTLS) problem [208], which can be formulated as:

$$\min \left\| \begin{bmatrix} \widehat{\boldsymbol{X}}^T & \widehat{\boldsymbol{Y}}^T & \widehat{\boldsymbol{I}}^T \end{bmatrix} - \begin{bmatrix} \boldsymbol{X}^T & \boldsymbol{Y}^T & \boldsymbol{I}^T \end{bmatrix} \right\|^2_{\sum^{-1}} \tag{6.17}$$

$$\widehat{\boldsymbol{Y}} = \mathbf{A}\widehat{\boldsymbol{X}} + \boldsymbol{C}\mathbf{1}^T \tag{6.18}$$

where $\boldsymbol{Y} = [\boldsymbol{P}, \boldsymbol{Q}]^T$; $\boldsymbol{X} = [\boldsymbol{V}, \boldsymbol{\delta}]^T$; $\widehat{(\bullet)}$ is the estimated value.

The expression $\|\cdot\|^2_{\sum^{-1}}$ represents the weighted matrix norm. For a given matrix $\boldsymbol{M}$, the weighted matrix norm is:

$$\|\boldsymbol{M}\|^2_{\sum^{-1}} := vec(\boldsymbol{M})^T \sum^{-1} vec(\boldsymbol{M}) \tag{6.19}$$

where $vec(\cdot)$ represents the operation that reshapes a matrix into a vector; $\sum^{-1}$ represents the

covariance matrix.

6.4.2 State Estimation based on the Proposed SC-GAIN

When there is a decrease in the number of PMUs, indicating fewer actual measurement data, the state estimation error based on the WTLS estimator will increase [203], and the pseudo-measurement obtained from equation (6.16) is unreliable. Therefore, we proposed a Generative Adversarial Network (GAN)-based approach to impute the missing data.

6.4.2.1 Conventional GAN-based learning structure

The GAN is a kind of unsupervised learning algorithm that can generate data with a realistic feature and has been gradually utilized in power system problems in recent years [209, 210]. The structure of GAN is shown in Fig. 6-2. It consists of two deep neural networks: Generator (*G*) and Discriminator (*D*) [211]. The input of the generator is a series of random numbers, and the output is the data that follows the real distribution. The input of the discriminator contains the real historical data (true) and the data generated by the generator (false). The task of the discriminator is to distinguish these two kinds of data, and hence the output of the discriminator is a scalar (0/1). The two networks are trained at the same time and form a zero-sum game framework. Through the training, GAN will reach an equilibrium the discriminator can no longer pick out the generated data, indicating that the generated data follow the real distribution.

Generator: Denote the input of the generator as a vector z under a prior distribution $z\sim p_z(z)$. Denote the true sampling distribution of the states of the power system as p_r. The objective of the generator is to learn a function $G\left(z;\theta_G\right)$ following distribution p_g that is as close to p_r as possible. Therefore, the value function of the generator can be formulated as (6.20).

Discriminator: Denote a multilayer perceptron $D\left(x;\theta_D\right)$ that outputs a scalar. The outputted scalar indicates the probability that data x is sampling from p_r rather than being generated. The objective of the discriminator is to maximize the probability of the correct label between the real data $E[D(x)]$ and the generated data $E[D(G(z))]$, shown as (6.21).

$$\max_G V\left(D,G\right)=\max_G\left\{E_{z\sim Pz(z)}\left[\log\left(D\left(G\left(z\right)\right)\right)\right]\right\} \tag{6.20}$$

$$\max_D V(D,G)=\max_D\begin{Bmatrix}E_{x\sim Pr(x)}\left[\log D\left(x\right)\right]\\+E_{z\sim Pz(z)}\left[\log\left(1-D\left(G\left(z\right)\right)\right)\right]\end{Bmatrix} \tag{6.21}$$

Equation (6.20) can be transformed to equation (6.22) as:

$$\min_G V(D,G) = \min_G \left\{ E_{z\sim Pz(z)} \left[\log\left(1 - D\left(G\left(z\right)\right)\right) \right] \right\} \tag{6.22}$$

When combining (6.21) and (6.22), the Nash equilibrium of the two-player iterative mini-max game can be found through solving (6.23).

$$\min_G \max_D V(G,D) = \min_G \max_D \left\{ \begin{matrix} E_{x\sim Pr(x)} \left[\log D(x) \right] \\ + E_{z\sim Pz(z)} \left[\log\left(1 - D\left(G\left(z\right)\right)\right) \right] \end{matrix} \right\} \tag{6.23}$$

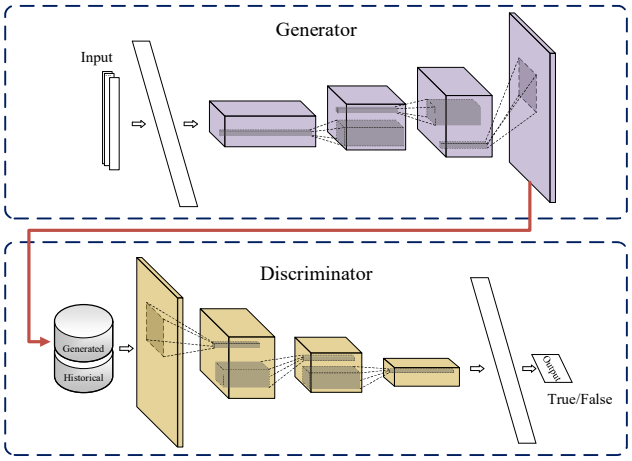

Fig. 6-2. Conventional GAN-based learning structure.

6.4.2.2 Proposed SC-GAIN for state estimation with missing data

Based on the specific characteristic of the power system, we proposed an SC-GAIN learning structure for the state estimation with missing data shown in Fig. 6-3. The SC-GAIN, whose full name is Semi-supervised Coupled Generative Adversarial Imputation Network, is a learning structure to impute the missing data based on the adversarial framework [212]. To make the learning structure better adapt to the electrical context, a coupled network is designed for the data in different domains so that the joint distribution of the voltage magnitude, phase angle, and branch current can be learned. Besides, the discriminator will judge whether the outputted data belongs to the phase-angle, voltage, current, or fake, indicating a semi-supervised learning process. The detailed design of SC-GAIN will be illustrated in the following parts.

To impute the missing data, the mask vector $\mathbf{M}=[M_1,M_2,\ldots M_n]$ is designed. The mask vector has the same dimension as the original data. If the elements in the original data are unobserved, mark the elements in the mask vector at the corresponding places as 0. Our aim is to impute the unobserved data whose masks equal 0.

The missing data of the PMUs include three domains, i.e., phase-angle, voltage, and branch current.

In power systems, these three domains have interconnections and are correlated. Combining the unique characteristics of the data in power systems, we aim to learn a joint distribution of the data in three different domains. Therefore, the true characteristics of the electric states in power systems are expected to be learned. Hence, we propose a coupled generative adversarial imputation network (C-GAIN) structure consisting of three coupled networks, i.e., $GAIN_A$, $GAIN_V$, and $GAIN_I$. Each network is responsible for imputing the missing data in its individual domain. Three networks are coupled by sharing the common weights, shown in Fig. 6-3. According to [213], the first layer of the network appears not to extract the features of a specific task but general in that they are applicable to many tasks. Features must eventually transit from general to specific by the last layer of the network. Therefore, the common features of the three domains can be learned in the proposed coupled network with sharing weight parameters. This specific design builds bridges between three independent tasks to enhance the learning performance, which can effectively prevent the circumstance that one task faces overfitting while the other faces underfitting.

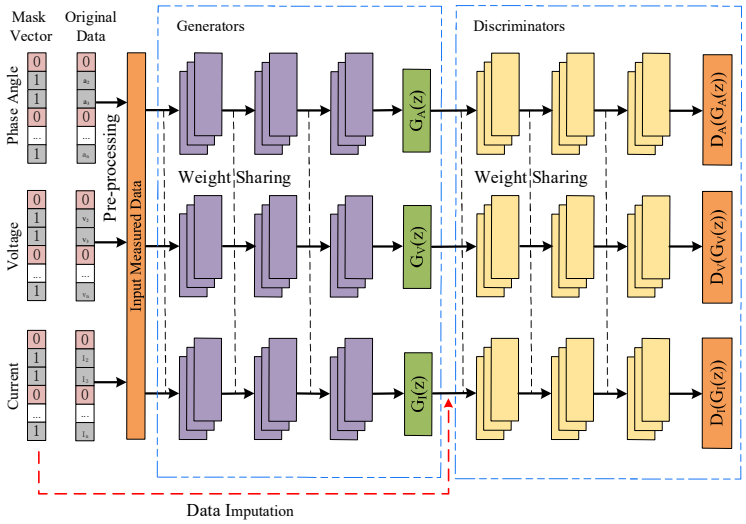

Fig. 6-3. Proposed SC-GAIN learning structure.

The input of the generator in the proposed network is the measured data, with unobserved data excluded from the original data in all domains. The input data is passed to the generators to impute the missing data. The generators have three convolutional layers, which share the common weight as hidden layers and one fully connected layer with unique weights as the output layer. The imputed values are recovered to the original data sequence according to the mask vector and then sent to the discriminators to see whether the imputation can cheat the discriminators. Each discriminator also has three convolutional layers and one fully connected layer. A zero-filling operation is conducted to ensure that

the three networks are homogeneous. The layers which share the common weight are actually merged into one channel. The whole propagation process can be summarized as follow: first, the input data in three domains are first spliced into one vector. Then, the input data pass through the first three convolutional layers. After that, the network is branched into three channels, each corresponding to different output layers. The raining/propagation process of the discriminator is similar. Therefore, the training of the SC-GAIN is the same as a normal multi-channel neural network.

The discriminator in a normal GAN outputs a probability that the data is imputed. In order to generate higher quality data, the GAN is extended to a semi-supervised context by forcing the discriminator to output the class label of the data. In other words, the discriminator should judge whether the outputted data belongs to the phase-angle, voltage, current, or fake.

The proposed SC-GAIN is trained according to the following value function:

$$\begin{aligned}&\min_{G_A G_V G_I}\max_{D_A D_V D_I} V(G_A,G_V,G_I,D_A,D_V,D_I)=\\&\sum E_{x\sim Pr(x)}\left[\sum_{c=1}^{3} y_{x,c}\log D(x)\right]+\sum E_{z\sim Pz(z)}\left[\log\left(1-D\left(G(z)\right)\right)\right]\end{aligned} \tag{6.24}$$

where c is the class of the label (1: phase angle; 2: voltage; 3: current; 4: fake); $y_{x,c}$ is the indicator (0 or 1). If the label is the same as the class of x, it equals 1; G_A, G_V, G_I and D_A, D_V, D_I are the generators and discriminators of the three domains marked in Fig. 6-3. It should be noted that G is the collective name of G_A, G_V, G_I, while D is the collective name of D_A, D_V, D_I.

6.4.3 Proposed Sensitivity Function Analysis Method

6.4.3.1 Network sensitivity function

In the real application, the DR aggregators do not have access to the network data, and they cannot solve the OPF problem to realize the operating envelope. However, it has been proved that the network sensitivity factor can provide quantified variation in the network variables due to the change in the power consumption in different types of network topologies. Denoting the network variable as $\varepsilon_{i,t}$, the operating envelope of the DR aggregators can be formulated in the form of (6.25) (linear form for voltage, active power, and reactive power; quadratic form for complex power and current).

$$\varepsilon_i^{\min} \le \varepsilon_{i,t} \le \varepsilon_i^{\max}, \left(\varepsilon_{i,t}\right)^2 \le \varepsilon_i^{(2)\max} \tag{6.25}$$

where $\varepsilon_i^{\min}$ and $\varepsilon_i^{\max}$ are the minimum and maximum state magnitude; $\varepsilon_i^{(2)\max}$ is the maximum

quadratic limit of the state.

In [75], linear regression is utilized to regress the sensitivity factor shown as:

$$\varepsilon_{i,t} = \widehat{\varepsilon}_{i,t} + o_i^P \Delta P_{i,t}, \varepsilon_{i,t} = \widehat{\varepsilon}_{i,t} + o_i^Q \Delta Q_{i,t} \tag{6.26}$$

where o_i^P and o_i^Q are the sensitivity factor, $\widehat{\varepsilon}_{i,t}$ is the estimated state variables from the DNO.

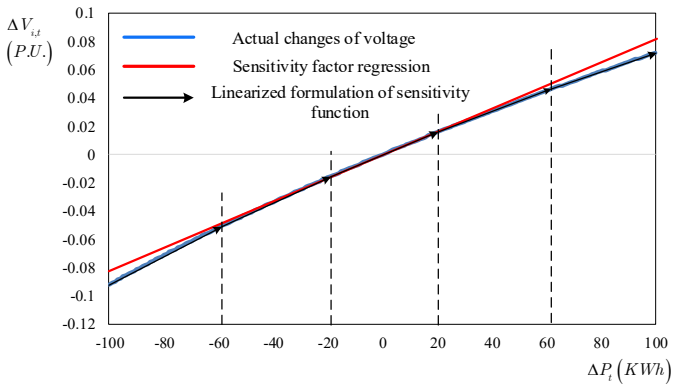

Fig. 6-4. Sensitivity function and sensitivity factor.

However, shown in Fig. 6-4, the accuracy of using linear regression to model the nonlinear problem is questioned. Therefore, in this chapter, we proposed a more accurate model. A sensitivity function is learned based on the big-data analysis shown as:

$$\varepsilon_{i,t} = \widehat{\varepsilon}_{i,t} + g_i^P\left(\Delta P_{i,t}\right), \varepsilon_{i,t} = \widehat{\varepsilon}_{i,t} + g_i^Q\left(\Delta Q_{i,t}\right) \tag{6.27}$$

where $g_i^{P_i}\left(\Delta P_{i,t}\right)$ and $g_i^{Q_i}\left(\Delta Q_{i,t}\right)$ are the sensitivity functions.

The theoretical analysis of the sensitivity function is explained in the Appendix.

6.4.3.2 Learning of the sensitivity functions

In this chapter, the sensitivity functions are learned based on a convolutional neural network (CNN). The proposed network structure is shown in Fig. 6-5. There are two channels. In Channel 1, the input data is the changes in the active or reactive power, and it consists of three dense layers. In Channel 2, the input data is the estimated state variables of the distribution network, and it consists of two convolutional layers and one dense layer. Two channels are then connected through a fully connected layer to map the outputs to the changes of the state variables.

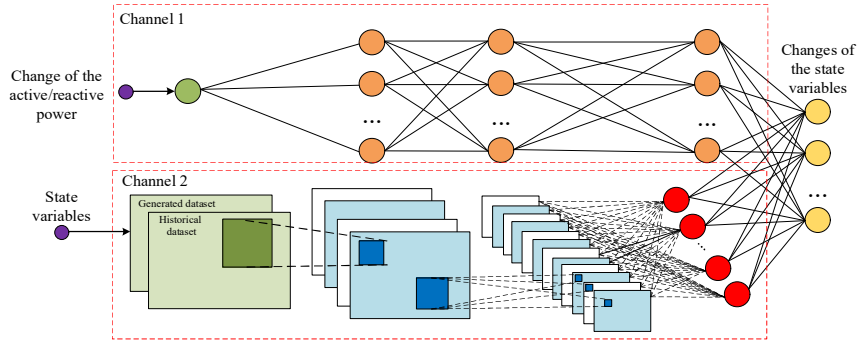

Fig. 6-5. Double-channel learning structure for sensitivity function.

The convolution layer shows good capability in feature extraction. Firstly, the features from the previous layer will be convolved by the learnable kernels. The procedure can be described as:

$$\mathbf{y}_j^l = f\left(\sum_{i \in M_j} \mathbf{x}_i^{l-1} \otimes \mathbf{k}_{ij}^l + b_j^l\right) \tag{6.28}$$

where $\mathbf{y}_j^l$ is the output of the j^{th} map in the l^{th} layer; $\mathbf{x}_i^{l-1}$ is the input of the i^{th} map in layer l-1; M_j is the set of the input maps; $\otimes$ denotes the convolutional operation; $\mathbf{k}_{ij}^l$ represents the weight of the filter of the corresponding convolutional layer and b_j^l is the bias, respectively.

Before being passed to the next layer, the output of the convolution layer needs to be activated. In this chapter, the sigmoid function is utilized as an activation function, shown as:

$$sig(x) = 1/\left(1+e^{-x}\right) \tag{6.29}$$

The dense layers or fully connected layers are expressed as:

$$\mathbf{y}^l = \mathrm{K}^l \mathbf{x}^{l-1} + \mathbf{b}^l \tag{6.30}$$

where K^l is the weight from layer l-1 to layer l; and $\mathbf{b}^l$ is the additive bias.

The Mean Squared Error (MSE) loss function is defined as:

$$L = \sum_z \left(\varepsilon_{i,t} - \tilde{\varepsilon}_{i,t}\right)^2 + \left\|k\right\|_2^2 \tag{6.31}$$

where $\tilde{\varepsilon}_{i,t}$ is the value of the label.

After the sensitivity function $g_i^P\left(\Delta P\right)$ and $g_i^Q\left(\Delta Q\right)$ are learned, the combined effect of the changes of active and reactive power on the state estimation can be further expressed in (6.32) and (6.33).

$$\varepsilon_{i,t} = \hat{\varepsilon}_{i,t} + g_i^P\left(\Delta P_{i,t}\right) + g_i^Q\left(\Delta Q_{i,t}\right) \tag{6.32}$$

$$\left(\varepsilon_{i,t}\right)^2 = \left(\hat{\varepsilon}_{i,t} + g_i^P\left(\Delta P_{i,t}\right) + g_i^Q\left(\Delta Q_{i,t}\right)\right)^2 \tag{6.33}$$

In the conventional model, such as [199], the DR aggregator is assumed to master all the system

information, so constraints (6.4)-(6.10) are considered in the optimization model. However, in reality, the DR aggregators do not have the capability to solve the optimization problem with constraints (6.4)-(6.10) embedded. So, the electricity network constraints (6.4)-(6.10) are not utilized in the proposed method of this chapter. Meanwhile, we proposed a novel DR framework based on the sensitivity functions. Then, constraints (6.4)-(6.10) are substituted by (6.32) and (6.33) in our proposed method.

6.5 Day-ahead and Real-time Demand Response with Operating Envelope based on Sensitivity Function

According to the proposed framework in Fig. 6-1, DR scheduling is a two-stage optimization problem. In the day-ahead scheduling, the DNO first predicts the network variables, such as the power injections, and produces the sensitivity functions. Then, the DR aggregators schedule the controllable resources based on the received sensitivity functions. At real-time scheduling, the DNO conducts the real-time state estimation introduced in section 6.4.1 and produces the sensitivity functions. Based on the received sensitivity functions and the day-ahead scheduling result, the DR aggregator will adjust the operation of the controllable resources.

6.5.1 Day-ahead Scheduling Stage

The model of day-ahead scheduling is similar to the conventional DR scheduling strategy in section 6.2. The objective function is (6.1), and the operational constraints of the devices are (6.51)-(6.64) in the Appendix. However, the difference is that the DR aggregator is not authorized to access the information of network variables, and it does not have the capability to solve the operating envelope constraints (6.4)-(6.10). Therefore, the operating envelope will be imposed based on the sensitivity functions.

As mentioned, the power injection at each bus is predicted the day ahead to produce the sensitivity functions. Then, $\Delta P_{i,t}$ and $\Delta Q_{i,t}$ can be calculated as:

$$\Delta P_{i,t} = P_{i,t}^{Tot} - \widehat{P}_{i,t}^{inj}, \Delta Q_{i,t} = Q_{i,t}^{Tot} - \widehat{Q}_{i,t}^{inj} \tag{6.34}$$

where $\widehat{P}_{i,t}^{inj}$ and $\widehat{Q}_{i,t}^{inj}$ are the predicted value of the active and reactive power consumption of the DR aggregator.

Hence, based on the received representative information, including the predicted system states $\hat{\varepsilon}_{i,t}$ and the sensitivity functions $g_i^P\left(\Delta P_{i,t}\right)$ and $g_i^Q\left(\Delta Q_{i,t}\right)$ related to the connection point of the DR

aggregators, the operating envelope constraints can be expressed as:

$$\varepsilon_{i,t} = \hat{\varepsilon}_{i,t} + g_i^P\left(\Delta P_{i,t}\right) + g_i^Q\left(\Delta Q_{i,t}\right) \tag{6.35}$$

$$\left(\varepsilon_{i,t}\right)^2 = \left(\hat{\varepsilon}_{i,t} + g_i^P\left(\Delta P_{i,t}\right) + g_i^Q\left(\Delta Q_{i,t}\right)\right)^2 \tag{6.36}$$

$$\varepsilon_i^{\min} \le \varepsilon_{i,t} \le \varepsilon_i^{\max}, \left(\varepsilon_{i,t}\right)^2 \le \varepsilon_i^{(2)\max} \tag{6.37}$$

where $\hat{\varepsilon}_{i,t}$ is the system variable predicted by the DNO in the day ahead.

6.5.2 Real-time Scheduling Stage

During the real-time control, there is a deviation in the predictive information, resulting in changes in DR schedules. The real-time operation problem of the aggregator can be solved by solving the objective function (6.38), where the decision variables are the active and reactive power adjustment ΔP_t and ΔQ_t.

$$\begin{aligned}&\min \sum_t \left(\lambda_t^P\left(P_{i,t}^{Tot} - \Delta P_{i,t}\right)\Delta t + \lambda_t^Q\left(Q_{i,t}^{Tot} - \Delta Q_{i,t}\right)\Delta t\right)\\ &+\alpha\sum_t \left\|\Delta P_{i,t}\right\| + \beta\sum_t \left\|\Delta Q_{i,t}\right\|\end{aligned} \tag{6.38}$$

where α and β are the penalty coefficients.

Similar to day-ahead scheduling, the active and reactive power adjustment of the controllable load can be further decomposed as equations (6.39)-(6.40):

$$\Delta P_{i,t} = \Delta P_{i,t}^{SL} + \Delta P_{i,t}^{ESS,CH} - \Delta P_{i,t}^{ESS,DS} + \Delta P_{i,t}^{HVAC} - \Delta P_{i,t}^{PV} \tag{6.39}$$

$$\Delta Q_{i,t}^{Tot} = \Delta Q_{i,t}^{SL} - \Delta Q_{i,t}^{ESS} + \Delta Q_{i,t}^{HVAC} - \Delta Q_{i,t}^{PV} \tag{6.40}$$

Also, the operation constraints (6.51)-(6.64) in the Appendix need to be satisfied.

The changes in the DR schedule may result in infeasibility. Therefore, the real-time DR with operating envelope should be solved based on the representative data sent by the DNO. The representative data include the estimated states $\widehat{\varepsilon}_{i,t}$ (obtained in sections 6.4.1 and 6.4.2) and the sensitivity functions $g_i^P\left(\Delta P_{i,t}\right)$ and $g_i^Q\left(\Delta Q_{i,t}\right)$ related to the connection point of the DR aggregators (obtained in section 6.4.3). The real-time operating envelope constraints can be expressed as:

$$\varepsilon_{i,t} = \widehat{\varepsilon}_{i,t} + g_i^P\left(\Delta P_{i,t}\right) + g_i^Q\left(\Delta Q_{i,t}\right) \tag{6.41}$$

$$\left(\varepsilon_{i,t}\right)^2 = \left(\widehat{\varepsilon}_{i,t} + g_i^P\left(\Delta P_{i,t}\right) + g_i^Q\left(\Delta Q_{i,t}\right)\right)^2 \tag{6.42}$$

$$\varepsilon_i^{\min} \le \varepsilon_{i,t} \le \varepsilon_i^{\max}, \left(\varepsilon_{i,t}\right)^2 \le \varepsilon_i^{(2)\max} \tag{6.43}$$

6.5.3 Linearization of the Sensitivity Function

However, the learned sensitivity functions $g_i^P\left(\Delta P\right)$ and $g_i^Q\left(\Delta Q\right)$ are nonlinear due to the convolutional layer and activation function. Hence, equations (6.35), (6.36), (6.41), and (6.42) become nonlinear constraints, which bring an extra computing burden.

To ensure that the optimization problem can be solved efficiently, linear piecewise functions are applied to approximate the learned sensitivity function shown in Fig. 6-4. The linear piecewise functions can be expressed as:

$$h\left(\Delta P_{i,t}\right)=\tilde{a}_k\Delta P_{i,t}+\tilde{b}_k,\Delta P_{i,t}\in\left[x_k,x_{k+1}\right] \tag{6.44}$$

$$c\left(\Delta Q_{i,t}\right)=\tilde{a}_m\Delta Q_{i,t}+\tilde{b}_m,\Delta Q_{i,t}\in\left[x_m,x_{m+1}\right] \tag{6.45}$$

where $h\left(\Delta P_{i,t}\right)$ and $c\left(\Delta Q_{i,t}\right)$ are the piecewise approximation function.

Then, constraint (6.41) can be converted to the mixed-integer linear constraints by introducing variables w_k and z_k shown as (6.46)-(6.50).

$$\Delta P_{i,t}=\sum_{k=1}^{K}w_k x_k \tag{6.46}$$

$$h\left(\Delta P_{i,t}\right)=\sum_{k=1}^{K}w_k h\left(\Delta P_{i,t}\right) \tag{6.47}$$

$$w_1\le z_1,w_2\le z_1+z_2,w_k\le z_{k-1}+z_k,w_K\le z_{K-1} \tag{6.48}$$

$$\sum_{k=1}^{K-1}z_k=1,\sum_{k=1}^{K}w_k=1 \tag{6.49}$$

$$z_k\in\left\{0,1\right\},w_k\in\left[0,1\right] \tag{6.50}$$

6.5.4 Whole Process of the Two-stage DR Scheduling

The whole process of the two-stage DR scheduling is presented in algorithm 6-1 steps. Algorithm 6-1 steps illustrate how day-ahead scheduling, real-time scheduling, state estimation, missing data imputation based on SC-GAIN, and sensitivity functions are integrated and connected. The day-ahead scheduling is conducted first to schedule the controllable resources for the next day. Due to the error between the day-ahead predictions and the real-time states of the network, the day-ahead scheduling may be infeasible during operation. Consequently, the dispatch of the controllable resources will be adjusted in real-time based on the up-to-date information. Both day-ahead and real-time scheduling contain the cooperation and communications between the DNO and DR aggregator.

Algorithm 6-1 steps: Two-stage DR scheduling

Day-ahead scheduling:

i. DNO predicts the network variables
ii. DNO produces the sensitivity function (section 6.4.3)
iii. DNO sends the regarding representative information to the DR aggregator
iv. DR aggregator schedules controllable resources in day ahead (section 6.5.1)

Real-time scheduling:

i. DNO collects the real-time measurements from PMU
ii. DNO imputes the missing value based on the SC-GAIN (section 6.4.2)
iii. DNO realizes the state estimation (section 6.4.1)
iv. DNO produces the sensitivity function (section 6.4.3)
v. DNO sends the regarding representative information to the DR aggregator
vi. DR aggregator adjusts the scheduling of the controllable resources in real-time based on the received representative information and the day-ahead scheduling results (section 6.5.2)

6.6 Case Studies

6.6.1 Experiment Setting

The proposed framework and methodology are verified on the IEEE 33-bus system. In case studies, two different scenarios are considered. In scenario one, the penetration of RES is relatively low, and the voltage profile of the network before DR is given in Fig. 6-6. In scenario two, the penetration of RES is relatively high, so the inverse current occurs in the network, and the voltage profile is given in Fig. 6-7. In both scenarios, the network suffers from voltage and thermal problems. In the simulation, we focus on the DR aggregator located at bus 18, which is a sensitive descendant bus. In order to show the scalability of the proposed framework and methodology, the simulation is also conducted on the IEEE 123-bus system.

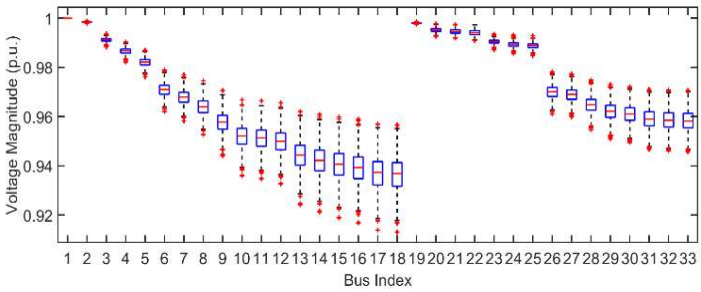

Fig. 6-6. Voltage profile of IEEE 33-bus system (scenario one).

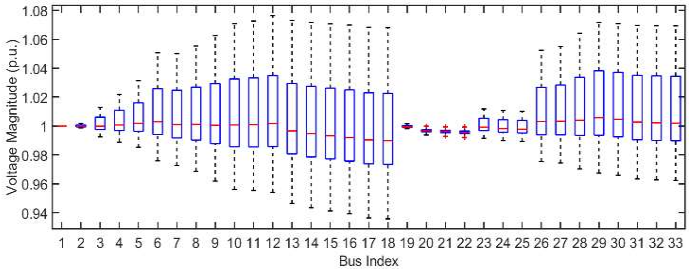

Fig. 6-7. Voltage profile of IEEE 33-bus system (scenario two).

TABLE 6-1. NETWORK STRUCTURE AND PARAMETERS OF SC-GAIN

Generator			
Layer Index	Channel 1	Channel 2	Channel 3
1	Input: 33*1	Input: 33*1	Input: 33*1
2	Convolution: 3*1,64, ReLu		
3	Convolution: 3*1,128, ReLu		
4	Convolution: 1*1,256 ReLu		
5	FC: 33, Linear	FC: 33, Linear	FC: 33, Linear
Discriminator			
Layer Index	Channel 1	Channel 2	Channel 3
1	Input: 33*1	Input: 33*1	Input: 33*1
2	Convolution: 3*1,64, ReLu		
3	Convolution: 3*1,128, ReLu		
4	Convolution: 1*1,256, ReLu		
5	FC: 4, Linear	FC: 4, Linear	FC: 4, Linear
6	Softmax	Softmax	Softmax

TABLE 6-2. NETWORK STRUCTURE AND PARAMETERS OF THE NEURAL NETWORK FOR THE LEARNING OF THE SENSITIVITY FUNCTIONS

Layer Index	Channel 1	Channel 2
1	Input: 1*1	Input: 99*1
2	FC: 32, ReLu	Convolution: 5*1,64, ReLu
3	FC: 64, ReLu	Convolution: 3*1,128, ReLu
4	FC: 128, ReLu	Convolution: 2*1,256, ReLu
5	/	FC: 128, Linear
6	FC: 128, Linear	
7	FC: 99, Linear	

6.6.2 State Estimation based on SC-GAIN

In the proposed framework, the DNO first estimates the states of the system in real-time based on the proposed SC-GAIN. Four cases are established in this section:

Case 1: The state estimation at Bus 13 in scenario one (low RES penetration).

Case 2: The state estimation at Bus 18 in scenario one.

Case 3: The state estimation at Bus 13 in scenario two (high RES penetration) considering a sudden

drop of PV output.

Case 4: The state estimation at Bus 18 in scenario two (high RES penetration) considering a sudden drop of PV output.

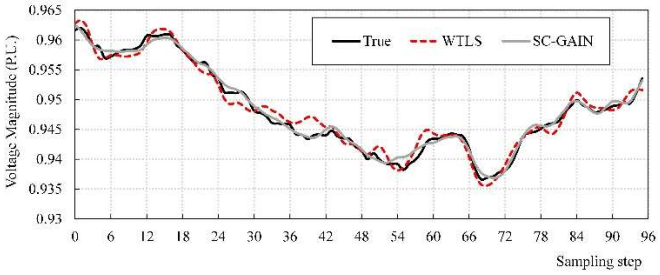

Fig. 6-8. Voltage magnitude estimation result of Case 1.

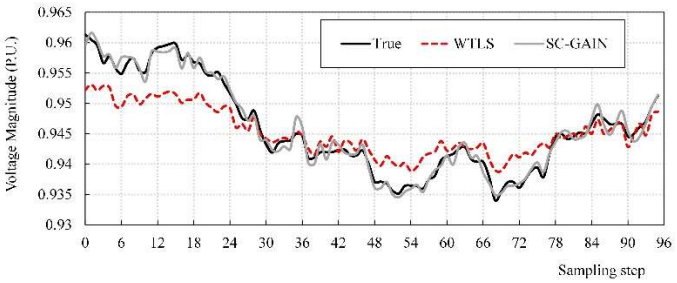

Fig. 6-9. Voltage magnitude estimation result of Case 2.

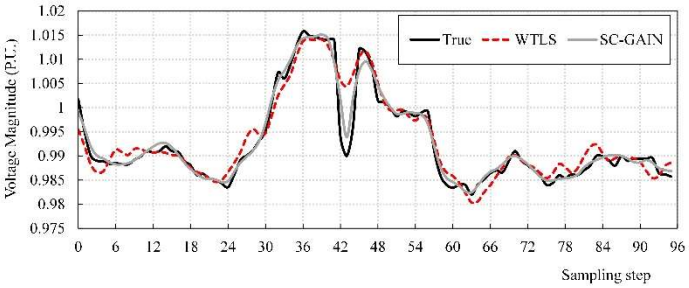

Fig. 6-10. Voltage magnitude estimation result of Case 3.

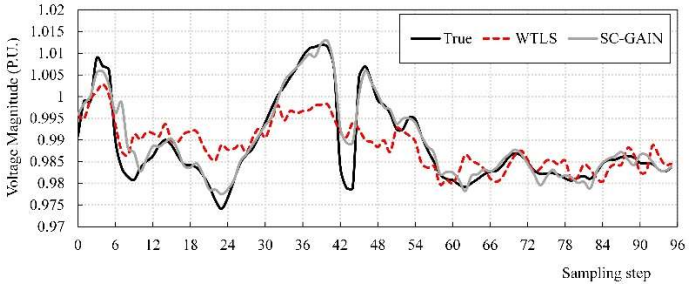

Fig. 6-11. Voltage magnitude estimation result of Case 4.

We first compare the state estimation result between the SC-GAIN algorithm and the WTLS estimator utilized in ref.[202] in terms of voltage magnitude. As for measurement, the PMUs are lost at buses 5, 9, 15, 18, 21, 25, and 30. In Case 1, shown in Fig. 6-8, both the WTLS estimator and SC-GAIN show relatively good estimation performance at bus 13, where there is a PMU measuring the voltage magnitude. In Case 2, shown in Fig. 6-9, there is a loss of PMU at bus 18, and the WTLS estimator shows bad

performance under incomplete information, but the proposed SC-GAIN can better deal with the missing data through data imputation. This is because when there are outliers (missing values), the squared error will be largely affected in (6.17) in the conventional WTLS method. However, in the proposed SC-GAIN, missing data are imputed, which largely reduces the squared error.

In Cases 3 and 4, we consider a sudden drop of PV output under the situation of high penetration of RES so that the outliers occur. It can be observed that the WTLS estimator and SC-GAIN algorithm have similar estimation accuracy under normal operation in Case 3, shown in Fig. 6-10. However, the WTLS estimator is vulnerable to outliers, while the SC-GAIN algorithm can bound the influence of a sudden change of the system states. In Case 4, it can be found that the SC-GAIN algorithm can better deal with the missing information and the outliers concurrently, as shown in Fig. 6-11. This is because the designed coupled network structure helps the estimator learn the joint distribution of the phase angle, voltage magnitude, and current, which can better reveal the true characteristics of the electric states in power systems.

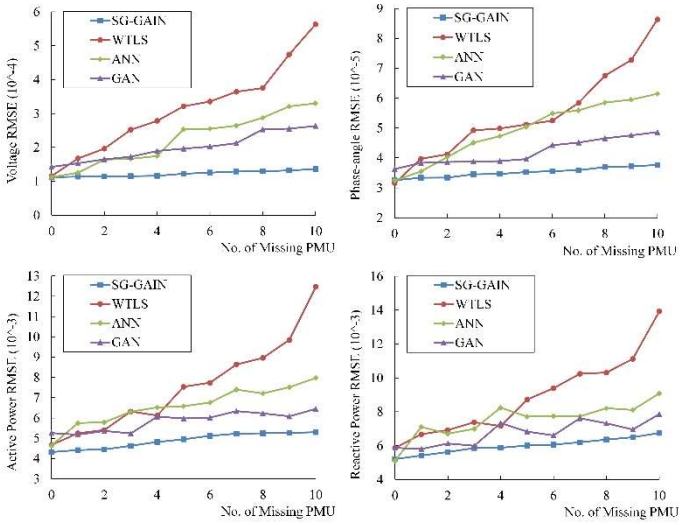

Fig. 6-12. State estimation error under the different numbers of missing PMUs on the IEEE 33-bus system.

In Fig. 6-12, we further compare the influence of the number of missing PMUs on the state estimation under four different methods, i.e., the proposed SC-GAIN, WTLS estimator [28], artificial neural network (ANN)-based estimation [203], and GAN-based estimation [204]. In Fig. 6-12, the Root Mean Squared Error (RMSE) of different measurements is provided. It can be concluded that the proposed SC-GAIN is the most robust method in all estimations with the increasing of the missing number of PMUs, followed by GAN, ANN, and WTLS.

To further show the scalability of the proposed method, these four methods are verified on the IEEE

123-bus system. Similar findings can be concluded, shown in Fig. 6-13. With the continuous increase of the missing number of PMUs, the RMSE of the WTLS estimator increases dramatically. As for ANN, the RMSE increases steadily first and rockets when the missing number of PMUs becomes large. The RMSE of GAN goes steadily up while the RMSE of SC-GAIN always remains at a relatively low level.

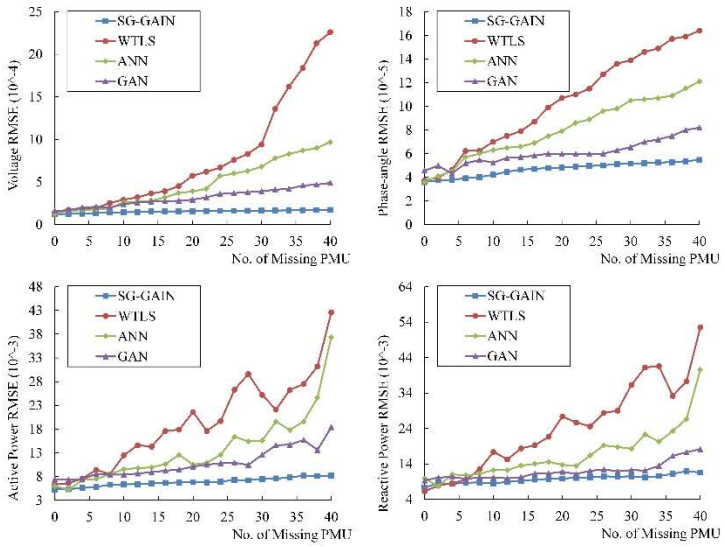

Fig. 6-13. State estimation error under the different numbers of missing PMUs on the IEEE 123-bus system.

6.6.3 DR of the Aggregator with Operating Envelope based on the Sensitivity Functions

Based on the accurate estimation of the system states, sensitivity functions can be learned based on CNN. In order to verify the effect of the learned sensitivity functions and the proposed DR with the operating envelope framework, three cases are established.

Case 1: DR neglecting the network constraints.

Case 2: DR with operating envelope based on sensitivity factor [75].

Case 3: DR with operating envelope based on the learned sensitivity functions.

Case 4: DR with physical network constraints (assume that the DR aggregator masters all the network information).

Figs. 6-14 to 6-17 show the real-time dispatch result of the controllable loads and smart inverters by the DR aggregators under four cases. Obviously, without considering the network constraints, the extremely high peak load occurs in Fig. 6-14. The voltage and current profiles of the three cases are shown in Figs. 6-18 and 6-19. The peak load will cause the violation of voltage and current, which is infeasible. In Case 1, the lowest nodal voltage reaches 0.935 p.u., and the highest branch current reaches around 170 A, which is 1.7 times the maximum capacity. The severe overloading is a risk for the network

assets and power quality. The result is not surprising since merely relying on the DR price signals will overestimate the true DR potential, which results in infeasibility in real-time dispatch.

In Case 2, the peak load is reduced in Fig. 6-15, and the nodal voltage and branch current violation problem is improved compared with Case 1, shown in Figs. 6-18 and 6-19. However, the violation still happens occasionally because of the inaccurate estimation of the sensitivity factor. The main reason is that the sensitivity factor can partially reflect the change of system states but still sacrifices certain accuracy. Hence, in Case 2, the DR capacity is also over-estimated, which may result in infeasibility.

In Case 3, the shiftable load is distributed more evenly than the previous two cases in Fig. 6-16, and the voltage and current violations are avoided in Figs. 6-18 and 6-19. The proposed methodology is effective to realize the DR with the operating envelope. It indicates that the sensitivity function is more accurate in estimating the changes in system states than the sensitivity factor.

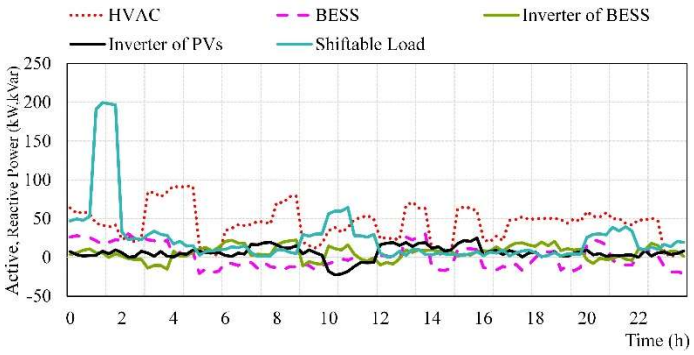

Fig. 6-14. Real-time DR operation in Case 1.

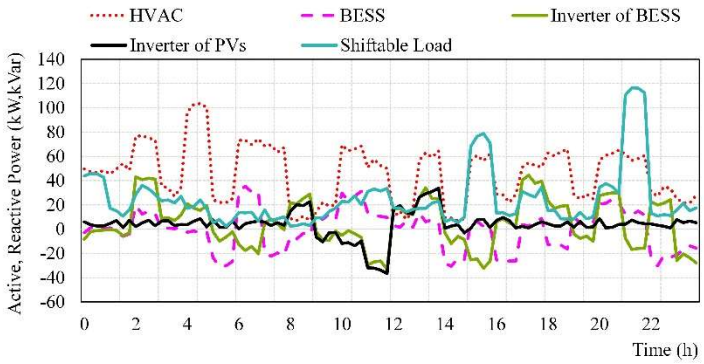

Fig. 6-15. Real-time DR operation in Case 2.

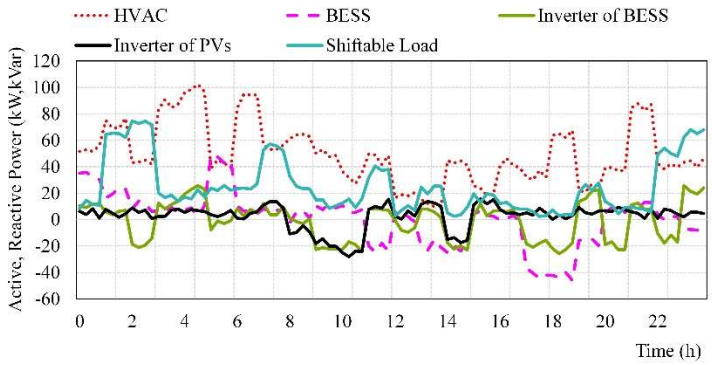

Fig. 6-16. Real-time DR operation in Case 3.

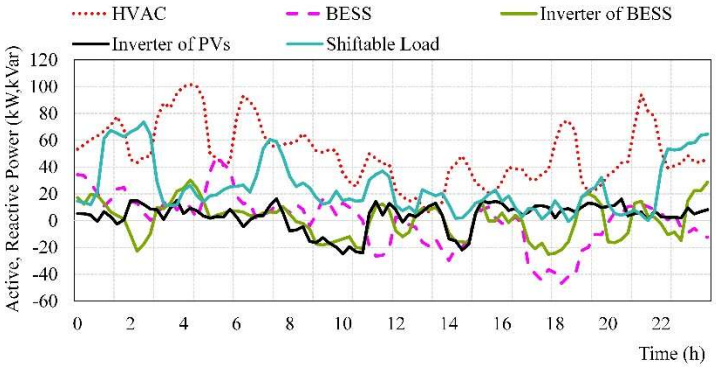

Fig. 6-17. Real-time DR operation in Case 4.

In Case 4, the DR aggregator is assumed to master all the network information, and the power flow is solved as constraints in the optimization problem. Also, the voltage and current profiles of Case 4 are within limits in Figs. 6-18 and 6-19. Compared Fig. 6-16 with Fig. 6-17, it can be found that the scheduling results of the two cases are very close. It indicates that the learned sensitivity functions can reflect the real status of the network, but the proposed methodology only requires limited information exchange.

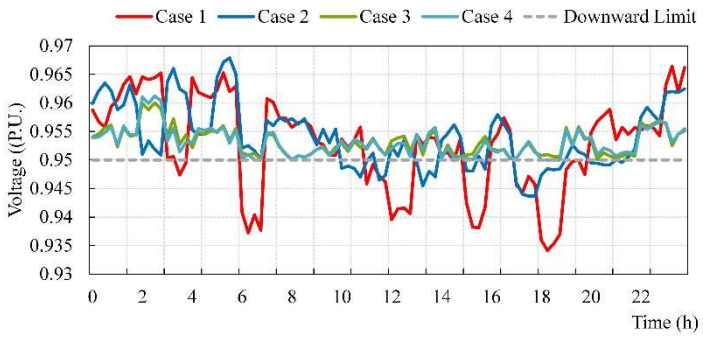

Fig. 6-18. Voltage profile of different cases.

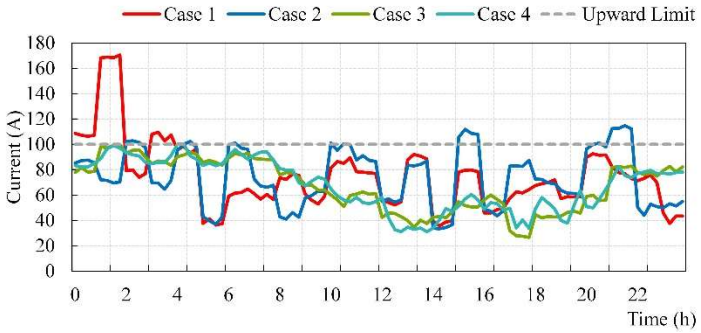

Fig. 6-19. Current profile of different cases.

TABLE 6-3. NETWORK CONSTRAINTS VIOLATION UNDER DIFFERENT STATE ESTIMATION METHODS ON IEEE 33-BUS SYSTEM

	Slight Violation Frequency (%)			Severe Violation Frequency (%)		
Number of Missing PMUs	2	5	7	2	5	7
SC-GAIN	0	0.03	0.12	0	0	0
WTLS	0.91	2.12	10.41	0.13	1.23	3.27
ANN	0.06	1.12	5.26	0	0.35	2.41
GAN	0	0.15	2.45	0	0	1.14

TABLE 6-3 further investigates the influence of the state estimation methods on the performance of the learned sensitivity functions. We define the voltage below 0.94 p.u. as a severe violation and the voltage between 0.95 p.u. and 0.94 p.u. as a slight violation. For the current, we define the current above 1.2 times the maximum capacity as a severe violation and below 1.2 times the maximum capacity as a slight violation. Combined with the result in Fig. 6-12, we can conclude that a more accurate and robust estimation method will result in better performance of the learned sensitivity functions. The proposed SC-GAIN is robust in dealing with missing data, and the frequency of severe violation is always 0 in TABLE 6-3. When there are 7 missing PMUs in the network, the slight violation frequency is only 0.12%, much smaller than that of WTLS (10.41%), ANN (5.26%), and GAN (2.45%).

TABLE 6-4. NETWORK CONSTRAINTS VIOLATION UNDER DIFFERENT STATE ESTIMATION METHODS ON IEEE 123-BUS SYSTEM

	Slight Violation Frequency (%)			Severe Violation Frequency (%)		
Number of Missing PMUs	10	20	40	10	20	40
SC-GAIN	0.02	0.25	1.25	0	0.05	0.76
WTLS	1.24	6.36	12.63	0.74	2.25	5.23
ANN	0.12	2.15	6.12	0.01	0.55	3.02
GAN	0.03	1.05	1.95	0.21	0.53	1.84

To improve the scalability of the proposed method and framework, we further verify our findings on the IEEE 123-bus system, shown in TABLE 6-4. When the missing number of the PMUs increases from

10 to 40, the slight violation based on the WTLS estimator increases from 1.24% to 12.63%, and the severe violation increases from 0.74% to 5.23%. But for the proposed SC-GAIN, the slight violation only increases from 0.02% to 1.25%, and the severe violation increases from 0% to 0.76%. Its performance is obviously better than the other three methods.

6.7 Challenges and Future Work

One of the challenges of this work is the generalization capability of the proposed data-driven models, including SC-GAIN for missing data imputation and the learning of the sensitivity functions. The demand level and the capacity of the renewable energy generator will continuously increase annually. Whether the currently trained model can adapt to future power system environments is challenging. One method to enhance the generalization capability is to add both the historical and generated data to the dataset according to the method in [214]. First, the future load is first predicted based on the long-term forecasting technologies presented in the literature [215]. Then, Gaussian noise is added to the predicted load level. Different scenarios are created for the possible allocation of the renewable energy generators in the future, and Monte Carlo simulations will run to decide the output of the renewable energy generation at each bus. The uncertain demand and renewable energy generation compose the generated data set. Both historical data and the generated data are fed for training. In this way, the trained model can perform well under different demand levels and generation mixes. In future work, an online learning process can be further developed to revise the trained model timely so that the trained model can adapt to the time-varying electricity network.

The second critical challenge is that the typology of the distribution network may change due to network expansion. When the typology of the network changes, the data-driven model needs to be re-trained since the dimension of the problem may change. However, owing to the development of heterogeneous transfer learning, a new model can be trained rapidly, and the methodology to extend the current model to the different network topology is considered for our future work.

6.8 Conclusion

In this chapter, a DR aggregation with the operating envelope framework is presented. In the proposed framework, the DR aggregators can use the limited representative signals sent by the DNO to realize the real-time dispatch of the controllable loads. The representative signals include the estimated states based on the proposed SC-GAIN algorithm and the learned sensitivity functions based on the data-driven

methodology. The proposed framework and methodologies are verified on the IEEE 33-bus system and IEEE 123-bus system. The simulation results show that, compared with the other state-of-art works, the proposed SC-GAIN algorithm can better deal with the missing data and sudden change of the network states in state estimation. Based on the learned sensitivity functions, the DR aggregators can realize the real-time DR considering the network constraints. Besides, the dispatch result of the proposed method is very close to the result directly considering the physical constraints in optimization. It indicates that the learned sensitivity functions can reflect the real status of the network, and the proposed methodology only requires limited information exchange. It is also found that a robust state estimation method can help DR aggregators better estimate the DR capacity by using sensitivity functions. Therefore, with the proposed state estimation method, the network constraint violation is less likely to occur.

6.9 Appendix

6.9.1 Device Operating Constraints

6.9.1.1 DGs with smart inverters

The DGs can generate and absorb reactive power when equipped with smart inverters. The constraints of the inverter-based DGs can be expressed as:

$$\left|Q_{j,t}^{PV,\max}\right| \le \sqrt{\left(S_j^{DG,\max}\right)^2 - P_{j,t}^{PV}} \tag{6.51}$$

$$-Q_{j,t}^{PV,\max} \le Q_{j,t}^{PV} \le Q_{j,t}^{PV,\max} \tag{6.52}$$

where $S_j^{DG,\max}$ is the maximum capacity of the smart inverters of the DGs; $Q_{j,t}^{PV,\max}$ is the maximum reactive power generation of the DGs.

6.9.1.2 BESS with smart inverters

Equation (6.53) describes the energy balance constraints of the BESS. Equations (6.54) and (6.55) describe the limit of the energy storage state and charging/discharging power. Equations (6.56) and (6.57) describe the reactive power capacity of the smart inverters.

$$E_{j,t+1}^{ESS} = E_{j,t}^{ESS} + P_{j,t}^{ESS,CH}\eta^C\Delta t - P_{j,t}^{ESS,DS}\Delta t / \eta^D \tag{6.53}$$

$$E_j^{ESS,\min} \le E_{j,t}^{ESS} \le E_j^{ESS,\max} \tag{6.54}$$

$$0 \le P_{j,t}^{ESS,CH/DS} \le P_{j,t}^{ESS,RT} \tag{6.55}$$

$$\left|Q_{j,t}^{ESS,\max}\right| \le \sqrt{\left(S_j^{ESS,\max}\right)^2 - \left(P_{j,t}^{ESS,CH}\right)^2 - \left(P_{j,t}^{ESS,DS}\right)^2} \tag{6.56}$$

$$-Q_{j,t}^{ESS,\max} \le Q_{j,t}^{ESS} \le Q_{j,t}^{ESS,\max} \tag{6.57}$$

where $E_{j,t}^{ESS}$ is the energy storage state of the BESS; η^C and η^D are the charging and discharging efficiency of the BESS; $E_j^{ESS,\min}$ and $E_j^{ESS,\max}$ are the minimum and maximum energy storage state of the BESS; $P_{j,t}^{ESS,RT}$ is the maximum charging and discharging rate of the BESS; $S_j^{ESS,\max}$ is the maximum capacity of smart inverters of the BESS; $Q_{j,t}^{ESS,\max}$ is the maximum reactive power generation of the BESS.

6.9.1.3 *HVAC*

For the HVAC units, the total aggregated active and reactive power consumption can be calculated by summing up the power of each HVAC unit shown as (6.58). Equation (6.59) describes the reactive power consumption of the HVAC units. The relationship between the indoor temperature and the power of the HVAC units is modeled based on the thermodynamic behavior [216] shown as (6.60). In order to ensure the comfort of the residents, the indoor temperature should be maintained within a specific range shown as (6.61). The aggregation method of the HVAC units can be further referred to [194].

$$P_{j,t}^{HVAC} = \sum_{h\in\Omega^{HVAC}} P_{h,t}^{HVAC}, Q_{j,t}^{HVAC} = \sum_{h\in\Omega^{HVAC}} Q_{h,t}^{HVAC} \tag{6.58}$$

$$Q_{h,t}^{HVAC} = P_{h,t}^{HVAC} \tan\left(\cos^{-1}\left(pf_{h,t}^{HVAC}\right)\right) \tag{6.59}$$

$$T_{h,t+1}^{in} = T_{h,t}^{in} e^{-1/R_h C_h} + \left(T_t^{am} - R_h P_{h,t}^{HVAC} \Delta t\right)\left(1 - e^{-1/R_h C_h}\right) \tag{6.60}$$

$$T_h^{ref} - \delta_h \le T_{h,t}^{in} \le T_h^{ref} + \delta_h \tag{6.61}$$

$$0 \le P_{h,t}^{HVAC} \le P_h^{HVAC,RT} \tag{6.62}$$

where Ω^{HVAC} is the set of HVAC units; $P_{h,t}^{HVAC}$ and $Q_{h,t}^{HVAC}$ are the active and reactive power consumption of the h^{th} HVAC; $pf_{h,t}^{HVAC}$ is the power factor of the HVAC; $T_{h,t}^{in}$ and T_h^{am} are the indoor and ambient temperature; R_h is the thermal resistance; C_h is the heat ratio of the air; T_h^{ref} is the reference temperature; δ_h is the maximum acceptable temperature deviation; $P_h^{HVAC,RT}$ is the maximum power of the HVAC.

HVAC units have very complicated mechanisms and multiple components, and the power factor in (6.59) is not a constant value. However, to simplify the problem in an energy dispatch problem, we

consider the average power factor of the HVAC units. Such simplification and assumption are common in the energy dispatch problem in electricity market operations [217].

6.9.1.4 Shiftable load

For the shiftable load, it should ensure that the total daily demand is satisfied, shown as:

$$Q_{j,t}^{SL} = pf_{j,t}^{SL} \cdot P_{j,t}^{SL} \tag{6.63}$$

$$\sum_{t} P_{j,t}^{SL} = P_{j}^{SL,D} \tag{6.64}$$

where pf_{t}^{SL} is the power factor of the shiftable load; $P_{j}^{SL,D}$ is the total active power demand.

6.9.2 Basic Theoretic Analysis of the Sensitivity Function

Using sensitivity analysis to estimate the state changes in the electricity network has its basic theory. Take the voltage as an example. Sensitivity data is readily obtained from the inverse of the standard Jacobian matrix used for the calculation of network bus voltages under the Newton-Raphson load-flow technique. The updated formula of the power system stated in the Newton-Raphson load-flow technique is given by:

$$\begin{aligned} &\begin{bmatrix} \Delta\delta_2 & \dots & \Delta\delta_n & \dfrac{\Delta|V_2|}{|V_2|} & \dots & \dfrac{\Delta|V_n|}{|V_n|} \end{bmatrix}^T \\ &= \mathbf{J}^{-1}\begin{bmatrix} \Delta P_2 & \dots & \Delta P_n & \Delta Q_2 & \dots & \Delta Q_n \end{bmatrix}^T \end{aligned} \tag{6.65}$$

Once the power flow is converged, the Jacobian specifies the partial derivatives (i.e., sensitivities) of P_X and Q_X with respect to $|V_Y|$ and δ_Y as a function of the current system state. The Jacobian matrix can be expressed as:

$$\mathbf{J} = \begin{bmatrix} \dfrac{\partial P_2}{\partial \delta_2} & \dots & \dfrac{\partial P_2}{\partial \delta_n} & |V_2|\dfrac{\partial P_2}{\partial |V_2|} & \dots & |V_n|\dfrac{\partial P_2}{\partial |V_n|} \\ \dots & \mathbf{J_{11}} & \dots & \dots & \mathbf{J_{12}} & \dots \\ \dfrac{\partial P_n}{\partial \delta_2} & \dots & \dfrac{\partial P_n}{\partial \delta_n} & |V_2|\dfrac{\partial P_2}{\partial |V_2|} & \dots & |V_n|\dfrac{\partial P_n}{\partial |V_n|} \\ \dfrac{\partial Q_2}{\partial \delta_2} & \dots & \dfrac{\partial Q_2}{\partial \delta_n} & |V_2|\dfrac{\partial Q_2}{\partial |V_2|} & \dots & |V_n|\dfrac{\partial Q_2}{\partial |V_n|} \\ \dots & \mathbf{J_{21}} & \dots & \dots & \mathbf{J_{22}} & \dots \\ \dfrac{\partial Q_n}{\partial \delta_2} & \dots & \dfrac{\partial Q_n}{\partial \delta_n} & |V_2|\dfrac{\partial Q_2}{\partial |V_2|} & \dots & |V_n|\dfrac{\partial Q_n}{\partial |V_n|} \end{bmatrix} \tag{6.66}$$

Combining the equation above, an incremental change in voltage can be yielded according to [218] as:

$$\Delta|V_Y| \approx \sum_{X}\left(\frac{\partial|V_Y|}{\partial P_X}\times\Delta P_X + \frac{\partial|V_Y|}{\partial Q_X}\times\Delta Q_X\right) \tag{6.67}$$

where $\Delta|V_Y|$ is the change in voltage magnitude at bus Y, ΔP_X and ΔQ_X are the changes in P and Q at bus X; $\partial|V_Y|/\partial P_X$ and $\partial|V_Y|/\partial Q_X$ are the voltage sensitivities to active power and reactive power changes.

The equation above is similar to our general formula based on sensitivity function, shown in (6.32). The difference is that we utilized the proposed sensitivity function $g_i^P(\cdot)$ and $g_i^Q(\cdot)$ based on data-driven analysis rather than the sensitivity factors $\partial|V_Y|/\partial P_X$ and $\partial|V_Y|/\partial Q_X$. The proposed method can better reflect the nonlinearity of the power system equations, which is more accurate.

7. PRICING FOR ELECTRIC VEHICLE CHARGING STATIONS BASED ON THE RESPONSIVENESS OF DEMAND

EVs have the promising potential to be effective in mitigating greenhouse gas emissions in the transportation sector. Hence, the penetration of EVs in some countries has experienced steady growth. However, the proliferation of EVs can cause negative impacts on the PDN and the TN. Thus, in this chapter, a dynamic pricing strategy for EVCSs is proposed to facilitate EVCSs to earn higher profits while alleviating the potential negative impacts on both PDN and TN. First, a pricing strategy, considering the competition effect established based on the TN, is formulated to facilitate the EVCS to attract the defined competitive charging demand. Second, a two-step approach is proposed to mathematically formulate the responsiveness of demand towards the charging price. Third, EV user behaviors are incorporated based on both an admission control scheme and a queueing model to further adjust the charging demand. We have conducted simulations to verify the effectiveness of the pricing strategy in a PDN and TN coupled system, which contains approximately 2000 EVs. Results show that the proposed pricing strategy can facilitate the EVCS to gain 14.2% more net charging profit on average compared with the other three cases. Moreover, the operational stability of the EVCS can be ensured because the proposed pricing strategy can result in the least queueing length volatility with moderate profit variance compared with the other three cases. Furthermore, the proposed pricing strategy can achieve spatial load shifting by incentivizing EVs to alter their station-selection decisions to avoid possible power congestion in the electricity network.

7.1 Introduction

EVs are believed to have the promising potential to reduce greenhouse gas emissions and urban air pollution if EVs are charged with renewable energy [41, 42]. As a result, EVs are burgeoning to gradually replace gasoline-based vehicles (GVs) [43]. Under this context, the synergistic effect of PDNs and TNs has become an emerging topic to discuss [44, 45]. To be specific, the growth of EVs will increase the EV traffic flow in TN. Then, the increasing EV traffic flow will increase the charging demand at the EVCSs, and the increased charging demand at EVCSs will further affect the operation of PDN. To this end, the increasing penetration of EVs can pose a potential impact on the security and stability of the PDN [44]. Additionally, the substitution of GVs with EVs might induce two types of potential risks for TN [45]. First, EVCSs are usually constructed on prosperous roads to obtain more traffic capture, but the

attraction of the additional EV flow will worsen the traffic condition. Second, the charging behavior of EV users might cause long queueing lengths within certain EVCSs. Hence, the EVCS plays an important role in guiding EV users' charging selection decisions through pricing strategy to mitigate the above-mentioned issues.

The pricing strategy of the EVCS is investigated in the literature. However, in some of the existing references [119, 120], EVCSs simply applied the DLMP as the charging price. Although DLMP has the advantage of stimulating EV loads to maintain the voltage, current, and power flow within acceptable limits and alleviate the congestion of PDN, using the DLMP can only cover the marginal costs of EVCSs. Thus, it fails to facilitate the EVCSs to gain higher profits. In practice, EVCSs are self-interested [121]. Hence, EVCSs can formulate their own pricing strategies to not only cover the cost of EVCSs but also gain higher profit [121-125]. Some references not only aimed to maximize charging profit but also aimed to enhance customer satisfaction or PDN stability via pricing strategy [126, 127]. Apart from increasing charging profit, in some references, the pricing strategy could enhance the QoS at the EVCS [128-131].

However, there are still three issues that remain unaddressed in the existing literature. First, although [124, 125] analyzed the competition among EVCSs based on a Stackelberg game model, the relationship between the TN and the price competition is ignored. In practice, the competition among EVCSs is established based on the TN. For example, when the EVCSs are close to each other, the competition between them might become intense. On the contrary, when the EVCSs are far from each other, the competition between them might become less intense. If two EVCSs are not related to each other in TN through traffic flow, they do not have a competitive relationship. Hence, the competition model in the literature, such as [124, 125], may overestimate the competition degree. Second, in some of the existing literature [120, 132, 133], the pricing strategy of the EVCS is formulated based on the demand responsiveness of individual EV users towards the charging price. For example, in [132], the pricing strategy is formulated by solving each EV decision problem based on travel time and charge cost minimization. Similarly, the pricing strategy of [133] utilized a congestion game to model the route-selection and station-selection behavior of each EV to minimize the travel duration and energy consumption costs. However, this type of pricing strategy formulated from the microscopic view of individual EV users showing the response of EVs towards the charging price is problematic in two aspects. First, the computational complexity of the pricing optimization of these references will increase

significantly as the number of EVs increases. Despite using the clustering method, it might still be computational complex to optimize the detailed EV charging behavior of each cluster. Second, it is almost impossible for EVCSs to have access to real-time or future data related to traffic flow conditions, SOC of individual EVs, and the traveling plan of individual EVs. Hence, the pricing strategy of [120, 132, 133] can only be applied to day-ahead pricing or long-term pricing where the energy price is pre-determined using historical data. As a result, it is more computationally efficient to formulate a pricing strategy for the EVCS from a more macroscopic view by considering the total demand responsiveness towards the charging price. There are research articles modeling the pricing strategy of EVCSs from an aggregated viewpoint by considering the aggregated charging demand, such as [121]. However, it is assumed in [121] that the total charging demand was inelastic to the charging price, which is obviously inappropriate. As an improvement, in [43], price elasticity was utilized to analyze the relationship between the charging price and the total charging demand. However, it should be noted that the queueing length at the EVCSs can also influence demand responsiveness. Therefore, the balance between charging price, total charging demand, and queueing length needs to be further investigated. Third, the impact of the queueing length on EV users' charging behaviors is not investigated [134]. EVs normally will need to queue before connecting to a plug during peak charging periods. However, the EV may leave the queue due to impatience when the queueing length is too long, which will reduce the QoS of the charging station and the EV satisfaction. Hence, to increase the effectiveness of the formulated pricing strategy, it is necessary to investigate the behaviors of EVs towards the queueing length.

Table 7-1 is added to summarize the pricing strategies in the literature as well as the proposed pricing strategy from five main aspects, namely, the modeling of PDN, the modeling of TN, the competition between EVCSs, the modeling of EV behaviors in station selection, routing, or charging process, and the charging demand responsiveness towards the charging price. Noted that demand responsiveness towards price means that the pricing strategy of EVCSs is formulated considering the demand responsiveness, which is further classified into four sub-aspects, i.e., the aggregated demand response, the individual demand response, the inelastic demand response, and the elastic demand response.

TABLE 7-1. METHODS SUMMATION REGARDING THE PRICING STRATEGY

	PDN	TN	Competition between EVCSs	EV behaviors	Demand responsiveness towards charging price			
					Aggregated response	Individual response	Inelastic response	Elastic response
[3]	-	-	-	-	√	-	-	√
[6]	√	√	-	-	-	-	-	-
[7]	√	√	-	-	-	-	-	-
[8]	-	-	-	-	√	-	√	-
[10]	√	-	-	-	-	-	-	-
[11]	-	-	√	-	-	-	-	-
[12]	-	-	√	-	√	-	-	√
[13]	√	-	-	-	√	-	-	√
[14]	√	-	-	√	-	-	-	-
[19]	√	√	-	-	-	√	-	√
[20]	√	√	-	√	-	√	-	-
Proposed	√	√	√	√	√	-	-	√

Thus, in this chapter, we propose a dynamic pricing strategy for the EVCS to address the above-mentioned research gaps. The main contributions of this chapter are as follows.

- First, a dynamic pricing strategy, considering the competition relationship between EVCSs, is proposed based on a coupled PDN and TN to maximize the net charging profit of the EVCS. Under this pricing strategy, more charging demand can be attracted. Additionally, the proposed pricing strategy can achieve spatial load shifting by incentivizing EV users to alter their station-selection decision to avoid congestion of the electricity network. Numerical results show that the proposed pricing strategy can facilitate the EVCS to gain 14.2% more net charging profit on average compared with the fixed pricing strategy.
- Second, a two-step approach is proposed to quantitatively formulate the total charging demand responsiveness towards the charging price based on the optimally assigned traffic flow. With this approach, the balance between the charging price, total charging demand, and the queueing length can be obtained. To be noted, in this chapter, we consider the total demand response of EV users from an aggregated viewpoint rather than considering the demand response of individual EV users. Numerical results in this chapter indicate that although the profit variance of the proposed model is slightly higher than that using a competitive pricing strategy, the queueing length volatility of the proposed pricing strategy is lower. Thus, a balance between the QoS at the EVCS and the charging

profit can be obtained.

- Third, combining both an admission control scheme and a queueing model, two types of EV user behaviors are modeled to further adjust the charging demand, i.e., refuse-to-join and impatient-leave. The modeling of these two types of EV behaviors can reflect the impact of queueing length on the charging demand. Additionally, it can better model the real situation to form a proper pricing strategy by considering EV behaviors.

7.2 EV Integrated Transportation System Modeling

7.2.1 Preliminaries

The original transportation system only analyzed the static traffic flow of GVs based on the User Equilibrium model [219], which is a macroscopic method to assign traffic flow using the estimated average traveling behavior of GVs. In this chapter, both GVs and EVs are considered. Thus, besides the physical road link, where the traveling behavior is modeled, the concept of the virtual link, i.e., the charging link, is introduced to model the queueing and charging behaviors of EVs at EVCSs [121]. As a result, the original TN is extended.

7.2.2 Objective Function

In this chapter, the User equilibrium model is used to reduce the road impedance of the traffic flow distribution of both GVs and EVs, shown as (7.1). Here, impedance is measured by the time spent on the road, including the traveling time on physical road links, as well as the queueing and charging time on charging links. The first term in (7.1) is the traveling time of both GV and EV users, which is based on the Bureau of Public Roads function [121]. The second term is the time EV users spend at EVCSs for queueing and charging, which is based on the Davidson function [121].

$$\min \sum_{a \in A} \left[\int_0^{x_{a,t}} t_a(\theta) d\theta \right] + \sum_{j \in \Omega_j} \left[\int_0^{x_{j,t}} t_j(\theta) d\theta \right] \tag{7.1}$$

where a is the index of the link in the transportation network; A is the set of links in the transportation system; $x_{a,t}$ is the traffic flow on link a at time t; t_a is the traveling time on link a; j is the index of the EVCS; Ω_j is the set of EVCSs in the transportation system; $x_{j,t}$ is the charging flow (the number of EVs) at EVCS j at time t; t_j is the queueing and charging time spent at EVCS j.

The traveling time t_a is further explained in equation (7.2) [121].

$$t_a\left(x_{a,t}\right)=t_a^0\times\left[1+0.15\left(x_{a,t}/\vartheta_a\right)^4\right] \tag{7.2}$$

where t_a^0 is the free-flow travel time on link *a* without congestion; ϑ_a is the traveling capacity of link *a*.

Additionally, the traffic flow of link *a* at time *t* is [121]:

$$x_{a,t}=\sum_{rs}\sum_{\beta\in\mathcal{B}^{rs,gv}}f_{\beta,t}^{rs,gv}\times\delta_{\beta,a}^{rs,gv}+\sum_{rs}\sum_{\beta\in\mathcal{B}^{rs,ev}}f_{\beta,t}^{rs,ev}\times\delta_{\beta,a}^{rs,ev} \tag{7.3}$$

where rs is the index of the origin-destination pair denoting trips; β is the index of the available path that GVs and EVs travel on; $f_{\beta,t}^{rs,gv}$ and $f_{\beta,t}^{rs,ev}$ are the GV and EV flow on paths β; $\delta_{\beta,a}^{rs,gv}$ and $\delta_{\beta,a}^{rs,ev}$ are the binary parameters indicating whether path β that GVs and EVs travel on will pass through link *a*; $\mathcal{B}^{rs,gv}$ and $\mathcal{B}^{rs,ev}$ are the path sets for GVs and EVs, respectively.

The time spent at EVCS t_j is shown in equation (7.4) [121].

$$t_j\left(x_{j,t}\right)=t_j^0\times\left[1+J\times\left(x_{j,t}/\left(\vartheta_j-x_{j,t}\right)\right)\right],x_{j,t}<\vartheta_j,\forall j \tag{7.4}$$

where t_j^0 is the minimum time spent at EVCS *j*; J is the delay parameter; ϑ_j is the service capacity of EVCS *j*.

Additionally, the charging flow that passes EVCS *j* is [121]:

$$x_{a,t}=\sum_{rs}\sum_{\beta\in\mathcal{B}^{rs,ev}}f_{\beta,t}^{rs,ev}\times\delta_{\beta,j}^{rs,ev} \tag{7.5}$$

where $\delta_{\beta,j}^{rs,ev}$ is the binary parameter indicating whether path β will pass through EVCS *j*.

7.2.3 Constraints of Transportation System

Equations (7.6) shows the non-negative constraints of traffic flow of both GVs and EVs on path β. Equation (7.7) describes the relationship between traffic demand from origin to destination and traffic flows on path β.

$$f_{\beta,t}^{rs,gv}\geq0,\forall\beta\in\mathcal{B}^{rs,gv},f_{\beta,t}^{rs,ev}\geq0,\forall\beta\in\mathcal{B}^{rs,ev} \tag{7.6}$$

$$\sum_{\beta\in\mathcal{B}^{rs,gv}}f_{\beta,t}^{rs,gv}=q_t^{rs,gv},\sum_{\beta\in\mathcal{B}^{rs,ev}}f_{\beta,t}^{rs,ev}=q_t^{rs,ev} \tag{7.7}$$

where $q_t^{rs,gv}$ and $q_t^{rs,ev}$ are the traffic demand of GV and EV.

Equation (7.8) indicates that if the mileage can support EVs to travel from the origin to the destination on the non-charging path, EVs can be assigned to the non-charging path. Otherwise, EV users should be

assigned to the charging path. However, if the mileage of EVs still cannot support the trip from the origin to the EVCS on the charging path, the traffic flow on this charging path should be assigned as 0, shown as equation (7.9). As a result, EVs will be assigned to other charging paths.

$$f_{\beta,t}^{rs,ev}\left[SOC^0-\sum\nolimits_{a\in A^\beta}\left(E^{ev}l_a/E^{ev,\max}\right)\right]\geq 0,\forall\beta\in\mathcal{B}^{ev,nc} \tag{7.8}$$

$$f_{\beta,t}^{rs,ev}\left[SOC^0-\left(E^{ev}l_j/E^{ev,\max}\right)\right]\geq 0,\forall\beta\in\mathcal{B}^{ev,c},\forall j\in\Omega_\beta^{rs} \tag{7.9}$$

where SOC^0 is the average initial SOC of EVs; E^{ev} is the average energy consumption measured in kWh/km; $E^{ev,\max}$ is the maximum capacity of EVs; $\mathcal{B}^{ev,nc}$ is the non-charging path set for EVs; $\mathcal{B}^{ev,c}$ is the charging path set for EVs; l_a is the length of link *a*, where $a\in A^\beta$; A^β is the set of links corresponding to the EV non-charging event (The non-charging event means EVs can travel from the origin to the destination of path β without charging); l_j is the distance between the origin to EVCS *j*; Ω_β^{rs} is the set of EVCSs that locates on path β with *rs* as the origin-destination pair.

In the literature, probability density functions are utilized to describe personal EV behaviors, such as daily mileage and arrival time [220]. Hence, in this chapter, we utilize Monte Carlo simulation to simulate the EV charging behaviors and then aggregate these EV behaviors to obtain the average value, including the average energy consumption of EVs, the average initial SOC, the charging demand, etc.

7.3 Problem Formulation and Proposed Framework

7.3.1 Problem Formulation

After optimizing the traffic flow on each path in section III via equations (7.1)-(7.9), the optimally assigned charging demand (amount of energy) on each charging path can be acquired and is expressed as $f_{\beta,t}^{rs,ev^*}\times d$, $\forall\beta\in\mathcal{B}^{ev,c}$, where $f_{\beta,t}^{rs,ev^*}$ is the optimized traffic flow of EVs on charging path β; d is the average EV demand. Although the total charging flow $f_{\beta,t}^{rs,ev^*}$ on path β passes through the EVCS, not all the total charging flow can be attracted by the EVCS if the total charging flow on path β also passes through another EVCS. This is because EVCSs might compete to attract the charging flow. As a result, only part of the total charging flow is attracted by the EVCS due to this competitive relationship between EVCSs. Thus, it is necessary to incorporate the competition relationship in model formulation. In some references, such as [125], although the competition between EVCSs is considered,

the relationship between the TN and the price competition is ignored. By contrast, we model the competition between EVCSs based on the optimally assigned traffic flow in the TN.

Fig. 7-1 is the simplified TN diagram showing the competition between EVCSs s1 and s2. In this chapter, we formulate a pricing strategy for EVCS s1 only, whereas EVCS s2 is the competitor of EVCS s1 (s1 represents EVCS s1 and s2 represents EVCS s2). In this diagram, the total demand of EV users that pass through both EVCSs (such as the blue line) is defined as the demand as ***total competitive demand***. The demand of EV users that pass through both EVCSs and is attracted by EVCS s1 is defined as ***competitive demand*** at EVCS s1. However, EVCS s1 will not compete against EVCS s2 to attract the demand of EV users that only pass through EVCS s1 (such as the green line). This is because this type of demand will only be serviced by EVCS s1. Thus, we define this type of demand as ***non-competitive demand***. Moreover, for the EV flow that does not pass through either EVCS s1 or s2, shown as the orange line, we define it as ***irrelevant flow***. In this case, EVCS s1 will optimize the charging price based on the sum of the competitive demand and the non-competitive demand at EVCS s1.

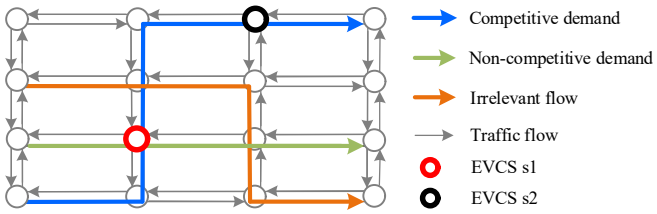

Fig. 7-1. Simplified TN that includes competition between EVCSs.

7.3.2 Proposed Framework

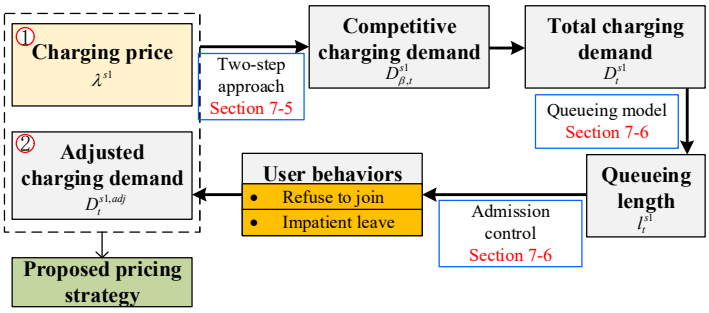

Fig. 7-2. The framework of the proposed charging price optimization process.

The framework of the proposed dynamic pricing strategy optimization process from the perspective of EVCS s1 is illustrated in Fig. 7-2. In Fig. 7-2, first, the relationship between charging price and competitive charging demand $D^{s1}_{\beta,t}$ attracted by EVCS s1 is modeled via the proposed two-step approach in section V, where β is the path that EVs travel on passes through both EVCSs s1 and s2. Second, the total charging demand D^{s1}_{t} of EVCS s1 is derived by summing up the competitive demand

and the non-competitive demand of EVCS s1. Detailed definitions of competitive demand and non-competitive demand can refer to section IV, part A. Third, queueing length l_t^{s1} is calculated based on the total charging demand D_t^{s1} and the queueing model in section VI. Fourth, there are two classes of EV user behaviors considered, i.e., refuse-to-join and impatient-leave. The probabilities leading to obtaining the proportion of EVs in both refuse-to-join and impatient-leave classes are modeled in equation (7.28) and equation (7.29), respectively. Fifth, the adjusted charging demand $D_t^{s1,adj}$ is derived based on user behaviors, shown as equation (7.34). Finally, based on the adjusted charging demand, the pricing strategy for EVCS s1 can be formulated.

The benefits of the proposed pricing strategy are twofold. First, in existing literature, such as [124, 125], although the competition between different EVCSs is included in price formulation, the impact of TN on such competition relationships is not considered. Hence, the competition between EVCSs might be overestimated. By contrast, our chapter models the competition between EVCSs based on TN. Hence, the charging demand, consisting of both the competitive demand and the non-competitive demand, can be more adequately formulated to facilitate the EVCS to set a proper charging price. Second, some references only modeled the relationship between the charging price and the charging demand. For example, [43] utilized price elasticity to model the relationship between the charging price and the charging demand. By contrast, our model not only analyzes the total demand responsiveness towards the charging price (shown as equations (7.19)-(7.21)) but also analyzes the recursive impact of the queueing length on the charging demand (shown as equation (7.34)). In other words, the balance between charging price, charging demand, and queueing length is obtained via the proposed pricing strategy.

7.4 Charging Demand Responsiveness toward Charging Price

In most cases, it is assumed that the driving patterns of EVs related to commuting are relatively unchanged in terms of temporality. Therefore, we mainly focus on the demand responsiveness of EVs along the assigned driving route. According to the definition of non-competitive demand defined in this chapter, this type of demand can only be serviced by EVCS s1. Hence, in this chapter, the responsiveness of non-competitive demand towards the charging price is not further discussed, and only the competitive demand responsiveness towards the charging price will be modeled. In the following parts, a two-step approach is proposed to derive the relationship between the competitive charging demand and charging price.

7.4.1 Step 1: Indifferent Charging Price

EVCSs s1 and s2 are two available stations. The charging price of EVCS s2 is assumed to be known. Before formulating the relationship between the competitive charging demand and the charging price, the ***indifferent price*** for EVCS s1 is derived in step 1. It is a price that can make the aggregated EV users indifferent about which EVCS to select. Here, there are two types of decision-makers, i.e., the aggregated EVs and EVCS s1. To be specific, EVs will make station-selection decisions (selecting EVCS s1 or EVCS s2), and EVCS s1 will derive the indifferent price based on the station-selection decision of EVs and the charging price of EVCS s2.

Hence, the decision-selection choice of EVs is modeled first. The payoffs (utility) of the EV users on station selection are influenced by the waiting time and the charging price at the EVCS. Thus, the utility of EV users who select EVCSs s1 and s2 can be expressed as equations (7.10) and (7.11), respectively.

$$U_{\beta,t}^{s1} = -\lambda^{wa} \times w_t^{s1} - \lambda_{\beta,t}^{s1} \times D_{\beta,t} \tag{7.10}$$

$$U_{\beta,t}^{s2} = -\lambda^{wa} \times w_t^{s2} - \lambda_t^{s2} \times D_{\beta,t} \tag{7.11}$$

where

$$w_t^{s1} = l_t^{s1} / \varepsilon_t^{s1,ar*}, w_t^{s2} = l_t^{s2} / \varepsilon_t^{s2,ar*} \tag{7.12}$$

where $U_{\beta,t}^{s1}$ and $U_{\beta,t}^{s2}$ are the utility of EV users who select EVCSs s1 and s2; λ^{wa} is the penalty coefficient of EV users that can transform waiting time into monetary value; w_t^{s1} and w_t^{s2} are the average waiting time at EVCS s1 and s2; $\lambda_{\beta,t}^{s1}$ is the charging price of EVCS s1 regarding the demand on path β; λ_t^{s2} is the charging price of EVCS s2; $D_{\beta,t}$ is the total competitive demand of EV users on path β; l_t^{s1} and l_t^{s2} are the queueing length at EVCS s1 and EVCS s2 at time *t* (detailed formulae of queueing length are shown in section VI, part B); $\varepsilon_t^{s1,ar*}$ and $\varepsilon_t^{s2,ar*}$ are the average arrival rate at EVCS s1 and EVCS s2 at time *t*.

When $U_{\beta,t}^{s1} = U_{\beta,t}^{s2}$, EV users are indifferent about selecting between EVCSs s1 and s2. Then, we can find the indifferent price $\lambda_{\beta,t}^{s1*}$ set by EVCS s1 results in $U_{\beta,t}^{s1} = U_{\beta,t}^{s2}$. Here, the expression of $\lambda_{\beta,t}^{s1*}$ is given by equation (7.14), which is derived via **proposition 1**.

Proposition 1: Let $\lambda_{\beta,t}^{s1} - \lambda_t^{s2} = \Delta\lambda_{\beta,t}$, the price difference $\Delta\lambda_{\beta,t}^{*}$ between EVCSs s1 and s2 that can make EV users indifferent about which EVCSs to select, i.e., the price difference that can make $U_{\beta,t}^{s1} = U_{\beta,t}^{s2}$, is as (7.13). The method used is to solve simultaneous equations related to the station-selection utility of EVs shown as (7.10) and (7.11). Detailed proof of deriving the price difference that

makes $U_{\beta,t}^{s1} = U_{\beta,t}^{s2}$ can refer to Appendix a.

$$\Delta\lambda_{\beta,t}^{*} = \frac{-\lambda^{wa}\left(w_t^{s1} - w_t^{s2}\right)}{D_{\beta,t}} \tag{7.13}$$

Then, based on the known charging price of EVCS s2 and (7.13), the indifferent price can be shown as:

$$\lambda_{\beta,t}^{s1*} = \lambda_t^{s2} + \Delta\lambda_{\beta,t}^{*} \tag{7.14}$$

7.4.2 Step 2: Demand Responsiveness towards Charging Price

In step 2, the indifferent price is treated as a known parameter to derive the responsiveness of the competitive demand towards the charging price. According to economic theory, demand and price are inversely related [170]. Thus, the exponential distribution can be applied in equation (7.15) to model the relationship between the competitive demand probability and the charging price of EVCS s1.

$$Pr_{D_{\beta,t}^{s1}} = \rho_{\beta,t} e^{-\rho_{\beta,t}\lambda_t^{s1}} \tag{7.15}$$

where $Pr_{D_{\beta,t}^{s1}}$ is the proportion of total competitive demand $D_{\beta,t}$ that is attracted by EVCS s1; $\rho_{\beta,t}$ is the coefficient that describes the relationship between the competitive demand probability and the charging price of EVCS s1, which can be obtained based on the indifferent price derived in step 1.

Note that $Pr_{D_{\beta,t}^{s1}}$ will be 50% when the EV users are indifferent about which EVCSs to select. As a result, we can plug in point ($\lambda_{\beta,t}^{s1*}$,50%) into equation (7.15) to derive the function regarding the coefficient $\rho_{\beta,t}$ of each path β at each time *t* as follows:

$$f\left(\rho_{\beta,t}\right) = \rho_{\beta,t} e^{-\rho_{\beta,t}\lambda_{\beta,t}^{s1*}} - 0.5 \tag{7.16}$$

Then, by applying the Newton-Raphson method, the coefficient can be derived [221].

$$\rho_{\beta,t,i+1} = \rho_{\beta,t,i} - \left[\frac{df\left(\rho_{\beta,t,i}\right)}{d\rho_{\beta,t}}\right]^{-1} f\left(\rho_{\beta,t,i}\right) \tag{7.17}$$

where $\rho_{\beta,t,i}$ is the value of coefficient at iteration *i* of path β.

Proposition 2: To ensure equation (7.16) has at least one root, the charging price should be within the range $\left(0, 2/e\right]$. However, the real charging price is within a range of $\lambda_t^{s1} \in \left(0, \lambda^{\max}\right]$, where $\lambda^{\max}$ is the maximum real charging price. Hence, an auxiliary price that is within the range of $\left(0, 2/e\right]$ is

introduced as an auxiliary variable to mathematically shrink the real charging price into the range of $\left(0,2/e\right]$ (The method used to derive the range of the auxiliary charging price is to find the global maximum point of equation (7.16). Then, the value of the charging price that makes $f\left(\rho_{\beta,t}\right)$=0 is when $\lambda_{\beta,t}^{s1*}=2/e$, and it is also the upper limit of the auxiliary charging price. Detailed proof of the way to derive this range can refer to in Appendix b.). As a result, the relationship between real charging price and auxiliary charging price is shown as (7.18).

$$\lambda_t^{aux,s1}=\frac{2/e}{\lambda^{\max}}\times\lambda_t^{s1},\ \ \lambda_t^{aux,s1}\in\left(0,2/e\right] \tag{7.18}$$

where $\lambda_t^{aux,s1}$ is the auxiliary price.

Thus, equation (7.15) should be modified to:

$$Pr_{D_{\beta,t}^{s1}}=\rho_{\beta,t}e^{-\rho_{\beta,t}\lambda_t^{aux,s1}} \tag{7.19}$$

After formulating the relationship between the charging demand probability and the charging price in (7.19), the competitive demand can be modeled shown as (7.20). Then, the total charging demand at EVCS s1 can be modeled by summing up all the competitive demand at EVCS s1 and all the non-competitive demand at EVCS s1 shown as equation (7.21). The first term represents all the competitive demand, and the second term represents all the non-competitive demand.

$$D_{\beta,t}^{s1}=D_{\beta,t}\times Pr_{D_{\beta,t}^{s1}} \tag{7.20}$$

$$D_t^{s1}=\sum_{\beta\in\mathcal{B}^{s1,s2}}D_{\beta,t}^{s1}+\sum_{\beta\in\mathcal{B}^{s1}}D_{\beta,t}^{s1} \tag{7.21}$$

where $\mathcal{B}^{s1,s2}$ is the set of paths that passes through both EVCSs s1 and s2; $\mathcal{B}^{s1}$ is the set of paths that only passes through EVCS s1.

The model used in this chapter can be generalized to multiple-charging stations. The method used is to focus on every two EVCSs (i.e., EVCS s1 and another EVCS) rather than solving simultaneous equations related to the station-selection utility of EVs. Details of the way to generalize the problem between two stations to multiple stations can refer to in Appendix c.

7.5 EV Behavior Modeling based on Admission Control and Queueing Model

As mentioned before, the long queueing length might lead to EV user impatience. Hence, it is necessary to incorporate EV user behaviors when formulating the pricing strategy to further adjust the charging demand formulated in (7.21). In this chapter, two types of behaviors are considered, i.e., refuse-to-join and impatient-leave. Details of definitions relating to the two types of behaviors can refer to

section VI, part C. Both an admission control scheme and a queueing model are utilized to model those two types of EV behaviors.

7.5.1 Admission Control Scheme

Before analyzing the physical queueing process at the EVCS, a virtual multi-sub-process admission control scheme based on the $M/T_D/n/n+b$ virtual queueing model is introduced [222]. In this admission process, M denotes the arrival rate of the EVs, which follows a Poisson distribution; T_D is the minimum inter-arrival time of two consecutively admitted EVs of the same sub-process (it is also the deterministic service time of one virtual charger); n denotes the number of sub-processes in the admission process (it is also the number of virtual chargers during the admission control process); b is the buffer of the admission process, which is zero.

Under the admission control, EVs will not be admitted if all the virtual chargers (sub-processes) are occupied. Otherwise, EVs will be admitted to the idle virtual charger within the deterministic service time T_D.

For example, consider an admission control scheme including two sub-processes, as shown in Fig. 7-3. When EV user 1 arrives, it is assigned to sub-process 1. When EV user 2 arrives, it cannot be assigned to sub-process 1 because the inter-arrival time between EV users 1 and 2 is shorter than the minimum inter-arrival time. In other words, sub-process 1 is occupied when EV user 2 arrives. Thus, EV user 2 is assigned to sub-process 2. When EV user 3 arrives, it can be assigned to sub-process 1 because this process is not occupied at that time. However, when EV user 4 arrives, none of the sub-processes can be assigned since both sub-processes are occupied at that time. As a result, EV user 4 will not be admitted to EVCS s1. When EV user 5 arrives, it can be assigned to sub-process 2.

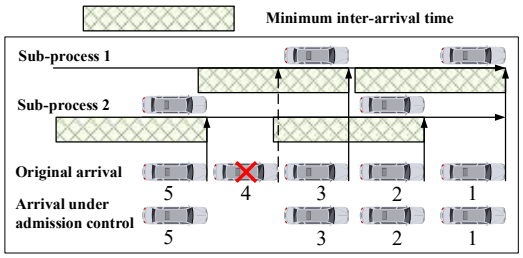

Fig. 7-3. Admission control example illustration.

The advantages of admission control are twofold. First, the admission process can ensure the stability of the physical queueing process by admitting enough users with a guaranteed QoS and avoiding the excessive delay of the admitted EVs [223]. Second, admission control can achieve a balance among the

waiting time, admission probability, and physical charger utilization.

The stability of the physical queueing process can be ensured when the deterministic service time during the admission process is larger than the physical service time at the EVCS, which can be expressed as equation (7.22) [222].

$$nT_D > \varpi^{s1} d / \mu_t^{s1} \tag{7.22}$$

where T_D is the minimum inter-arrival time of one sub-process; n is the number of sub-process in the admission control process; ϖ^{s1} is the total number of physical EV chargers at EVCS s1; μ_t^{s1} is the charging rate per EV charger.

To modify (7.22) into an equation, we have:

$$T_D = \varphi \varpi^{s1} d / n \mu_t^{s1} \tag{7.23}$$

where φ is a coefficient that is larger than 1.

As a result, the admission probability is [224]:

$$Pr_t^{adm} = 1 - \frac{\left(T_D \times \varepsilon_t^{s1,ar}\right)^n \times e^{-T_D \times \varepsilon_t^{s1,ar}}}{\Gamma\left(n+1, T_D \times \varepsilon_t^{s1,ar}\right)} \tag{7.24}$$

where Pr_t^{adm} is the admission probability; $\varepsilon_t^{s1,ar}$ is the arrival rate at EVCS s1 at time *t*.

7.5.2 Queueing Model

After the admission control, the admitted EVs will be physically waiting in the queue. The expression of the queueing length can be shown as equation (7.25), which is based on the total charging demand at EVCS s1. In this chapter, the *M*/*M*$_2$/*N* queuing model is applied in the queueing process, where *M* denotes the arrival rate of the EVs; *M2* denotes the charging rate; *N* denotes the number of physical EV chargers at EVCS s1 [225].

$$l_t^{s1} = \frac{\left(\varepsilon_t^{s1,ar} / \mu_t^{s1}\right)^{\varpi^{s1}} \times \varepsilon_t^{s1,ar} / \left(\mu_t^{s1} \varpi^{s1}\right)}{\varpi^{s1}! \left(1 - \varepsilon_t^{s1,ar} / \left(\mu_t^{s1} \varpi^{s1}\right)\right)^2} \times Pr_{0,t}^{s1} \tag{7.25}$$

$$Pr_{0,t}^{s1} = \left[\sum_{k=0}^{\varpi^{s1}-1} \frac{1}{k!} \left(\frac{\varepsilon_t^{s1,ar}}{\mu_t^{s1}} \right)^k + \frac{1}{\varpi^{s1}!} \frac{\mu_t^{s1}}{\mu_t^{s1} - \varepsilon_t^{s1,ar}} \left(\frac{\varepsilon_t^{s1,ar}}{\mu_t^{s1}} \right)^{\varpi^{s1}} \right]^{-1} \tag{7.26}$$

$$\varepsilon_t^{s1,ar} = D_t^{s1} / d \tag{7.27}$$

where $Pr_{0,t}^{s1}$ is the probability that all chargers are standing by at EVCS s1 at time *t*; k is the number of chargers standing by at EVCS s1.

7.5.3 Modified Charging Demand Considering EV Behaviors

7.5.3.1 *Behavior modeling based on queuing model only*

Based on the queueing model, we can model EV user behaviors at EVCS s1, which can be categorized into two types, i.e., *refuse to join* and *impatient leave*.

Refuse to join: When the EV users arrive at the EVCS, they find the queueing length too long and thus refuse to join the queue, even if the total EV number in the EVCS is less than the maximum queueing capacity.

The probability that EV users will refuse to join the charging service provided by EVCS s1 is as (7.28) [134].

$$Pr_t^{RTJ} = e^{-\left(l_t^{s1}-\varpi^{s1}\right)\sigma} \tag{7.28}$$

where Pr_t^{RTJ} is the probability that EV users will refuse to join the queue at EVCS s1; σ is the parameter that defines the probability decrease rate.

Impatient leave: When the EV users become impatient, they will leave the EVCS, even if the queueing length is not too long.

The number of EVs that leave the queue at time t is relevant to the queueing length at EVCS at time t and assumed to be $\delta ln\left(l_t^{s1}-\varpi^{s1}+1\right)$, where δ is the non-negative adjusting factor [134]. Thus, the probability that the EV users will be impatient and leave the EVCS is:

$$Pr_t^{IL} = \delta ln\left(l_t^{s1}-\varpi^{s1}+1\right)\Big/ l_t^{s1} \tag{7.29}$$

where Pr_t^{IL} is the probability that the EV users will be impatient and leave the queue at EVCS s1.

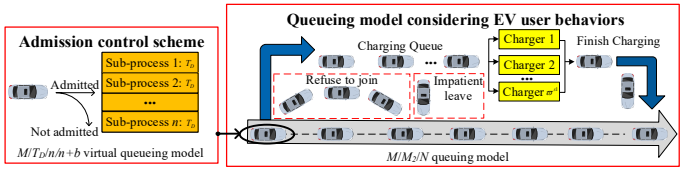

Fig. 7-4. The admission control scheme and queueing model.

7.5.3.2 *Behavior modeling based on both admission control and queueing model*

However, it is improper to apply the probability of refuse-to-join and impatient-leave straight away to model EV user behaviors. Because it is assumed that the behavior of EV users occurs after the admission control of the EVCS s1, shown in Fig. 7-4. In Fig. 7-4, both the admission control process and the queueing process are illustrated. It can be found that only EVs that are admitted can join the physical queue. Thus, the conditional probability based on Bayes' theorem is used to reflect the occurrence

sequence of admission and queueing [226]. The formulae relating to the conditional probability under the context of admission control and queueing model are shown as equations (7.30)-(7.33). Note that equation (7.33) utilizes the conditional probability to emphasize the occurrence sequence of admission control and the behavior of EV users.

$$Pr_t\left(RTJ\middle|adm\right)=\frac{Pr_t^{RTJ}\times Pr_t\left(adm\middle|RTJ\right)}{Pr_t^{adm}} \tag{7.30}$$

$$Pr_t\left(IL\middle|adm\right)=\frac{Pr_t^{IL}\times Pr\left(adm\middle|IL\right)}{Pr_t^{adm}} \tag{7.31}$$

$$Pr_t\left(adm\middle|RTJ\right)=1, Pr_t\left(adm\middle|IL\right)=1 \tag{7.32}$$

$$Pr_t\left(RTJ\middle|adm\right)=\frac{Pr_t^{RTJ}}{Pr_t^{adm}},\ \ Pr_t\left(IL\middle|adm\right)=\frac{Pr_t^{IL}}{Pr_t^{adm}} \tag{7.33}$$

where $Pr_t\left(adm\middle|RTJ\right)$ is the conditional probability that EV users, who refuse to join the queue at EVCS s1, are admitted by EVCS s1; $Pr_t\left(adm\middle|IL\right)$ is the conditional probability that EV users, who are impatient and will leave the EVCS s1, are admitted by EVCS s1; $Pr_t\left(RTJ\middle|adm\right)$ is the conditional probability that the admitted EV users refuse to join the queue at EVCS s1; $Pr_t\left(IL\middle|adm\right)$ is the probability that the admitted EV users are impatient and will leave EVCS s1.

In this chapter, the total charging demand at EVCS s1 is adjusted considering the EV user behaviors shown in (7.34), which is formulated based on equations (7.21), (7.24), and (7.33). Noted that our model is also adaptive to the case where there is no need to queue, in which case the adjusted demand $D_t^{s1,adj}$ in equation (7.34) will be equal to the total charging demand at EVCS s1 D_t^{s1}. This is because when there is no need to queue, the admission probability will be 1, and the behavior of refuse-to-join and impatient leave will not occur.

$$D_t^{s1,adj}=D_t^{s1}\times Pr_t^{adm}\times\left(1-Pr_t\left(RTJ\middle|adm\right)\right)\cdot\left(1-Pr_t\left(IL\middle|adm\right)\right) \tag{7.34}$$

where $D_t^{s1,adj}$ is the total adjusted demand at EVCS s1.

7.6 Proposed Pricing Strategy

7.6.1 Objective Function and Constraints

Based on the adjusted charging demand, we can formulate the pricing strategy for EVCS s1. The aim of EVCS s1 is to decide on charging prices that can maximize the net profit during the charging process, shown as equation (7.35). The first term shows the revenue of the charging service. The second term

shows the electricity purchasing cost. And the third and fourth terms are the operational cost during the charging service and the daily fixed cost. Equation (7.39) aims to remain the hourly average charging price set by EVCS s1 at an average charging price level. Normally, the average charging price level is determined based on the average energy consumption level of EV users and the average market charging price level [121].

$$\max . \sum_{t=1}^{T} \left(\lambda_t^{s1} \times D_t^{s1,adj} - \lambda_t^{BG} \times D_t^{s1,adj} \right) - C^{oper} - C^{inv} \tag{7.35}$$

s.t. equations (7.18)-(7.21), (7.24), (7.33), and (7.34).

$$C^{oper} = \sum_{t=1}^{T} D_t^{s1,adj} \times \varsigma \tag{7.36}$$

$$P^{s1,\min} \Delta t \le D_t^{s1,adj} \le P^{s1,\max} \Delta t \tag{7.37}$$

$$0 < \lambda_t^{s1} \le \lambda^{\max} \tag{7.38}$$

$$\sum_{t=1}^{T} \left(\lambda_t^{s1} \right) / T = \lambda^{PL} \tag{7.39}$$

where λ_t^{BG} is the electricity purchasing price of the electricity grid; λ^{PL} is the average charging price level; C^{oper} is the daily operational cost at EVCS s1; C^{inv} is the daily fixed cost at EVCS s1; ς is the unit operational cost.; $P^{s1,\min}$ and $P^{s1,\max}$ are the minimum and maximum power of the charger at EVCS s1, and they are measured in kW.

7.6.2 Power System Constraints

Furthermore, PDN constraints are included. This is because when a lower price is set by EVCS s1, more charging demand can be attracted from EVCS 2, which can lead to PDN congestion and instability, such as voltage instability, in the area where EVCS s1 locates. Hence, it is necessary to incorporate the power flow constraints to ensure that the price set by EVCS s1 can achieve spatial load shifting by incentivizing EV users to alter their station-selection decisions to avoid possible power congestion in the electricity network. Note that the EVCS and PDN are coupled via the power of EV charging loads at electricity bus q $P_{q,t}^{EV}$.

$$P_{pq,t} + P_{q,t}^{g} - r_{pq} \frac{\left(P_{pq,t} \right)^2 + \left(Q_{pq,t} \right)^2}{V_{q,t}^2} = \sum_{k \in K} P_{qk,t} + P_{q,t}^{EV} \tag{7.40}$$

$$Q_{pq,t} + Q_{q,t}^{g} - x_{pq} \frac{\left(P_{pq,t} \right)^2 + \left(Q_{pq,t} \right)^2}{V_{q,t}^2} = \sum_{k \in K} Q_{qk,t} \tag{7.41}$$

$$V_{q,t}^2 - V_{p,t}^2 = 2\left(r_{pq} P_{pq,t} + x_{pq} Q_{pq,t} \right) - \left(r_{pq}^2 + x_{pq}^2 \right) \frac{\left(P_{pq,t} \right)^2 + \left(Q_{pq,t} \right)^2}{V_{q,t}^2} \tag{7.42}$$

$$\underline{V_q} \le V_{q,t} \le \overline{V_q}, \sqrt{\left(P_{pq,t}\right)^2 + \left(Q_{pq,t}\right)^2} \le \overline{S_{pq}} \tag{7.43}$$

where $P_{pq,t}$ ($Q_{pq,t}$) is the active (reactive) power flow from bus p to bus q; $P^g_{q,t}$ ($Q^g_{q,t}$) is the active (reactive) power generated at bus q; r_{pq} (x_{pq}) is the resistance (reactance) from bus p to bus q; $V_{q,t}$ is the nodal voltage; $P_{qk,t}$ ($Q_{qk,t}$) is the active (reactive) power flow from bus q to bus k; $P^{EV}_{q,t}$ is the power of EV charging loads at bus q; $\overline{(\bullet)}$ and $\underline{(\bullet)}$ are the upward and downward limits.

7.6.3 Interdependency between Sub-models

In (7.35), the charging price λ^{s1}_t and the adjusted total charging demand $D^{s1,adj}_t$ are two important variables. They are related based on the sub-models introduced in the previous sections.

The **first sub-model** is the TN modeling presented in section III. It aims to derive the optimally assigned charging flow and use it as a known parameter in section V to derive the indifferent price. And based on the indifferent price, the relationship between charging price and total charging demand is formulated. As a result, section III and the following sections have a sequential relationship.

The **second sub-model** is the two-step approach presented in section V. It aims to formulate the relationship between total charging demand and charging price shown as (7.21) based on the indifferent price. And this relationship is one of the constraints of the optimization problem stated in section VII.

The **third sub-model** is the admission-based EV behavior modeling presented in section VI. It formulates the relationship between total charging demand and adjusted total charging demand in (7.34) based on equations (7.21), (7.24), and (7.33). And this relationship is also one of the constraints of the optimization problem stated in section VII.

The relationships formulated in section V and section VI are two constraints that are embedded into the optimization problem in section VII. Hence, the whole process is coherent and correlated.

7.6.4 Operational Framework

In this framework, we are formulating a dynamic pricing strategy for EVCS s1 to maximize the net profit of EVCS s1 based on future predicted data, including the traffic demand and the electricity purchasing price, etc. A rolling horizon is applied as an optimization framework to solve this real-time pricing optimization problem. The rolling optimization is conducted every 15 minutes. The optimized charging price of the first time interval will be used as the real-time charging price. For the rest optimized charging prices, they will be used as future reference charging prices. In the real application, the real-time charging price, along with the future reference prices, will be broadcasted to EV users to facilitate

EV users in making energy charging decisions.

7.6.5 Solver to Solve the Optimization Problem

In this chapter, the original problem is a convex optimization (However, it is not a quadratic optimization because there is a second-order cone constraint due to DistFlow equations). Since the formulated problem is convex, the interior-point method can find the optimal solution, which can be referred to [227]. As a result, the solver used is the Interior Point Optimizer (IPOPT) solver, which is an open-source solver suitable to solve large-scale non-linear optimization problem. As our problem is convex and the scale of the optimization problem is relatively small (because we solve the problem from the macroscopic level and the EV charging demand is aggregated), the solver can find the optimal solution accurately and efficiently. To be noted, the increasing number of EVs will not affect the computation time of our model. Hence, scalability will not be a problem for the proposed model.

7.7 Case Study

7.7.1 Experiment Setting

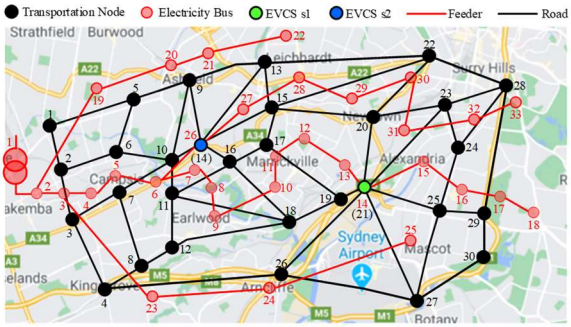

Fig. 7-5. A coupled power distribution network and transportation network.

The proposed dynamic pricing strategy is verified in the IEEE 33-bus power distribution system coupled with the 30-node transportation system, shown in Fig. 7-5. In this diagram, the traffic network is simplified from an actual district in Sydney, Australia, which includes 30 nodes and 53 arterial roads. The power distribution system has one 110 kV substation. To be noted, the PDN and TN are coupled based on EVCS s1 and EVCS s2 located at bus 14 (node 21) and bus 26 (node 14), respectively [228]. Note that our model can be applied to other transportation topologies. The distance or location of the EVCSs will not affect the scalability of the model.

TABLE 7-2. CHARGING STATION AND ELECTRIC VEHICLE PARAMETERS

Electric vehicle charging station parameters			
Number of chargers	$\varpi^{s1}=40$	Number of sub-processes	$n=5$
Maximum power of	$P^{s1,\max}=100$	Charging rate	$\mu_t^{s1}=2$

the charger (kW)		(veh/hr)	
Electric vehicle parameters			
Average charging demand (kWh)	$d = 20$	Maximum capacity (kWh)	$E^{ev,\max} = 45$
Average energy consumption (kWh/km)	$E^{ev} = 0.5$	Average initial state-of-charge (%)	$SOC^0 = 45\%$

The parameters relating to EVCS s1 and EVs are listed in Table 7-2. For the EVCS, the parameters related to the admission control (i.e., number of sub-processes) and the physical queueing processes (i.e., number of chargers, maximum power of the charger, and charging rate) are included. For EVs, the parameters related to the EV battery (i.e., maximum capacity, average energy consumption, and average initial SOC) and average charging demand are listed.

The simulations were completed by a PC with an Intel Core (TM) i7-9750 CPU @ 2.60 GHz with 16.00 GB RAM. The computation time of the pricing optimization problem is around 5 minutes and 47 seconds.

7.7.2 Simulation Results

Four case studies are carried out to prove the effectiveness of the proposed dynamic pricing strategy.

Case 1 Base case: Fixed pricing strategy for EVCS without considering transportation system modeling.

Case 2 Optimal pricing strategy for EVCS considering transportation system modeling without modeling the relationship between charging demand and charging price [121].

Case 3 Competitive pricing strategy for EVCS without considering transportation system modeling that models the relationship between charging demand and charging price. However, the impact of queueing length on charging demand is ignored [125].

Case 4 Proposed dynamic pricing strategy for EVCS with a coupled PDN and TN that incorporates demand responsiveness towards charging price and the recursive impact of queueing length on charging demand.

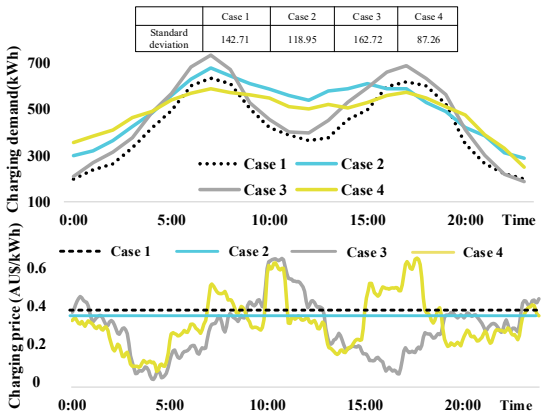

Fig. 7-6. Charging demand and charging price at EVCS s1 of four cases.

In Fig. 7-6, the charging demand and charging price at EVCS s1 of the four cases are illustrated. It can be found that the standard deviation of the charging demand of case 4 is the smallest compared with the other three cases at 87.26. Hence, case 4 has the least fluctuating charging demand. To be specific, a lower price is set by EVCS s1 as the spatial incentive to attract more EVs to shift the station-selection decision to EVCS s1 during the off-peak charging hours. As a result, the charger utilization during the off-peak charging period can be enhanced. By contrast, a higher price is set by EVCS s1 as the spatial incentive for EV users to shift the station-selection decision to EVCS s2 during peak charging hours. As a result, queueing length and waiting time at EVCs s1 can be reduced. Additionally, the problem of congestion on the electricity network can be mitigated. Moreover, it can be found that the charging demand of case 4 during the peak charging period at around 6:00 to 9:00 and 16:00 to 19:00 is the lowest. This is not only because of the high charging price but also because the proposed model introduces the admission control scheme to guarantee the stability of the physical queueing process. Thus, the number of EVs is further controlled when there is a peak charging demand. By comparison, case 3 has the highest charging demand during the peak charging period. This is because the competitive pricing strategy under case 3 aims to attract more charging demand from the competitor, i.e., EVCS s2. However, this pricing strategy of case 3 neglects to ensure the QoS at the EVCS. Thus, the long queueing length might occur during the peak charging period, which might lead to customer dissatisfaction.

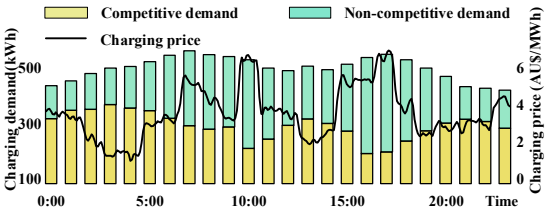

Fig. 7-7. Competitive and non-competitive charging demand of case 4.

Fig. 7-7 further specifies the component of the total charging demand of case 4, i.e., the competitive demand and the non-competitive demand. It can be found that the competitive demand is influenced by the charging price. The higher the charging price is, the lower the competitive demand will be, and vice versa. This is because the demand and price follow an inversely related relationship, as mentioned in section V, part B. By contrast, the non-competitive demand is irresponsive to the charging price.

TABLE 7-3. COMPARISON OF THREE TYPES OF PERFORMANCE INDICATORS

Criteria	Detailed items	Case 1	Case 2	Case 3	Case 4
Attractiveness	Total daily demand (MWh)	10.02	10.57	12.16	11.81
Profitability	Charging revenue (AU$)	3908	4017	4108	4547
	Purchasing cost (AU$)	501	528	608	590
	Charging profit (AU$)	3407	3489	3500	3957
Operation stability	Profit variance	421	385	352	369
	Queueing length volatility	115	104	128	93

In Table 7-3, four cases are compared from three aspects of criteria, i.e., *attractiveness*, *profitability*, and *operation stability* of EVCS s1, to verify the effectiveness of the proposed pricing strategy. For *attractiveness*, the more total charging demand is serviced by EVCS s1, the more attractive EVCS s1 will be. It can be found that case 3 has the highest charging demand at 12.16 MWh per day compared with the other three cases. This is because the pricing strategy of case 3 considers the competitive relationship between EVCSs. Hence, a lower price is set to attract more charging demand. Although case 4 also considers the competitive relationship between EVCSs, the total daily demand is slightly lower than that of case 3 at 11.81 MWh. This is because the competition relationship in case 4 is established based on the TN. As a result, the degree of competition is not overestimated, and the formulated charging price will be higher than that of case 3. For *profitability*, it can be found that case 4 has the highest charging profit at 3957 AU$. For *operation stability,* it is further evaluated from two sub-aspects, i.e., profit variance and queueing length volatility. Although the profit variance of case 4 is only the second-lowest among the other three cases, the queueing length volatility under case 4 is the lowest at 93. Thus, a balance between the QoS at the EVCS and the charging profit can be obtained.

Fig. 7-8 illustrates the hourly charging profits and hourly queueing length of EVCS s1 of the four cases. As for hourly profits, it can be found that case 4 has the highest hourly average charging profits, and case 3 has the least profit fluctuation measured by variance. By contrast, case 1 has the lowest hourly average charging profits with the most profit fluctuation. As for hourly queueing length, case 4 has the least queueing length volatility, whereas the queueing length of case 3 is the most volatile, which can

also be verified via Table 7-3.

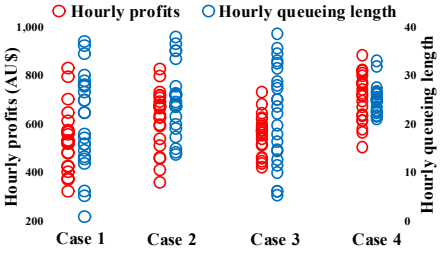

Fig. 7-8 Hourly charging profits and queueing length of EVCS s1 under four cases

Moreover, the charger occupation frequency of each case is presented. In Fig. 7-9, it can be found that 90% of the time, more than 50% of the chargers (>20 chargers) are occupied under case 4. By contrast, the occupation frequency for cases 1, 2, and 3 when the number of chargers being occupied is more than 20 is 54.2%, 75%, and 63%, respectively. This indicates that the proposed model significantly enhances the charger utilization ratio by ensuring that most of the time, most of the chargers are working. Furthermore, the more evenly distributed the occupation frequency is, the more fluctuating the queueing length will be. It can be found that the occupation frequency of case 4 is the least evenly distributed. Thus, the queueing length under case 4 is the most stable one compared with the other three cases, which can also be verified via Table 7-3.

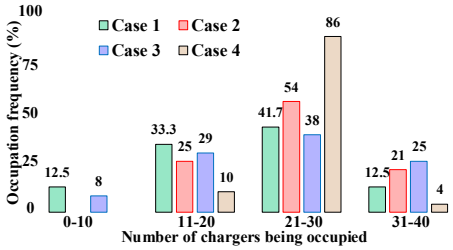

Fig. 7-9. Charger occupation frequency of each case.

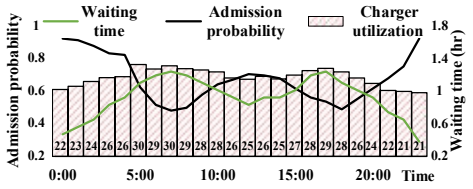

Fig. 7-10. The effect of the admission control on the waiting time, admission probability, and charger utilization of the proposed model.

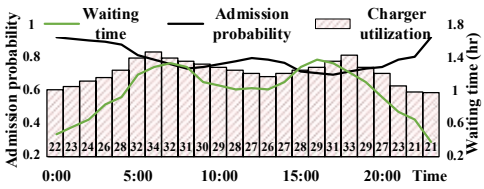

Fig. 7-11. The effect of the admission control on the waiting time, admission probability, and charger utilization of [222].

Furthermore, the proposed model is compared with the pricing strategy used in [222], where admission control is considered, but no EV user behaviors are modeled, holding other things constant. It can be found that the admission probability for the proposed model in Fig. 7-10 is lower than using the pricing strategy of [222] in Fig. 7-11 when there is a peak charging demand from 6:00 to 9:00 and 16:00 to 19:00. Thus, fewer EVs are admitted. As a result, the waiting time of the proposed model is shorter, and the charger utilization is lower during that peak charging period. This is because EVCS s1 aims to avoid excessive delay of service by considering the EV user behaviors when formulating the pricing strategy. Thus, the number of EVs is further controlled during the peak charging period compared with using the pricing strategy of [222].

TABLE 7-4. COMPARISON OF PDN LOSS COST AND DOWNWARD VIOLATION OF THE FOUR CASES

	Case 1	**Case 2**	**Case 3**	**Case 4**
PDN loss cost (AU$)	272	264	276	240
Minimum voltage (p.u.)	0.9445	0.9532	0.9354	0.9654

Additionally, the impact of the pricing strategy on the PDN is further analyzed from two aspects, i.e., PDN loss cost and downward voltage violation. In Table 7-4. It can be found that case 4 has the lowest PDN loss cost at 240 AU$ with a minimum voltage of 0.9654 p.u. This is because the proposed pricing strategy can reduce peak load at EVCS s1. Hence, the problem of downward voltage violation is avoided, and the PDN congestion is mitigated. By contrast, the PDN loss cost of case 3 is the highest, and there are downward violations for both cases 1 and 3.

TABLE 7-5. EFFECT OF DIFFERENT PRICING STRATEGIES ON EACH EVCS

		Case 1	**Case 2**	**Case 3**	**Case 4**
Total charging demand (MWh)	**EVCS s1**	10.02	10.57	12.16	11.81
	EVCS s2	12.88	12.01	10.75	11.60
Total charging profit (AU$)	**EVCS s1**	3407	3489	3500	3957
	EVCS s2	3887	3627	3246	3503

In Table 7-5, the effect of different pricing strategies on both EVCS s1 and EVCS s2 are analyzed. In case 1 (as a base case), the EVCS s2 attracts more charging demand than EVCS s1. When further considering the TN model, it can be found that the total charging demand of EVCS s1 under case 2 is higher than that under case 1. This is because, in case 2, a more proper pricing strategy is formulated based on the estimated charging demand, which is derived via TN modeling. Consequently, the total charging profit of EVCSs1 under case 2 is higher than that under case 1. At the same time, the charging

demand at EVCS s2 is reduced, which results in a lower profit. In case 3, the competitive relationship between EVCSs s1 and s2 is incorporated. Hence, EVCS s1 can attract more charging demand from EVCS s2, and the total charging demand and total profit of EVCSs1 in case 3 are higher than that of cases 1 and 2. Nevertheless, this competitive relationship is not established based on TN, and the degree of competition might be overestimated. As a result, EVCS s1 may set a low price to enhance competition ability in attracting charging demand but sacrifice the profits. Therefore, although the charging demand of EVCS s1 increases to a large extent in case 3, the increase in profit is not obvious. In case 4, the competitive relationship is established based on TN, which better investigates the competition relationship between two EVCSs. Therefore, EVCS s1 in case 4 can achieve the highest profit.

7.7.3 Sensitivity Analysis

In Fig. 7-12, the impact of the arrival rate and the number of sub-processes on the admission probability is illustrated. It can be found that an increase in the arrival rate will reduce the admission probability. On the contrary, the increase in the number of sub-process will increase the admission probability.

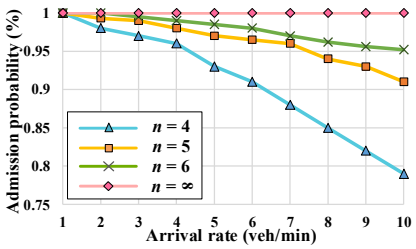

Fig. 7-12. The impact of arrival rate and the number of sub-processes on admission probability.

In Fig. 7-13, the impact of the arrival rate and average charging demand on average waiting time is illustrated. It can be found that an increase in either the arrival rate or the average charging demand will increase the average waiting time.

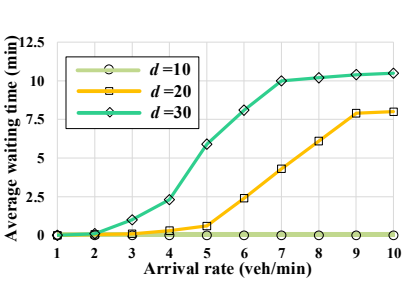

Fig. 7-13. The impact of arrival rate and average charging demand on average waiting time.

7.8 Conclusion

In this chapter, a dynamic pricing strategy for the EVCS is proposed considering a coupled PDN and

TN and the responsiveness of demand. First, a pricing strategy, considering the competition effect established based on the TN, is formulated. Second, a two-step approach is proposed to formulate the responsiveness of demand towards the charging price. Third, the EV user behaviors are incorporated based on both an admission control scheme and a queueing model to further adjust the charging demand. The effectiveness of the proposed pricing strategy is verified via the simulation results. The potential benefits of the proposed pricing strategy are threefold in terms of attractiveness, profitability, and stability. To be specific, the proposed pricing strategy can be applied to facilitate the EVCS to attract more charging demand and gain more charging profit. Additionally, the proposed pricing strategy can achieve spatial load shifting by incentivizing the EV users to alter their station-selection decision to avoid possible power congestion in the electricity network. Hence, the stability of PDN can be ensured. Moreover, our proposed model presents the balance between charging price and queueing length. This balance prevents the EVCS from setting a very low charging price which leads to a long queueing length. Therefore, congestion caused by the queueing length within the EVCS in TN can be avoided.

7.9 Appendix

a. ***Proof of Proposition 1***:

$$U_{\beta,t}^{s1} = U_{\beta,t}^{s2} \tag{7.44}$$

$$U_{\beta,t}^{s1} - U_{\beta,t}^{s2} = -\lambda^{wa} \times \left(w_t^{s1} - w_t^{s2} \right) - D_{\beta,t} \times \left(\lambda_{\beta,t}^{s1} - \lambda_t^{s2} \right) = 0 \tag{7.45}$$

Let $\lambda_{\beta,t}^{s1} - \lambda_t^{s2} = \Delta\lambda_{\beta,t}^{*}$, then we have:

$$\Delta\lambda_{\beta,t}^{*} = \frac{-\lambda^{wa}\left(w_t^{s1} - w_t^{s2} \right)}{D_{\beta,t}} \tag{7.46}$$

b. ***Proof of Proposition 2***: According to the monotonicity of the function shown as equation (7.16), there is only one global maximum point [229]. Thus, we can simply let $f\left(\rho_{\beta,t}\right)$=0 to obtain the unique root. Then we have:

$$0.5 = \rho_{\beta,t} e^{-\rho_{\beta,t}\lambda_{\beta,t}^{s1*}} \tag{7.47}$$

$$ln(0.5) = ln\left(\rho_{\beta,t}\right) - \rho_{\beta,t}\lambda_{\beta,t}^{s1*} \tag{7.48}$$

Then, we define $\gamma\left(\rho_{\beta,t}\right)$ as:

$$\gamma\left(\rho_{\beta,t}\right) = ln\left(\rho_{\beta,t}\right) - \rho_{\beta,t}\lambda_{\beta,t}^{s1*} - ln(0.5) \tag{7.49}$$

Next, taking the derivative of $\gamma\left(\rho_{\beta,t}\right)$, we have:

$$\frac{d\gamma\left(\rho_{\beta,t}\right)}{d\rho_{\beta,t}}=\frac{1}{\rho_{\beta,t}}-\lambda_{\beta,t}^{s1*}=0 \tag{7.50}$$

$$\rho_{\beta,t}=1/\lambda_{\beta,t}^{s1*} \tag{7.51}$$

Finally, by plugging the root value of the coefficient into equation (7.16), the global maximum point can be expressed as $\left(1/\lambda_{\beta,t}^{s1*},1/\left(\lambda_{\beta,t}^{s1*}e\right)-0.5\right)$. Thus, the value of the charging price that makes $f\left(\rho_{\beta,t}\right)$ =0 is when $\lambda_{\beta,t}^{s1*}=2/e$, and it is also the upper limit of the auxiliary charging price, shown as Fig. 7-14.

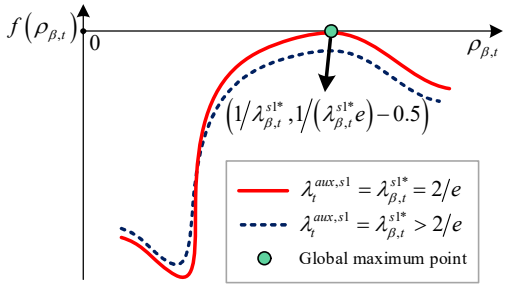

Fig. 7-14. Mathematical graph explanation of **Proposition 2**.

In Fig. 7-14, the global maximum point is found when $\lambda_{\beta,t}^{s1*}=2/e$. Be noted that $\lambda_{\beta,t}^{s1*}$ is the auxiliary charging price which is different from the real charging price. However, when $\lambda_{\beta,t}^{s1*}>2/e$, there is no root for $f\left(\rho_{\beta,t}\right)$, i.e., no root for equation (16). Hence, the auxiliary price should be within the range $\left(0,2/e\right]$.

c. Extend the two-station problem to a multiple-station problem

The two-station selection model can be extended to a multiple-station problem based on the two-step approach presented in section V. When there are multiple EVCSs (more than two EVCSs), the indifferent price among them can be derived by solving simultaneous equations related to the station-selection utility of EVs shown as (7.10) and (7.11). However, the existence of such an indifferent price (solutions of the simultaneous equations) cannot be ensured. Hence, we derive the indifferent price by focusing on every two EVCSs (i.e., EVCS s1 and another EVCS).

First, the indifferent price for each pair of EVCSs will be derived in the same way as step 1 presented in section V, part A.

Second, based on the derived indifferent price of each pair of EVCSs, the relationships between the competitive demand probability and the charging price of EVCS s1 can be formulated using the same approach of step 2 presented in section V, part B shown as (7.52). Note that if there are *n* EVCSs, there

will be *n*-1 equations describing such a relationship.

$$Pr_{D_{\beta,t}^{s1}} = \rho_{\beta,t}^{s1,sj} e^{-\rho_{\beta,t}^{s1,sj}\lambda_t^{s1}}, sj \in \Omega_{sj \neq s1} \tag{7.52}$$

where $\rho_{\beta,t}^{s1,sj}$ is the coefficient that describes the relationship between the competitive demand probability and the charging price of EVCS s1 considering the EVCS pair of EVCS s1 and EVCS sj; $\Omega_{sj \neq s1}$ is the set of EVCSs excluding EVCS s1.

Third, the ratio of the competitive demand probability of EVCS s1 and the competitive demand probability of another EVCS within the pair satisfies (7.53).

$$\frac{Pr_{D_{\beta,t}^{s1}}}{Pr_{D_{\beta,t}^{sj}}} = \frac{\rho_{\beta,t}^{s1,sj} e^{-\rho_{\beta,t}^{s1,sj}\lambda_t^{s1}}}{1-\rho_{\beta,t}^{s1,sj} e^{-\rho_{\beta,t}^{s1,sj}\lambda_t^{s1}}} \tag{7.53}$$

Additionally, the summation of the competitive demand probability of all the EVCSs should be 1 shown as (7.54).

$$Pr_{D_{\beta,t}^{s1}} + \sum\nolimits_{sj \in \Omega_{sj \neq s1}} Pr_{D_{\beta,t}^{sj}} = 1 \tag{7.54}$$

Substitute equation (7.19) with both (7.53) and (7.54), the constraints are generalized from a two-station problem to a multiple-station problem. The generalized constraints of both (7.53) and (7.54) will be the constraints of the pricing optimization problem in (7.35).

Finally, to verify whether the generalized constraints are applicable to the special case where only two EVCSs are considered, (7.53) and (7.54) can be simplified into (7.55) and (7.56), respectively.

$$\frac{Pr_{D_{\beta,t}^{s1}}}{1-Pr_{D_{\beta,t}^{s1}}} = \frac{\rho_{\beta,t}^{s1,s2} e^{-\rho_{\beta,t}^{s1,s2}\lambda_t^{s1}}}{1-\rho_{\beta,t}^{s1,s2} e^{-\rho_{\beta,t}^{s1,s2}\lambda_t^{s1}}} \tag{7.55}$$

$$Pr_{D_{\beta,t}^{s1}} + Pr_{D_{\beta,t}^{s2}} = 1 \tag{7.56}$$

Combining both (7.55) and (7.56), we can derive (7.57), which is the exact derivation in section V.

$$Pr_{D_{\beta,t}^{s1}} = \rho_{\beta,t}^{s1,s2} e^{-\rho_{\beta,t}^{s1,s2}\lambda_t^{s1}} = \rho_{\beta,t} e^{-\rho_{\beta,t}\lambda_t^{s1}} \tag{7.57}$$

As a result, those generalized constraints are also applicable to the two-station problem.

8. INDIVIDUALIZED PRICING OF ENERGY STORAGE SHARING BASED ON DISCOUNT SENSITIVITY

With the increasing use of distributed renewable energy to generate electricity, energy storage sharing has become more promising because it is capable of smoothing renewable power generation and reducing energy purchasing costs. In this chapter, we present a two-stage pricing mechanism between the coordinator who operates the shared energy storage and the prosumers who are borrowing the shared capacity from the coordinator. Individualized pricing is derived via the two-stage pricing process. It is a pricing strategy that can facilitate the coordinator to capture the most considerable possible net profits through price discrimination. First, prosumers are clustered into different groups using the data-driven approach. Then, novel concepts of bulk capacity borrowing and discount sensitivity are introduced to model the individualized pricing for the first time. As a result, the price structures and the price levels can be jointly optimized. From the simulation results, it can be found that the proposed individualized pricing can increase the net profits of the coordinator, enhance the utilization efficiency of the energy storage system, and reduce the energy consumption costs of the prosumers.

8.1 Introduction

With the increasing penetration of renewable resources, such as rooftop PV generation [39], greenhouse gas emissions can be reduced. However, renewable resources are difficult to operate reliably due to their intermittent and unstable features [40]. Thus, the energy storage system (ESS) is employed to smooth the spatial and temporal imbalance between the load demand and the renewable energy generation. Nevertheless, the investment costs of ESS are substantial, and the costs are entirely borne by the end-users. Furthermore, because of the random usage patterns of different residents, the utilization of the residential ESS is inefficient. To this end, the concept of energy storage sharing is introduced where the centrally controlled ESS can provide storage services to the end-users as if they were using the behind-the-meter ESS.

In the literature, the research on energy storage sharing could be divided into two layers, the *physical layer* and the *virtual layer* [48]. The *physical layer* mainly focuses on voltage and capacity control, network power loss minimization, and system strengthening [230]. In this chapter, the scope falls into the virtual layer, mainly *developing pricing mechanisms* [140, 231-235]. As for *developing pricing mechanisms,* there are mainly two types of pricing strategies. The first type is based on the clearing

scheme. In the existing literature, there are two commonly used clearing schemes. The first type of clearing is based on the non-cooperative game, such as [67]. The second type of clearing is based on the auction, such as [68]. The advantages and disadvantages of the two types of existing clearing schemes are explained as follows:

For the advantages, first, the common advantage of the two types of clearing schemes is that the end-users have the initiatives to participate in the sharing market. To be specific, the end-users can actively adjust their sharing strategies according to their energy demand, excess energy, and cost functions. As a result, the costs and the demand-supply information are fully considered in the clearing process. Second, for the clearing scheme based on the non-cooperative game, the global optima can be found in a totally distributed fashion. With the introduced distributed transaction technology, the clearing process can be conducted without a third party [67]. This means the end-users can purchase (sell) energy from (to) the other end-users with their privately compromised prices [67]. Thus, the information privacy of the end-users can be protected with limited information exchanges.

For the disadvantages, first, the non-cooperative game clearing and the auction-based clearing of energy sharing modeled the sharing process like an energy trading process. In such a sharing scheme, the pure consumers could participate and benefit by purchasing electricity at a relatively low sharing price in the clearing process even if they made less contribution toward the energy sharing [48]. It would lead to that pure consumer being less incentivized to invest in DERs so that the development of the DERs could be hindered. Second, the end-users were directly participating in the electricity market. As a result, they would encounter high risks due to the fluctuating sharing price. Additionally, the end-users normally lacked the expertise in risk-hedging.

Thus, it is necessary to propose a pricing strategy to realize the insulation between the end-users and the electricity market. Insulation means that the end-users do not directly participate in the electricity market. Hence, the sharing coordinator is introduced to insulate the prosumers and the sharing market so that the risks of the prosumers caused by the price fluctuation can be hedged. To this end, the second type of pricing strategy is introduced, where the coordinator is responsible for formulating the sharing price to realize the insulation between the prosumers and the sharing market. However, current literature failed to shift the energy usage profile of prosumers who had similar characteristics. This is because the individual sensitivity towards price change is neglected. Hence, a pricing strategy that can further

incentivize the prosumers needs to be investigated.

To solve the problems, we propose an individualized pricing strategy for energy storage sharing. The main contributions of this chapter are as follows:

- First, a two-stage pricing model for energy storage sharing has been presented based on the clustering of different load patterns. In the proposed model, the price structure and the price level for capacity sharing are jointly optimized.
- Second, novel concepts of bulk capacity borrowing and discount sensitivity are introduced to model individualized pricing for the first time. Bulk capacity borrowing and discount sensitivity are utilized to incentivize more prosumers to participate in the capacity sharing process and enhance the sharing profits of the coordinator.
- Third, a new business mode is formulated to determine a more reasonable payment rule for energy storage sharing. Traditionally, prosumers who are engaged in energy storage sharing will be charged according to the net discharging at a specific time. However, in our chapter, the concept of the capacity borrowing state is introduced, which can better reveal the essence of the sharing economy. That means the payment rule is closely related to the time length of borrowing.

8.2 Overview of Proposed Two-Stage Pricing Framework

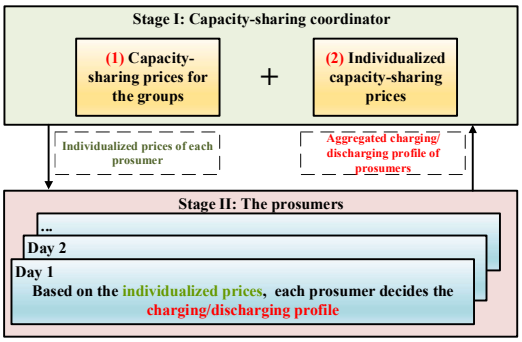

Fig. 8-1. Proposed two-stage pricing framework.

In Fig. 8-1, the proposed two-stage pricing framework is presented. In stage I, the coordinator who operates the shared energy storage will determine the capacity-sharing price for each individual prosumer. The coordinator will first determine the TOU capacity-sharing prices for each group based on the group marginal costs and the risk premium. Then, after applying the concepts of discount sensitivity and bulk capacity borrowing, the capacity-sharing price will be further individualized. Finally, the individualized prices will be passed to stage II. In stage II, the prosumers will react to the individualized prices and decide their charging/discharging profiles. Then the optimal profiles will be passed to the coordinator in

stage I. This iterative process will continue until reaching an equilibrium.

8.3 Conventional Pricing Mechanism Without Price Discrimination

Conventionally, the energy storage coordinators use equations (8.1) and (8.2) to determine the price r for energy storage sharing. Other ESS and system constraints can be referred to [69]. The energy storage price in the conventional pricing mechanism is the same for all the prosumers at any time of the day. And the prosumers will be charged according to the net discharging profile at time *t*.

$$\max NP_{co} = R_{co}(r) - C_{co}^{cap}(X,P) - \sum_{j=1}^{J}\sum_{t=1}^{T} C_{co}^{oper}\left(P_{j,t}^{ch}, P_{j,t}^{dis}\right) \tag{8.1}$$

s.t.
$$R_{co}(r) = \mathbb{E}\left[r \times \sum_{j=1}^{J}\sum_{t=1}^{T}\left(P_{j,t}^{dis} - P_{j,t}^{ch}\right)\right] \tag{8.2}$$

where NP_{co} is the daily net profit of the coordinator under the conventional model; $R_{co}(r)$ is the expected daily revenue over all scenarios under the conventional model; $\mathbb{E}$ is the expectation function; $P_{j,t}^{ch} / P_{j,t}^{dis}$ is the charging/discharging profile of prosumer *j* at time *t*; T is the total time period within a day; J is the total number of the prosumers; $C_{co}^{cap}(X,P)$ is the total daily capital cost of the coordinator under the conventional model; X and *P* are the capacity and power of the storage devices; $C_{co}^{oper}\left(P_{j,t}^{ch}, P_{j,t}^{dis}\right)$ is the operational cost for serving prosumer *j* at time *t*.

However, the price determined by the conventional pricing mechanism is the same for all the prosumers, which neglects the price elasticity of prosumers. Additionally, the prosumers are charged according to their net discharging at each time. By comparison, our pricing model individualizes the capacity sharing prices for each prosumer based on bulk capacity borrowing and discount sensitivity. Furthermore, prosumers will be charged according to the capacity borrowing state, which is a new charging method that involves the time accumulation effect.

8.4 Proposed Discount Sensitivity Based on Price Discrimination

8.4.1 The Mechanism and Benefits of Price Discrimination

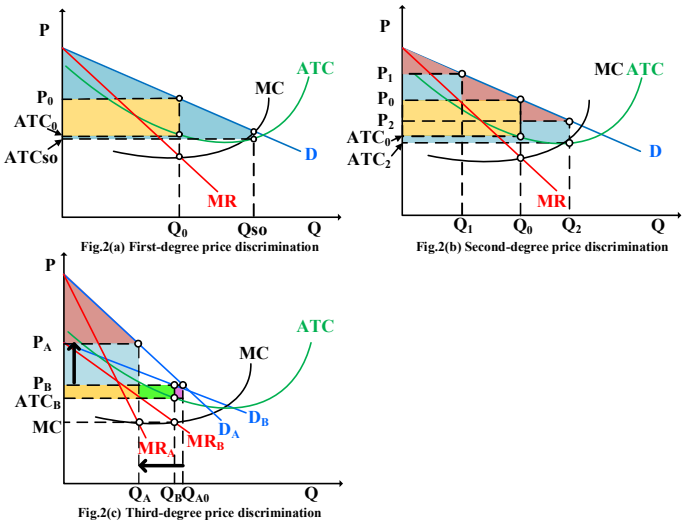

Fig. 8-2. Mechanism of three degrees of price discrimination.

To customize the capacity-sharing price, price discrimination will be applied. Figs. 8-2(a), 8-2(b), and 8-2(c) show the mechanism of first-degree, second-degree, and third-degree discrimination, respectively. In this diagram, the social welfare, coordinator surplus, and prosumer surplus are illustrated. Here, social welfare is defined as the total extra benefit or happiness enjoyed by the prosumers (i.e., the prosumer surplus) and the coordinator (i.e., the coordinator surplus) who feel they got a reasonable price for the 'product' being exchanged [170]. In this chapter, the product is the shared capacity. A detailed explanation of Fig. 8-2 can be referred to as ***Theorem 1.*** In Fig. 8-2, *P* is the capacity sharing price; *Q* is the amount of capacity borrowed by the prosumers; *D* is the demand curve; *MC* is the marginal cost; MR is the marginal revenue; *ATC* is the average sharing cost of the coordinator.

Theorem 1*: Price discrimination can be utilized by the coordinator to increase the net profits during the capacity sharing process.*

Proof: *First-degree price discrimination:* This type of price discrimination can be used when the coordinator knows the maximum price the prosumers can accept [170]. When no price discrimination is applied, the coordinator will use the Profit Maximization Rule, i.e., *MC*=*MR*, in economics to maximize the profits of capacity sharing [170]. As a result, the optimal sharing amount and the corresponding sharing price can be found at Q_0 and P_0 at an average cost of ATC_0, shown in Fig. 8-2 (a). Thus, the coordinator surplus is $(P_0\text{-}ATC_0)\times Q_0$, which is the yellow area. When first-degree price discrimination is applied, the socially optimal amount of capacity to share is Q_{so} at an average cost of ATC_{so}. Thus, the coordinator surplus is the blue area plus the yellow area, which is larger than the coordinator surplus when no price discrimination is applied. However, in practice, it is difficult for the coordinator to acquire

the maximum price the prosumers can accept. Thus, it is not suitable for this chapter.

Second-degree price discrimination: This type of price discrimination can be used when the coordinator wants to enhance sales by charging the prosumers less capacity-sharing price when the prosumers borrow more capacity. When no price discrimination is applied, the coordinator surplus is $(P_0\text{-}ATC_0)\times Q_0$, which is the yellow area shown in Fig. 8-2 (b) that can be derived the same way as before. To realize second-degree discrimination, two additional capacity-sharing prices are formulated by the coordinator. As a result, the prosumers can either borrow Q_1 amount of shared capacity at capacity sharing price P_1 or borrow Q_2 amount of shared capacity at capacity sharing price P_2 ($P_2 < P_0 < P_1$). Here, ATC_2 is the average cost to share Q_2 amount of capacity. Thus, the coordinator surplus is composed of three parts. Namely, $(P_1\text{-}ATC_2)\times Q_1$, $(P_0\text{-}ATC_2)\times(Q_0\text{-}Q_1)$, and $(P_2\text{-}ATC_2)\times(Q_2\text{-}Q_0)$, which is the blue area and the yellow area that is larger than the coordinator surplus when no price discrimination is applied. Thus, second-degree discrimination can be utilized to enhance the profits of the coordinator. A detailed formula can refer to equation (8.17).

Third-degree price discrimination: This type of price discrimination can be applied when the coordinator wants to encourage more new prosumers to participate in the capacity-sharing process by charging prosumers different sharing prices according to their price elasticity. For illustration simplicity, in Fig. 8-2 (c), there are two prosumers borrowing the capacity from the coordinator, i.e., prosumer A and prosumer B. It is assumed that prosumer A has relatively inelastic demand while prosumer B has relatively elastic demand. The average cost of the coordinator to share Q_B amount of capacity can be found at ATC_B. When no price discrimination is applied, the capacity sharing prices for both prosumer A and prosumer B are the same at P_B. Thus, the optimal capacity sharing amount for prosumers A and B can be found at Q_{A0} and Q_B, respectively. As a result, the coordinator surplus composes of two parts: $(P_B\text{-}ATC_B)\times Q_{A0}$ (the yellow, green, and pink areas) and $(P_B\text{-}ATC_B)\times Q_B$ (the yellow and green areas). To realize third-degree price discrimination, the capacity sharing price for prosumer B remains at P_B while a higher price is charged for prosumer A at P_A. Thus, the coordinator surplus includes $(P_A\text{-}ATC_B)\times Q_A$ (the yellow and blue areas) and $(P_B\text{-}ATC_B)\times Q_B$ (the yellow and green areas), which is larger than the coordinator surplus when no price discrimination is applied. Thus, third-degree price discrimination can be applied to increase the net profits of the coordinator. Detail can refer to as ***Theorem 2*** and equation (8.17).

8.4.2 The Proposed Discount Sensitivity

Inspired by the economic theory of third-degree discrimination mentioned above, the concept of discount sensitivity is introduced.

For discount rate, it is defined as the capacity sharing price reduction given to the prosumer when the prosumer is borrowing capacity from the coordinator in a bulk amount. In other words, the more capacity is borrowed by the prosumers, the more discounts will be given to the prosumers.

Discount sensitivity is a quantitative measure of the percentage changes in capacity borrowed by the prosumers when there is a one percent increase in the capacity sharing discount rate, holding everything else constant.

Theorem 2: The following relationship between the discount rate and the discount sensitivity in equation (8.3) can ensure maximized profits for the coordinator. The discount sensitivity information can be collected via the questionnaire, which will not be the focus of this chapter. The relationship can be explained in equation (8.3):

$$\frac{D_{g,j,t}}{D_{g,q,t}} = \frac{1+\left[1/f_q\left(D_{g,q,t}\right)\right]}{1+\left[1/f_j\left(D_{g,j,t}\right)\right]} \tag{8.3}$$

where $D_{g,j,t}$ is the discount rate for prosumer *j* at time *t*; $f_j\left(D_{g,j,t}\right)$ is the discount sensitivity for prosumer *j*; $D_{g,q,t}$ is the discount rate for prosumer *q* who is within the same group as prosumer *j*; $f_q\left(D_{g,q,t}\right)$ is the discount sensitivity for prosumer *q* who is within the same group as prosumer *j*.

***Proof of equation* (8.3):** Equation (8.4) ensures that *MC*=*MR*, and it illustrates the optimal relationship of the capacity-sharing prices of prosumers *j* and *q* with the price elasticities of prosumers *j* and *q*. Replacing the price elasticity in equation (8.4) to the proposed discount sensitivity in equation (8.3), the properties of the two equations will be the same.

$$\frac{P_j}{P_q} = \frac{1+\left(1/f_q\right)}{1+\left(1/f_j\right)} \tag{8.4}$$

where P_j and P_q are the capacity sharing price of prosumers *j* and *q* within the same cluster, and detail of clustering can refer to section V; f_j and f_q are the price elasticity of prosumers *j* and *q*.

***Deduction of equation* (8.4):** The relationship between the price elasticity and the capacity sharing price shown in equation (8.4) can be found when the Profit Maximization Rule is satisfied, i.e., *MC*=*MR* must be satisfied [170].

As for the MR_j (MR_q) of the coordinator, it can be derived by taking the derivative of the total sharing revenue curve of the coordinator gained from prosumer j (q) to the amount of capacity borrowed by prosumer j (q). For illustration simplicity, let $R_{j(q)} = P_{j(q)} Q_{j(q)}$, where $R_{j(q)}$ is the total sharing revenues of the coordinator gained from prosumer j (q), $P_{j(q)}$ is the capacity sharing price for prosumer j (q), and $Q_{j(q)}$ represents the capacity borrowing amount of prosumer j (q). Then the general form of $MR_{j(q)}$ can be written as:

$$MR_{j(q)} = P_{j(q)} + Q_{j(q)} \frac{dP_{j(q)}}{dQ_{j(q)}} = P_{j(q)} \left(1 + \frac{1}{f_{j(q)}} \right) \tag{8.5}$$

where

$$f_{j(q)} = \frac{r_{j(q)}}{Q_{j(q)}} \times \frac{dQ_{j(q)}}{dr_{j(q)}} \tag{8.6}$$

where $f_{j(q)}$ is the price elasticity of prosumer j (q).

As for the MC of the coordinator, it is derived by taking the derivative of the total sharing cost curve of the coordinator to the amount of capacity borrowed by the prosumers. Additionally, the MC of serving prosumers within different groups varies, while the MC is the same for serving prosumers within the same group. To be specific, the total sharing costs of the coordinator include two types of costs, i.e., the capital costs and the operational costs, which can be referred to equation (8.19). It can be found that the capital costs and operational costs are irrelevant to the charging/discharging decision of either prosumer j or q. However, they are related to the aggregated charging/discharging decisions of prosumers j and q and all the other prosumers that are clustered in the same group as prosumers j and q. Thus, the MC is the same for serving either prosumer j or q. Let $MR_j=MC$, $MR_q=MC$, then $MR_j=MR_q$, and the capacity prices for prosumers j and q are related to the price elasticities of prosumers j and q as follows:

$$P_j \left(1 + \frac{1}{f_j} \right) = P_q \left(1 + \frac{1}{f_q} \right) \Rightarrow \frac{P_j}{P_q} = \frac{1 + \left(1 / f_q \right)}{1 + \left(1 / f_j \right)} \tag{8.7}$$

8.5 Load Pattern Analysis Based on Clustering

To implement price discrimination mentioned above, the prosumers will be firstly classified into different clusters. Currently, there are many clustering algorithms based on data-driven, such as *K*-Means, Affinity propagation, Ward hierarchical clustering, Birch, etc. In this chapter, we applied the Density-Based Spatial Clustering of Applications with Noise (DBSCAN) algorithm to the load profile clustering

problem. It has the advantage of no need to determine the number of clustering categories *K* in advance [180], and it can effectively deal with noise points [181]. Before introducing its principle, some concepts should be defined.

Density at a point *P*: Number of points within a circle of radius *Eps* (ε) from point *P*. In this chapter, we use a rule-based method based on the k-distance graph to determine the *Eps* [236].

Dense Region: For each point in the cluster, the circle with radius ε contains at least a minimum number of points (*MinPts*).

The Epsilon neighborhood of a point *P* in the database *D* is defined as : $N(p)=\{q\in D|\, dist(p,q)\leq\varepsilon\}$.

Core point: If $|N(p)|\geq MinPts$, *P* is a core point.

Border Point: the point has fewer neighbors than *MinPts* within its ϵ-neighborhood (*N*), but it lies in the neighborhood of another core point.

Noise: the point is any data point, neither core nor border point. The principle of DBSCAN is iteratively aggregating the objects that can be reached directly from these core objects. The pseudocode of the DBSCAN algorithm is shown as [42]:

***DBSCAN* Algorithm Pseudocode:**

```
main DBSCAN (D, Eps, MinPts):
   mark all objects in dataset D as unvisited
   C=0
   for (each objects P in D) do
      mark P as visited
      Neigh_Pts=Region_Query (P, Eps)
      if sizeof (Neigh_Pts) < MinPts
         then Mark P as Noise
         else create P as core point
         C=next cluster
         Expand_Cluster (P, Neigh_Pts, C, Eps, MinPts)
   end
function Expand_Cluster (P, Neigh_Pts, C, Eps, MinPts):
      add P to cluster C
    for (each point P' in Neigh_Pts):
            if P' is unvisited
          mark P' as visited
          Neigh_Pts'=Region_Query (P', Eps)
          if sizeof (Neigh_Pts') >= MinPts
```

Neigh_Pts= *Neigh_Pts* joined with. *Neigh_Pts'*

if *P'* does not belong to any cluster

Add *P'* to cluster *C*

end

function *Region_Query* (*P*, *Eps*)**:**

Return all points belonging to *Eps* Neighborhood of *P* (including *P*)

Both the historical demand curves and the power generation of local PV panels/wind generators are considered for clustering. The energy consumption pattern and the renewable resource generation of end-users can be explored from their historical information data.

First, through DBSCAN clustering techniques, prosumers are classified into 4 types according to their load demand patterns. In Fig. 8-3, prosumers of type 1 prefer to use electricity during the morning and the afternoon periods. For types 2 and 3, there is only one peak load period. Regard type 4, it represents a load pattern that is less volatile during the day. Five prosumers have been randomly chosen from each type, which is illustrated on the right side of Fig. 8-3. Within each type, the prosumers have slightly different load demands.

Second, the prosumers are further manually clustered according to the type of renewable resources the prosumers have, i.e., PV generation or wind generation. Therefore, the prosumers are further classified into 8 clusters, i.e., 4 clusters for prosumers using the PV generation and the rest 4 clusters using energy from the wind generator.

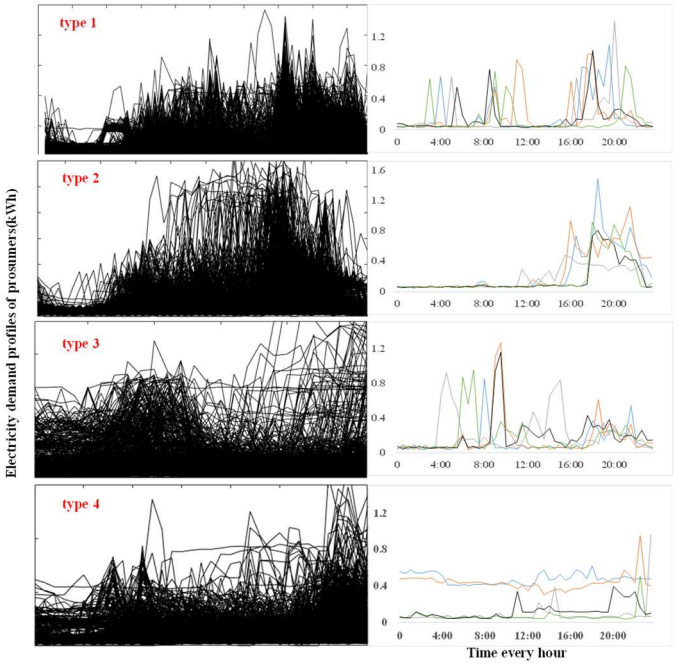

Fig. 8-3. Data-driven-based clustering on the prosumer load demand profiles.

There are three main reasons that we cluster the prosumers based on the load profile and the type of renewable energy sources. First, it is more intuitive and visualized to cluster prosumers based on their demand and renewable resource generation compared with clustering based on demand elasticity. Second, it is easier to collect information related to the demand and PV panels/wind generation than the demand elasticity of prosumers. This is because the demand elasticity needs to be collected based on questionnaires to the prosumers on how they would change the capacity borrowing amount when there is a one percent change in capacity sharing price, which might be inaccurate. Third, our pricing strategy aims to incentivize and coordinate prosumers with complimentary usage patterns to participate in the capacity-sharing process, which is beneficial for reducing congestion and increasing the utilization efficiency of the shared ESS.

8.6 Proposed Two-stage Pricing Strategy

8.6.1 Stage I: Problem from the Perspective of the Coordinator

Conventionally, the energy storage sharing is charged according to the net discharging of the prosumer, i.e., $P_{j,t}^{dis} - P_{j,t}^{ch}$. In this chapter, a new charging method is proposed, where the prosumers will be charged based on the capacity borrowing state $e_{g,j,t}$. It is the accumulated net charging of each prosumer that considers both the size of the capacity borrowed and the time length of the borrowing.

$$e_{g,j,t+1} = e_{g,j,t} + \left(P_{g,j,t}^{ch} \times \eta^{ch} - P_{g,j,t}^{dis} / \eta^{dis} \right) \times \Delta t \tag{8.8}$$

where $e_{g,j,t}$ is the capacity borrowing state of prosumer *j* at time *t*; $P_{g,j,t}^{ch}$ is the charging profile of prosumer *j* at time *t*; $P_{g,j,t}^{dis}$ is the discharging profile of prosumer *j* at time *t*; η^{ch} is the charging efficiency; η^{dis} is the discharging efficiency.

Compared with the conventional charging approach, the proposed method shows the advantage of considering the time accumulation effect. When the prosumers have a longer borrowing time or a larger borrowing capacity, they will incur a higher capacity sharing cost. Therefore, the prosumers are compelled to return the borrowed capacity in time. As a result, the proposed method better complies with the essence of the sharing economy, where the right of use of idle resources needs to be transferred to those in need in time.

For the individualized pricing strategy, first, the group TOU prices of the capacity sharing will be

derived based on the marginal costs and risk premium of the coordinator. Then, the capacity-sharing price will be further individualized based on the proposed bulk capacity borrowing and the discount sensitivity.

8.6.1.1 Group-based Pricing on Capacity Sharing

The group-based capacity-sharing price can be determined based on two parts, i.e., the marginal costs and the risk premium of the coordinator [71].

$$r_{g,i} = r_{g,i}^{mc} + r^{rp} \tag{8.9}$$

where $r_{g,i}$ is the group capacity-sharing price of price block *i*, $i \in N^{pb}$ (N^{pb} is the number of price blocks); $r_{g,i}^{mc}$ is the marginal cost; r^{rp} is the risk premium determined by the profit variation of serving all the prosumers.

The binary variable $y_{g,i,t}$ that indicates the coverage of price block *i* is introduced to optimize the price structure. Equation (8.10) ensures that each time *t* exclusively belongs to a price block. For equation (8.11), it ensures that only consecutive periods can be segmented into the same price block [66, 71]. Details are as follows:

$$\sum_{i=1}^{N^{pb}} y_{g,i,t} = 1 \tag{8.10}$$

$$\left| y_{g,i,1} - y_{g,i,T} \right| + \sum_{t=2}^{T} \left| y_{g,i,t} - y_{g,i,t-1} \right| = 2 \tag{8.11}$$

where N^{pb} is the number of price blocks.

The marginal cost $r_{g,i}^{mc}$ involves the capital cost and the operational cost of energy storage sharing. The calculation of the capital cost involves discounting the investment cost of the shared ESS to each hour using the capital recovery factor (CRF) [237]. The equation of marginal cost of the coordinator is shown as:

$$r_{g,i}^{mc} = \left(\sum_{t=1}^{T} r_{g,t}^{mc} \times y_{g,i,t} \right) \Big/ \sum_{t=1}^{T} y_{g,i,t} \tag{8.12}$$

$$r_{g,t}^{mc} = \left(m \times C_t^{Cap} + C_{g,t}^{Oper} \right) \Big/ \sum_{j \in g} \left(P_{g,j,t}^{ch} + P_{g,j,t}^{dis} \right) \tag{8.13}$$

$$C_t^{Cap} = \frac{IC^{Inv} \times \kappa}{\left(1 - 1 \Big/ (1+\kappa)^{\vartheta} \right) \times 365 \times 24} \tag{8.14}$$

$$C_{g,t}^{Oper} = \sum_{j \in g} \left(P_{g,j,t}^{ch} + P_{g,j,t}^{dis} \right) \times \lambda \tag{8.15}$$

where $r_{g,t}^{mc}$ is the group capacity-sharing price of time *t*; m is the number of energy storage devices invested by the coordinator; C_t^{Cap} is the capital cost of the energy storage at time *t*; $C_{g,t}^{Oper}$ is the operating cost of the coordinator at time *t*; IC^{Inv} is the initial investment cost of the shared ESS; κ is the annual discount rate; ϑ is the life cycle of the ESS; λ is the operational fee.

As for the risk premium, it can be shown as:

$$r^{rp} = V_{Day}^{CVaR,mc} \Big/ \sum_{g=1}^{G} \sum_{t=1}^{T} \left(P_{g,j,t}^{ch} + P_{g,j,t}^{dis} \right) \tag{8.16}$$

where $V_{Day}^{CVaR,mc}$ is the daily conditioned value-at-risk (CVaR) of the coordinator, details can be referred to equation (8.20); G is the number of clusters of the prosumers, i.e., 8 groups.

8.6.1.2 Individualized Pricing on Shared Capacity

The individualized pricing further customizes the group-based price. It has two advantages. First, it quantifies the individual discount given to the prosumers on the energy storage borrowed. Second, it is the first model to integrate both second-degree and third-degree discrimination, which can refer to equation (8.17). Two concepts are applied, namely bulk capacity borrowing and discount sensitivity.

For **bulk capacity borrowing**: To reflect the mechanism of second-degree price discrimination, the concept of bulk capacity borrowing is introduced. It is a strategy of the coordinator to incentivize and engage the prosumers in the energy storage sharing by offering different price reductions according to the different capacity borrowing state $e_{g,j,t}$ of each prosumer *j*. In other words, the more capacity is borrowed, the more price reductions will be given to the prosumers, which is a similar idea to bulk purchasing in economic theory [238]. Thus, bulk capacity borrowing is related to the capacity borrowing state $e_{g,j,t}$. Details can be referred to equation (8.17).

We use $\tau_j \times e_{g,j,t}$ to express the price reduction given by the coordinator to the prosumer, where τ_j is the reduction coefficient that transfers the capacity borrowing state of the prosumer to the price reduction.

As for **discount sensitivity**: To reflect the mechanism of third-degree price discrimination, the concept of discount sensitivity is introduced. It is the sensitivity of the prosumers towards the price discounts on capacity sharing. In this chapter, the coordinator will charge prosumers different prices by considering the price discount sensitivity of each individual prosumer, which can be referred to equation (8.17). Moreover, the discount rate and the discount sensitivity have a relationship as equation (8.3). Detailed

proof of the derivation of equation (8.3) can refer to ***Theorem 2*** in section IV, part B.

The individualized price based on bulk capacity borrowing and discount sensitivity is shown as:

$$r_{g,j,t}^{adj}=\sum_{i=1}^{N^{pb}} y_{g,i,t}\times\left[r_{g,i}\times\left(1-D_{g,j,t}\times f_j\left(D_{g,j,t}\right)\right)-\tau_j\times e_{g,j,t}\right] \tag{8.17}$$

where $r_{g,j,t}^{adj}$ is the individualized capacity-sharing price.

8.6.1.3 Model for Coordinator based on Individualized Pricing

Based on the individualized pricing in equation (8.17), the coordinator will jointly optimize the capacity sharing price structure $y_{g,i,t}$ and the price level $r_{g,j,t}^{adj}$. The decision variables include the group capacity-sharing price level of price block i $r_{g,i}$ and the price structure of price block i $y_{g,i,t}$.

The objective is to minimize the total costs of the coordinator, including the sharing costs and the CVaR costs. The objective function and the related constraints are shown below:

$$\min\left(C_{Day}^{TC}+\beta^{mc}\times V_{Day}^{CVaR,mc}\right) \tag{8.18}$$

where

$$C_{Day}^{TC}=m\times C_{Day}^{Cap}+C_{Day}^{Oper} \tag{8.19}$$

s.t. equations (8.9)-(8.16).

where C_{Day}^{TC} is the total sharing cost of the coordinator; $\beta^{mc}\in[0,\infty)$ is the weighting factor between the total revenue and the total cost of the coordinator, the higher the value is, the more risk-averse the coordinator is [71].

The Conditional value-at-risk (CVaR) model is selected as the risk measurement. Compared with other risk methods, CVaR is more advantageous due to its monotonicity and sub-additivity [239].

$$V_{Day}^{CVaR,mc}=V_{Day}^{VaR,mc}+\frac{\sum_{n^s=1}^{N^s}\left(-NP_{Day}-V_{Day}^{VaR,mc}\right)^+}{\left(1-\alpha\right)\times N^s} \tag{8.20}$$

$$V_{Day}^{VaR,mc}=\inf\left\{t_\alpha\mid\Pr\left[x_{C_{Day}^{TC}}\geq t_\alpha\right]=1-\alpha\right\} \tag{8.21}$$

where $V_{Day}^{VaR,mc}$ is the corresponding value-at-risk value; N^s is the number of samples; NP_{Day} is the net profit of the coordinator of a day; $x_{C_{Day}^{TC}}$ is the test statistic relating to the total cost of the coordinator; t_α is the t critical value at a given confidence level α.

In our model, prosumers will pay the capacity sharing fee based on the recorded capacity borrowing state $e_{g,j,t}$, which can be referred to equation (8.8). Hence, the profit of the coordinator is:

$$NP_{Day} = \sum_{j=1}^{J} \sum_{t=1}^{T} \left\{ r_{g,j,t}^{adj} \times e_{g,j,t} \times \left[1 - f\left(r_{g,j,t}^{adj} \right) \right] \right\} - C_{Day}^{TC} \tag{8.22}$$

$$f\left(r_{g,j,t}^{adj} \right) = \delta \times \left(r_{g,j,t}^{adj} - r_{0,t}^{adj} \right) \Big/ r_{0,t}^{adj} \tag{8.23}$$

where $f\left(r_{g,j,t}^{adj} \right)$ is the price elasticity of prosumer *j*; δ is the price change coefficient; $r_{0,t}^{adj}$ is the nominal capacity-sharing price at time *t*.

The ESS constraints are as follows:

$$E_{t+1} = E_t + \sum_{j=1}^{J} \left(P_{g,j,t}^{ch} \times \eta^{ch} - P_{g,j,t}^{dis} \Big/ \eta^{dis} \right) \times \Delta t \tag{8.24}$$

$$0 \le P_{g,j,t}^{ch} \times \eta^{ch} \times \Delta t \le m \times p_{\max} \times \Delta t - E_t \tag{8.25}$$

$$P_{\min} \le P_{g,j,t}^{ch} \le P_{\max} \tag{8.26}$$

where E_t is the energy storage state at time *t*; $P_{\min}$ and $P_{\max}$ are the minimum and maximum charging amount.

8.6.2 Stage II: Problem from the Perspective of the Prosumers

In stage II, based on the optimized capacity-sharing price $r_{g,j,t}^{adj}$ in stage I, the prosumers will determine the optimal electric power to charge/discharge at each time period. The prosumers can use the electric power generated from rooftop PV cells or wind generators $\boldsymbol{P_j^{DRE}} = \left\{ P_{g,j,t}^{PV}, P_{g,j,t}^{Wind}, \forall t \in T \right\}$. If the DERs are more than the load demand, the prosumers can have two options. The energy can be stored in the shared ESS, which will incur a capacity sharing cost of $C_{g,j}^{ESS}$. The energy can also be sold to the external grid and gain a profit of R_j^G. If the DERs are inadequate to satisfy the demand, the prosumers can first use the previously stored energy from the shared ESS. Then, if the load demand is still not satisfied, the prosumers can purchase the energy externally from the grid by paying C_j^G. The energy transaction between the grid and the prosumer is $\boldsymbol{P_j^G} = \left\{ P_{g,j,t}^{BG}, P_{g,j,t}^{SG}, \forall t \in T \right\}$. Equation (8.27) illustrates the power demand and supply relationship.

$$P_{g,j,t}^{D} = \boldsymbol{P_j^{DRE}} - P_{g,j,t}^{ch} + P_{g,j,t}^{dis} - P_{j,t}^{SG} + P_{j,t}^{BG} \tag{8.27}$$

where $P_{g,j,t}^{D}$ is the load demand of prosumer *j* at time *t*.

The objective is to minimize the energy procurement cost and the capacity sharing cost. The objective function is as follows:

$$\max R^G - C^G - C^{ESS} = \sum_{j=1}^{J}\sum_{t=1}^{T}\left[P_{j,t}^{SG} \times r_t^{sell}\right] - \sum_{j=1}^{J}\sum_{t=1}^{T}\left[P_{j,t}^{BG} \times r_t^{buy}\right] - \sum_{j=1}^{J}\sum_{t=1}^{T}\left\{r_{g,j,t}^{adj} \times e_{g,j,t} \times \left[1 - f\left(r_{g,j,t}^{adj}\right)\right]\right\} \tag{8.28}$$

s.t. equations (8.8), (8.25)-(8.27)

where r_t^{buy} is the purchasing price from the grid at time t; r_t^{sell} is the selling price to the grid at time t.

8.7 Case Study

8.7.1 Experiment Setting

In the case study, all data are collected by the Smart Grid, Smart City project in Australia [240]. The original data is collected every 15 minutes. However, to simplify the calculation, the time resolution is changed to 1 hour.

Three case studies are examined:

Case 1: Base case: energy capacity sharing based on the same capacity price for all the prosumers [69].

Case 2: TOU pricing: energy capacity sharing based on TOU pricing [71].

Case 3: Individualized pricing: energy capacity sharing based on the proposed individualized pricing strategy.

Fig. 8-4 shows the historical daily load demand of the simulated prosumers. Five prosumers are selected from each cluster. From left to right, every five prosumers form a cluster. It also indicates the variance and means of the daily load demand. It can be found that #16-#20, i.e., cluster 4, and #36-#40, i.e., cluster 8, have the lowest variance among the other clusters. This indicates the load pattern of these prosumers is relatively stable.

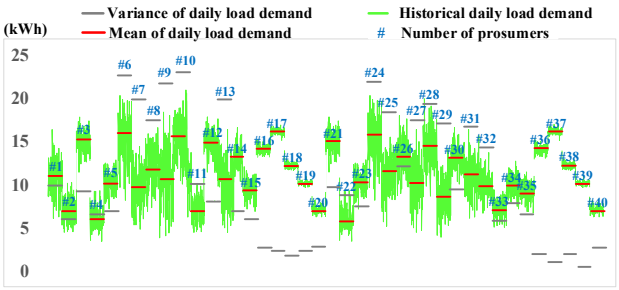

Fig. 8-4. Daily electricity usage of each prosumer.

8.7.2 Simulation Results on Energy Storage Sharing

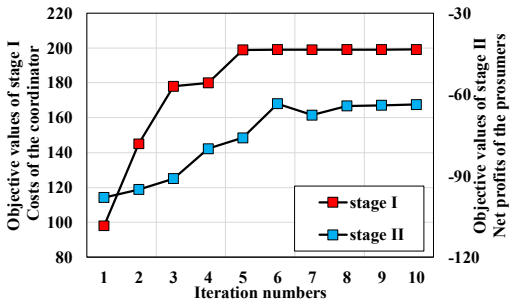

Fig. 8-5. Objective convergence for stages I and II.

Fig. 8-5 illustrates the objective convergence for stages I and II. It can be found that the initial net profit of the prosumers is low because the initial capacity sharing price is set too high. By adjusting the capacity sharing price to a lower level, prosumers are more incentivized to participate in the capacity sharing process. Thus, the net profit of the prosumers is increasing. As a result, the costs of the coordinator will increase. Generally, the cost of the coordinator in stage I and the net profit of the prosumers in stage II are positively correlated. To incentivize prosumers to participate in capacity sharing, the capacity sharing price is adjusted by the coordinator. As a result, the prosumers will respond to the capacity sharing price by adjusting their charging/discharging profiles. Consequently, the net profit of the prosumers will increase, which will lead to an increase in the operational cost of the coordinator. The iteration continues until the equilibrium is reached, i.e., the optimal capacity sharing price and the optimal charging/discharging profiles are obtained.

Fig. 8-6 (a), (b), and (c) illustrate the charging/discharging profiles of prosumers of the three cases. The positive and negative values correspond to charging and discharging, respectively. It can be found that under case 1, massive charging/discharging behaviors occur simultaneously, which is verified via the superposition of the lines across the time scale. For example, the solid green lines and the dotted pink lines at the time of 17:00 are intense. This phenomenon can be explained by the behavior of the prosumers that coincides with each other to conduct either charging or discharging. Consequently, this may result in congestion or inefficient storage usage. As for case 2, prosumers are classified into different clusters based on the historical demand curves and power generation of local PV panels/wind generators, which is the same clustering method used in case 3. Although the charging/discharging behavior of prosumers is more dispersed compared with case 1, superposition still exists within each group. To further disperse the charging/discharging behavior, the individualized pricing method is proposed and studied in case 3. The results show that the charging/discharging behavior can be further dispersed compared with case 2.

Fig. 8-6 (d) presents the hourly average net profit of the three cases, and the shaded areas represent the fluctuation of each case. Among them, the proposed method has both higher net profit and lower variation of profit.

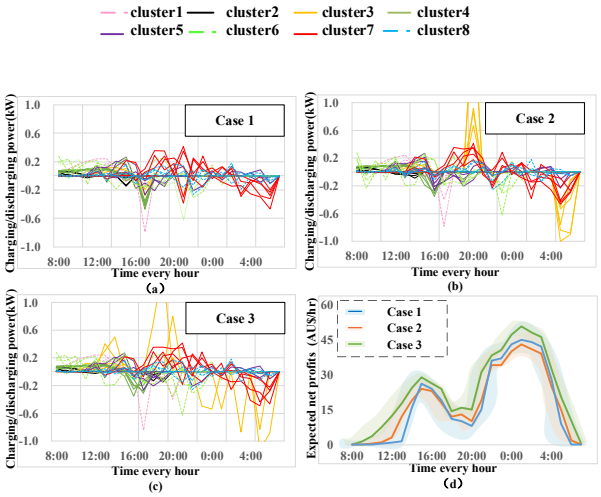

Fig. 8-6. Charging/discharging decision and the net profits comparison.

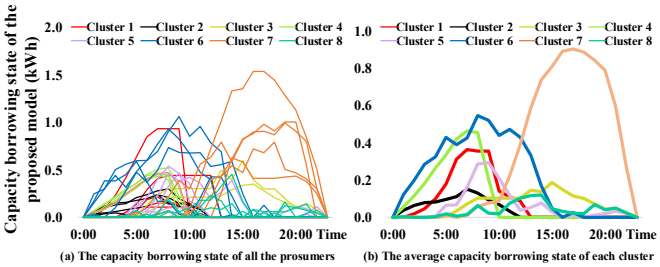

Fig. 8-7. Capacity borrowing state of the proposed model.

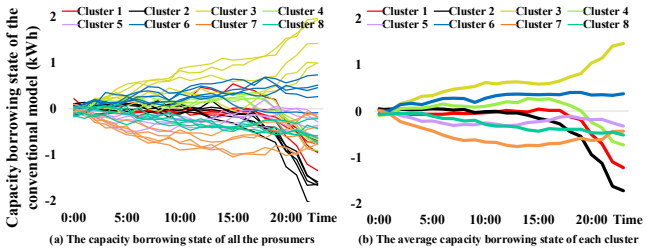

Fig. 8-8. Capacity borrowing state of the conventional model.

For the proposed model in Fig. 8-7, the prosumers will be charged according to the capacity borrowing state. Fig. 8-7 (a) shows the capacity borrowing state of all the prosumers, and Fig. 8-7 (b) shows the average capacity borrowing state of each cluster. In Fig. 8-7, the increase in the capacity borrowing state means that the prosumers are borrowing more capacity from the shared ESS. The decrease in the capacity borrowing state means that the prosumers are returning the borrowed capacity. Thus, the capacity borrowing state is always non-negative in our proposed model since prosumers do not need to return the

borrowed capacity if the capacity borrowing state is reduced to zero. It can be found that although the prosumers have different capacity borrowing state profiles, the borrowing states of all the prosumers will eventually reduce to zero. It indicates that the prosumers are compelled to return the borrowed capacity in time, which is in alignment with the essence of sharing economy. Hence, the long-term occupation of the shared capacity can be avoided because the prosumers are incentivized by the proposed pricing strategy to return the borrowed capacity eventually. As a result, congestion in the usage of the shared ESS can be mitigated.

By contrast, for the conventional model, the prosumers will be charged according to the net discharging profile at time *t*, which can be referred to section III [69]. When the prosumers charge electricity to the shared ESS, the coordinator will pay the prosumers. On the other hand, when the prosumers are discharging electricity from the shared ESS, the coordinator will get paid by the prosumers. Thus, the whole process is modeled as a trading process rather than sharing. In order to compare the conventional model with our proposed method, the capacity borrowing state is also calculated according to equation (29). Fig. 8-8 (a) shows the capacity borrowing state of all the prosumers under the conventional model, and Fig. 8-8 (b) shows the average capacity borrowing state of each cluster. In Fig. 8, it can be found that some prosumers continuously charge electricity to the shared ESS while others continuously discharge electricity from the shared ESS. Therefore, the capacity borrowing state profiles appear to be a dispersed shape. In such a mechanism, the pure consumers can participate and benefit by purchasing electricity at a relatively low sharing price even though they contribute less to the sharing process [48]. As a result, the conventional sharing mechanism achieves higher savings for the pure consumers at the cost of the prosumers with DERs, which is unfair for the prosumers. In comparison, the introduction of the capacity borrowing state in our proposed model incentives the consumers to invest in DERs so that they can better be engaged in the proposed sharing mechanism.

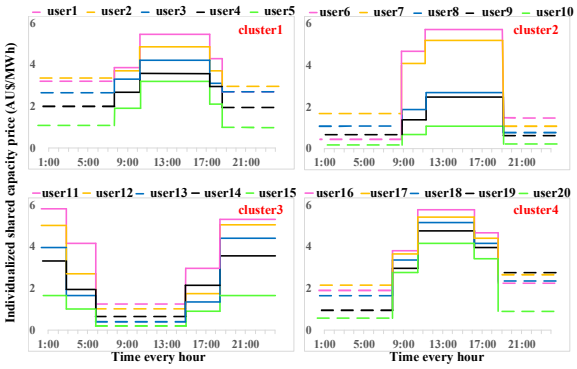

Fig. 8-9. Individualized pricing on PV-based prosumers.

Fig. 8-9 shows the individualized price structure and price level of PV-based prosumers. The prosumers within clusters 1-4 use PV cells to generate electricity, and the load patterns are illustrated in Fig. 8-3 involving double-peak (one in the morning, another in the afternoon), a single peak in the evening, a single peak in the morning, and a flatter one. By applying customized pricing, clusters 1-4 have different capacity-sharing price levels and price structures. Although each prosumer numbered from 1 to 20 is priced differently, the prosumers within the same cluster have the same price structures.

Fig. 8-10 shows the individualized price structure and price level of the wind-based prosumers. The prosumers within clusters 5-8 utilize energy from wind generators, and the load patterns are the same four types mentioned above. By applying customized pricing, clusters 5-8 have different capacity-sharing price levels and price structures. Although each prosumer numbered from 21 to 40 is priced differently, the prosumers within the same cluster have the same price structures. Furthermore, compared with PV-based prosumers, the price level within each cluster is more volatile.

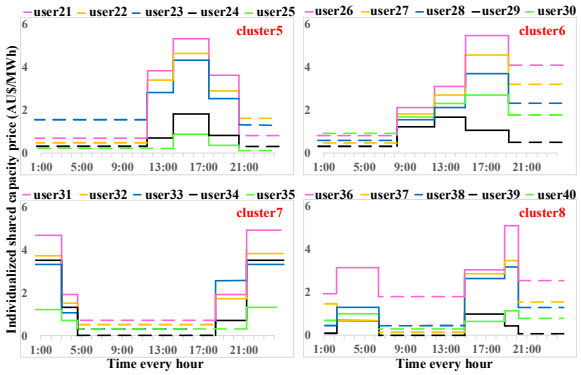

Fig. 8-10. Individualized pricing on wind-based prosumers.

8.7.3 Effectiveness Evaluation

Fig. 8-11 compares the energy storage usage efficiency of the self-sufficient model where prosumers purchase their own ESS and the model where the ESS is managed by the coordinator. For the self-sufficient model, it means prosumers purchase energy storage devices individually. By contrast, the capacity sharing model encourages prosumers to borrow the capacity from the shared ESS managed by the coordinator (i.e., cases 1-3). It can be found that the state of charge of the self-sufficient model has lower capacity usage efficiency compared with the coordinator-facilitated sharing model. For example, the usage efficiency of user 31 in the self-sufficient model from 12:00 to 16:00 is lower than 20%. By contrast, the lowest efficiency of the three cases mentioned above is more than 30%. Additionally, the proposed sharing model ensures a higher storage usage efficiency compared with cases 1 and 2.

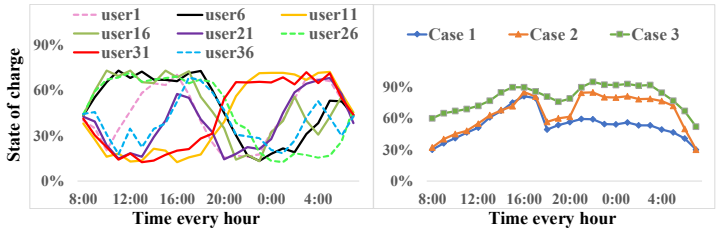

Fig. 8-11. SOC efficiency of the self-sufficient model and the sharing model.

Except for the normal evaluation approaches, such as expected net profits and variance, the coefficient of variation (CV) is introduced in Table 8-1 to compare one data series to another when the means of the data series are varied [241]. Since the scale of each case is varied, the CV is a suitable criterion to compare the risks of the three cases. It is calculated as the ratio of the standard deviation of the net profits of the coordinator divided by the expected net profits of the coordinator, which can be shown as $CV = \sigma\left(NP_{Day}\right)/\mathbb{E}\left(NP_{Day}\right)$.

Table 8-1 shows the simulation results from the perspectives of the whole community, including the coordinator side and prosumers side. For the coordinator, the results indicate that both the daily sharing revenue (693 AU$) and net sharing profit (551 AU$) of case 3 is higher than in the other two cases. As for the risk analysis, case 3 incurs the lowest variance and CV, which indicates that the profit variation risks of the coordinator are the lowest. Furthermore, case 1 results in the largest discounted daily capital cost. This is because when the charging/discharging profiles of the prosumers are similar, the coordinator needs to invest more to have a larger energy storage capacity to satisfy the peak charging/discharging demand. On the contrary, for case 3, the charging/discharging behavior of the prosumers is more dispersed than in either case 1 or case 2. As a result, fewer storage devices are invested, and the discounted daily capital cost is smaller compared with the other two cases. However, as more prosumers are involved, the operational cost under case 3 is larger than that under the other two cases.

For the simulation results of Table 8-1 from the perspective of the prosumers, the energy cost is the lowest for case 3 at 27 AU$ per day compared to the other two cases. Another indicator is the self-sufficiency ratio. It is a ratio to indicate the degree of utilization of the DERs to satisfy load demand within the community of the coordinator and the prosumers. To be noted, the excess energy stored in the shared ESS for future use is also accounted for self-sufficiency. And it can be expressed as $SSR = \left(E_{PV/wind} + E_{Dis}\right)/E_L$, where $E_{PV/wind}$ is the aggregated renewable energy; E_{Dis} is the aggregated electric power from the energy storage devices that are discharged to satisfy load demand;

E_L is the aggregated load demand [138]. It can be found that the *SSR* of case 3 is improved to 65%, which is 20% and 8% higher than case 1 and case 2, respectively. This is because more prosumers are incentivized to store their excess renewable energy in the shared ESS rather than directly sell it to the utility grid.

In Table 8-1, it can be found that the net profit of the coordinator is the highest at 551 AU$, and the energy cost of the prosumers is the lowest at 27 AU$. Thus, social welfare is increasing. This is because the individualized capacity sharing price can incentivize more new prosumers to participate in the sharing process and reduce energy procurement from the utility grid. As a result, the increase of profits of the coordinator is not at the cost of reducing the prosumer surplus. Instead, it is at the cost of reducing the electricity selling revenues of the utility grid. Thus, a win-win situation between the coordinator and the prosumers can occur.

TABLE 8-1. COMPARISON OF DIFFERENT CASES BASED ON GAINS AND RISKS FROM THE PERSPECTIVES OF THE COORDINATOR AND THE PROSUMERS

		Case 1		**Case 2**		**Case 3**	
Coordinator	**Revenues**	Expected revenues	557	Expected revenues	606	Expected revenues	693
	Costs	Capital costs	93	Capital costs	84	Capital costs	72
		Operation costs	57	Operation costs	64	Operational costs	70
	Net profits	Expected net profits	407	Expected net profits	458	Expected net profits	551
	Variance	299.85		242.17		196.37	
	Coefficient of variation	0.0426		0.0340		0.0254	
Prosumer	**Energy costs**	52		38		27	
	Self-sufficiency	45%		57%		65%	

Fig. 8-12 evaluates the relationship of the price change coefficient δ in equation (8.23), individualized capacity-sharing price $r_{g,j,t}^{adj}$, and capacity borrowing state $e_{g,j,t}$ of the prosumer. The shaded areas of the green and red lines are the variation range of all the prosumers simulated. It can be found that an increase in price reduces the capacity borrowing state $e_{g,j,t}$ that means prosumers will respond to an increase in price by reducing the usage of the shared capacity, and vice versa. This relationship is presented by the green line. For the red line, $\delta = 1.1$ is the critical point in this chapter. When δ is larger than 1.1, the capacity-sharing price decreases and $e_{g,j,t}$ increases to a point (e_1, P_1). On the contrary, when δ is smaller than 1.1, the capacity-sharing price increases and $e_{g,j,t}$ decreases

to a point (e_2, P_2).

8.7.4 Sensitivity Analysis

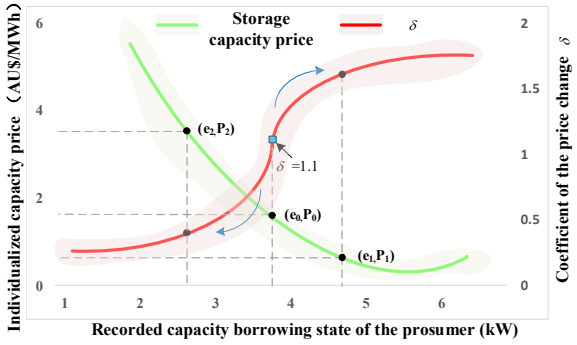

Fig. 8-12. Relationship between coefficient of price change, capacity borrowing state, and capacity sharing price.

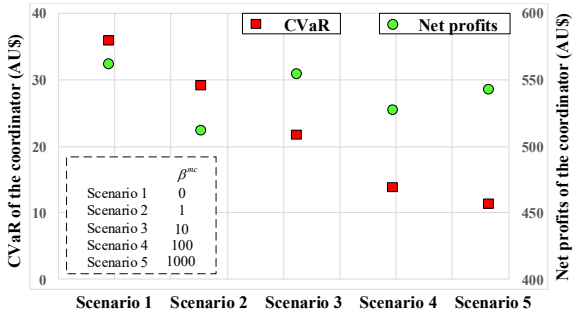

Fig. 8-13. CVaR and net profits of coordinator with varied weighting factors.

Fig. 8-13 illustrates the change of CVaR and net profits of the coordinator when β^{mc} varies in each scenario. From scenarios 1 to 5, β^{mc} increases from 0 to 1000. When β^{mc} increases, it indicates that the coordinator is more risk-averse [71]. Thus, CVaR moves in the opposite direction with β^{mc}.

8.8 Discussion

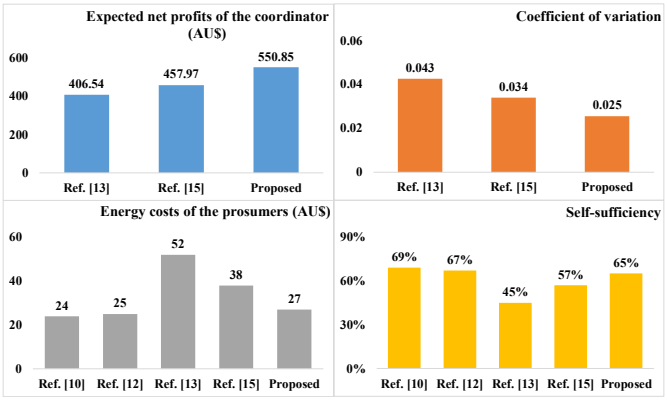

Fig. 8-14. Comparison of different references with the proposed model.

To further discuss the effectiveness of the proposed pricing strategy, two types of pricing strategies are compared in Fig. 8-14. The first type is based on the clearing scheme, which includes the pricing strategy based on the non-cooperative game as [67] and the auction-based pricing strategy as [68]. The

second type of pricing strategy is formulated by the sharing coordinator that can realize the insulation between the prosumers and the sharing market. It includes the fixed pricing strategy that is the same for all the prosumers as [69], the TOU pricing strategy sets different prices for different groups of prosumers, as [71], and the proposed individualized pricing strategy.

From the perspective of the coordinator, it can be found that the proposed model has the highest amount of net profit, reaching 550.85 AU$ per day. This is because the individualized price fully considers the discount sensitivity, price elasticity, and demand of the prosumers. Thus, it can incentivize more new prosumers to participate in the sharing process. As a result, the sharing profit of the coordinator will increase. By contrast, using the fixed pricing strategy in [69] results in the lowest net profit for the coordinator. This is because the electricity usage behavior of the prosumers is ignored. As a result, the prosumers are less incentivized to participate in the sharing process under the same sharing price. Thus, the sharing profit of the coordinator is reduced. For the CV value of the coordinator (detailed definition can be referred to section VII, part C), the proposed model has the lowest CV value of 0.025. This means the individualized pricing strategy can ensure the coordinator has the smallest profit fluctuation. However, using the fixed pricing strategy of [69] results in the highest CV value at 0.043.

From the perspective of the prosumers, it can be found that the energy cost of using the clearing-based pricing strategies, i.e., the non-cooperative game and auction-based pricing [67, 68], is the lowest. This is because the prosumers can have the initiatives to participate in the sharing market by actively adjusting their sharing strategies according to their energy demand, excess energy, and cost functions. As a result, the cost and the demand-supply information are fully considered in the clearing process. Thus, the prosumers are incentivized to participate in the sharing process to store the excess energy for later usage, which is cost-saving for the prosumers. Although the energy cost of our model is higher than using the clearing-based pricing strategy, our model can insulate the prosumers from the risky sharing market (i.e., price volatility in the market). This is because the prosumers normally lack risk-hedging and bidding knowledge. Additionally, the energy cost of our model is lower than using the method of [69] and [71]. As for the self-sufficiency ratio, it can be found that the self-sufficiency ratio using the clearing-based pricing is the highest. This is because the prosumers will reduce the energy procurement from the grid. For our model, the self-sufficiency ratio is lower than using the clearing-based pricing strategy but higher than using the pricing strategies of [69, 71].

Although the energy costs of the clearing-based pricing strategy are lower and the self-sufficiency ratio is higher compared with the proposed pricing strategy, the proposed pricing strategy is more advantageous in hedging the risks caused by price fluctuation, as shown in Fig. 8-15. In Fig. 8-15, it can be found that the variance in energy cost of the clearing-based pricing strategies of [67, 68] is 0.125 and 0.09243, respectively. By contrast, the variance in energy cost of the coordinator-based pricing strategies of [69, 71] and the proposed pricing strategy is lower, at 0.07639, 0.04222, and 0.02021, respectively. It indicates that the prosumers will encounter higher risks in the energy market under the clearing-based pricing strategy. To be noted, the presented results assume that the prosumers have risk-hedging knowledge, so risk control is considered in the analytical model. However, in practical practice, the prosumers normally lack the expertise/knowledge of risk-hedging. As a result, the variance of energy costs might be even higher than the presented results in Fig. 8-15. On the other hand, the coordinator as a corporation has better knowledge of risk-hedging than the prosumer as an individual. Therefore, the coordinator-based pricing strategy can better hedge the market risk for the prosumers via insulating the prosumers from the risky sharing market. Moreover, compared the proposed method with the other coordinator-based pricing strategies [69, 71], the proposed pricing strategy results in the lowest energy costs. Hence, the proposed pricing strategy not only can save energy costs but also can hedge risks for the prosumers compared with cases 1 and 2.

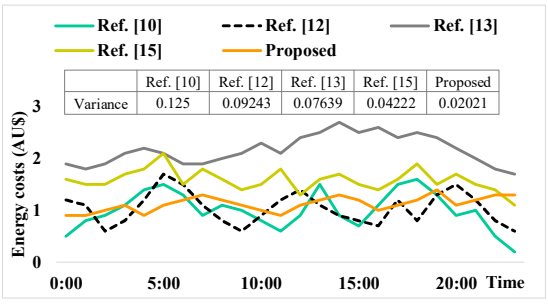

Fig. 8-15. Energy cost volatility comparisons from the view of the prosumers.

8.9 Future Works and Conclusions

The proposed work can be further extended in two aspects. First, the work can be extended by integrating both capacity sharing and energy sharing, in which the prosumers can either borrow capacity or energy from the coordinator. Second, an integrated energy sharing system, including both electricity sharing and hydrogen sharing, can be developed. Future works can be focused on two aspects. First, besides the cost-based pricing strategy, i.e., marginal costs plus premium, a pricing strategy that

incorporates more dynamic demand information can be developed. Second, we can consider using an advanced DBSCAN algorithm, such as adaptive DBSCAN, to choose the *Eps* automatically [242]. In this way, artificial intervention in the clustering process can be avoided, and the complete automation of the clustering process can be realized. Besides, data mining on the characteristic identification of the prosumers, including the demand elasticity, electricity usage habits, and sociodemographic characteristics, can be further realized. Based on these features, a refined clustering of the prosumers can be realized to help the coordinator formulate a more reasonable pricing strategy.

To conclude, a two-stage pricing model for energy capacity sharing has been presented based on the clustering of different net load patterns of prosumers. Both the price structure and the price level of the capacity-sharing price for individual prosumers are optimized. Novel concepts of bulk capacity borrowing and discount sensitivity are proposed to individualize the capacity-sharing price. Simulation results indicate that compared with the conventional pricing and time-of-use pricing, the proposed individualized pricing not only increases the net profits of the coordinator but also increases the efficiency of storage usage. Additionally, the risks measured by the coefficient of variation are reduced, which means proposed pricing can ensure more stable sharing profits for the coordinator. Furthermore, the individualized pricing strategy can result in lower energy costs for the prosumers.

9. CREDIT-BASED PRICING AND PLANNING STRATEGIES FOR HYDROGEN AND ELECTRICITY ENERGY STORAGE SHARING

With the increasing penetration of intermittent renewable resources, the energy demand is more fluctuating. Thus, the concept of energy sharing is brought up to smooth the energy demand of the prosumers and to ensure system stability. In this chapter, a two-stage credit-based sharing model between the coordinator who manages the shared energy storage system (ESS) and the prosumers who borrow the capacity and energy from the coordinator is presented. Both capacity and energy sharing are integrated via the proposed credit-based sharing model. As for energy sharing, two forms of energy are considered: electricity and hydrogen. In addition, both cost-based and demand-based pricing strategies are introduced to customize the sharing prices so that the coordinator can obtain larger net profits and the prosumers can reduce their energy purchase costs. According to the simulation results, the proposed model is beneficial for both the coordinator and the prosumers. For the coordinator, the net profits can be enhanced, and the storage usage efficiency has been increased from an average of 39% to 62% compared with the conventional model. From the perspective of the prosumers, the self-sufficiency ratio and the willingness-to-participate ratio are increased by 14.5% and 20%, respectively, compared with that under the conventional model. Moreover, it is cost-saving for the prosumers to participate in the credit-based sharing process.

9.1 Introduction

The installation of distributed energy resources (DERs), such as rooftop PVs, is promising in reducing greenhouse gas emissions [39]. However, the power generated by the DERs is intermittent, which will cause system stability and security issues [40]. Thus, the energy storage system (ESS) is implemented to smooth the power generation. The benefits of the battery energy storage system (BESS) have been well recognized in terms of generation backup, transmission alleviation, voltage control, frequency regulation, etc. Apart from BESS, the power-to-gas (P2G) is also a promising ESS technology since the process of electricity-hydrogen conversion is carbon-free if electricity is from renewable energy [55, 56]. P2G devices can convert excess electricity into hydrogen through water electrolysis, and the energy is stored in the form of gas. Then, the gas can be converted back to electricity by the installed gas generators and fuel cells when needed [34]. Therefore, applying the P2G as an additional ESS can increase the flexibility of the integrated multi-carrier energy system and provide the customer with reliable services.

As one form of energy, hydrogen offers an opportunity for sector coupling between the electricity, gas, and transport sectors. According to [82], hydrogen is a versatile energy carrier that can be served as an input into a range of industrial processes. The application of hydrogen can enable deep decarbonization across the energy and industrial sectors. Hydrogen can also facilitate the transition to high penetration of intermittent renewable generation in the electricity network. Moreover, governments are putting more emphasis on the application of hydrogen. The Australian government formulates a series of development strategies for the hydrogen industry [82]. The National Hydrogen Roadmap report of the *Commonwealth Scientific and Industrial Research Organization (CSIRO), Australia,* states that the most significant near-term opportunity is blending hydrogen into the existing natural gas network for heating systems in buildings [82]. With the advancement of the P2G technology in the future, excess renewable energy could be economically stored on a large scale in the form of gas (natural gas or hydrogen).

However, the capital costs of the ESS are still expensive at this stage. To reduce the investment costs, the concept of energy storage sharing has been put forward. As a result, it is more economical for a group of prosumers to share the ESS invested and managed by the coordinator rather than investing in the self-built ESS [73, 74]. Thus, to adapt to the increasing trend of sharing economy, proper sharing mechanisms and relevant pricing strategies in an integrated energy system need to be developed to enhance the comprehensiveness of the sharing model.

In the literature, some references focused on the operation strategy in an energy-sharing market. For example, [46, 135-137]. Apart from the operation strategy, some references investigated the pricing strategy in the energy-sharing market. For example, [72, 138, 139] There is also literature focused on the operation strategy of capacity sharing, such as [47, 69, 140]. Except for operational strategy, some literature studied the pricing strategy for capacity sharing. For example, [68-70]

There are still three issues that remain unaddressed in the existing literature. As for the first issue, most of the references did not reveal the essence of the sharing economy. For example, refs [46, 47] modeled energy sharing as an energy trading process. In such a trading process, pure consumers could participate and benefit from the sharing economy by purchasing electricity at a relatively low price [48]. However, they made less contribution toward energy sharing. It would result in the end-users being less incentivized to invest in DERs. As for the prosumers, they were also less incentivized to participate in energy sharing. Furthermore, the current literature lacked the link between capacity and energy sharing.

It is expected to formulate a method that can integrate both sharing services. For the second factor, the existing literature on energy sharing utilized the same sharing price for all end-users. It neglected that different end-users had different energy consumption profiles. Consequently, using the same sharing price could not incentivize individual end-user, for example, in [28, 69, 78], the same sharing price was formulated for all the prosumers, which was derived via the optimization process. Without applying a customized pricing strategy, the prosumers would not be willing to participate in the sharing process. Furthermore, the pricing strategy of these references did not make use of the dynamic demand-supply information, such as [69, 72]. Such a pricing strategy would reduce the profit of the coordinator [141]. For the third factor, most of the references only considered the virtual layer of the sharing process, i.e., the pricing strategy, the operation management, the incentivizing mechanism, etc., whereas the physical layer of the sharing process was ignored. For example, [69, 138, 139] neglected the voltage and capacity constraints and network power loss. Thus, these references cannot ensure the security of the power system in the sharing process.

Therefore, in this chapter, we propose credit-based pricing and planning strategies for capacity and energy sharing. The coordinator will invest and manage the ESS, while the prosumers will borrow the capacity and energy from the coordinator. The main contributions are as follows:

- First, a novel business model of credit-based sharing has been proposed to integrate both capacity sharing and energy sharing. The time accumulation effect has been considered via the proposed credit points, which can better reveal the essence of the sharing economy. Additionally, the payment rule is closely related to the time length and amount of the shared capacity and the shared energy that the prosumers borrow. When the credit is positive, the prosumers borrow the capacity of the ESS managed by the coordinator; when the credit is negative, the prosumers are borrowing the energy from the ESS either in the form of electricity or hydrogen.
- Second, two pricing strategies have been proposed to increase the total net profits of the coordinator and the willingness of the prosumers to participate in the sharing process. Customized pricing strategies are applied to capacity and energy sharing, respectively. When the credit is positive, the proposed cost-based pricing is applied to determine the price of the shared capacity; when the credit is negative, the proposed demand-based pricing is applied to determine the price of the shared energy, which has fully utilized the dynamic demand-supply information.

- Third, the energy storage system planning model is proposed. Physical constraints on ESS planning are considered to enhance the security of the power system. Additionally, integrated energy systems, including both the electricity network and the gas network, are examined. A 55-bus electricity network coupled with an 18-bus gas network has been employed to test the effectiveness of the credit-based sharing model.

9.2 The Framework of the Two-stage Credit-Based Sharing Model

9.2.1 Explanation of the Two-stage Sharing Process

In this chapter, the coordinator and the prosumers are the main participants in the capacity-sharing and energy-sharing process. In the proposed sharing framework, both electricity and hydrogen are involved. As mentioned in the introduction section, the utilization of hydrogen is increasing due to its feature of reducing greenhouse gas emissions. Additionally, hydrogen has a promising future to enhance energy flexibility. With the advancement of the P2G devices, excess renewable energy could be economically stored on a large scale in the form of gas. Thus, according to [78], a multi-carrier energy system can increase the flexibility of the energy system, provide the prosumers with reliable services, and reduce the transmission burden of the utility grid.

It is assumed that one coordinator manages the shared ESS and provides sharing services to a cluster of prosumers denoted by $J = \{1, 2, \ldots j, \ldots J\}$. The coordinator intends to maximize the profits within a day. A two-stage optimization problem between the coordinator and the prosumers is formulated. A detailed explanation is presented in Fig. 9-1:

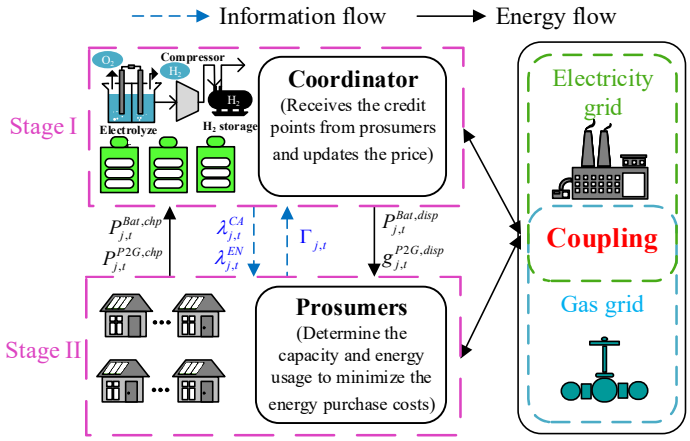

Fig. 9-1. The framework of the two-stage sharing process.

Stage I: The objective function of the coordinator in stage I is to maximize the daily net profits of the coordinator incurred during the energy sharing and capacity sharing process, which can be referred to

(9.15). Three decisions need to be made by the coordinator in this stage. First, the coordinator will determine the optimal planning of the shared ESS, i.e., the location and capacity of the ESS. Second, the coordinator will determine the capacity sharing price $\lambda_{j,t}^{CA}$ and energy sharing price $\lambda_{j,t}^{EN}$ based on the credit point $\Gamma_{j,t}$ of each prosumer. The credit is calculated according to the capacity and energy borrowing profile of each prosumer sent from stage II. Third, the coordinator will decide the amount of energy to trade with both the electricity grid and the gas grid. Finally, the capacity and energy sharing prices are transferred to stage II.

Stage II: The objective function of the prosumers in stage II is to minimize the capacity sharing and energy sharing costs, electricity purchasing costs, and hydrogen purchasing costs, which can be referred to (9.40). Two decisions need to be made by the prosumers. First, the prosumers will determine the capacity and energy borrowing profiles based on the sharing prices $\lambda_{j,t}^{CA}$ and $\lambda_{j,t}^{EN}$ provided by the coordinator in stage I [185]. The borrowing profiles include the electric power charged to the battery devices from prosumer j $P_{j,t}^{Bat,chp}$, the electric power discharged from the battery devices to prosumer j $P_{j,t}^{Bat,disp}$, the electric power delivered to the electrolyzer from prosumer j $P_{j,t}^{P2G,chp}$, and the hydrogen outflow from the P2G devices to prosumer j $g_{j,t}^{P2G,disp}$. Second, the prosumers will determine the electric power to purchase from the electricity grid $P_{j,t}^{ELE,BG}$, the electric power to sell to the electricity grid $P_{j,t}^{ELE,SG}$, and the amount of hydrogen to purchase from the gas grid $g_{j,t}^{H_2,BG}$. Finally, the capacity and energy borrowing profiles are transferred to stage I.

9.2.2 The Proposed Credit-Based Sharing Model

To standardize the amount of capacity occupied and the amount of energy shared, a credit-based sharing mechanism has been proposed. In this mechanism, the credit is a score that the coordinator records for each prosumer regarding their accumulated borrowing decision on either capacity or energy. The time accumulation effect has been considered via the proposed credit point $\Gamma_{j,t}$, which means it is closely related to the time length that the prosumers borrow the shared capacity and the shared energy. The equation relating to the credit is:

$$\begin{aligned}\Gamma_{j,t+1} = \Gamma_{j,t} &+ \left(P_{j,t}^{Bat,chp} \times \eta^{Bat,ch} - P_{j,t}^{Bat,disp} \Big/ \eta^{Bat,dis}\right) \times \Delta t \\ &+ \left(P_{j,t}^{P2G,chp} \times \eta^{P2G,ch} - g_{j,t}^{P2G,disp} \times \alpha \Big/ \eta^{P2G,dis}\right) \times \Delta t\end{aligned} \tag{9.1}$$

where $\Gamma_{j,t}$ is the credit points of prosumer j at time t; α is the unit conversion factor that converts GJ to MWh; $\eta^{Bat,ch}$ ($\eta^{Bat,dis}$) is the charging (discharging) efficiency of the battery devices; $\eta^{P2G,ch}$

($\eta^{P2G,dis}$) is the efficiency of the P2G devices.

Axiom 1: *When* $\Gamma_{j,t} > 0$*, it means the prosumers are using the capacity of the ESS.* This is similar to borrowing a storage locker. The costs of borrowing the shared capacity C_j^{CA} are influenced by the amount of capacity borrowed and the amount of time occupied where $C^{CA} = \sum_{j=1}^{J} \sum_{t=1}^{T} \left(\Gamma_{j,t} \times \lambda_{j,t}^{CA} \right)^{+}$.

Axiom 2: *When* $\Gamma_{j,t} < 0$*, the prosumers are borrowing energy from the coordinator in the form of either electricity or hydrogen with* $W_{j,t}^{ELE} + W_{j,t}^{H_2} = 1$ (where $W_{j,t}^{ELE}$ and $W_{j,t}^{H_2}$ are the proportion of the energy demanded by the prosumer in the form of electricity and hydrogen) [243]. This can be compared to borrowing money from the bank. Prosumers pay the borrowing fee to the **coordinator** for borrowing a certain amount of energy. The payment is no longer needed when the prosumers have returned the same amount of energy to the coordinator ($\Gamma_{j,t}$=0). The energy borrowing costs C_j^{EN} are also influenced by the energy borrowed and the borrowing time length where $C^{EN} = \sum_{j=1}^{J} \sum_{t=1}^{T} \left(-\Gamma_{j,t} \times \lambda_{j,t}^{EN} \right)^{+}$.

9.2.3 Brief Comparison of the Proposed Model with the Conventional Sharing Model

The detailed mechanism of the conventional sharing model can be found in the following section, i.e., section IV, part A [69]. The proposed model differs from the conventional sharing model in the following three aspects:

First, in the conventional sharing model [69], only the capacity sharing process is considered. Whereas in the proposed model, both energy sharing and capacity sharing are integrated via the proposed credit-based sharing model.

Second, conventional sharing modeled the sharing process like a trading process. In the proposed model, the process of sharing is emphasized with a return of the shared capacity and shared energy, which reveals the sharing economy.

Third, the price of shared energy is derived directly via the optimization process under the conventional model. By comparison, in the proposed model, two pricing strategies are used to customize the prices of the shared energy and the shared capacity. As a result, both the net profits of the coordinator and the willingness of the prosumers can be enhanced.

9.3 The Proposed Credit-based Pricing Strategy

9.3.1 Conventional Pricing Model

Conventionally, the coordinators will use equations (9.2) and (9.3) determine the price of the capacity sharing with the aim of maximizing the net profits [69]. It is the detailed model of **case 2** mentioned in

section VIII, part A. Equation (9.3) is the capacity-sharing revenue of the coordinator under the conventional model. The revenue of the coordinator equals the capacity sharing price multiplies the net charging profile of the prosumers. It can be found that all the prosumers are charged with the same capacity sharing price [69]. The formulae are shown as follows:

$$\max NP_{co} = R_{co}\left(\lambda_t^{CA}\right) - C_{co}^{cap}\left(X,P\right) - C_{co}^{oper}\left(P_{j,t}^{ch}, P_{j,t}^{dis}\right) \tag{9.2}$$

s.t.

$$R_{co}\left(\lambda_t^{CA}\right) = \mathbb{E}\left[\sum_{j=1}^{J}\sum_{t=1}^{T}\lambda_t \times \left(P_{j,t}^{ch} - P_{j,t}^{dis}\right)\right] \tag{9.3}$$

where $R_{co}\left(\lambda_t^{CA}\right)$ is the total revenues of the capacity sharing under the conventional pricing model; λ_t^{CA} is the capacity sharing price; $P_{j,t}^{ch}$ is the charging profile of prosumer *j* at time *t*; $P_{j,t}^{dis}$ is the discharging profile of prosumer *j* at time *t*; T is the total time periods within a day; J is the total numbers of the prosumers; $C_{co}^{cap}\left(X,P\right)$ is the daily capital costs of the coordinator under the conventional pricing model; X and P are the capacity and power scheduling of the prosumers; $C_{co}^{oper}\left(P_{j,t}^{ch}, P_{j,t}^{dis}\right)$ is the daily operational costs of the coordinator under the conventional pricing model; NP_{co} is the daily net profits of the coordinator under the conventional pricing model.

9.3.2 Proposed Cost-Based Pricing on Shared Capacity

In this section, the cost-based pricing strategy is proposed to derive the capacity sharing price due to the following two advantages of this pricing strategy. First, the capacity sharing market is a relatively new research area. As a result, the demand-supply information of the market is unrepresentative. Thus, it is inappropriate to price the shared capacity from the perspective of the prosumers by using the demand-based pricing strategy. Second, the cost-based pricing strategy can guarantee a positive profit for the coordinator [244]. This is because the mechanism of cost-based pricing is to determine a price that not only covers the capacity sharing costs of the coordinator but also facilitates the coordinator to earn extra profits, i.e., the premium, during capacity sharing.

A binary variable $y_{j,i,t}$ is used to optimize the time-of-use (TOU) price structure, and it indicates the coverage of the price block *i*. In this chapter, the TOU price is utilized. There are several price blocks in the TOU pricing, and each price block has a different price level and time duration. The TOU pricing strategy should be subject to equations (9.4)-(9.5). Equation (9.4) aims to ensure that each time period belongs to only one price block. Equation (9.5) indicates that only consecutive time periods can form a price block [71].

$$\sum_{i=1}^{N^{pb}} y_{j,i,t} = 1 \tag{9.4}$$

$$\left| y_{j,i,1} - y_{j,i,T} \right| + \sum_{t=2}^{T} \left| y_{j,i,t} - y_{j,i,t-1} \right| = 2 \tag{9.5}$$

where $y_{j,i,t}$ is the binary variable utilized to optimize the TOU price structure; N^{pb} is the number of price blocks

The capacity price is assumed to compose of two parts: the marginal costs λ_t^{mc} incurred during the capacity sharing process and the price premium of capacity sharing δ_t. In some practice, the price premium is normally empirically determined by the decision-maker according to the required rate of return. However, in our proposed method, the optimal price premium δ_t is obtained by solving an optimization problem rather than the empirical setting. The expression of the capacity sharing price is explained below:

$$\lambda_{j,t}^{CA} = \mathbb{E}\left(y_{j,i,t} \times \left[\lambda_t^{mc} \times \left(1 + \delta_t\right) \right] \right) \tag{9.6}$$

where $\lambda_{j,t}^{CA}$ is the capacity sharing price for prosumer *j* at time *t*.

The marginal costs can be derived as follows:

$$\lambda_t^{mc} = \frac{\left(C_t^{Bat+P2G,cap} + C_t^{Bat+P2G,oper} \right)}{\sum_{j=1}^{J} \left(P_{j,t}^{Bat,chp} + P_{j,t}^{P2G,chp} \right) \times \Delta t} \tag{9.7}$$

where $$C_t^{Bat+P2G,cap} = \Lambda \left(\mu^{Bat} \times IC^{Bat} + \mu^{P2G} \times IC^{P2G} \right) \tag{9.8}$$

$$C_t^{Bat+P2G,oper} = \sum_{j=1}^{J} \left(P_{j,t}^{Bat,chp} + P_{j,t}^{Bat,disp} \right) \times \vartheta^{Bat} + \sum_{j=1}^{J} \left[P_{j,t}^{P2G,chp} + \left(g_{j,t}^{P2G,disp} \times \alpha \right) \right] \times \vartheta^{P2G} \tag{9.9}$$

where $C_t^{Bat+P2G,cap}$ is the discounted hourly capital costs of the battery and P2G devices; $C_t^{Bat+P2G,oper}$ is the operational costs during the capacity sharing process; μ^{Bat} and μ^{P2G} are the total number of the battery and P2G devices that are installed; IC^{Bat} and IC^{P2G} are the investment costs per battery and P2G devices; Λ is the discount factor that discounts the capital costs of the ESS into every *t* period; ϑ^{Bat} and ϑ^{P2G} are the operating costs per battery and P2G devices.

9.3.3 Proposed Demand-Based Pricing on Shared Energy

Different from the pricing strategy on shared capacity, a demand-based pricing strategy is proposed to determine the price of the shared energy [245]. The advantages of this pricing method are also two-fold. First, demand-based pricing is suitable for pricing shared energy. Energy sharing is widely studied in the existing literature, such as [46, 136, 246]. Thus, the energy sharing market is relatively more mature than

the capacity sharing market. Therefore, information on the energy demand and energy supply is representative and can reflect the genuine value of the shared energy. Second, demand-based pricing can dynamically respond to the demand-supply variation. It is a pricing strategy that is based on demand-supply information, which can reflect the market information on a timely basis. Compared with cost-based pricing, demand-based pricing can prevent the coordinator from selling at too high a price that is unattractive to the prosumers or selling at too low a price, which results in losing profits of the coordinator that prosumers would otherwise have been willing to pay.

Here, the concept of supply-demand ratio SDR_t is applied to reflect the dynamic demand-supply information. It is a ratio calculated by dividing the amount of energy supply at time *t* by the total amount of energy demand at time *t* [138, 247]. By adapting to the proposed sharing model, it can be found in equation (9.10) that the energy supply means the energy available from the energy storage devices (both the P2G and the battery devices) managed by the coordinator. Additionally, energy demand is the energy borrowing amount of the prosumers. The expression SDR_t can be shown as:

$$SDR_t = \frac{\left(E_t^{Bat} + S_t^{P2G} \times LHV^H \times \mathrm{M}^{-1} \times \alpha\right)}{\sum_{j=1}^{J}\left(P_{j,t}^{Bat,disp} + g_{j,t}^{P2G,disp} \times \alpha\right) \times \Delta t} \tag{9.10}$$

$$E_t^{Bat} = \sum_{k \in K} E_{k,t}^{Bat} \tag{9.11}$$

$$S_t^{P2G} = \sum_{q \in Q} S_{q,t}^{P2G}, S_{q,0}^{P2G} = S_{q,T}^{P2G} \tag{9.12}$$

where E_t^{Bat} is the energy storage state of the battery devices at time *t*; $E_{k,t}^{Bat}$ is the energy storage state of the battery devices at bus *k* at time *t*; S_t^{P2G} is the energy storage state of the P2G device at time *t*; M is the molar volume of gas (L/mol); LHV^H is the lower heat value of the hydrogen (GJ/Mol); $S_{q,t}^{P2G}$ is the energy storage state of the P2G device at bus *q* at time *t*.

Although our proposed pricing model for energy sharing is empirically adopted, it is based on a reasonable theoretical basis. The rationale for using SDR_t is that the relationship between price and SDR_t is inversely related, which is based on empirical experience and relevant economic theory [248]. To be specific, the increase of SDR_t will reduce the energy sharing price $\lambda_{j,t}^{EN}$. However, when SDR_t approaches infinity, the energy sharing price is not lower than the selling price to the utility grid $\lambda_t^{ELE,SG}$. Otherwise, the coordinator will lose incentives to provide energy-sharing services. On the contrary, the decrease of SDR_t will increase the energy sharing price $\lambda_{j,t}^{EN}$. However, the energy sharing price will

not be higher than the purchasing price from the utility grid λ_t^{buy}. Otherwise, the prosumers will lose incentives to participate in energy sharing. Additionally, when SDR_t =0, the energy sharing price equals the energy purchasing price λ_t^{buy}. Moreover, when SDR_t =1, the energy sharing price equals the energy selling price to the utility grid $\lambda_t^{ELE,SG}$ plus a compensating price β. Here β is the compensating price that is used to ensure that the coordinator is incentivized to share energy. Thus, the energy sharing price is bounded by a range [$\lambda_t^{ELE,SG}$, λ_t^{buy}].

Thus, the relationship between the energy sharing price and SDR_t can be shown as (9.13)-(9.14) and illustrated in Fig. 9-2, which can refer to [138, 247]. A detailed deduction can be referred to [248]. To be noted, since the prosumers can purchase both electricity and hydrogen from the utility grid, the weighted purchase price from the utility grid is formulated as (9.14).

$$\lambda_{j,t}^{EN}=\begin{cases}\dfrac{\left(\lambda_t^{ELE,SG}+\beta\right)\times\lambda_t^{buy}}{\left(\lambda_t^{buy}-\lambda_t^{ELE,SG}-\beta\right)SDR_t+\lambda_t^{ELE,SG}+\beta} & 0\le SDR_t\le 1\\ \left(\lambda_t^{ELE,SG}+\dfrac{\beta}{SDR_t}\right) & SDR_t>1\end{cases} \tag{9.13}$$

$$\lambda_t^{buy}=\left(W_{j,t}^{ELE}\times\lambda_t^{ELE,BG}+W_{j,t}^{H_2}\times\lambda_t^{H_2,BG}\right) \tag{9.14}$$

where $\lambda_{j,t}^{EN}$ is the energy sharing price for prosumer *j* at time *t*; λ_t^{buy} is the weighted energy purchasing price; $\lambda_t^{ELE,BG}$ ($\lambda_t^{ELE,SG}$) is the energy purchasing (selling) price in the electricity grid; $\lambda_t^{H_2,BG}$ is the hydrogen purchasing price in the gas grid; β is the compensating price that is used to ensure that the coordinator is incentivized to share energy; $W_{j,t}^{ELE}$ and $W_{j,t}^{H_2}$ are the proportion of the energy demand of prosumer *j* in the form of electricity and hydrogen.

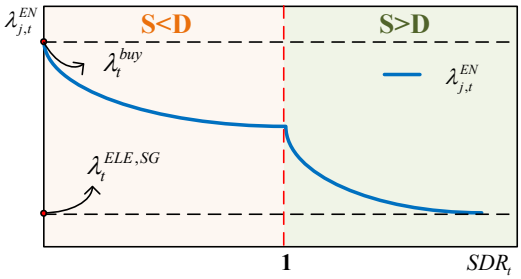

Fig. 9-2. Relationship between SDR_t and the energy sharing price

In brief, our SDR_t model is different from the existing SDR_t models in the following three aspects. First, our model is designed specifically for energy sharing rather than energy trading in the existing SDR_t models. Second, multi-forms of energy sharing have been considered in the formulation. Both

electricity and hydrogen have been incorporated in the model shown as equation (9.14). Third, the compensating price β is used to ensure that the coordinator is incentivized to share energy.

9.4 Stage I: Problem from the Perspective of Energy Storage Coordinator

9.4.1 Revenues and Costs of the Energy Storage Sharing

In stage I, apart from trading with the electricity grid and the gas grid, the coordinator will also determine the capacity sharing price and the energy sharing price. For equation (9.15), the objective is to maximize the daily total net profits of the coordinator incurred during the capacity sharing and energy sharing process. The decision variables of (9.15) include the number of batteries μ_k^{Bat} to install at bus *k*, the number of the P2G devices μ_q^{P2G} to install at bus *q*, the capacity sharing price for prosumer *j* at time *t* $\lambda_{j,t}^{CA}$, the energy sharing price for prosumer *j* at time *t* $\lambda_{j,t}^{EN}$, the binary variable $y_{j,i,t}$ that is introduced to optimize the TOU price structure, the electric power discharged from the battery devices that is sold to the electricity grid $P_{k,t}^{Bat,SG}$, the electric power purchased from the electricity grid that is charged to the battery devices $P_{k,t}^{Bat,BG}$, the electric power purchased from the electricity grid that is delivered to the electrolyzer $P_{q,t}^{P2G,BG}$, the hydrogen outflow from the P2G devices that is sold to the gas grid $g_{q,t}^{P2G,SG}$, the hydrogen inflow to the P2G devices that is purchased from the gas grid $g_{q,t}^{P2G,BG}$, σ_k and σ_q which are used to indicate whether the battery and the P2G will be installed at the electricity bus and the gas bus.

The objective function is shown as:

$$\begin{aligned}\max .NP^{co} = {} & R^{CA} + R^{EN} + NP^{ELE} + NP^{H_2} \\ & - C^{Bat+P2G} - C^{ELE/H_2,NW}\end{aligned} \tag{9.15}$$

9.4.1.1 Revenues from capacity sharing R^{CA} and energy sharing R^{EN}:

$$R^{CA} = \sum_{j=1}^{J}\sum_{t=1}^{T}\left(\lambda_{j,t}^{CA} \times \Gamma_{j,t}\right)^{+} \tag{9.16}$$

$$R^{EN} = \sum_{j=1}^{J}\sum_{t=1}^{T}\left(-\lambda_{j,t}^{EN} \times \Gamma_{j,t}\right)^{+} \tag{9.17}$$

When $\Gamma_{j,t} > 0$, the coordinator will calculate the revenues on capacity sharing based on the optimized capacity price $\lambda_{j,t}^{CA}$. When $\Gamma_{j,t} < 0$, the coordinator will calculate the revenues on energy sharing based on the optimized energy price $\lambda_{j,t}^{EN}$.

9.4.1.2 Daily net profits from energy trading with both electricity and gas grids:

$$NP^{ELE} = \sum_{k\in K}\sum_{t=1}^{T}\left(\lambda_t^{ELE,SG} \times P_{k,t}^{Bat,SG}\right) - \sum_{k\in K}\sum_{t=1}^{T}\left(\lambda_t^{ELE,BG} \times P_{k,t}^{Bat,BG}\right) - \sum_{q\in Q}\sum_{t=1}^{T}\left(\lambda_t^{ELE,BG} \times P_{q,t}^{P2G,BG}\right) \tag{9.18}$$

$$NP^{H_2} = \sum_{q\in Q}\sum_{t=1}^{T}\left(\lambda_t^{H_2,SG} \times g_{q,t}^{P2G,SG}\right) - \sum_{q\in Q}\sum_{t=1}^{T}\left(\lambda_t^{H_2,BG} \times g_{q,t}^{P2G,BG}\right) \tag{9.19}$$

where NP^{ELE} and NP^{H_2} are the net profits from trading with the electricity grid and the gas grid.

9.4.1.3 The total daily capital and operational costs of energy storage devices:

$$C^{Bat+P2G} = \sum_{t=1}^{T}\left(C_t^{Bat+P2G,cap} + C_t^{Bat+P2G,oper}\right) \tag{9.20}$$

9.4.1.4 The network loss:

$$C^{ELE,NW} = \sum_{t=1}^{T}\left(r_{mk} \times {l_{mk,t}}^2 \times \lambda_t^{ELE,BG}\right) \tag{9.21}$$

$$C^{H_2,NW} = \sum_{t=1}^{T}\left[\zeta \times S_{pq,t}^{pipe} + \zeta \times \left(S_{pq,t}^{pipe}\right)^3\right] \tag{9.22}$$

where $C^{ELE,NW}$ and $C^{H_2,NW}$ are the network loss of both the electricity grid and the gas grid [78]; r_{mk} is the resistance of line *mk*; $l_{mk,t}$ is the line current magnitude on distribution line *mk*; ζ is the gas pipeline cost coefficient; $S_{pq,t}^{pipe}$ is the gas flow from pipelines *p* to *q* at time *t*.

9.4.2 Constraints of the Electricity Network

9.4.2.1 Electricity storage system constraints

Different from the traditional centralized ESS, the proposed sharing model not only satisfies the load via energy purchase from the grid but also offers sharing services among the prosumers. In other words, $P_{k,t}^{Bat,ch} = P_{k,t}^{Bat,BG} + P_{k,t}^{Bat,chp}$ and $P_{k,t}^{Bat,dis} = P_{k,t}^{Bat,SG} + P_{k,t}^{Bat,disp}$, where $P_{k,t}^{Bat,ch}$ is the total electric power charged to the battery devices at bus *k* at time *t*; $P_{k,t}^{Bat,dis}$ is the total electric power discharged from the battery devices at bus *k* at time *t*; $P_{k,t}^{Bat,chp}$ is the electric power charged to the battery devices from the prosumers at bus *k* at time *t*; $P_{k,t}^{Bat,disp}$ is the electric power discharged from the battery to the prosumers at bus *k* at time *t*.

Moreover, a binary variable is introduced. For instance, σ_k is used in equation (9.24) to indicate whether the battery will be installed at bus *k*, and it satisfies $\sum_{k\in K}\sigma_k = Z$. Detailed constraints are:

$$E_{k,t+1}^{Bat} = E_{k,t}^{Bat} + P_{k,t}^{Bat,ch} \times \eta^{Bat,ch} \times \Delta t - P_{k,t}^{Bat,dis} \times \Delta t / \eta^{Bat,dis} \tag{9.23}$$

$$0 \le P_{k,t}^{Bat,ch} \le P_{\max}^{Bat,ch} \times \sigma_k, 0 \le P_{k,t}^{Bat,dis} \le P_{\max}^{Bat,dis} \times \sigma_k \tag{9.24}$$

$$0 \le E_{k,t}^{Bat} \le E_{\max}^{Bat} \times \mu_k^{Bat}, 0 \le \mu_k^{Bat} \le \sigma_k \times \overline{Cap^{Bat}} \tag{9.25}$$

where $P_{\max}^{Bat,ch}$ and $P_{\max}^{Bat,dis}$ are the maximum charging and discharging power of the battery; Z is the total number of sharing stations; μ_k^{Bat} is the number of the battery devices to install at bus *k*,

$\mu^{Bat} = \sum_{k \in K} \mu_k^{Bat}$; $E_{\max}^{Bat}$ is the maximum capacity of the battery; $\overline{Cap^{Bat}}$ is the upper limit of the installed battery.

The electric power charged to the battery devices from the prosumers at bus *k* at time *t*, i.e., $P_{k,t}^{Bat,chp}$, is derived by aggregating the charging decision of the prosumers who belong to bus *k*, shown as (9.26):

$$P_{k,t}^{Bat,chp} = \sum_{j \in k} P_{j,t}^{Bat,chp} \tag{9.26}$$

where $P_{j,t}^{Bat,chp}$ is the electric power charged to the battery devices from prosumer *j* at time *t*; $P_{k,t}^{Bat,chp}$ is the electric power charged to the battery devices from the prosumers at bus *k* at time *t*.

In addition, the electric power discharged from the battery to the prosumers at bus *k* at time *t*, i.e., $P_{k,t}^{Bat,disp}$, is derived by aggregating the discharging decision of the prosumers who belong to bus *k*, which is shown as (9.27):

$$P_{k,t}^{Bat,disp} = \sum_{j \in k} P_{j,t}^{Bat,disp} \tag{9.27}$$

where $P_{j,t}^{Bat,disp}$ is the electric power discharged from the battery devices to prosumer *j* at time *t*; $P_{k,t}^{Bat,disp}$ is the electric power discharged from the battery to the prosumers at bus *k* at time *t*.

9.4.2.2 Power flow equation

Constraints relating to the electricity network are explained:

$$\begin{aligned} & P_{mk,t}^{B} - \sum_{n} P_{kn,t}^{B} + P_{k,t}^{PV} + P_{k,t}^{ST} - P_{k,t}^{L} \\ & = P_{k,t}^{Bat,ch} \times \eta^{Bat,ch} - P_{k,t}^{Bat,dis} \Big/ \eta^{Bat,dis} + r_{mk} \frac{\left(P_{mk,t}^{B}\right)^2 + \left(Q_{mk,t}^{B}\right)^2}{V_{k,t}^2} \end{aligned} \tag{9.28}$$

$$Q_{mk.t}^{B} - \sum_{n} Q_{kn.t}^{B} + Q_{k,t}^{ST} - Q_{k,t}^{L} = x_{mk} \frac{\left(P_{mk,t}^{B}\right)^2 + \left(Q_{mk,t}^{B}\right)^2}{V_{k,t}^2} \tag{9.29}$$

$$V_{k,t}^2 - V_{m,t}^2 = 2\left(r_{mk} P_{mk,t}^{B} + x_{mk} Q_{mk,t}^{B}\right) - \left(r_{mk}^2 + x_{mk}^2\right) \frac{\left(P_{mk,t}^{B}\right)^2 + \left(Q_{mk,t}^{B}\right)^2}{V_{k,t}^2} \tag{9.30}$$

$$\underline{V_k} \le V_{k,t} \le \overline{V_k}, \sqrt{\left(P_{mk,t}^{B}\right)^2 + \left(Q_{mk,t}^{B}\right)^2} \le \overline{S_{mk}^{B}} \tag{9.31}$$

where $P_{mk,t}^{B}$ and $Q_{mk,t}^{B}$ are the active and reactive branch power flow from bus *m* to bus *k*; $P_{k,t}^{PV}$ is the output of the PVs; $P_{k,t}^{ST}$ and $Q_{k,t}^{ST}$ are the active and the reactive power from the substation; $P_{k,t}^{L}$ and

$Q_{k,t}^{L}$ are the active and reactive load at bus k; $V_{k,t}$ is the nodal voltage; r_{mk} and x_{mk} are the resistance and the reactance of feeder; $\overline{(\bullet)}$ and $\underline{(\bullet)}$ are the upward and downward limits.

9.4.3 Constraints of the Gas Network

9.4.3.1 Gas storage system constraints

The energy storage sharing in an electricity and hydrogen integrated system has the advantage of energy flexibility. Hence, the trading among the coordinator, prosumers, and the gas grid should be considered. Furthermore, to ensure the operation of the gas grid, the gas grid constraints (9.32)-(9.39) should be considered.

Similar to the electricity grid, a binary variable is introduced in the gas storage system. For instance, σ_q is used to indicate whether the P2G will be installed at bus q, $\sum_{q\in Q}\sigma_q = Z$. Detailed constraints are explained as follows:

$$\begin{aligned} S_{q,t+1}^{P2G} = S_{q,t}^{P2G} &+ \left(g_{q,t}^{elz} + g_{q,t}^{P2G,BG}\right)\times \mathrm{M}\times \eta^{P2G,ch} \Big/ LHV^{H} \\ &- \left(g_{q,t}^{P2G,disp} + g_{q,t}^{P2G,SG}\right)\times \mathrm{M} \Big/ \left(\eta^{P2G,dis}\times LHV^{H}\right) \end{aligned} \tag{9.32}$$

$$g_{q,t}^{elz} = \eta^{elz}\times\left(P_{q,t}^{P2G,chp} + P_{q,t}^{P2G,BG}\right)\times\Delta t\times\alpha^{-1}, \forall t \tag{9.33}$$

$$P_{q,t}^{elz} = P_{q,t}^{P2G,BG} + P_{q,t}^{P2G,chp} \tag{9.34}$$

$$0 \le P_{q,t}^{elz} \le P_{q,\max}^{elz}, P_{q,\max}^{elz} \le \overline{P^{elz}}\times\sigma_q \tag{9.35}$$

$$0 \le S_{q,t}^{P2G} \le S_{\max}^{P2G}\times\mu_q^{P2G}, 0 \le \mu_q^{P2G} \le \sigma_q \times \overline{Cap^{P2G}} \tag{9.36}$$

where $g_{q,t}^{elz}$ is the hydrogen from the electrolyzer that is stored in the gas tank at bus q at time t; $P_{q,t}^{P2G,chp}$ is the electric power delivered to the P2G electrolyzer from the prosumers at bus q; $P_{q,t}^{P2G,BG}$ is the electric power purchased from the electricity grid that is delivered to the electrolyzer; $g_{q,t}^{P2G,BG}$ is the hydrogen inflow to the P2G devices that is purchased from the gas grid; $g_{q,t}^{P2G,disp}$ is the hydrogen outflow from the P2G devices to the prosumers at bus q; $g_{q,t}^{P2G,SG}$ is the hydrogen outflow from the P2G devices that is sold to the gas grid; $\overline{P^{elz}}$ is the upper power limit of the electrolyzer; $P_{q,\max}^{elz}$ is the maximum power limit of the electrolyzer; μ_q^{P2G} is the number of the P2G devices to install at bus q,

$\mu^{P2G} = \sum_{q \in Q} \mu_q^{P2G}$; $\overline{Cap^{P2G}}$ is the upper limit of the installed P2G. Similar to equations (9.26) and (9.27), $P_{q,t}^{P2G,chp}$ and $g_{q,t}^{P2G,disp}$ can be derived by aggregating all the energy usage profiles of the prosumers at corresponding buses.

9.4.3.2 Gas pipeline gas flow

The gas flow of the pipeline can be expressed by the Weymouth flow equation [249, 250].

$$S_{pq,t}^{pipe} = \mathrm{sgn}\left(\rho_{p,t}, \rho_{q,t}\right) \times \Phi_{pq} \times \sqrt{\left|\rho_{p,t}{}^2 - \rho_{q.t}{}^2\right|} \tag{9.37}$$

where $S_{pq,t}^{pipe}$ is the gas flow from pipelines p to q at time t; $\mathrm{sgn}\left(\rho_{p,t}, \rho_{q,t}\right)$ denotes the gas flow direction; $\rho_{p,t}$ and $\rho_{q,t}$ are the gas pressure at bus p and bus q; Φ_{pq} is the pipeline constant.

9.4.3.3 Gas compressor

The gas consumption of the compressor $G_{pq,t}^{comp}\left(H_{pq,t}\right)$ can be shown as follows [243]:

$$G_{pq,t}^{comp}\left(H_{pq,t}\right) = \alpha_{3,pq}^{comp} + \alpha_{2,pq}^{comp} \times H_{pq,t} + \alpha_{1,pq}^{comp} \times \left(H_{pq,t}\right)^2 \tag{9.38}$$

where $H_{pq,t}$ is the horsepower consumption of the compressor station; $\alpha_{1,pq}^{comp}$, $\alpha_{2,pq}^{comp}$, and $\alpha_{3,pq}^{comp}$ are the conversion factors between the horsepower consumption and the gas consumption of the compressor.

9.4.3.4 Nodal gas balance model

The flow balance equation indicates that the gas flowing into bus q equals the overall gas flowing out of bus q.

$$\begin{aligned} & G_{q,t}^{well} + \sum_{p \in Q} S_{pq,t}^{pipe} - \sum_{p \in Q} S_{qp,t}^{pipe} - \sum_{p \in Q} G_{pq,t}^{comp}\left(H_{pq,t}\right) \times \eta_{pq}^{comp} - G_{q,t}^{GL} \\ & = \left(g_{q,t}^{elz} + g_{q,t}^{P2G,BG}\right) \times \mathrm{M} \times \eta^{P2G,ch} \Big/ LHV^{H} \\ & - \left(g_{q,t}^{P2G,disp} + g_{q,t}^{P2G,SG}\right) \times \mathrm{M} \Big/ \left(\eta^{P2G,dis} \times LHV^{H}\right) \end{aligned} \tag{9.39}$$

where $G_{q,t}^{well}$ is the gas generation from the gas well; $G_{q,t}^{GL}$ is the gas load.

9.5 Stage II: Problem from the Perspective of Prosumers

After knowing the prices of the shared capacity and the shared energy, the prosumers will determine the optimal capacity and energy borrowing amount. The prosumers will use the energy generated by PVs. If there is surplus energy, the energy can be stored in the *ESS* operated by the coordinator and incur

capacity borrowing costs $C^{CA}=\sum_{j=1}^{J}\sum_{t=1}^{T}\left(\Gamma_{j,t}\times\lambda_{j,t}^{CA}\right)^{+}$, or the energy can be sold to the external electricity grid and gain profits $R^{ELE,SG}=\sum_{j=1}^{J}\sum_{t=1}^{T}\left(P_{j,t}^{ELE,SG}\times\lambda_{t}^{ELE,SG}\right)$; If the self-generated energy is inadequate to satisfy the demand of the prosumers, the prosumers could purchase the electricity and hydrogen externally from the electricity grid and the gas grid by paying $C^{ELE,BG}=\sum_{j=1}^{J}\sum_{t=1}^{T}\left(P_{j,t}^{ELE,BG}\times\lambda_{t}^{ELE,BG}\right)$ for the purchased electricity and $C^{H_2,BG}=\sum_{j=1}^{J}\sum_{t=1}^{T}\left(g_{j,t}^{H_2,BG}\times\lambda_{t}^{H_2,BG}\right)$ for the purchased hydrogen. Alternatively, prosumers could borrow the energy from the coordinator and incur energy borrowing costs $C^{EN}=\sum_{j=1}^{J}\sum_{t=1}^{T}\left(-\Gamma_{j,t}\times\lambda_{j,t}^{EN}\right)^{+}$.

For equation (9.40), the objective of the prosumers in stage II is to minimize the capacity sharing and energy sharing costs, electricity purchasing costs, and gas purchasing costs. The decision variables include the credit point of prosumer *j* at time *t* $\Gamma_{j,t}$, the electric power charged to the battery devices from the prosumer *j* at time *t* $P_{j,t}^{Bat,chp}$, the electric power discharged from the battery devices to prosumer *j* at time *t* $P_{j,t}^{Bat,disp}$, the electric power delivered to the electrolyzer from prosumer *j* at time *t* $P_{j,t}^{P2G,chp}$, the hydrogen outflow from the P2G devices to prosumer *j* (GJ) $g_{j,t}^{P2G,disp}$, the electric power sold to the electricity grid from prosumer *j* $P_{j,t}^{ELE,SG}$, the electric power purchased from the electricity grid by prosumer *j* $P_{j,t}^{ELE,BG}$, and the amount of hydrogen purchased by prosumer *j* from the gas grid $g_{j,t}^{H_2,BG}$. The objective function is shown as:

$$\min .C^{CA}+C^{EN}+\left(C^{ELE,BG}-R^{ELE,SG}\right)+C^{H_2,BG} \tag{9.40}$$

s.t.

$$P_{j,t}^{ELE,BG}-P_{j,t}^{ELE,SG}+P_{j,t}^{Bat,disp}-P_{j,t}^{Bat,chp}-P_{j,t}^{P2G,chp}=P_{j,t}^{l,ELE} \tag{9.41}$$

$$g_{j,t}^{H_2,BG}+g_{j,t}^{P2G,disp}=g_{j,t}^{l,H_2} \tag{9.42}$$

where $P_{j,t}^{l,ELE}$ and $g_{j,t}^{l,H_2}$ are the electricity and the hydrogen net load of prosumer *j*.

9.6 Solver to Solve the Optimization Problem

The gas network loss (9.22) is non-linear. To improve the computational efficiency, piecewise linear approximation has been utilized to linearize (9.22). Details can be referred to [243]. The pipeline gas flow constraint is non-linear. We used the first-order Taylor series approximation to linearize (9.37).

Details can be referred to [243]. Equations (9.16) and (9.17) are non-linear because they contain the maximum functions. They can be linearized by introducing auxiliary variables [71]. Equation (9.5) is the structural constraint of the TOU price, which contains the absolute value. To linearize constraint (9.5), binary variables are introduced [71]. For equation (9.28), it is non-convex and non-linear due to term $\frac{\left(P_{mk,t}^{B}\right)^2+\left(Q_{mk,t}^{B}\right)^2}{V_{k,t}^2}$, which equals the squared line current magnitude l_{mk}^2. To convexify equation (9.28), $l_{mk}^2=\left(\left(P_{mk,t}^{B}\right)^2+\left(Q_{mk,t}^{B}\right)^2\right)\Big/V_{k,t}^2$ is relaxed as $l_{mk}^2\geq\left(\left(P_{mk,t}^{B}\right)^2+\left(Q_{mk,t}^{B}\right)^2\right)\Big/V_{k,t}^2$, and the second-order cone constraint is $\left\|\left(2P_{mk,t}^{B},2Q_{mk,t}^{B},V_{k,t}^2-l_{mk}^2\right)\right\|_2\leq V_{k,t}^2+l_{mk}^2$. After linearizing the other non-linear constraints mentioned above, the mixed-integer second-order cone programming (MISOCP) can be utilized to solve the problem [136]. CPLEX is utilized as the optimization solver.

The optimization problem is solved in the following procedures. First, the stage II problem is solved based on the initial capacity and energy sharing prices. Then, the stage I problem is solved based on the charging/discharging profiles optimized in stage II. Next, the optimized sharing prices in stage I will be passed to stage II. This iterative process will end until reaching an equilibrium, i.e., the optimal capacity/energy sharing price and the optimal charging/discharging profiles are achieved. A detailed explanation of the iterative process regarding the information exchange can be referred to in Fig. 9-1 [136].

9.7 Case Study

9.7.1 Experiment Setting

The proposed credit-based capacity and energy sharing model is verified on a 55-bus electricity network coupled with an 18-bus gas network. The electricity network is the modified IEEE European Low Voltage Test Feeder. The detailed parameters, such as resistance r_{km} and reactance of the feeders x_{km} can be referred to [228]. The nominal voltage is set as 415V. For the gas network, the pipeline constant Φ_{pq} can be referred to [243]. The electricity and hydrogen demand profiles are shown in Fig. 9-3.

The uncertainties in this chapter contain the output of the DERs, the electricity and hydrogen price of the utility grid, and the electricity and hydrogen demand of the prosumers. These uncertainties are modeled by probability density functions, and then Monte Carlo Simulation is utilized to address

uncertainty problems by modeling their probability density functions.

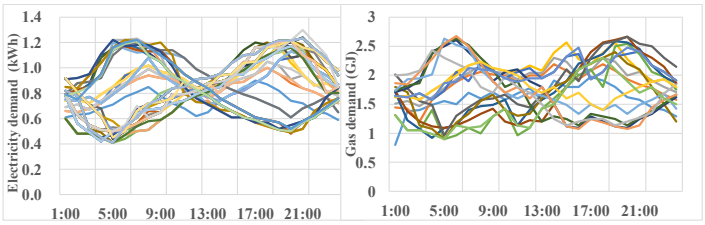

Fig. 9-3. The electricity and hydrogen demand profiles

Three case studies were carried out to prove the effectiveness of the proposed credit-based sharing model.

In **case 1,** *the base case* without capacity or energy sharing is presented.

In **case 2,** *the conventional model* with the capacity sharing process is examined [69]. This model is explained in section IV, part A.

In **case 3,** *the proposed credit-based sharing model* is evaluated.

The following case study is divided into three parts. In the first part, the ESS planning results are provided. In the second part, the result of the operation of the shared ESS in different cases is analyzed. To be specific, the results of **cases 1-3** are compared from the aspects of load components, SOC state, the financial indicators, the willingness-to-participate ratio, the self-sufficiency ratio, etc. Moreover, the proposed pricing model using both the battery and P2G devices has been compared with only using the battery. In the third part, the proposed pricing strategy is analyzed. In addition, the proposed pricing strategy is further compared with only using the cost-based pricing strategy for both energy and capacity sharing.

9.7.2 The ESS Planning Results

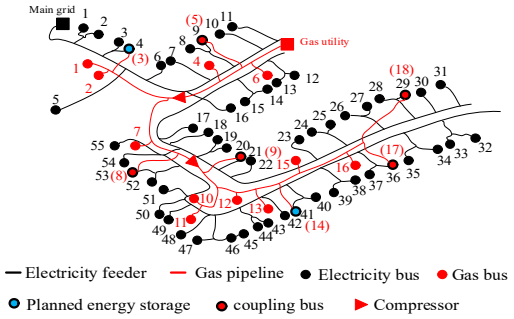

Fig. 9-4. Physical planning of the sharing stations.

In Fig. 9-4, the physical planning of the ESS is illustrated [136]. Both the candidate coupling bus and the optimized ESS planning are presented. The **location** of the battery devices is derived via equations (9.24)-(9.25) in section V, part B (1). The **location** of the P2G devices is derived via equations (9.35)-

(9.36) in section V, part C (1). As for the **capacity** of the battery devices and the P2G devices, it is embedded in equation (9.8). All the measurements are transferred into energy units. Thus, after the optimization process, the total capacity of the battery and the P2G devices are 920 kWh and 240 kWh, respectively. There are two optimal sharing stations. For the first sharing station, it is planned at electricity bus 4 (gas bus 3) with 378 kWh battery and 87 kWh P2G. For the second sharing station, it is planned at electricity bus 41 (gas bus 14) with 542 kWh battery and 153 kWh P2G.

9.7.3 Operation of Shared ESS in Different Cases

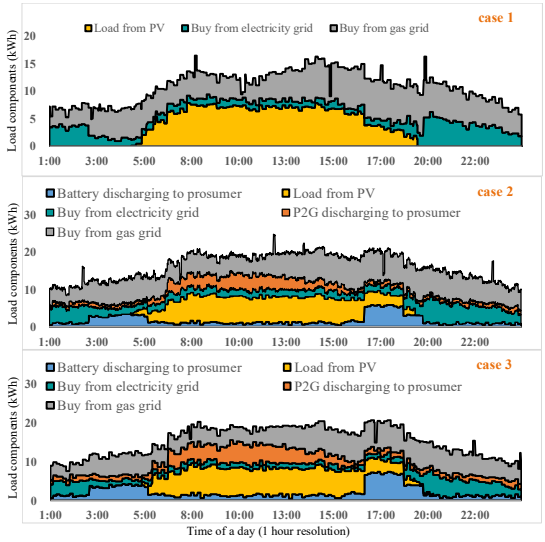

Fig. 9-5. The load components comparison of the three cases.

Fig. 9-5 illustrates the case comparison of the load components of all the prosumers in the three cases. For **case 1**, no energy or capacity sharing is involved. Thus, it can be found that the load includes three parts, i.e., the load from PV, energy purchased from the electricity grid, and energy purchased from the gas grid. By comparison, prosumers in **case 2** can borrow capacity from the coordinator to store excess energy for later use when the energy price in the utility grid is high. For **case 3**, the load components in the early morning and late evening are similar to **case 2**. During the daytime, there is more energy discharged from the battery and the P2G in **case 3** compared with **case 2**, which indicates that prosumers in **case 3** are engaged in borrowing energy from the coordinator at a price that is lower than the energy purchasing price in the utility grid. As a result, the proposed model can further reduce the energy purchase cost of prosumers from the utility grid.

Fig. 9-6 and Fig. 9-7 show the SOC and the total net profits of the coordinator under both **case 2** and **case 3**. It can be found that the SOC of both the battery and the P2G devices in **case 3** is higher than that

in **case 2** in general. This is because the credit-based sharing model has incentivized more prosumers to participate in the capacity and energy-sharing process. Thus, the overall energy storage usage efficiency is enhanced, which can be presented as the ascending of the SOC. Additionally, the enhancement of the overall energy storage usage efficiency can be verified via Table 9-1 quantitatively. It can be found that the storage usage efficiency can be increased from 39% to 62%.

Table 9-1 shows the result comparison from the perspective of both the prosumers and the coordinator. The financial indicators on energy costs of the prosumers and the total net profits of the coordinator are analyzed. In addition, other indicators like the willingness-to-participate (WTP) ratio and the self-sufficiency ratio (SSR) are analyzed. For **case 1**, only the energy costs and the self-sufficiency ratio can be analyzed [138]. Two concepts will be introduced. The first is the willingness-to-participate ratio $WTP = N_{lc} / N_{total}$, where N_{lc} is the number of prosumers that have reduced energy costs after participating in the sharing process, and N_{total} is the total number of prosumers participating in the sharing process [138]. It is a ratio used to indicate the degree of willingness of the prosumers to participate in the sharing process. The higher the ratio, the more incentivized the prosumers are. The second is the self-sufficiency ratio $SSR = \left(E_{PV} + E_{Dis}\right) / E_L$, where E_{Dis} is the aggregated energy from the energy storage devices are discharged to satisfy load need [138]. It is a ratio used to indicate the degree of self-sufficiency within the community of the prosumers and the coordinator. From the perspective of the prosumers, the SSR has increased by 14.5%, and the WTP ratio has increased by 20% under **case 3** compared with that under **case 2**. And it is cost-saving for the prosumers to participate in the sharing process under the proposed model. For the coordinator, the average daily total net profits of the coordinator in **case 3** have increased to 264.11 AU$ compared with **case 2**. Here, the total net profits calculation can be referred to equation (9.15). Moreover, the payback period of the energy storage devices is reduced to 5.6 years. Additionally, storage usage efficiency is increased from an average of 39% to 62%.

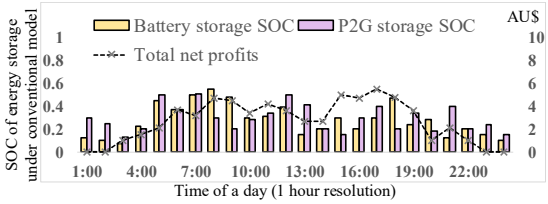

Fig. 9-6. The SOC and total net profits under **case 2**.

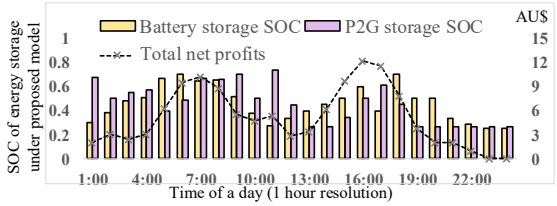

Fig. 9-7. The SOC and total net profits under **case 3**.

TABLE 9-1. RESULT COMPARISON OF DIFFERENT CASES FROM THE PERSPECTIVE OF THE PROSUMERS AND THE COORDINATOR

		Case 1	**Case 2**	**Case 3**
Prosumers	Energy costs	154 AU$	110.92 AU$	80.54 AU$
	SSR	54%	55%	63%
	WTP ratio	N/A	65%	78%
Coordinator	Total net profits	N/A	197.38 AU$	264.11 AU$
	Payback period	N/A	7.2 years	5.6 years
	Storage usage	N/A	39%	62%

In Table 9-2, the advantages of using battery plus P2G are illustrated from both the perspective of the prosumers and the coordinator. For the prosumers, it can be found that the energy cost of using the battery plus P2G is 80.54 AU$, which is lower than that of using the battery alone. Additionally, the WTP ratio of using the battery plus P2G is 6% higher than only using the battery. From the perspective of the coordinator, it can be found that the total net profits of using the battery plus P2G are higher than only using the battery. Moreover, the ESS efficiency can be enhanced using the battery plus P2G.

TABLE 9-2. RESULT COMPARISON OF USING ONLY THE BATTERY AND USING BOTH THE BATTERY AND THE P2G

		Battery (only electricity is considered)	**Battery+P2G** (both electricity and hydrogen are considered)
Prosumers	Energy costs	108.75 AU$	80.54 AU$
	WTP	72%	78%
Coordinator	Total net profits	207.82 AU$	264.11 AU$
	ESS efficiency	58%	62%

9.7.4 Analysis of the Proposed Pricing Strategy

In Fig. 9-8, the credit points of the prosumers are illustrated. Three clusters of prosumers are classified according to the load pattern of the prosumers via the Density-Based Spatial Clustering of Applications

with Noise (DBSCAN) algorithm [251]. They are double-peak in the morning and afternoon (cluster 1), single-peak in the afternoon (cluster 2), and single-peak in the morning (cluster 3), respectively. For cluster 1, the prosumers are borrowing energy from 4:00 to 10:00 and 16:00 to 20:00, and borrowing capacity from 11:00 to 16:00 on average. For cluster 2, the prosumers are borrowing capacity from 11:00 to 14:00 and borrowing energy from 6:00 to 8:00 and 15:00 to 20:00 on average. Combining the simulation results of the capacity and energy sharing prices in Fig. 9-10, it can be found that although the capacity and energy sharing prices of cluster 2 converge to a relatively low level, the prosumers in cluster 2 are still less engaged in participating in capacity and energy sharing compared with the other two clusters. As for cluster 3, the prosumers borrow energy from 7:00 to 13:00 and borrow capacity from 14:00 to 19:00 on average.

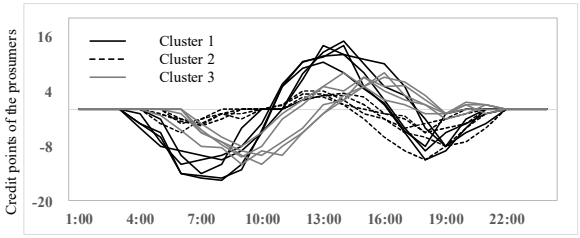

Fig. 9-8. The credit points change of three types of clusters.

Fig. 9-9 shows the load components of prosumers 1, 2, and 3 from clusters 1, 2, and 3, respectively. All three prosumers are willing to use the shared energy to cover their peak load. For prosumers 1 and 2 they prefer hydrogen from P2G from around 6:00 to 13:00 to satisfy the hydrogen need. And they store the excess energy generated from the PV panels into the battery for later use. As for prosumer 3, less hydrogen is borrowed from the P2G compared with the other two prosumers.

In Fig. 9-10, three prosumers are selected from the three clusters to show the customized pricing on capacity and energy sharing. The price above the horizontal axis represents the capacity sharing price, while the price below is the energy sharing price. Prosumer 1 has six price blocks in total, within which there are two peak price blocks: 5:00 to 8:00 for energy sharing and 14:00 to 17:00 for capacity sharing. For prosumer 2, three price blocks are illustrated, and the price variation is not immense. For prosumer 3, four price blocks are shown, with one peak price block for energy sharing from 10:00 to 12:00 and one peak price block for capacity sharing from 14:00 to 16:00.

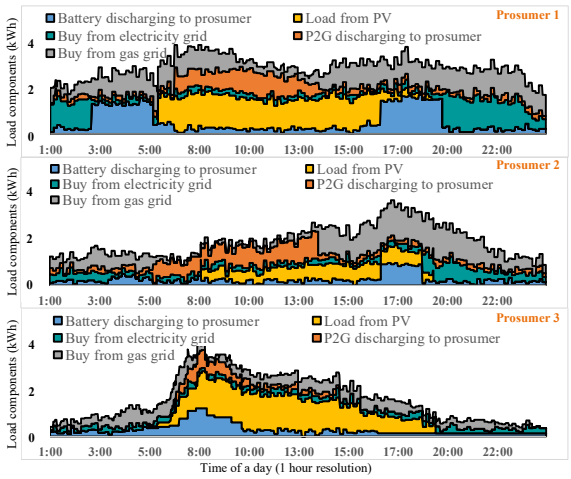

Fig. 9-9. The load components of the three prosumers.

In Table 9-3, the comparisons between using one pricing strategy and using two pricing strategies are illustrated. It can be found that, compared with merely using cost-based pricing for both capacity sharing and energy sharing, using two pricing strategies, i.e., the proposed pricing strategy, can save the energy costs for the prosumers by 17.85 AU$ per day. Additionally, both the SSR and WTP ratios can be increased. For the coordinator, using the proposed pricing strategy can ensure higher total net profits and ESS usage efficiency. Moreover, compared with using the cost-based pricing strategy, the payback period of the proposed strategy can be shortened by 1.2 years.

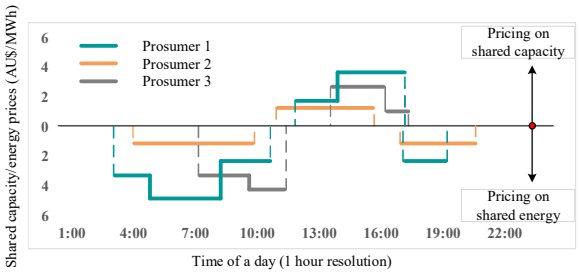

Fig. 9-10. The prices of shared capacity and shared energy.

TABLE 9-3. COMPARISONS BETWEEN USING ONE PRICING STRATEGY AND USING TWO PRICING STRATEGIES

		Cost-based	**Cost-based+demand-based**
Prosumers	Energy costs	98.39 AU$	80.54 AU$
	SSR	58%	63%
	WTP ratio	69%	78%
Coordinator	Total net profits	240.4 AU$	264.11 AU$
	Payback period	6.8 years	5.6 years
	ESS efficiency	57%	62%

9.8 Conclusion

This chapter proposed a two-stage credit-based capacity and energy sharing model to combine both capacity and energy sharing. Two pricing strategies have been proposed to customize the capacity and energy sharing prices to benefit both the coordinator and the prosumers. Simulation results indicate that the proposed credit-based sharing model not only can increase the total net profits and storage usage efficiency of the coordinator but can also enhance the self-sufficiency ratio and the willingness-to-participate ratio of the prosumers. Moreover, both the payback period of the coordinator and the energy costs of the prosumers can be reduced compared with the base case and the conventional model.

10. PICING STRATEGY FOR ENERGY SUPPLEMENT SERVICES OF HYBRID ELECTRIC VEHICLES CONSIDERING BOUNDED-RATIONALITY AND ENERGY SUBSTITUTION EFFECT

Electric vehicles (EVs) have experienced rapid growth in recent years due to the concern about climate change. Meanwhile, hydrogen has become a versatile energy carrier that can be used in the EV industry. Thus, apart from pure EVs, hydrogen fuel cell EVs (FCEVs) and plug-in hybrid hydrogen and electric vehicles (PH2EVs) are also promising solutions for replacing gasoline vehicles. With the penetration of these alternative fuel vehicles, it is necessary to formulate proper strategies to guide EV charging and refueling. Hence, in this chapter, a dynamic pricing strategy for integrated electricity charging and hydrogen refueling stations (IEHSs) is proposed to guide the charging/refueling decisions of EVs and ensure the operation of IEHSs, power distribution network (PDN), and gas network (GN). First, a tri-level dynamic pricing strategy is proposed considering the interactions among EVs, IEHSs, and both PDN and GN. Second, the bounded rationality of EVs in station selection is modeled based on cognitive theory. Third, energy substitution for PH2EVs between electricity charging and hydrogen refueling is analyzed. Simulation results show that the proposed pricing strategy can increase the utility of EVs, enhance the profit of IEHSs, and mitigate the congestion of both PDN and GN.

10.1 Introduction

EVs outweigh gasoline vehicles in terms of energy-saving and environmental protection [128]. In practice, the plug-in electric vehicle (PEV) is a common type of EV powered by electricity that is undergoing dramatic development. However, the proliferation of PEVs might increase queueing length and waiting time even at the fast-charging stations, which can bring about reduced comfort for PEV users. In recent years, hydrogen has become a versatile energy carrier that can be served as an input into a range of industrial processes, including the EV industry [78]. As a result, fuel cell electric vehicle (FCEV) has emerged as another type of EV that is powered by hydrogen. Compared the FCEV with PEV, energy supplement duration is significantly reduced via hydrogen refueling. Thus, the problem of long waiting times can be mitigated. However, FCEV can result in higher energy costs than PEV. Hence, plug-in hybrid hydrogen and electric vehicle (PH2EV), which consumes either electricity or hydrogen, can be served as a new promising type of EV to balance energy supplement duration and energy cost.

Additionally, the penetration of PH2EVs can increase the flexibility and alternatives of energy. However, the random charging pattern of various types of EVs can lead to difficulties in charging/refueling management of IEHSs as well as congestions to the power distribution network (PDN) and gas network (GN) [44]. Thus, it is necessary to develop proper strategies to guide the charging/refueling of EVs.

In the existing literature, the pricing strategy formulated by energy supplement stations is a commonly used approach to manage EV charging/refueling. Research articles mainly formulated the pricing strategy by considering the interests of stations, EVs, and a combination of both. There is literature that focuses on increasing the profit of the station, such as [121-123, 125]. There is also literature paying attention to EV user satisfaction, such as [128-130]. In terms of literature that investigated pricing strategy from the perspective of both stations and EVs, how to balance the competing objectives of profitability enhancement, customer satisfaction assurance, and PDN security is investigated, such as [126, 127].

Therefore, in this chapter, we propose a dynamic pricing strategy for integrated electricity charging and hydrogen refueling stations (IEHSs). Here, IEHSs can provide both electricity charging and hydrogen refueling services. The main contributions of this chapter are threefold.

- First, a tri-level pricing strategy for IEHSs is formulated considering the integration among EVs, IEHSs, and both the PDN and GN. In this pricing strategy, the temporal shift of EVs within one IEHS and the spatial shift of EVs among multiple IEHSs are modeled. With the proposed tri-level pricing mechanism, IEHSs can ensure the charging/refueling services based on the dynamic charging/refueling response of EVs while mitigating the congestion of both the PDN and GN.
- Second, to ensure the effectiveness of the pricing strategy in guiding EV behaviors, the bounded rationality of EVs in station selection is rigorously modeled based on the cognitive hierarchy (CH) theory. To be specific, EVs are categorized into heterogeneous cognitive levels, and the strategic thinking process of EVs that they will make decisions by considering the decisions of other EVs with lower cognitive levels is analyzed.
- Third, the energy substitution effect of PH2EVs when making energy purchasing decisions is mathematically modeled. On the one hand, the optimal energy purchasing mixture of electricity and hydrogen is derived based on the consumer choice theory. On the other hand, the relationship between energy demand and energy price is established based on both the self-price elasticity and

cross-price elasticity.

10.2 the Framework of the Proposed Trilevel Model

The proposed tri-level framework considers the optimization and interaction of three types of participants at three levels, as shown in Fig. 10-1. At the **upper level**, both the PDN and GN will determine the electricity generation $P^{g}_{q,t}$, gas generation $G^{well}_{h,t}$, and the DLMP $\lambda^{PDN}_{q,t}$ and $\lambda^{GN}_{h,t}$ at each electricity and gas bus based on information related to the baseload and the energy demand of EVs from the lower level. At the **middle level**, after receiving the DLMP information from the upper level and the energy purchasing demand of all the EVs from the lower level, IEHSs will make energy pricing decisions $\lambda^{ELE}_{j,t}$ and $\lambda^{H_2}_{j,t}$ for both electricity charging and hydrogen refueling. Apart from optimizing energy price, the queueing information, i.e., the waiting time information $t^{wait}_{j,t}$, will be estimated by the IEHSs. Moreover, the coupon $\mathfrak{C}_{j,t}$ will be offered to attract more EVs during off-peak periods. At the **lower level**, EV users will make station selection $x_{i,j,t}$, routing $f_{\beta^{i}_{rs},i,t}$, and energy purchasing decisions $D^{ELE}_{i,j,t}$ and $D^{H_2}_{i,j,t}$ based on information relating to energy purchasing price, the estimated waiting time, and the offered coupon at IEHSs received from the middle level.

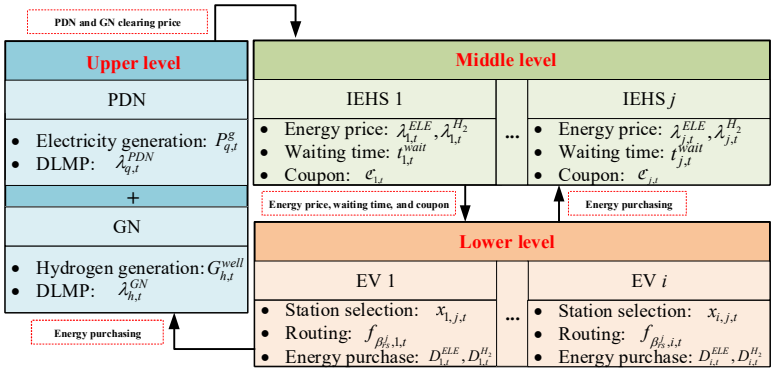

Fig. 10-1. Proposed tri-level framework and information flow.

10.3 Lower Level: EV Decision-making with Bounded Rationality and Energy Substitution

At the **lower level**, the decision-making of EVs is optimized based on information from the middle level. In addition, the bounded rationality of EVs and the energy substitution between electricity charging and hydrogen refueling are investigated.

10.3.1 Preliminaries

EVs will make station selection decisions considering other EVs' decisions to avoid long queues at

stations. However, in practice, EVs usually have bounded rationality (cognitive limits) in making such decisions [252, 253]. Thus, in this chapter, the CH theory is utilized to model the bounded rationality of EVs.

Under the CH theory, EVs can be categorized according to their cognitive levels into an infinite number of levels indexed $k=0,1,...,\infty$. The number of EV users at each level follows a Poisson distribution shown as (10.1) [254, 255].

$$f(k)=e^{-\tau}\tau^{k}/k! \tag{10.1}$$

where τ is the average cognitive level of all the EVs.

To be specific, level 0 EVs will make decisions randomly without considering other EVs' decisions. For a level 1 EV user, she or he will only consider the decision-making of EVs who have lower cognitive levels, i.e., level 0 EVs. In general, for level *k* EV, she or he will make decisions by considering other EVs' decisions that have lower cognitive levels, i.e., level 0 to level *k*-1. Additionally, level *k* EV assumes that he or she is the only person at level *k* [254, 255].

10.3.2 Objective Function

In this chapter, the coupon provided by IEHS *j* is utilized to incentivize EV users with different cognitive levels in station selection decision-making. The total coupon offered by IEHS *j* is fixed at each time and will be evenly shared among EVs. As a result, the more EVs select IEHS *j,* the less coupon will be received by each EV who selects IEHS *j*. Hence, level *k*>0 EV users will make station selection decisions by considering the station selection decisions of lower-level EVs based on the CH theory to maximize their utility [254, 255].

As a result, the objective function of EV user *i* at level *k*>0 can be written as (10.2). In (10.2), the first term is the coupon received by EV user *i* after considering the station selection decision of other EVs who have lower cognitive levels. The second term y_i is the net profit apart from coupons.

$$\arg_{\left\{x_{i,j,t},f_{\beta_{rs}^{j},i,t},D_{i,j,t},D_{i,j,t}^{ELE},D_{i,j,t}^{H_2}\right\}}\max U_i=\sum_{t=1}^{T}\left(x_{i,j,t}\mathfrak{C}_{j,t}\Big/\left(\frac{n_{j,t}}{\mathfrak{F}}\right)\right)+y_i \tag{10.2}$$

where $x_{i,j,t}$ is the binary variable indicating whether EV user *i* will select IEHS *j*; $f_{\beta_{rs}^{j},i,t}$ is the binary variable indicating whether EV user *i* will choose path $\beta_{rs,i}^{j}$ at time *t*; $\beta_{rs,i}^{j}$ is the path EV user *i* travels on that starts from the origin of EV user *i* to IEHS *j*; $D_{i,j,t}$ is the total energy demand of EV user *i* at

time t; $D_{i,j,t}^{ELE}$ and $D_{i,j,t}^{H_2}$ are electricity and hydrogen demand of EV user i at IEHS j at time t; U_i is the utility of EV user i; T is the total time slots with a day; $\mathscr{C}_{j,t}$ is the total coupon offered by IEHS j at time t; $n_{j,t}$ is the number of EVs selecting IEHS j perceived by EV user i; $\mathscr{F}$ is the total fraction of lower-level EVs perceived by EV user i.

Note that the decision-making process based on the CH theory is an iterative and strategic thinking process, whereas (10.2) merely expresses the decision-making process of one EV user at one cognitive level. As a result, **Algorithm 10-1** is elaborated to explain the progressive decision-making process of all EVs.

Algorithm 1: EVs' Decision-making based on the CH Theory

Input: Coupon $\mathscr{C}_{j,t}$; electricity charging price $\lambda_{j,t}^{ELE}$; hydrogen refueling price $\lambda_{j,t}^{H_2}$; estimated waiting time $t_{j,t}^{wait}$; average cognitive level of all the EVs τ; the total number of EVs I; tolerant error ς; set of IEHSs Ω_j.

Compute $x_{i,j,t}, f_{\beta_{ns}^l,i,t}, D_{i,j,t}, D_{i,j,t}^{ELE}, D_{i,j,t}^{H_2}$.

Set $k=\mathscr{F}=n_{j,t}^i=0$; $\omega_{0,j,t}^i=1/|\Omega_j|$.

repeat

$f(k)=e^{-\tau}\tau^k/k!$; $\mathscr{F}=\mathscr{F}+f(k)$; $k=k+1$.

for each $j\in\Omega_j$ **do**

$n_{j,t}^i=n_{j,t}^i+f(k)\times\omega_{k,j,t}^i\times I$.

$\overline{\mathscr{C}_{j,t}}=\left(\mathscr{C}_{j,t}/\left(n_{j,t}^i/\mathscr{F}\right)\right)$.

end for

$U_i=y_i+\sum_{j\in\Omega_j}\sum_{t=1}^{T}x_{i,j,t}\overline{\mathscr{C}_{j,t}}$.

$x_{i,j,t}, f_{\beta_{ns}^l,i,t}, D_{i,j,t}, D_{i,j,t}^{ELE}, D_{i,j,t}^{H_2}=\arg\max U_i$.

---

for each $j \in \Omega_j$ **do**

if $U_i \geq 0$ **then** $\omega_{k,j,t}^{i} = 1 \Big/ \left|\Omega_j\right|$.

else $\omega_{k,j,t}^{i} = 0$.

end for

until $\mathfrak{F} > 1 - \varsigma$

Output: CH equilibrium Solution: $n_{j,t}^{i\ *} = n_{j,t}^{i}$.

Definition: $Pr_{k,j,t}$ is defined as the probability of level *k* EV to select IEHS *j* perceived by level *k*+1 EV. After optimizing the utility function U_i of EV user *i*, the value of $\omega_{k,j,t}$, i.e., the probability that level *k* EV users to select IEHS *j*, can be derived. To be specific, when the utility of EV user *i* (level k+1 EV user) in choosing IEHS *j* is larger than zero, i.e., $U_i \geq 0$, $\forall j \in \Omega_j$, level *k*+1 EV users will assume that level *k* EV users would simply randomize among all the IEHSs when making the station-selection decision. As a result, $\omega_{k,j,t} = 1 \Big/ \left|\Omega_j\right|$. On the contrary, when the utility of EV user *i* is smaller than zero, i.e., $U_i < 0$, level *k*+1 EV users will assume that level *k* EV users would not choose IEHS *j*. Hence, $\omega_{k,j,t} = 0$. To be noted, $\omega_{k,j,t}$ is the station-selection probability of level *k* EV users perceived by level *k*+1 EV users based on the assumption that level *k* EV users would simplify the station-selection problem due to lower cognitive level, which is not the same as the station-selection binary variable $x_{i,j,t}$ of EV user *i* that is optimized based on utility maximization. U_i is the utility of level *k*+1 EV when IEHS *j* is selected, after considering the station selection strategies of level 0 to level *k* EVs.

Initialization: The cognitive level of EVs is initialized as *k*=0, and the total fraction of EVs that is considered by level *k* EV is initialized as $\mathfrak{F}$ =0. Additionally, we initialize the number of EVs selecting IEHS *j* as $n_{j,t}$ =0.

Iteration process: At iteration *k*, the number of level *k* EVs who select IEHS *j* can be computed. Based on the station selection decisions of level 0 to level *k* EVs, level *k*+1 EV can optimize the utility.

a). Utility: The fraction of level *k* EV $f(k)$ and the number of EVs selecting IEHS *j* $n_{j,t}$ are computed. Then, the coupon received by each EV who selects IEHS *j* can be calculated as $C_{j,t} \Big/ \left(n_{j,t} / \mathfrak{F}\right)$.

Next, the decision variables can be optimized to maximize the utility of EV *i* at level *k*+1.

b). Station selection: For level *k*+1 EV, the IEHS that can provide the maximum utility will be selected.

Output: The iterative process continues until $\tilde{\mathcal{F}} > 1-\varsigma$, which indicates that the reasoning of almost all the EVs is considered. Then, the total number of EVs selecting IEHS *j* can be calculated as $n_{j,t}^{*} = n_{j,t}, \forall j \in \Omega_j$. Moreover, the electricity demand $D_{j,t}^{ELE}$ and hydrogen demand $D_{j,t}^{H_2}$ of all the EVs that select IEHS *j* can be derived.

The net profit of EV user *i*, apart from the coupon, is further explained in (10.3). Equation (10.3) shows the purchasing utility, time cost, and energy purchasing cost of EV. Moreover, the relationship between the total amount of energy purchased $D_{i,j,t}$ and purchasing utility can be expressed as (10.4) [256].

$$y_i = \sum_{t=1}^{T} \left[\begin{array}{l} U_{i,t}^{pur} \times Pr_{t\ i}^{u} - \sigma\left(t_{\beta_{rs,i}^{j},i}^{tra} + t_{i,t}^{wait} + t_{i,t}^{sta}\right) - \\ -C_{i,t}^{ELE} - C_{i,t}^{H_2} \end{array} \right] \tag{10.3}$$

$$U_{i,t}^{pur} = \alpha_i \log\left(D_{i,j,t} + 1\right) \tag{10.4}$$

where Pr_t^u is the probability of the utility gained from energy purchasing; σ is the parameter that can transfer time into monetary value; $t_{\beta_{rs,i}^{j},i}^{tra}$ is the traveling time on path $\beta_{rs,i}^{j}$; $t_{i,t}^{wait}$ is the waiting time of EV user *i*; $t_{i,t}^{sta}$ is the charging/refueling time of EV user *i*; $C_{i,t}^{ELE}$ and $C_{i,t}^{H_2}$ are the electricity and hydrogen energy cost of EV user *i* at time *t*; α_i is the coefficient of the purchasing utility function of EV *i*.

The traveling time, waiting time, charging time, and energy purchasing cost are further explained via equations (10.5)-(10.8), respectively. Equation (10.5) shows the traveling time of EV *i* on path $\beta_{rs,i}^{j}$. Equation (10.6) shows that the waiting time of EV user *i* is the same as the waiting time estimated by IEHS *j* $t_{j,t}^{wait}$ only if IEHS *j* is selected by EV user *i*, i.e., when $x_{i,j,t}$ is 1.

$$t_{\beta_{rs,i}^{j},i}^{tra} = l_{\beta_{rs,i}^{j},i} \times f_{\beta_{rs,i}^{j},i,t} \Big/ \bar{v}_i \tag{10.5}$$

$$t_{i,t}^{wait} = t_{j,t}^{wait} \times x_{i,j,t} \tag{10.6}$$

$$t_{i,t}^{sta} = D_{i,j,t}^{ELE} \Big/ P_j^{ELE} \times \eta_j^{ELE} + D_{i,j,t}^{H_2} \Big/ g_j^{H_2} \times \eta_j^{H_2} \tag{10.7}$$

$$C_{i,t}^{ELE} = \lambda_{j,t}^{ELE} \times D_{i,j,t}^{ELE}, C_{i,t}^{H_2} = \lambda_{j,t}^{H_2} \times D_{i,j,t}^{H_2} \tag{10.8}$$

where $l_{\beta_{rs}^j,i}$ is the length of path $\beta_{rs,i}^j$; $\bar{v}_i$ is the average driving velocity of EV *i*; P_j^{ELE} and $g_j^{H_2}$ are the electricity charging rate and hydrogen refueling rate; η_j^{ELE} and $\eta_j^{H_2}$ are the charging and refueling efficiency.

10.3.3 Decision-making Constraints

To further model the decision-making process of the EV users, three types of decisions are explained in detail, namely, the station selection, the routing, and the purchasing decision.

10.3.3.1 Station selection decision constraints

At first, EVs will make a station selection decision. Besides the offered coupon, EV use *i* will take the waiting time into consideration as well when making the station selection decision shown as (10.9). Equation (10.9) indicates that if the estimated waiting time at IEHS *j* is longer than the maximum waiting time EV user *i* can accept, EV user *i* will not choose IEHS *j*. As a result, $x_{i,j,t}$ will be 0. Otherwise, EV user *i* will choose IEHS *j* and $x_{i,j,t}$ will be 1. Equation (10.10) ensures that EV user makes at most one selection decision daily.

$$x_{i,j,t}\left(t_{j,t}^{wait} - t_i^{\max}\right) \le 0 \tag{10.9}$$

$$\sum_{j\in\Omega_j}\sum_{t=1}^{T}\left(x_{i,j,t}\right) \le 1 \tag{10.10}$$

where $t_i^{\max}$ is the maximum waiting time EV user *i* can accept.

10.3.3.2 Routing decision constraints

Once EV user *i* selects IEHS *j*, he or she will encounter another decision on routing selection. When making the navigation decision, the SOC of EV *i* must be able to cover the trip from the origin of EV user *i* to IEHS *j* shown as (10.11). Equation (10.11) shows that if the mileage can support the EV to travel from the origin of EV user *i* to IEHS *j*, EV user *i* will choose path $\beta_{rs,i}^j$. As a result, $f_{\beta_{rs}^j,i,t}$ will be 1. Otherwise, $f_{\beta_{rs}^j,i,t}$ will be 0. As a result, EV user *i* will choose another path. (10.12) indicates that path $\beta_{rs,i}^j$ can only be selected when IEHS *j* is selected by EV user *i*, i.e., when $x_{i,j,t}$ equals 1. As a result, $f_{\beta_{rs}^j,i,t}$ may be 1. On the contrary, if IEHS *j* is not selected by EV user *i*, $x_{i,j,t}$ will be 0 and

$f_{\beta_{rs}^j,i,t}$ will be 0.

$$f_{\beta_{rs}^j,i,t}\left[SOC_{i,t}-\left(E_i^{ev}l_{\beta_{rs}^j,i}/E_i^{\max}\right)\right]\geq 0,\forall\beta_{rs,i}^j\in b^{ev,c} \tag{10.11}$$

$$f_{\beta_{rs}^j,i,t}\leq x_{i,j,t} \tag{10.12}$$

where $SOC_{i,t}$ is the initial SOC of EV i at time t when making the navigation decision; E_i^{ev} is the average energy consumption per km of EV i; $E_i^{\max}$ is the maximum capacity.

10.3.3.3 Purchasing decision constraints

a). Energy substitution for PH2EVs

When arriving at IEHS j, EV users will make energy purchasing decisions. For PH2EVs, there exists an energy substitution effect between electricity charging and hydrogen refueling. To model such an energy substitution effect, we first derive the optimal purchasing mixture of electricity demand and hydrogen demand. Then, the impact of energy price on energy purchasing amount is modeled using self-price and cross-price elasticities.

First, there exists a substitution relationship between the demand for electricity and hydrogen to satisfy the total energy demand, shown as (10.13). The first term represents energy from electricity purchasing, and the second term is energy from hydrogen purchasing. According to consumer choice theory, (10.13) is defined as the *indifference curve* that describes a combination of two goods (i.e., electricity and hydrogen) that give the EV user equal utility, thereby making the EV user indifferent, shown as in Fig. 2 [170, 257].

$$f_i^{EAC}\left(D_{i,j,t}^{ELE}\right)+f_i^{GAC}\left(f_i^{GCC}\left(D_{i,j,t}^{H_2}\right)\right)=D_{i,j,t} \tag{10.13}$$

where f_i^{EAC}, f_i^{GAC}, and f_i^{GCC} are the input-output function of electricity AC, hydrogen AC, and hydrogen CC, respectively.

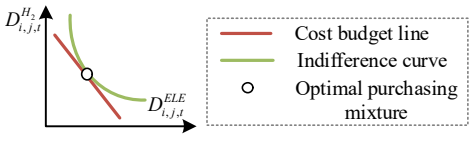

Fig. 10-2. Cost budget line and indifference curve of the PH2EV user.

Moreover, the concept of *cost budget line* is introduced to balance energy purchasing cost and the charging/refueling time cost of EV users when making the energy purchasing decisions shown as (10.14) and Fig. 10-2.

$$\lambda_{j,t}^{ELE} \times D_{i,j,t}^{ELE} + \lambda_{j,t}^{H_2} \times D_{i,j,t}^{H_2} + \sigma \times t_{i,t}^{sta} = \mathfrak{B}_{i,t} \tag{10.14}$$

where $\mathfrak{B}_{i,t}$ is the cost budget of EV user *i*, including both energy purchasing cost and charging/refueling time cost.

We further model the energy substitution of the PH2EVs to determine the *optimal purchasing mixture* of input energy that balances the purchasing cost and charging/refueling time cost.

According to the consumer choice theory, the optimal combination of two goods can be found at the tangent point of the indifference curve and the cost budget line, shown in Fig. 2 [170]. Hence, we need to find the slope of both curves. For the slope of the cost budget line of the PH2EVs, it is $-\left[\lambda_{j,t}^{ELE} + \left(\sigma / P_j^{ELE} \eta_j^{ELE}\right)\right] / \left[\lambda_{j,t}^{H_2} + \left(\sigma / g_j^{H_2} \eta_j^{H_2}\right)\right]$. And the slope of the indifference curve is:

$$\frac{dD_{i,j,t}^{H_2}}{dD_{i,j,t}^{ELE}} = -\frac{f_i^{EAC'}\left(D_{i,j,t}^{ELE}\right)}{f_i^{GAC'}\left(f_i^{GCC}\left(D_{i,j,t}^{H_2}\right)\right) \cdot f_i^{GCC'}\left(D_{i,j,t}^{H_2}\right)} \tag{10.15}$$

Then, let the slope of the cost budget line equal to the slope of the indifference curve, we have (10.16):

$$\frac{\lambda_{j,t}^{ELE} + \left(\sigma / P_j^{ELE} \eta_j^{ELE}\right)}{\lambda_{j,t}^{H_2} + \left(\sigma / g_j^{H_2} \eta_j^{H_2}\right)} = \frac{f_i^{EAC'}\left(D_{i,j,t}^{ELE}\right)}{f_i^{GAC'}\left(f_i^{GCC}\left(D_{i,j,t}^{H_2}\right)\right) \cdot f_i^{GCC'}\left(D_{i,j,t}^{H_2}\right)} \tag{10.16}$$

In this chapter, it is assumed that the conversion function of hydrogen follows $D_{i,j,t}^{H_2} = a_1 \times \left(D_{i,j,t}^{out}\right)^2$, where a_1 is the conversion coefficients. Additionally, η_i^{EAC} and η_i^{GAC} are the electricity AC and hydrogen AC conversion efficiency of EV user *i*. Thus, by plugging in the conversion efficiency and conversion function to (10.13), we have:

$$\eta_i^{EAC} \times D_{i,j,t}^{ELE} + \eta_i^{GAC} \times \sqrt{D_{i,j,t}^{H_2} / a_1} = D_{i,j,t} \tag{10.17}$$

Then, combining both equations (10.16) and (10.17), the optimal purchasing mixture of electricity and hydrogen for the PH2EV can be obtained, shown as (10.18). It can be found that an increase in electricity price and refueling rate (or a reduction in hydrogen price and charging rate) will increase the hydrogen demand.

$$\frac{\lambda_{j,t}^{ELE} + \left(\sigma / P_j^{ELE} \eta_j^{ELE}\right)}{\lambda_{j,t}^{H_2} + \left(\sigma / g_j^{H_2} \eta_j^{H_2}\right)} = \frac{2\eta_i^{EAC} \sqrt{a_1 \cdot D_{i,j,t}^{H_2}}}{\eta_i^{GAC}} \tag{10.18}$$

Second, the relationship between energy price and energy demand is modeled using both self-price elasticity and cross-price elasticity, shown as (10.19)-(10.20). Here, self-price elasticity measures the

responsiveness of demand for one type of energy towards the energy price of the same type of energy. For cross-price elasticity, it analyzes the responsiveness between one type of energy price and the demand for another type of energy[71, 258].

$$\lambda_{j,t}^{ELE} = \alpha^{ELE} - \beta_{i,t}^{E} \times D_{i,j,t}^{ELE} - \varepsilon_{i,t}^{H-E} \times D_{i,j,t}^{H_2}, \varepsilon_{i,t}^{H-E} > 0 \tag{10.19}$$

$$\lambda_{j,t}^{H_2} = \alpha^{H_2} - \beta_{i,t}^{H} \times D_{i,j,t}^{H_2} - \varepsilon_{i,t}^{E-H} \times D_{i,j,t}^{ELE}, \varepsilon_{i,t}^{E-H} > 0 \tag{10.20}$$

where α^{ELE} and α^{H_2} are the highest historical energy price for electricity charging and hydrogen refueling, respectively; $\beta_{i,t}^{E}$ and $\beta_{i,t}^{H}$ are the self-price elasticity on electricity charging and hydrogen refueling, respectively; $\varepsilon_{i,t}^{H-E}$ is the cross-price elasticity of EV *i* which measures the impact of electricity price on hydrogen refueling; $\varepsilon_{i,t}^{E-H}$ is the cross-price elasticity of EV *i* which measures the impact of hydrogen price on electricity charging.

b). General constraints for all types of EVs

Equations (10.21)-(10.23) further constraint the total energy demand of any type of EVs. Equation (10.21) shows that the total energy demand of EV user *i* should be no larger than the sum of the remaining EV capacity and the traveling consumption. Equation (10.22) indicates that only when IEHS *j* is selected by EV user *i*, i.e., $x_{i,j,t}$ equals 1, can EV user *i* decide the amount of electricity and hydrogen to purchase from IEHS *j*. Equation (10.23) shows the total daily energy demand plus the initial energy storage state should be larger than the traveling consumption plus the required energy storage remaining amount.

$$D_{i,j,t} \le E_i^{\max} - E_{i,0} + E_i^{ev} \times l_{\beta_{rs}^j,i} \times f_{\beta_{rs}^j,i,t} \tag{10.21}$$

$$D_{i,j,t} \le x_{i,j,t} \times D^{\max} \tag{10.22}$$

$$\sum_{j \in \Omega_j} \sum_{t=1}^{T} \left(D_{i,j,t} \right) \ge E_i^{ev} \times l_{\beta_{rs}^j,i} \times f_{\beta_{rs}^j,i,t} + E_{i,T} - E_{i,0} \tag{10.23}$$

where $D^{\max}$ is the maximum energy demand; $E_{i,0}$ is the initial energy storage state of EV user *i*; $E_{i,T}$ is the required end-of-day energy storage state.

10.4 Middle Level: IEHS Pricing Strategy

At the **middle level**, IEHS *j* will decide the energy price for electricity charging and hydrogen refueling based on information received from EV users at the lower level and the PDN and GN at the upper level.

Besides determining the pricing strategy, information relating to the waiting time at IEHS j will be estimated and passed down to EV users at the lower level to facilitate EV users in station selection and energy purchasing. Furthermore, the coupon is utilized to incentivize EV users in station selection and enhance the profit of the IEHS.

10.4.1 Objective Function and Constraints

The objective function of IEHS j can be referred to (10.24), which includes five parts: the charging revenue R^{cha}, energy purchasing cost C^{pc}, operational costs C^{oper}, fixed costs C^{fix}, and the coupon $\mathcal{C}_{j,t}$.

$$\arg_{\left\{\lambda_{j,t}^{ELE},\lambda_{j,t}^{H_2}\right\}} \max U_j = R_j^{cha} - C_j^{pc} - C_j^{oper} - C_j^{fix} - \mathcal{C}_{j,t} \tag{10.24}$$

s.t.

$$R_j^{cha} = \sum_{t=1}^{T}\left(\lambda_{j,t}^{ELE} \times D_{j,t}^{ELE}\right) + \sum_{t=1}^{T}\left(\lambda_{j,t}^{H_2} \times D_{j,t}^{H_2}\right) \tag{10.25}$$

$$C_j^{pc} = \sum_{t=1}^{T}\left(x_{jq} \times \lambda_{q,t}^{PDN} \times D_{j,t}^{ELE}\right) + \sum_{t=1}^{T}\left(x_{jh} \times \lambda_{h,t}^{GN} \times D_{j,t}^{H_2}\right) \tag{10.26}$$

$$C_j^{oper} = \lambda_j^{oper} \times \sum\nolimits_{i\in\Omega_j} D_{i,j,t} \tag{10.27}$$

$$\mathcal{C}_{j,t} = \gamma \Big/ \sum\nolimits_{i\in\Omega_j} x_{i,j,t} \tag{10.28}$$

where U_j is the utility of IEHS j; x_{jq} and x_{jh} are the binary parameter indicating whether IEHS j is coupled with electricity bus q or gas bus h; γ is the coupon transfer factor.

10.4.2 Queueing Information Estimation

The waiting time at the IEHS can be calculated based on the queuing model, shown as (10.29) [225]. Additionally, the average arrival rate $\varepsilon_{j,t}$ and average charging/refueling rate $\mu_{j,t}$ can be calculated, shown as (10.32) [225]. For (10.32), the number of EVs arriving at time t $n_{j,t}^{arri}$ can be obtained via the infrared sensor installed at the entry of the IEHS. And the number of EVs being charged/refueled at time t $n_{j,t}^{serv}$ can be obtained via the charging/refueling plugs [225].

$$t_{j,t}^{wait} = l_{j,t} \Big/ \varepsilon_{j,t} \tag{10.29}$$

where

$$l_{j,t} = \frac{\left(\varepsilon_{j,t}/\mu_{j,t}\right)^{s_j} \times \left(\varepsilon_{j,t}/\mu_{j,t}s_j\right)}{s_j!\left[1-\left(\varepsilon_{j,t}/\mu_{j,t}s_j\right)\right]^2} \times Pr_{0,j,t} \tag{10.30}$$

$$Pr_{0,j,t}=\left[\sum_{k_j=0}^{s_j-1}\frac{1}{k_j!}\left(\frac{\varepsilon_{j,t}}{\mu_{j,t}}\right)^{k_j}+\frac{1}{s_j!}\frac{\mu_{j,t}}{\mu_{j,t}-\varepsilon_{j,t}}\left(\frac{\varepsilon_{j,t}}{\mu_{j,t}}\right)^{s_j}\right]^{-1} \tag{10.31}$$

$$\varepsilon_{j,t}=\left(n_{j,t-1}^{arri}+n_{j,t}^{arri}\right)\Big/2\Delta t,\mu_{j,t}=\left(n_{j,t-1}^{serv}+n_{j,t}^{serv}\right)\Big/2\Delta t \tag{10.32}$$

where $l_{j,t}$ is the queueing length at IEHS j at time t; s_j is the total number of physical charging/refueling plugs at IEHS j; $Pr_{0,j,t}$ is the probability that all charging/refueling plugs are standing by at IEHS j; k_j is the number of charging/refueling plugs that is standing by.

10.5 Upper Level: PDN and GN Modeling

At the **upper level**, the PDN and GN will determine the market-clearing price DLMP based on both the baseload and the aggregated EV energy demand from the lower level. Additionally, the electricity and hydrogen generation will be determined as well.

10.5.1 Objective Function

The objective function of PDN and GN is to optimize the power and hydrogen generation and DLMP to minimize the total operation cost, shown as (10.33). Note that the dual variables $\lambda_{q,t}^{PDN}$ and $\lambda_{h,t}^{GN}$ of power balance constraint (10.34) and gas flow balance constraint (10.40) are the electricity and hydrogen DLMP at bus q and bus h, respectively, which can be obtained by solvers like Gurobi [121].

$$\begin{aligned}&\arg_{\left\{P_{q,t}^{g},G_{h,t}^{well},\lambda_{q,t}^{PDN},\lambda_{h,t}^{GN}\right\}}\min U^{grid}=\lambda_t^{ELE,BG}\sum\nolimits_{d\in\Omega_d}P_{d,t}^{ELE}+\\&\sum\nolimits_{q\in\Omega_q}\left[a_q\left(P_{q,t}^{g}\right)^2+b_qP_{q,t}^{g}+c_q\right]+\lambda_t^{H_2,BG}\sum\nolimits_{d\in\Omega_d}G_{d,t}^{H_2}+\\&\sum\nolimits_{h\in\Omega_h}\left[a_h\left(G_{h,t}^{well}\right)^2+b_hG_{h,t}^{well}+c_h\right]\end{aligned} \tag{10.33}$$

where U^{grid} is the utility of both PDN and GN; $P_{q,t}^{g}$ is the active power generated at bus q; $P_{d,t}^{ELE}$ is the electricity purchasing amount at upper grid d at time t; Ω_d is the set of upper grids; Ω_q and Ω_h are the PDN and GN bus sets; $G_{h,t}^{well}$ is the gas generation from the gas well at time t; $G_{d,t}^{H_2}$ is the hydrogen purchasing amount at upper grid d at time t; $\lambda_t^{ELE,BG}$ and $\lambda_t^{H_2,BG}$ are the upper grid market-clearing price of electricity and hydrogen; a_q, b_q, c_q, and a_h, b_h, c_h are the generation cost coefficients of the PDN and the GN.

10.5.2 Power Network Constraints

Equations (10.34) and (10.35) shows the active and reactive power balances at each bus. Equation

(10.36) shows the voltage drop/rise on each line. Equation (10.37) shows the relationship between the power flow, squared bus voltage magnitude, and the squared line current magnitude, which is non-convex.

$$P_{pq,t} + P^{g}_{q,t} - r_{pq} \times i_{pq,t} = \sum\nolimits_{k\in\Omega_k} P_{qk,t} + P^{ev}_{q,t} + P^{L}_{q,t} : \lambda^{PDN}_{q,t} \tag{10.34}$$

$$Q_{pq,t} + Q^{g}_{q,t} - x_{pq} \times i_{pq,t} = \sum\nolimits_{k\in\Omega_k} Q_{qk,t} \tag{10.35}$$

$$V^2_{q,t} - V^2_{p,t} = 2\left(r_{pq}P_{pq,t} + x_{pq}Q_{pq,t}\right) - \left(r^2_{pq} + x^2_{pq}\right) i_{pq,t} \tag{10.36}$$

$$i_{pq,t} = \left(P^2_{pq,t} + Q^2_{pq,t}\right) \Big/ V^2_{q,t} \tag{10.37}$$

$$\underline{V_q} \le V_{q,t} \le \overline{V_q} \tag{10.38}$$

$$\sqrt{P^2_{pq,t} + Q^2_{pq,t}} \le \overline{S_{pq}} \tag{10.39}$$

where $P_{pq,t}$ ($Q_{pq,t}$) is the active (reactive) power flow from bus p to bus q; $Q^{g}_{q,t}$ is the reactive power generated at bus q; r_{pq} (x_{pq}) is the resistance (reactance) from bus p to bus q; $i_{pq,t}$ is the squared current magnitude on the distribution line pq; $V_{q,t}$ is the nodal voltage; $P_{qk,t}$ ($Q_{qk,t}$) is the active (reactive) power flow from bus q to bus k; $P^{ev}_{q,t}$ is the electricity demand of EVs at bus q; $P^{L}_{q,t}$ is the electricity baseload demand; $\overline{(\bullet)}$ and $\underline{(\bullet)}$ are the upward and downward limits.

10.5.3 Gas Network Constraints

Equation (10.40) shows the flow balance equation that the gas flowing into bus h equals the overall gas flowing out of bus h. Equation (10.41) shows the gas flow of the pipeline, which can be expressed by the Weymouth flow equation[54, 249]. Equation (10.43) is the gas consumption of the compressor [243].

$$\begin{aligned} &G^{well}_{h,t} + \sum\nolimits_{g\in\Omega_g} F^{pipe}_{gh,t} - \sum\nolimits_{g\in\Omega_g} G^{comp}_{gh,t} \cdot \eta^{comp}_{gh} = \\ &\sum\nolimits_{n\in\Omega_n} F^{pipe}_{hn,t} + G^{ev}_{h,t} + G^{L}_{h,t} : \lambda^{GN}_{h,t} \end{aligned} \tag{10.40}$$

$$F^{pipe}_{gh,t} = \operatorname{sgn}\left(\rho_{g,t}, \rho_{h,t}\right) \times \Psi_{gh} \times \sqrt{\left|\rho_{g,t}{}^2 - \rho_{h,t}{}^2\right|} \tag{10.41}$$

$$\operatorname{sgn}\left(\rho_{g,t}, \rho_{h,t}\right) = \begin{cases} 1; & if\ \rho_{g,t} \ge \rho_{h,t} \\ -1; & if\ \rho_{g,t} < \rho_{h,t} \end{cases} \tag{10.42}$$

$$G^{comp}_{gh,t} = \zeta^3_{gh} + \zeta^2_{gh} \times H_{gh,t} + \zeta^1_{gh} \times \left(H_{gh,t}\right)^2 \tag{10.43}$$

where $F^{pipe}_{gh,t}$ is the gas flow from pipelines g to h; $F^{pipe}_{hn,t}$ is the gas flow from pipelines h to n; $G^{comp}_{gh,t}$

is the gas consumption of the compressor; $G_{h,t}^{ev}$ is the gas demand of EVs at bus h; $G_{h,t}^{L}$ is the gas baseload; $\mathrm{sgn}\left(\rho_{g,t},\rho_{h,t}\right)$ denotes the gas flow direction; $\rho_{g,t}$ and $\rho_{h,t}$ are the gas pressure at bus g and bus h; Ψ_{gh} is the pipeline constant; $H_{gh,t}$ is the horsepower consumption of the compressor station; ζ_{gh}^{1}, ζ_{gh}^{2}, and ζ_{gh}^{3} are the conversion factors between the horsepower consumption and the gas consumption.

10.6 Case Study

10.6.1 Experiment Setting

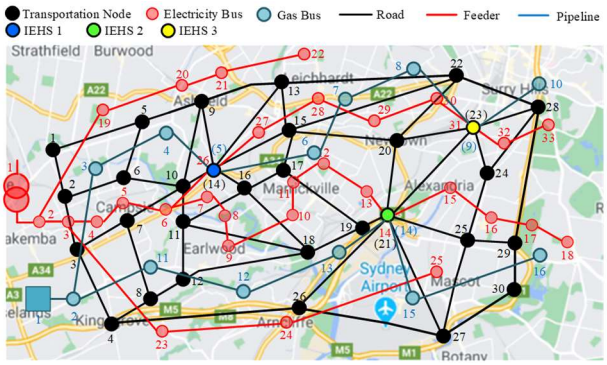

Fig. 10-3. A coupled power distribution, gas, and transportation networks.

The proposed dynamic pricing strategy is verified in the IEEE 33-bus power distribution system coupled with the 16-bus gas network and the 30-node transportation system, shown in Fig. 10-3. In this diagram, the traffic network is simplified from an actual district in Sydney, Australia, which includes 30 nodes and 53 arterial roads. The power distribution system has one 110kV substation. The coupling points are three IEHSs, namely IEHS 1 at electricity bus 26 (node 14 or gas bus 5), IEHS 2 at electricity bus 14 (node 21 or gas bus 14), and IEHS 3 at electricity bus 31 (node 23 or gas bus 9) [228].

10.6.2 Simulation Results

Three case studies are carried out to prove the effectiveness of the proposed pricing strategy.

Case 1 Fixed pricing strategy for IEHS without considering energy substitution, under the assumption of 100% EV rationality.

Case 2 Dynamic pricing strategy for IEHS without considering energy substitution, under the assumption of 100% EV rationality [121].

Case 3 Dynamic pricing strategy for IEHS considering energy substitution, under the assumption of 100% EV rationality [258].

Case 4 Proposed tri-level pricing strategy for IEHSs considering energy substitution and EV user bounded rationality in decision making.

10.6.2.1 Middle level: simulation results for IEHSs

Figs. 10-4 to 10-7 show the energy price at the three IEHSs under cases 1-4, respectively. For case 1 in Fig. 10-4, the electricity charging price of the three IEHSs is fixed, and it is the highest compared with the other three cases. For case 2 in Fig. 10-5, the dynamic electricity charging price is low during off-peak periods, i.e., in both morning and evening. For cases 3 and 4, both electricity charging and hydrogen refueling price are illustrated in Figs. 10-6 and 10-7 because energy substitution is considered. Moreover, comparing case 4 with case 3, the energy price during the off-peak periods is lower. This is because IEHSs under case 4 offer a coupon to incentivize EV users to make station selection decisions during those periods.

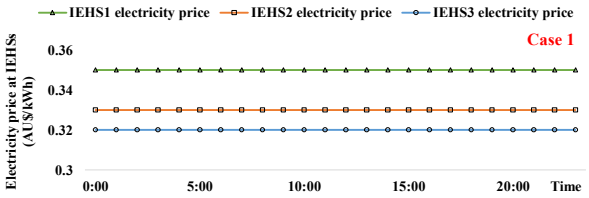

Fig. 10-4. Electricity charging price of three IEHSs under case 1.

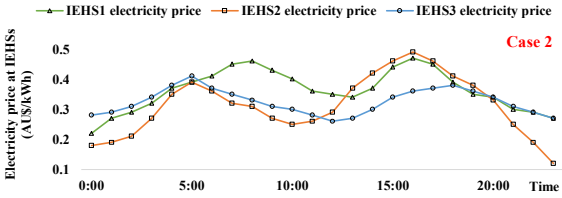

Fig. 10-5. Electricity charging price of three IEHSs under case 2.

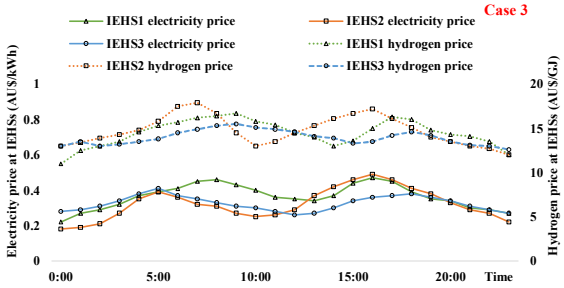

Fig. 10-6. Electricity and hydrogen price of three IEHSs under case 3.

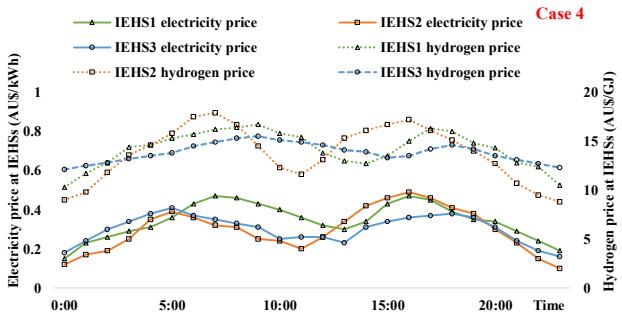

Fig. 10-7. Electricity and hydrogen price of three IEHSs under case 4.

TABLE 10-1. CASE COMPARISONS FROM THE PERSPECTIVE OF IEHSS

Criteria	Detailed items	Case 1	Case 2	Case 3	Case 4
Attractiveness	Average demand (kWh)	430	759	988	1,187
Profitability	Average revenue (AU$)	142	235	264	305
	Average cost (AU$)	89	127	139	151
	Average profit (AU$)	53	108	125	154

In Table 10-1, four cases are compared from two aspects of criteria, i.e., *attractiveness* and *profitability*, to verify the effectiveness of the proposed pricing strategy. For *attractiveness*, the more demand is serviced by the IEHS, the more attractive the station will be. It can be found that IEHSs under case 4 are the most attractive for EV users because it has the highest average demand at 1,187 kWh per day compared with the other three cases. For *profitability*, it can be found that although the average cost of case 4 is the highest at 151 AU$, the average revenue for providing services to EV users is the highest at 305 AU$. Hence, case 4 has the highest average profit at 154 AU$.

10.6.2.2 Lower level: simulation results for EVs

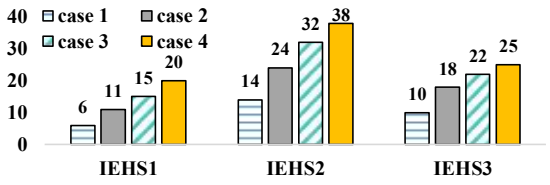

Fig. 10-8. Aggregated station selection choice at three IEHSs.

Fig. 10-8 shows the aggregated daily station selection choice at three IEHSs. It can be found that case 1 results in the lowest daily penetration of EVs. For cases 2 and 3, more EVs select the three IEHSs compared with case 1 because the dynamic pricing strategy takes the responsiveness of EV demand into consideration. As a result, when the demand is low, a lower price will be charged to attract more EV demand, and vice versa. However, case 3 can attract more EVs because less service time at IEHSs will

occur due to the availability of energy substitution between electricity charging and hydrogen refueling. For case 4, the number of EVs that select the three IEHSs is the highest. This is because a coupon is utilized to further incentivize more EVs to select IEHSs during off-peak periods.

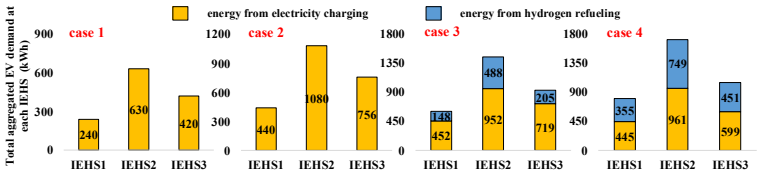

Fig. 10-9. Aggregated energy purchasing amount at three IEHSs.

Fig. 10-9 shows the aggregated energy purchasing amount of EV users at the three IEHSs, consisting of energy from electricity charging and hydrogen refueling. In cases 1 and 2, no energy substitution is considered. Hence, only electricity is purchased by EV users. Compared case 2 with case 1, the electricity demand for the three IEHSs is higher. As for cases 3 and 4, energy substitution between electricity charging and hydrogen refueling is incorporated. Compared case 4 with case 3, total demand is higher for the three IEHSs. Moreover, the proportion of energy from hydrogen refueling is larger. This is because EV users will make an energy purchasing decision considering the balance between energy cost and charging/refueling time cost under case 4. Hence, the proportion of energy from hydrogen refueling is increased to reduce the charging duration.

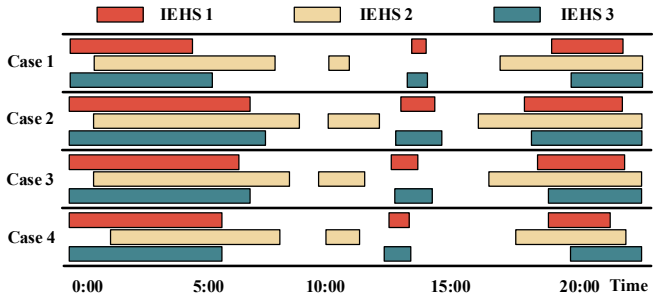

Fig. 10-10. Aggregated service time at three IEHSs.

Fig. 10-10 shows the aggregated service time of EVs at the three IEHSs under the four cases. The aggregated service time for the three IEHSs mainly covers the early morning and evening period as well as at around 12:00 pm. It can be found that the three IEHSs under case 1 have a shorter service time than case 2 because more energy demand is serviced under case 2. For case 3, the aggregated service time is reduced compared with case 2. This is because energy substitution is considered. Hence, EV users can substitute hydrogen with electricity to reduce service time. As an improvement, the aggregated service time is further reduced under case 4.

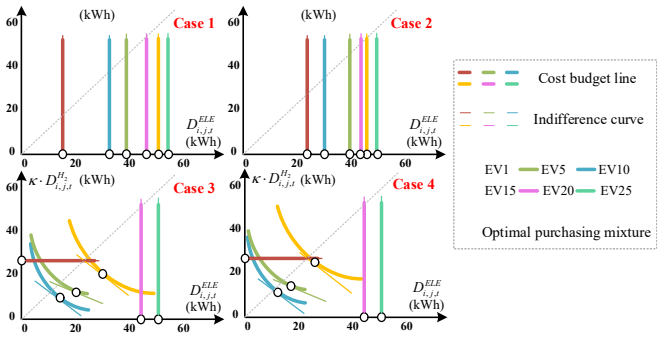

Fig. 10-11. Optimal purchasing decisions of 6 EV users under the four cases.

In Fig. 10-11, the optimal energy purchasing decisions of 6 chosen EV users that select the three IEHSs under the four cases are illustrated. Note that κ is used to transform the unit of hydrogen, i.e., GJ, into the kWh. In cases 1 and 2, no energy substitution is considered. Hence, EVs only purchase electricity. Note that the electricity demand of EVs in case 1 is more dispersed than that of case 2. This is because the dynamic pricing strategy utilized in case 2 can better smooth the energy demand than the fixed pricing strategy used in case 1. For cases 3 and 4, energy substitution is considered. Hence, a mixture of energy is purchased. It can be found that the proportion of energy from hydrogen purchasing of EVs 5, 10, and 15 in case 4 is higher than that of case 3, which is verified by the optimal purchasing mixtures of the three EVs. This is because EV users balance the energy cost and the time cost when making the energy purchasing decision under case 4. Hence, a larger proportion of energy from hydrogen is evidenced.

TABLE 10-2. CASE COMPARISONS FROM THE PERSPECTIVE OF EVS

	Case 1	Case 2	Case 3	Case 4
Average energy cost (AU$)	12.8	11.4	12.2	11.7
Average traveling time (hr/veh)	0.50	0.50	0.45	0.45
Average waiting time (hr/veh)	0.32	0.25	0.18	0.19
Average service time (hr/veh)	0.33	0.26	0.20	0.15
Average utility (AU$)	12.5	20.7	24.5	33.8

Table 10-2 shows the average energy costs, average time (traveling, waiting, and service), and average utility of all the EV users under four cases. It can be found that case 4 has the second-lowest average energy cost at 11.7 AU$. Comparing cases 3 and 4 with cases 1 and 2, the waiting time and service time are reduced due to energy substitution. Among them, case 4 has the least average service time because EV users under case 4 have considered not only energy cost but also charging/refueling time cost when making the energy purchasing decision. Hence, the proportion of hydrogen purchasing is increased to reduce the service duration. Furthermore, the average utility of EV users under case 4 is the highest at 33.8 AU$.

10.6.2.3 Upper level: simulation results for the grid

TABLE 10-3. CASE COMPARISONS FROM THE PERSPECTIVE OF PDN AND GN

		Case 1	Case 2	Case 3	Case 4
PDN	**PDN loss cost (AU$)**	281	274	256	239
	Minimum voltage (p.u.)	0.9445	0.9532	0.9554	0.9593

In table 10-3, the impact of the pricing on the PDN is analyzed from two aspects, i.e., PDN loss cost and downward voltage violation. It can be found that case 4 has the lowest PDN loss cost at 239 AU$ with a minimum voltage of 0.9593 p.u. This is because the proposed pricing strategy can smooth the load at IEHSs. Hence, the problem of downward voltage violation is avoided, and the PDN congestion is mitigated.

10.7 Conclusions

The stochastic charging/refueling behaviors of EVs can result in operational challenges to IEHSs and both PDN And GN. Hence, in this chapter, we propose a tri-level dynamic pricing strategy for IEHSs to guide EV behaviors. First, a tri-level pricing strategy is formulated by incorporating the interaction among EVs at the lower level, IEHSs at the middle level, and both PDN and GN at the upper level. Second, the cognitive theory is applied to model the bounded rationality of EVs in station selection, in which EVs will make station selection decisions considering other EVs' decisions. Third, energy substitution of the PH2EVs is investigated. Simulation results indicate that the proposed pricing strategy can increase the utility of EVs, enhance the profit of IEHSs, and mitigate congestion of both PDN and GN. In the next chapter, the overall work will be summarized, and future research topics/opportunities will be described as well.

11. CONCLUSION AND FUTURE WORK

In recent years, the energy market has developed with uttermost rapidity in terms of two aspects. First, the penetration of renewable generations has gradually replaced parts of the traditional ways to generate energy, such as fossil fuel generation. However, the intermittent and unstable nature of renewable generation can lead to energy supply uncertainty, which might exacerbate the imbalance between energy supply and demand. Second, with the introduction of DERs, new categories of markets besides traditional wholesale and retail markets are emerging, including the energy sharing market, renewable energy trading market, P2P trading, etc. However, market participants might encounter various types of uncertainties, including DER supply uncertainty, end-user behavior uncertainty, wholesale market price uncertainty, etc. Hence, we propose risk hedging strategies that can be used to guide various market participants in new categories of markets to hedge risks and enhance utilities. The major contributions can be summarized as follows:

- First, the rigorous mathematical models of profits in three types of markets are presented for the gas generator, namely, the spot market, the ancillary market, and the financial market. In this model, the revenues and costs have been calculated to derive the relative investment weights among the three markets. Within the financial market, two types of options are utilized and accommodated to the operation mechanism of the gas generator. Both the financial and physical tools have to be considered to hedge the risks of the gas generator. As for the physical tools, P2G has been chosen due to its promising future application. Within both the ancillary market and the spot market, a comprehensive bidding process is also examined. Within the bidding process, the probability of succeeding in a bid is figured out via a data-driven method that enables deep learning of the previous bidding strategies. Moreover, a novel investment decision strategy among the three markets based on the portfolio model has been proposed. By considering the budget limitations of the gas generator, portfolio theory has to be applied to determine the optimal weight of the three markets and the optimal weight of short put and short call options within the financial market. By plotting the minimum variance frontier, the efficient frontier can be found [151]. Then the utility curve will be used to tangent the efficient frontier. It can serve as a reliable method for asset management for the gas generator that participates in the spot, the ancillary, and the financial market.
- Second, a rigorous risk-hedging model based on insurance is proposed for the retailer to hedge the

risks at the transmission level. The conventional risk hedging insurance lacked the consideration of the risk preference of the retailer on the total loss value caused by EEs [117]. As a result, the insurance purchased will be ineffective and undesirable for the retailer. By contrast, in this chapter, an economic adjusting index is introduced to represent the different risk aversion levels of the retailer toward the low probability but high loss events, i.e., the EEs. The larger the adjusting index is, the more risk-averse the retailer is. As a result, the larger the loss value caused by the EEs is. Therefore, the retailer is more willing to pay for the insurance premium to get a higher chance of receiving monetary compensation from the insurance, and vice versa. Furthermore, a risk management strategy based on the strangle weather derivatives and ESS is designed for the retailer to hedge the risks at the distribution level. The traditional risk hedging tools like options and forward contracts relied heavily on the forecast of the electricity prices, such as [36, 37, 118]. However, the increasing penetration of DERs will further amplify the fluctuation of demands and prices, which will increase the forecast difficulty. By using the proposed strangle weather derivative and the ESS, the reliance on the prediction of the prices is avoided.

- Third, a rigorous option-based DR mechanism based on both call and put options are implemented to shift the consumption patterns of the EV users managed by the EVA to mitigate demand-supply imbalance. For the call option, it is designed for the retailer to reduce peak demand when the energy supply is smaller than demand by compelling the EVA to discharge a certain amount of electricity. For the put option, it is designed for the retailer to increase demand when the energy supply is higher than the demand by compelling the EVA to charge a certain amount of electricity.
- Fourth, DNO and the DR aggregator belonging to different agents can cooperate to realize the real-time price-based DR with operating envelope via limited exchanges of representative information. Therefore, the DR aggregator can choose a preferable usage profile within the operating envelope, which provides more initiatives to the DR aggregator. The improvement of the DR scheduling structure to coordinate the DR aggregator and DNO is of great practical significance. With the proposed framework, the DR aggregator is not required to obtain unauthorized data at a higher level, and less communication burden will be brought to the cyber-physical network. Since less information exchange is required, data security problems will be unlikely to occur.
- Fifth, a dynamic pricing strategy, considering the competition relationship between EVCSs, is

proposed based on a coupled PDN and TN to maximize the net charging profit of the EVCS. Under this pricing strategy, more charging demand can be attracted. Additionally, the proposed pricing strategy can achieve spatial load shifting by incentivizing EV users to alter their station-selection decision to avoid congestion of the electricity network. Moreover, a two-step approach is proposed to quantitatively formulate the total charging demand responsiveness towards the charging price based on the optimally assigned traffic flow. With this approach, the balance between the charging price, total charging demand, and the queueing length can be obtained.

- Sixth, a two-stage pricing model for energy storage sharing coordinator has been presented based on the clustering of different load patterns. In the proposed model, the price structure and the price level for capacity sharing are jointly optimized. Novel concepts of bulk capacity borrowing and discount sensitivity are introduced to model individualized pricing for the first time. Bulk capacity borrowing and discount sensitivity are utilized to incentivize more prosumers to participate in the capacity sharing process and enhance the sharing profits of the coordinator. In addition, a new business mode is formulated to determine a more reasonable payment rule for energy storage sharing. Traditionally, prosumers who are engaged in energy storage sharing will be charged according to the net discharging at a specific time. However, in our chapter, the concept of the capacity borrowing state is introduced, which can better reveal the essence of the sharing economy. That means the payment rule is closely related to the time length of borrowing.
- Seventh, a novel business model of credit-based sharing has been proposed to integrate both capacity sharing and energy sharing. The time accumulation effect has been considered via the proposed credit points, which can better reveal the essence of the sharing economy. Additionally, the payment rule is closely related to the time length and amount of the shared capacity and the shared energy that the prosumers borrow. When the credit is positive, the prosumers are borrowing the capacity of the ESS managed by the coordinator; when the credit is negative, the prosumers are borrowing the energy from the ESS either in the form of electricity or hydrogen. Moreover, two pricing strategies have been proposed to increase the total net profits of the coordinator and the willingness of the prosumers to participate in the sharing process. Customized pricing strategies are applied to capacity and energy sharing, respectively. When the credit is positive, the proposed cost-based pricing is applied to determine the price of the shared capacity; when the credit is negative,

the proposed demand-based pricing is applied to determine the price of the shared energy, which has fully utilized the dynamic demand-supply information.

- Eighth, a tri-level pricing strategy for IEHSs is formulated considering the integration among EVs, IEHSs, and both the PDN and GN. In this pricing strategy, the temporal shift of EVs within one IEHS and the spatial shift of EVs among multiple IEHSs are modeled. With the proposed tri-level pricing mechanism, IEHSs can ensure the charging/refueling services based on the dynamic charging/refueling response of EVs while mitigating the congestion of both the PDN and GN. To ensure the effectiveness of the pricing strategy in guiding EV behaviors, the bounded rationality of EVs in station selection is rigorously modeled based on the cognitive hierarchy (CH) theory. To be specific, EVs are categorized into heterogeneous cognitive levels, and the strategic thinking process of EVs that they will make decisions by considering the decisions of other EVs with lower cognitive levels is analyzed. Furthermore, the energy substitution effect of PH2EVs when making energy purchasing decisions is mathematically modeled. On the one hand, the optimal energy purchasing mixture of electricity and hydrogen is derived based on the consumer choice theory. On the other hand, the relationship between energy demand and energy price is established based on both the self-price elasticity and cross-price elasticity.

In the future, one of the challenges of this work is the generalization capability of the proposed data-driven models, including SC-GAIN for missing data imputation and the learning of the sensitivity functions. The demand level and the capacity of the renewable energy generator will continuously increase annually. Whether the currently trained model can adapt to future power system environments is challenging. One method to enhance the generalization capability is to add both the historical and generated data to the dataset according to the method in [214]. First, the future load is first predicted based on the long-term forecasting technologies presented in the literature [215]. Then, Gaussian noise is added to the predicted load level. Different scenarios are created for the possible allocation of renewable energy generators in the future, and Monte Carlo simulations will run to decide the output of the renewable energy generation at each bus. The uncertain demand and renewable energy generation compose the generated data set. Both historical data and the generated data are fed for training. In this way, the trained model can perform well under different demand levels and generation mixes. In future work, an online learning process can be further developed to revise the trained model timely so that the

trained model can adapt to the time-varying electricity network. The second critical challenge is that the typology of the distribution network may change due to network expansion. When the typology of the network changes, the data-driven model needs to be re-trained since the dimension of the problem may change. However, owing to the development of heterogeneous transfer learning, a new model can be trained rapidly, and the methodology to extend the current model to the different network topology is considered for our future work.

Second, we can consider using an advanced DBSCAN algorithm, such as adaptive DBSCAN, to choose the *Eps* automatically [242]. In this way, artificial intervention in the clustering process can be avoided, and the complete automation of the clustering process can be realized. Besides, data mining on the characteristic identification of the prosumers, including the demand elasticity, electricity usage habits, and sociodemographic characteristics, can be further realized. Based on these features, a refined clustering of the prosumers can be realized to help the coordinator formulate a more reasonable pricing strategy.

REFERENCES

[1] H. Yang, S. Zhang, J. Qiu, D. Qiu, M. Lai, and Z. Dong, "CVaR-constrained optimal bidding of electric vehicle aggregators in day-ahead and real-time markets," *IEEE Transactions on Industrial Informatics,* vol. 13, no. 5, pp. 2555-2565, 2017.

[2] D. McConnell *et al.*, "Retrospective modeling of the merit-order effect on wholesale electricity prices from distributed photovoltaic generation in the Australian National Electricity Market," *Energy Policy,* vol. 58, pp. 17-27, 2013.

[3] I. MacGill, "Electricity market design for facilitating the integration of wind energy: Experience and prospects with the Australian National Electricity Market," *Energy Policy,* vol. 38, no. 7, pp. 3180-3191, 2010.

[4] S. Chu and A. Majumdar, "Opportunities and challenges for a sustainable energy future," *nature,* vol. 488, no. 7411, pp. 294-303, 2012.

[5] N. Panwar, S. Kaushik, and S. Kothari, "Role of renewable energy sources in environmental protection: A review," *Renewable and sustainable energy reviews,* vol. 15, no. 3, pp. 1513-1524, 2011.

[6] S. P. Sukhatme and J. Nayak, *Solar energy*. McGraw-Hill Education, 2017.

[7] J. Boland, S. Farah, and L. Bai, "Forecasting of Wind and Solar Farm Output in the Australian National Electricity Market: A Review," *Energies,* vol. 15, no. 1, p. 370, 2022.

[8] R. McKenna *et al.*, "High-resolution large-scale onshore wind energy assessments: A review of potential definitions, methodologies and future research needs," *Renewable Energy,* vol. 182, pp. 659-684, 2022.

[9] S. F. Stefenon *et al.*, "Time series forecasting using ensemble learning methods for emergency prevention in hydroelectric power plants with dam," *Electric Power Systems Research,* vol. 202, p. 107584, 2022.

[10] S. Wright, M. Frost, A. Wong, and K. A. Parton, "Australian Renewable-Energy Microgrids: A Humble Past, a Turbulent Present, a Propitious Future," *Sustainability,* vol. 14, no. 5, p. 2585, 2022.

[11] G. Todeschini *et al.*, "Medium-term variability of the UK's combined tidal energy resource for a net-zero carbon grid," *Energy,* vol. 238, p. 121990, 2022.

[12] C. Auguste, J.-R. Nader, P. Marsh, I. Penesis, and R. Cossu, "Modelling the influence of Tidal Energy Converters on sediment dynamics in Banks Strait, Tasmania," *Renewable Energy,* vol. 188, pp. 1105-1119, 2022.

[13] J. C. Kurnia, M. S. Shatri, Z. A. Putra, J. Zaini, W. Caesarendra, and A. P. Sasmito, "Geothermal energy extraction using abandoned oil and gas wells: Techno-economic and policy review," *International Journal of Energy Research,* vol. 46, no. 1, pp. 28-60, 2022.

[14] L. Bartholomew, "Australian onshore petroleum acreage and releases 2022," *The APPEA Journal,* vol. 62, no. 2, pp. S544-S554, 2022.

[15] M. Irfan, R. M. Elavarasan, M. Ahmad, M. Mohsin, V. Dagar, and Y. Hao, "Prioritizing and overcoming biomass energy barriers: Application of AHP and G-TOPSIS approaches," *Technological Forecasting and Social Change,* vol. 177, p. 121524, 2022.

[16] M. Li *et al.*, "Scenario modelling of biomass usage in the Australian electricity grid," *Resources, Conservation and Recycling,* vol. 180, p. 106198, 2022.

[17] X. Luo, W. Shi, Y. Jiang, Y. Liu, and J. Xia, "Distributed peer-to-peer energy trading based on

game theory in a community microgrid considering ownership complexity of distributed energy resources," *Journal of Cleaner Production,* vol. 351, p. 131573, 2022.

[18] S. Lai, J. Qiu, Y. Tao, and J. Zhao, "Individualized Pricing of Energy Storage Sharing Based on Discount Sensitivity," *IEEE Transactions on Industrial Informatics,* 2021.

[19] B. Meng, R. C. Loonen, and J. L. Hensen, "Performance variability and implications for yield prediction of rooftop PV systems–Analysis of 246 identical systems," *Applied Energy,* vol. 322, p. 119550, 2022.

[20] A. Rajabi, S. Elphick, J. David, A. Pors, and D. Robinson, "Innovative approaches for assessing and enhancing the hosting capacity of PV-rich distribution networks: An Australian perspective," *Renewable and Sustainable Energy Reviews,* vol. 161, p. 112365, 2022.

[21] A. A. Kebede, T. Kalogiannis, J. Van Mierlo, and M. Berecibar, "A comprehensive review of stationary energy storage devices for large scale renewable energy sources grid integration," *Renewable and Sustainable Energy Reviews,* vol. 159, p. 112213, 2022.

[22] B. Bibak and H. Tekiner-Mogulkoc, "The parametric analysis of the electric vehicles and vehicle to grid system's role in flattening the power demand," *Sustainable Energy, Grids and Networks,* vol. 30, p. 100605, 2022.

[23] Y. Zhang, F. Gao, H. You, Z. Li, B. Zou, and Y. Du, "Recent advances in one-dimensional noble-metal-based catalysts with multiple structures for efficient fuel-cell electrocatalysis," *Coordination Chemistry Reviews,* vol. 450, p. 214244, 2022.

[24] F. J. Jamshidian, S. Gorjian, and M. Shafieefar, "Techno-economic assessment of a hybrid RO-MED desalination plant integrated with a solar CHP system," *Energy Conversion and Management,* vol. 251, p. 114985, 2022.

[25] Y. Huang, Y. Wang, and N. Liu, "Low-carbon economic dispatch and energy sharing method of multiple Integrated Energy Systems from the perspective of System of Systems," *Energy,* vol. 244, p. 122717, 2022.

[26] A. Narune and E. Prasad, "Renewable Energy Market by Type (Hydroelectric Power, Wind Power, Bioenergy, Solar Energy, and Geothermal Energy), and End Use (Residential, Commercial, Industrial, and Others): Global Opportunity Analysis and Industry Forecast, 2018–2025," *Report EN,* vol. 17140, 2019.

[27] A. Pena-Bello, D. Parra, M. Herberz, V. Tiefenbeck, M. K. Patel, and U. J. Hahnel, "Integration of prosumer peer-to-peer trading decisions into energy community modelling," *Nature Energy,* vol. 7, no. 1, pp. 74-82, 2022.

[28] L. Miles and V. Kapos, "Reducing greenhouse gas emissions from deforestation and forest degradation: global land-use implications," *science,* vol. 320, no. 5882, pp. 1454-1455, 2008.

[29] M. Y. Jaber, C. H. Glock, and A. M. El Saadany, "Supply chain coordination with emissions reduction incentives," *International Journal of Production Research,* vol. 51, no. 1, pp. 69-82, 2013.

[30] J. Woodcock *et al.*, "Public health benefits of strategies to reduce greenhouse-gas emissions: urban land transport," *The Lancet,* vol. 374, no. 9705, pp. 1930-1943, 2009.

[31] J. Zheng *et al.*, "Regional development and carbon emissions in China," *Energy Economics,* vol. 81, pp. 25-36, 2019.

[32] Q. Munir, H. H. Lean, and R. Smyth, "CO2 emissions, energy consumption and economic growth in the ASEAN-5 countries: A cross-sectional dependence approach," *Energy Economics,* vol. 85, p. 104571, 2020.

[33] J. C. Hull, "Options, Futures, And Other Derivatives (Eight Edition)," *New Jersey: PrenticeHall,* 2012.

[34] S. Clegg and P. Mancarella, "Integrated modeling and assessment of the operational impact of power-to-gas (P2G) on electrical and gas transmission networks," *IEEE Transactions on Sustainable Energy,* vol. 6, no. 4, pp. 1234-1244, 2015.

[35] Y. Tao, J. Qiu, S. Lai, J. Zhao, and Y. Xue, "Carbon-oriented Electricity Network Planning and Transformation," *IEEE Transactions on Power Systems,* vol. 36, no. 2, pp. 1034-1048, 2020.

[36] Y. Zheng, Z. Y. Dong, F. J. Luo, K. Meng, J. Qiu, and K. P. Wong, "Optimal allocation of energy storage system for risk mitigation of DISCOs with high renewable penetrations," *IEEE Transactions on Power Systems,* vol. 29, no. 1, pp. 212-220, 2013.

[37] S. Palamarchuk, "Dynamic programming approach to the bilateral contract scheduling," *IET generation, transmission & distribution,* vol. 4, no. 2, pp. 211-220, 2010.

[38] X. Liu *et al.*, "A Planning-oriented Resilience Assessment Framework for Transmission Systems under Typhoon Disasters," *IEEE Transactions on Smart Grid,* 2020.

[39] W. Huang, N. Zhang, J. Yang, Y. Wang, and C. Kang, "Optimal configuration planning of multi-energy systems considering distributed renewable energy," *IEEE Transactions on Smart Grid,* vol. 10, no. 2, pp. 1452-1464, 2017.

[40] S. Y. Abujarad, M. Mustafa, and J. Jamian, "Recent approaches of unit commitment in the presence of intermittent renewable energy resources: A review," *Renewable and Sustainable Energy Reviews,* vol. 70, pp. 215-223, 2017.

[41] G. G. Zanvettor, M. Casini, R. S. Smith, and A. Vicino, "Stochastic Energy Pricing of an Electric Vehicle Parking Lot," *IEEE Transactions on Smart Grid,* 2022.

[42] Y. Tao, J. Qiu, S. Lai, X. Zhang, and G. Wang, "Collaborative Planning for Electricity Distribution Network and Transportation System Considering Hydrogen Fuel Cell Vehicles," *IEEE Transactions on Transportation Electrification,* vol. 6, no. 3, pp. 1211-1225, 2020.

[43] Z. Ding, Y. Lu, L. Zhang, W.-J. Lee, and D. Chen, "A stochastic resource-planning scheme for PHEV charging station considering energy portfolio optimization and price-responsive demand," *IEEE Transactions on Industry Applications,* vol. 54, no. 6, pp. 5590-5598, 2018.

[44] S. Sun, Q. Yang, and W. Yan, "Optimal temporal-spatial PEV charging scheduling in active power distribution networks," *Protection and Control of Modern Power Systems,* vol. 2, no. 1, pp. 1-10, 2017.

[45] C. Zhang, X. Zhao, M. Shahidehpour, W. Li, L. Wen, and Z. Yang, "Reliability assessment of coordinated urban transportation and power distribution systems considering the impact of charging lots," *IEEE Access,* vol. 8, pp. 30536-30547, 2020.

[46] S. Cui, Y.-W. Wang, Y. Shi, and J.-W. Xiao, "A New and Fair Peer-to-Peer Energy Sharing Framework for Energy Buildings," *IEEE Transactions on Smart Grid,* vol. 11, no. 5, pp. 3817-3826, 2020.

[47] J. Jo and J. Park, "Demand-Side Management with Shared Energy Storage System in Smart Grid," *IEEE Transactions on Smart Grid,* vol. 11, no. 5, pp. 4466-4476, 2020.

[48] W. Tushar, T. K. Saha, C. Yuen, D. Smith, and H. V. Poor, "Peer-to-peer trading in electricity networks: an overview," *IEEE Transactions on Smart Grid,* vol. 11, no. 4, pp. 3185-3200, 2020.

[49] S. Lai, J. Qiu, and Y. Tao, "Option-based portfolio risk hedging strategy for gas generator based on mean-variance utility model," *Energy Conversion and Economics,* vol. 3, no. 1, pp. 20-30, 2022.

[50] S. Ahmed, M. Elsholkami, A. Elkamel, J. Du, E. B. Ydstie, and P. L. Douglas, "Financial risk management for new technology integration in energy planning under uncertainty," *Applied energy,* vol. 128, pp. 75-81, 2014.

[51] D. M. Chance and R. Brooks, *Introduction to derivatives and risk management*. Cengage Learning, 2015.

[52] J. Kettunen, A. Salo, and D. W. Bunn, "Optimization of electricity retailer's contract portfolio subject to risk preferences," *IEEE Transactions on Power Systems,* vol. 25, no. 1, pp. 117-128, 2009.

[53] J. A. Schachter and P. Mancarella, "Demand response contracts as real options: a probabilistic evaluation framework under short-term and long-term uncertainties," *IEEE Transactions on Smart Grid,* vol. 7, no. 2, pp. 868-878, 2015.

[54] S. Lai, J. Qiu, Y. Tao, and J. Zhao, "Risk hedging for gas power generation considering power-to-gas energy storage in three different electricity markets," *Applied Energy,* vol. 291, p. 116822, 2021.

[55] Y. Xiao, X. Wang, P. Pinson, and X. Wang, "A local energy market for electricity and hydrogen," *IEEE Transactions on Power Systems,* vol. 33, no. 4, pp. 3898-3908, 2017.

[56] G. Pan, W. Gu, Y. Lu, H. Qiu, S. Lu, and S. Yao, "Accurate Modeling of a Profit-Driven Power to Hydrogen and Methane Plant Toward Strategic Bidding Within Multi-Type Markets," *IEEE Transactions on Smart Grid,* vol. 12, no. 1, pp. 338-349, 2020.

[57] S. Lai, J. Qiu, Y. Tao, and X. Sun, "Demand Response Aggregation with Operating Envelope Based on Data-driven State Estimation and Sensitivity Function Signals," *IEEE Transactions on Smart Grid,* 2022.

[58] L. Yao, W. H. Lim, and T. S. Tsai, "A real-time charging scheme for demand response in electric vehicle parking station," *IEEE Transactions on Smart Grid,* vol. 8, no. 1, pp. 52-62, 2016.

[59] Q. Chen *et al.*, "Dynamic price vector formation model-based automatic demand response strategy for PV-assisted EV charging stations," *IEEE Transactions on Smart Grid,* vol. 8, no. 6, pp. 2903-2915, 2017.

[60] Z. Tan, P. Yang, and A. Nehorai, "An optimal and distributed demand response strategy with electric vehicles in the smart grid," *IEEE Transactions on Smart Grid,* vol. 5, no. 2, pp. 861-869, 2014.

[61] F. Rassaei, W.-S. Soh, and K.-C. Chua, "Distributed scalable autonomous market-based demand response via residential plug-in electric vehicles in smart grids," *IEEE Transactions on Smart Grid,* vol. 9, no. 4, pp. 3281-3290, 2016.

[62] S. Talari, M. Shafie-Khah, Y. Chen, W. Wei, P. D. Gaspar, and J. P. Catalao, "Real-time scheduling of demand response options considering the volatility of wind power generation," *IEEE Transactions on Sustainable Energy,* vol. 10, no. 4, pp. 1633-1643, 2018.

[63] D. Muthirayan, D. Kalathil, S. Li, K. Poolla, and P. Varaiya, "Selling Demand Response Using Options," *IEEE Transactions on Smart Grid,* vol. 12, no. 1, pp. 279-288, 2020.

[64] M. Fahrioglu and F. L. Alvarado, "Designing incentive compatible contracts for effective demand management," *IEEE Transactions on power Systems,* vol. 15, no. 4, pp. 1255-1260, 2000.

[65] S.-I. Azuma, D. Sato, K. Kobayashi, and N. Yamaguchi, "Detection of defaulting participants of demand response based on sparse reconstruction," *IEEE Transactions on Smart Grid,* vol. 11, no. 1, pp. 368-378, 2019.

[66] S. Lai, J. Qiu, and Y. Tao, "Credit-based Pricing and Planning Strategies for Hydrogen and Electricity Energy Storage Sharing," *IEEE Transactions on Sustainable Energy,* 2021.

[67] S. Cui, Y.-W. Wang, and J.-W. Xiao, "Peer-to-peer energy sharing among smart energy buildings by distributed transaction," *IEEE Transactions on Smart Grid,* vol. 10, no. 6, pp. 6491-6501, 2019.

[68] W. Tushar *et al.*, "Energy storage sharing in smart grid: A modified auction-based approach," *IEEE Transactions on Smart Grid,* vol. 7, no. 3, pp. 1462-1475, 2016.

[69] D. Zhao, H. Wang, J. Huang, and X. Lin, "Virtual energy storage sharing and capacity allocation," *IEEE Transactions on Smart Grid,* vol. 11, no. 2, pp. 1112-1123, 2019.

[70] X. Xu *et al.*, "Data-driven game-based pricing for sharing rooftop photovoltaic generation and energy storage in the residential building cluster under uncertainties," *IEEE Transactions on Industrial Informatics,* vol. 17, no. 7, pp. 4480-4491, 2020.

[71] J. Yang, J. Zhao, F. Wen, and Z. Dong, "A model of customizing electricity retail prices based on load profile clustering analysis," *IEEE Transactions on Smart Grid,* vol. 10, no. 3, pp. 3374-3386, 2018.

[72] A. Fleischhacker, H. Auer, G. Lettner, and A. Botterud, "Sharing solar PV and energy storage in apartment buildings: resource allocation and pricing," *IEEE Transactions on Smart Grid,* vol. 10, no. 4, pp. 3963-3973, 2018.

[73] D. L. Rodrigues, X. Ye, X. Xia, and B. Zhu, "Battery energy storage sizing optimisation for different ownership structures in a peer-to-peer energy sharing community," *Applied Energy,* vol. 262, p. 114498, 2020.

[74] Y. Xia, Q. Xu, J. Zhao, and X. Yuan, "Two-stage robust optimisation of user-side cloud energy storage configuration considering load fluctuation and energy storage loss," *IET Generation, Transmission & Distribution,* vol. 14, no. 16, pp. 3278-3287, 2020.

[75] V. Rigoni, D. Flynn, and A. Keane, "Coordinating demand response aggregation with LV network operational constraints," *IEEE Transactions on Power Systems,* vol. 36, no. 2, pp. 979-990, 2020.

[76] M. D. de Souza Dutra and N. Alguacil, "Optimal residential users coordination via demand response: An exact distributed framework," *Applied Energy,* vol. 279, p. 115851, 2020.

[77] M. Vahid-Ghavidel, N. Mahmoudi, and B. Mohammadi-Ivatloo, "Self-scheduling of demand response aggregators in short-term markets based on information gap decision theory," *IEEE Transactions on Smart Grid,* vol. 10, no. 2, pp. 2115-2126, 2018.

[78] Y. Tao, J. Qiu, S. Lai, and J. Zhao, "Integrated Electricity and Hydrogen Energy Sharing in Coupled Energy Systems," *IEEE Transactions on Smart Grid,* vol. 12, no. 2, pp. 1149-1162, 2020.

[79] J. Tan and L. Wang, "Real-time charging navigation of electric vehicles to fast charging stations: A hierarchical game approach," *IEEE transactions on smart grid,* vol. 8, no. 2, pp. 846-856, 2015.

[80] L. Thibault, G. De Nunzio, and A. Sciarretta, "A unified approach for electric vehicles range maximization via eco-routing, eco-driving, and energy consumption prediction," *IEEE Transactions on Intelligent Vehicles,* vol. 3, no. 4, pp. 463-475, 2018.

[81] G. Li, Q. Sun, L. Boukhatem, J. Wu, and J. Yang, "Intelligent vehicle-to-vehicle charging navigation for mobile electric vehicles via VANET-based communication," *IEEE Access,* vol. 7, pp. 170888-170906, 2019.

[82] S. Bruce *et al.*, "National hydrogen roadmap," *Australia: CSIRO,* 2018.

[83] A. Mohamed, V. Salehi, T. Ma, and O. Mohammed, "Real-time energy management algorithm for plug-in hybrid electric vehicle charging parks involving sustainable energy," *IEEE Transactions on Sustainable Energy,* vol. 5, no. 2, pp. 577-586, 2013.

[84] T. Chen, B. Zhang, H. Pourbabak, A. Kavousi-Fard, and W. Su, "Optimal routing and charging of an electric vehicle fleet for high-efficiency dynamic transit systems," *IEEE Transactions on Smart Grid,* vol. 9, no. 4, pp. 3563-3572, 2016.

[85] G. Kneževic, S. Nikolovski, and P. Marić, "Electricity spot market simulation involving bilateral contracts hedging," in *2011 8th International Conference on the European Energy Market (EEM)*, 2011: IEEE, pp. 122-127.

[86] J. A. Batten, H. Kinateder, P. G. Szilagyi, and N. F. Wagner, "Can stock market investors hedge energy risk? Evidence from Asia," *Energy Economics,* vol. 66, pp. 559-570, 2017.

[87] H. M. Ghadikolaei, A. Ahmadi, J. Aghaei, and M. Najafi, "Risk constrained self-scheduling of hydro/wind units for short term electricity markets considering intermittency and uncertainty," *Renewable and Sustainable Energy Reviews,* vol. 16, no. 7, pp. 4734-4743, 2012.

[88] C. Budny, R. Madlener, and C. Hilgers, "Economic feasibility of pipe storage and underground reservoir storage options for power-to-gas load balancing," *Energy Conversion and Management,* vol. 102, pp. 258-266, 2015.

[89] H. Khani and H. E. Z. Farag, "Optimal day-ahead scheduling of power-to-gas energy storage and gas load management in wholesale electricity and gas markets," *IEEE Transactions on Sustainable Energy,* vol. 9, no. 2, pp. 940-951, 2017.

[90] B. Lyseng *et al.*, "System-level power-to-gas energy storage for high penetrations of variable renewables," *international journal of hydrogen energy,* vol. 43, no. 4, pp. 1966-1979, 2018.

[91] J. Yang, N. Zhang, Y. Cheng, C. Kang, and Q. Xia, "Modeling the operation mechanism of combined P2G and gas-fired plant with CO 2 recycling," *IEEE Transactions on smart grid,* vol. 10, no. 1, pp. 1111-1121, 2018.

[92] R. Zhang, T. Jiang, F. F. Li, G. Li, H. Chen, and X. Li, "Coordinated Bidding Strategy of Wind Farms and Power-to-Gas Facilities using a Cooperative Game Approach," *IEEE Transactions on Sustainable Energy,* 2020.

[93] Y. Li, W. Liu, M. Shahidehpour, F. Wen, K. Wang, and Y. Huang, "Optimal operation strategy for integrated natural gas generating unit and power-to-gas conversion facilities," *IEEE Transactions on Sustainable Energy,* vol. 9, no. 4, pp. 1870-1879, 2018.

[94] X. Xing, J. Lin, Y. Song, and Q. Hu, "Maximum Production Point Tracking of a High-Temperature Power-to-Gas System: A Dynamic-Model-Based Study," *IEEE Transactions on Sustainable Energy,* vol. 11, no. 1, pp. 361-370, 2019.

[95] M. Arnesano, A. P. Carlucci, and D. Laforgia, "Extension of portfolio theory application to energy planning problem–The Italian case," *Energy,* vol. 39, no. 1, pp. 112-124, 2012.

[96] X. Li, Z. Qin, and S. Kar, "Mean-variance-skewness model for portfolio selection with fuzzy returns," *European Journal of Operational Research,* vol. 202, no. 1, pp. 239-247, 2010.

[97] V. Mohan, J. G. Singh, and W. Ongsakul, "Sortino ratio based portfolio optimization considering EVs and renewable energy in microgrid power market," *IEEE Transactions on Sustainable Energy,* vol. 8, no. 1, pp. 219-229, 2016.

[98] A. Perez, R. Moreno, R. Moreira, M. Orchard, and G. Strbac, "Effect of battery degradation on multi-service portfolios of energy storage," *IEEE Transactions on Sustainable Energy,* vol. 7,

no. 4, pp. 1718-1729, 2016.

[99] G. Fernandes, L. L. Gomes, and L. E. T. Brandão, "A risk-hedging tool for hydro power plants," *Renewable and Sustainable Energy Reviews,* vol. 90, pp. 370-378, 2018.

[100] Y. Wen, C. Chung, and X. Liu, "Hierarchical Interactive Risk Hedging of Multi-TSO Power Systems," *IEEE Transactions on Power Systems,* vol. 33, no. 3, pp. 2962-2974, 2017.

[101] R. Aid, L. Campi, and N. Langrené, "A Structural Risk-Neutral Model for Pricing and Hedging Power Derivatives," *Mathematical Finance: An International Journal of Mathematics, Statistics and Financial Economics,* vol. 23, no. 3, pp. 387-438, 2013.

[102] G. A. V. Sanchez, J. M. Alzate, A. I. Cadena, and J. M. Benavides, "Setting up standard power options to hedge price-quantity risk in a competitive electricity market: the colombian case," *IEEE Transactions on Power Systems,* vol. 26, no. 3, pp. 1493-1500, 2010.

[103] X. Yan, C. Gu, H. Wyman-Pain, and F. Li, "Capacity share optimization for multiservice energy storage management under portfolio theory," *IEEE Transactions on Industrial Electronics,* vol. 66, no. 2, pp. 1598-1607, 2018.

[104] A. Mehdizadeh, N. Taghizadegan, and J. Salehi, "Risk-based energy management of renewable-based microgrid using information gap decision theory in the presence of peak load management," *Applied energy,* vol. 211, pp. 617-630, 2018.

[105] R.-P. Liu, S. Lei, C. Peng, W. Sun, and Y. Hou, "Data-Based Resilience Enhancement Strategies for Electric-Gas Systems Against Sequential Extreme Weather Events," *IEEE Transactions on Smart Grid,* 2020.

[106] C. Sun, X. Wang, and Y. Zheng, "An ensemble system to predict the spatiotemporal distribution of energy security weaknesses in transmission networks," *Applied Energy,* vol. 258, p. 114062, 2020.

[107] R. J. Hyndman and S. Fan, "Density forecasting for long-term peak electricity demand," *IEEE Transactions on Power Systems,* vol. 25, no. 2, pp. 1142-1153, 2009.

[108] Z. Zhang *et al.*, "Optimal Alliance Strategies Among Retailers Under Energy Deviation Settlement Mechanism in China's Forward Electricity Market," *IEEE Transactions on Power Systems,* vol. 35, no. 3, pp. 2059-2071, 2019.

[109] M. Alipour, K. Zare, H. Zareipour, and H. Seyedi, "Hedging strategies for heat and electricity consumers in the presence of real-time demand response programs," *IEEE Transactions on Sustainable Energy,* vol. 10, no. 3, pp. 1262-1270, 2018.

[110] S. Kwon, L. Ntaimo, and N. Gautam, "Optimal day-ahead power procurement with renewable energy and demand response," *IEEE Transactions on Power Systems,* vol. 32, no. 5, pp. 3924-3933, 2016.

[111] L. Han, T. Morstyn, and M. McCulloch, "Incentivizing prosumer coalitions with energy management using cooperative game theory," *IEEE Transactions on Power Systems,* vol. 34, no. 1, pp. 303-313, 2018.

[112] D. Muthirayan, D. Kalathil, S. Li, K. Poolla, and P. Varaiya, "Selling Demand Response Using Options," *IEEE Transactions on Smart Grid,* 2020.

[113] A. S. Dagoumas and M. L. Polemis, "An integrated model for assessing electricity retailer's profitability with demand response," *Applied Energy,* vol. 198, pp. 49-64, 2017.

[114] S. Nojavan, R. Nourollahi, H. Pashaei-Didani, and K. Zare, "Uncertainty-based electricity procurement by retailer using robust optimization approach in the presence of demand response exchange," *International Journal of Electrical Power & Energy Systems,* vol. 105, pp. 237-248,

2019.

[115] A. Ahmadi, M. Charwand, and J. Aghaei, "Risk-constrained optimal strategy for retailer forward contract portfolio," *International Journal of Electrical Power & Energy Systems,* vol. 53, pp. 704-713, 2013.

[116] R. Karandikar, S. Khaparde, and S. Kulkarni, "Strategic evaluation of bilateral contract for electricity retailer in restructured power market," *International Journal of Electrical Power & Energy Systems,* vol. 32, no. 5, pp. 457-463, 2010.

[117] H. Yang, J. Qiu, K. Meng, J. H. Zhao, Z. Y. Dong, and M. Lai, "Insurance strategy for mitigating power system operational risk introduced by wind power forecasting uncertainty," *Renewable Energy,* vol. 89, pp. 606-615, 2016.

[118] S. Nojavan, K. Zare, and B. Mohammadi-Ivatloo, "Optimal stochastic energy management of retailer based on selling price determination under smart grid environment in the presence of demand response program," *Applied energy,* vol. 187, pp. 449-464, 2017.

[119] W. Wei, S. Mei, L. Wu, M. Shahidehpour, and Y. Fang, "Optimal traffic-power flow in urban electrified transportation networks," *IEEE Transactions on Smart Grid,* vol. 8, no. 1, pp. 84-95, 2016.

[120] W. Wei, L. Wu, J. Wang, and S. Mei, "Network equilibrium of coupled transportation and power distribution systems," *IEEE Transactions on Smart Grid,* vol. 9, no. 6, pp. 6764-6779, 2017.

[121] Y. Cui, Z. Hu, and X. Duan, "Optimal Pricing of Public Electric Vehicle Charging Stations Considering Operations of Coupled Transportation and Power Systems," *IEEE Transactions on Smart Grid,* 2021.

[122] Y. Kim, J. Kwak, and S. Chong, "Dynamic pricing, scheduling, and energy management for profit maximization in PHEV charging stations," *IEEE Transactions on Vehicular Technology,* vol. 66, no. 2, pp. 1011-1026, 2016.

[123] V. Moghaddam, A. Yazdani, H. Wang, D. Parlevliet, and F. Shahnia, "An online reinforcement learning approach for dynamic pricing of electric vehicle charging stations," *IEEE Access,* vol. 8, pp. 130305-130313, 2020.

[124] Y. Zhang, Y. Zhou, C. Jiang, Y. Wang, R. Zhang, and G. Chen, "Plug-in Electric Vehicle Charging With Multiple Charging Options: A Systematic Analysis of Service Providers' Pricing Strategies," *IEEE Transactions on Smart Grid,* vol. 12, no. 1, pp. 524-537, 2020.

[125] W. Yuan, J. Huang, and Y. J. A. Zhang, "Competitive charging station pricing for plug-in electric vehicles," *IEEE Transactions on Smart Grid,* vol. 8, no. 2, pp. 627-639, 2015.

[126] C. Luo, Y.-F. Huang, and V. Gupta, "Stochastic dynamic pricing for EV charging stations with renewable integration and energy storage," *IEEE Transactions on Smart Grid,* vol. 9, no. 2, pp. 1494-1505, 2017.

[127] M. Seyedyazdi, M. Mohammadi, and E. Farjah, "A combined driver-station interactive algorithm for a maximum mutual interest in charging market," *IEEE Transactions on Intelligent Transportation Systems,* vol. 21, no. 6, pp. 2534-2544, 2019.

[128] Y. Zhang, P. You, and L. Cai, "Optimal charging scheduling by pricing for EV charging station with dual charging modes," *IEEE Transactions on Intelligent Transportation Systems,* vol. 20, no. 9, pp. 3386-3396, 2018.

[129] I. Zenginis, J. Vardakas, N. Zorba, and C. Verikoukis, "Performance evaluation of a multi-standard fast charging station for electric vehicles," *IEEE transactions on smart grid,* vol. 9, no. 5, pp. 4480-4489, 2017.

[130] Z. Moghaddam, I. Ahmad, D. Habibi, and M. A. Masoum, "A coordinated dynamic pricing model for electric vehicle charging stations," *IEEE Transactions on Transportation Electrification,* vol. 5, no. 1, pp. 226-238, 2019.

[131] D. Said and H. T. Mouftah, "A novel electric vehicles charging/discharging management protocol based on queuing model," *IEEE Transactions on Intelligent Vehicles,* vol. 5, no. 1, pp. 100-111, 2019.

[132] M. Alizadeh, H.-T. Wai, M. Chowdhury, A. Goldsmith, A. Scaglione, and T. Javidi, "Optimal pricing to manage electric vehicles in coupled power and transportation networks," *IEEE Transactions on control of network systems,* vol. 4, no. 4, pp. 863-875, 2016.

[133] B. Sohet, Y. Hayel, O. Beaude, and A. Jeandin, "Hierarchical Coupled Driving-and-Charging Model of Electric Vehicles, Stations and Grid Operators," *IEEE Transactions on Smart Grid,* vol. 12, no. 6, pp. 5146-5157, 2021.

[134] X. Zhang, K. W. Chan, H. Li, H. Wang, J. Qiu, and G. Wang, "Deep-learning-based probabilistic forecasting of electric vehicle charging load with a novel queuing model," *IEEE transactions on cybernetics,* vol. 51, no. 6, pp. 3157-3170, 2020.

[135] S. Cui, Y.-W. Wang, C. Li, and J.-W. Xiao, "Prosumer Community: A Risk Aversion Energy Sharing Model," *IEEE Transactions on Sustainable Energy,* vol. 11, no. 2, pp. 828-838, 2019.

[136] X. Xu, J. Li, Y. Xu, Z. Xu, and C. S. Lai, "A Two-stage Game-theoretic Method for Residential PV Panels Planning Considering Energy Sharing Mechanism," *IEEE Transactions on Power Systems,* vol. 35, no. 5, pp. 3562-3573, 2020.

[137] L. Han, T. Morstyn, and M. D. McCulloch, "Scaling Up Cooperative Game Theory Based Energy Management using Prosumer Clustering," *IEEE Transactions on Smart Grid,* vol. 12, no. 1, pp. 289-300, 2020.

[138] C. Long, J. Wu, Y. Zhou, and N. Jenkins, "Peer-to-peer energy sharing through a two-stage aggregated battery control in a community Microgrid," *Applied Energy,* vol. 226, pp. 261-276, 2018.

[139] S. Yin, Q. Ai, J. Li, Z. Li, and S. Fan, "Energy Pricing and Sharing Strategy Based on Hybrid Stochastic Robust Game Approach for a Virtual Energy Station with Energy Cells," *IEEE Transactions on Sustainable Energy,* vol. 12, no. 2, pp. 772-784, 2020.

[140] W. Zhong, K. Xie, Y. Liu, C. Yang, and S. Xie, "Multi-Resource Allocation of Shared Energy Storage: A Distributed Combinatorial Auction Approach," *IEEE Transactions on Smart Grid,* vol. 11, no. 5, pp. 4105-4115, 2020.

[141] K. Mochtar and D. Arditi, "Pricing strategy in the US construction industry," *Construction Management & Economics,* vol. 19, no. 4, pp. 405-415, 2001.

[142] K. J. Reddy and N. Sudhakar, "High voltage gain interleaved boost converter with neural network based MPPT controller for fuel cell based electric vehicle applications," *IEEE Access,* vol. 6, pp. 3899-3908, 2018.

[143] J. Zhang, Y. Pei, J. Shen, L. Wang, T. Ding, and S. Wang, "Charging strategy unifying spatial-temporal coordination of electric vehicles," *IEEE Access,* vol. 8, pp. 74853-74863, 2020.

[144] F. Elghitani and E. F. El-Saadany, "Efficient assignment of electric vehicles to charging stations," *IEEE Transactions on Smart Grid,* vol. 12, no. 1, pp. 761-773, 2020.

[145] S. M. Danish, K. Zhang, H.-A. Jacobsen, N. Ashraf, and H. K. Qureshi, "BlockEV: Efficient and secure charging station selection for electric vehicles," *IEEE Transactions on Intelligent Transportation Systems,* 2020.

[146] Y. Jin, J. Xu, S. Wu, L. Xu, and D. Yang, "Enabling the wireless charging via bus network: Route scheduling for electric vehicles," *IEEE Transactions on Intelligent Transportation Systems,* vol. 22, no. 3, pp. 1827-1839, 2020.

[147] M. M. De Weerdt, S. Stein, E. H. Gerding, V. Robu, and N. R. Jennings, "Intention-aware routing of electric vehicles," *IEEE Transactions on Intelligent Transportation Systems,* vol. 17, no. 5, pp. 1472-1482, 2015.

[148] A. M. Bozorgi, M. Farasat, and A. Mahmoud, "A time and energy efficient routing algorithm for electric vehicles based on historical driving data," *IEEE Transactions on Intelligent Vehicles,* vol. 2, no. 4, pp. 308-320, 2017.

[149] T. Zhang, W. Chen, Z. Han, and Z. Cao, "Charging scheduling of electric vehicles with local renewable energy under uncertain electric vehicle arrival and grid power price," *IEEE Transactions on Vehicular Technology,* vol. 63, no. 6, pp. 2600-2612, 2013.

[150] A.-M. Koufakis, E. S. Rigas, N. Bassiliades, and S. D. Ramchurn, "Offline and online electric vehicle charging scheduling with V2V energy transfer," *IEEE Transactions on Intelligent Transportation Systems,* vol. 21, no. 5, pp. 2128-2138, 2019.

[151] J. C. Hull, "Option, Futures and other Derivatives," ed: Pearson Education, 2009.

[152] X. Zhang *et al.*, "Game-theoretic planning for integrated energy system with independent participants considering ancillary services of power-to-gas stations," *Energy,* vol. 176, pp. 249-264, 2019.

[153] S.-E. S. Yu, K.-H. Huarng, M.-Y. L. Li, and C.-Y. Chen, "A novel option pricing model via fuzzy binomial decision tree," *International Journal of Innovative Computing, Information and Control,* vol. 7, no. 2, pp. 709-718, 2011.

[154] R. Vaila, J. Chiasson, and V. Saxena, "A Deep Unsupervised Feature Learning Spiking Neural Network with Binarized Classification Layers for EMNIST Classification," *arXiv preprint arXiv:2002.11843,* 2020.

[155] M. Yousefi and E. J. M. Carranza, "Geometric average of spatial evidence data layers: a GIS-based multi-criteria decision-making approach to mineral prospectivity mapping," *Computers & Geosciences,* vol. 83, pp. 72-79, 2015.

[156] S. L. Fjesme, "Foreign market portfolio concentration and performance," *Financial Management,* 2019.

[157] P. Michaillat and E. Saez, "A New Keynesian model with wealth in the utility function," National Bureau of Economic Research, 2018.

[158] L. Zhang, L. Botti, and S. Petit, "Destination performance: Introducing the utility function in the mean-variance space," *Tourism Management,* vol. 52, pp. 123-132, 2016.

[159] S. Nakagawa, P. C. D. Johnson, and H. Schielzeth, "The coefficient of determination R 2 and intra-class correlation coefficient from generalized linear mixed-effects models revisited and expanded," *Journal of the Royal Society Interface,* vol. 14, no. 134, p. 20170213, 2017.

[160] A. E. M. Operator. National electricity market: data dashboard: aggregated data files,

[161] H. H. Huang, Y. M. Shiu, and P. S. Lin, "HDD and CDD option pricing with market price of weather risk for Taiwan," *Journal of Futures Markets: Futures, Options, and Other Derivative Products,* vol. 28, no. 8, pp. 790-814, 2008.

[162] J. Qiu *et al.*, "A probabilistic transmission planning framework for reducing network vulnerability to extreme events," *IEEE Transactions on Power Systems,* vol. 31, no. 5, pp. 3829-3839, 2015.

[163] X. Chen, J. Qiu, L. Reedman, and Z. Y. Dong, "A Statistical Risk Assessment Framework for Distribution Network Resilience," *IEEE Transactions on Power Systems,* vol. 34, no. 6, pp. 4773-4783, 2019.

[164] I.-L. Securities, "The handbook of insurance-linked securities," 2009.

[165] R. T. Rockafellar and S. Uryasev, "Optimization of conditional value-at-risk," *Journal of risk,* vol. 2, pp. 21-42, 2000.

[166] S. D. Campbell and F. X. Diebold, "Weather forecasting for weather derivatives," *Journal of the American Statistical Association,* vol. 100, no. 469, pp. 6-16, 2005.

[167] S. Bhattacharya, A. Gupta, K. Kar, and A. Owusu, "Cross hedging strategies for solar energy production using weather derivatives," *Available at SSRN 2642685,* 2016.

[168] A. L. F. Serafim, "Performance of VIX straddle and strangle strategies in portfolio management," 2018.

[169] A. g. b. o. meterology, "Weather and climate data: long term temperature data," 2020, doi: http://www.bom.gov.au/climate/data/index.shtml?bookmark=201.

[170] N. G. Mankiw, *Principles of economics*. Cengage Learning, 2020.

[171] C. Huang, H. Zhang, Y. Song, L. Wang, T. Ahmad, and X. Luo, "Demand response for industrial micro-grid considering photovoltaic power uncertainty and battery operational cost," *IEEE Transactions on Smart Grid,* 2021.

[172] F. Rassaei, W.-S. Soh, and K.-C. Chua, "Demand response for residential electric vehicles with random usage patterns in smart grids," *IEEE Transactions on Sustainable Energy,* vol. 6, no. 4, pp. 1367-1376, 2015.

[173] F. Luo, Z. Y. Dong, K. Meng, J. Qiu, J. Yang, and K. P. Wong, "Short-term operational planning framework for virtual power plants with high renewable penetrations," *IET Renewable Power Generation,* vol. 10, no. 5, pp. 623-633, 2016.

[174] Y. Sun, H. Yue, J. Zhang, and C. Booth, "Minimization of residential energy cost considering energy storage system and EV with driving usage probabilities," *IEEE Transactions on Sustainable Energy,* vol. 10, no. 4, pp. 1752-1763, 2018.

[175] P. Li, D. Yu, M. Yang, and J. Wang, "Flexible look-ahead dispatch realized by robust optimization considering CVaR of wind power," *IEEE Transactions on Power Systems,* vol. 33, no. 5, pp. 5330-5340, 2018.

[176] C. Zhang, Y. Xu, and Z. Y. Dong, "Probability-weighted robust optimization for distributed generation planning in microgrids," *IEEE Transactions on Power Systems,* vol. 33, no. 6, pp. 7042-7051, 2018.

[177] Z. Cui *et al.*, "Optimal strategies for distribution network reconfiguration considering uncertain wind power," *CSEE Journal of Power and Energy Systems,* vol. 6, no. 3, pp. 662-671, 2020.

[178] M. Shabanzadeh, M.-K. Sheikh-El-Eslami, and M.-R. Haghifam, "The design of a risk-hedging tool for virtual power plants via robust optimization approach," *Applied Energy,* vol. 155, pp. 766-777, 2015.

[179] D. Songhuai, Z. Xinghua, M. Lu, and X. Hui, "A novel nucleolus-based loss allocation method in bilateral electricity markets," *IEEE Transactions on Power Systems,* vol. 21, no. 1, pp. 28-33, 2006.

[180] K. Khan, S. U. Rehman, K. Aziz, S. Fong, and S. Sarasvady, "DBSCAN: Past, present and future," in *The Fifth International Conference on the Applications of Digital Information and Web Technologies (ICADIWT 2014)*, 2014: IEEE, pp. 232-238.

[181] D. Birant and A. Kut, "ST-DBSCAN: An algorithm for clustering spatial–temporal data," *Data & Knowledge Engineering,* vol. 60, no. 1, pp. 208-221, 2007.

[182] S. Wang, S. Bi, and Y.-J. A. Zhang, "Demand response management for profit maximizing energy loads in real-time electricity market," *IEEE Transactions on Power Systems,* vol. 33, no. 6, pp. 6387-6396, 2018.

[183] K. Stenner, E. R. Frederiks, E. V. Hobman, and S. Cook, "Willingness to participate in direct load control: The role of consumer distrust," *Applied Energy,* vol. 189, pp. 76-88, 2017.

[184] A. Taşcıkaraoğlu, N. G. Paterakis, O. Erdinç, and J. P. S. Catalao, "Combining the flexibility from shared energy storage systems and DLC-based demand response of HVAC units for distribution system operation enhancement," *IEEE Transactions on Sustainable Energy,* vol. 10, no. 1, pp. 137-148, 2018.

[185] S. Zheng *et al.*, "Incentive-Based Integrated Demand Response for Multiple Energy Carriers Considering Behavioral Coupling Effect of Consumers," *IEEE Transactions on Smart Grid,* vol. 11, no. 4, pp. 3231-3245, 2020.

[186] S. Zheng, Y. Sun, B. Li, B. Qi, X. Zhang, and F. Li, "Incentive-based integrated demand response for multiple energy carriers under complex uncertainties and double coupling effects," *Applied Energy,* p. 116254, 2020.

[187] Z. Liu, Y. Zhao, and X. Wang, "Long-term economic planning of combined cooling heating and power systems considering energy storage and demand response," *Applied Energy,* vol. 279, p. 115819, 2020.

[188] B. Qela and H. T. Mouftah, "Peak load curtailment in a smart grid via fuzzy system approach," *IEEE Transactions on Smart Grid,* vol. 5, no. 2, pp. 761-768, 2014.

[189] Q. Li, Y. Xu, and C. Ren, "A hierarchical data-driven method for event-based load shedding against fault-induced delayed voltage recovery in power systems," *IEEE Transactions on Industrial Informatics,* vol. 17, no. 1, pp. 699-709, 2020.

[190] Y. Zhang, M. H. Hajiesmaili, S. Cai, M. Chen, and Q. Zhu, "Peak-aware online economic dispatching for microgrids," *IEEE Transactions on Smart Grid,* vol. 9, no. 1, pp. 323-335, 2016.

[191] K. M. Tsui and S.-C. Chan, "Demand response optimization for smart home scheduling under real-time pricing," *IEEE Transactions on Smart Grid,* vol. 3, no. 4, pp. 1812-1821, 2012.

[192] J. H. Yoon, R. Baldick, and A. Novoselac, "Dynamic demand response controller based on real-time retail price for residential buildings," *IEEE Transactions on Smart Grid,* vol. 5, no. 1, pp. 121-129, 2014.

[193] R. Lu, R. Bai, Y. Huang, Y. Li, J. Jiang, and Y. Ding, "Data-driven real-time price-based demand response for industrial facilities energy management," *Applied Energy,* p. 116291, 2020.

[194] M. Song, W. Sun, Y. Wang, M. Shahidehpour, Z. Li, and C. Gao, "Hierarchical scheduling of aggregated TCL flexibility for transactive energy in power systems," *IEEE Transactions on Smart Grid,* vol. 11, no. 3, pp. 2452-2463, 2019.

[195] M. B. Anwar and M. O'Malley, "Strategic participation of residential thermal demand response in energy and capacity markets," *IEEE Transactions on Smart Grid,* pp. 1-1, 2021, doi: 10.1109/TSG.2021.3053639.

[196] J. S. Vardakas, N. Zorba, and C. V. Verikoukis, "A survey on demand response programs in smart grids: Pricing methods and optimization algorithms," *IEEE Communications Surveys & Tutorials,* vol. 17, no. 1, pp. 152-178, 2014.

[197] P. Faria and Z. Vale, "Demand response in electrical energy supply: An optimal real time pricing

approach," *Energy,* vol. 36, no. 8, pp. 5374-5384, 2011.

[198] S. C. Ross, N. Ozay, and J. L. Mathieu, "Coordination between an aggregator and distribution operator to achieve network-aware load control," in *IEEE Milan PowerTech*, 2019 2019 IEEE, pp. 1-6.

[199] A. Hassan, R. Mieth, M. Chertkov, D. Deka, and Y. Dvorkin, "Optimal load ensemble control in chance-constrained optimal power flow," *IEEE Transactions on Smart Grid,* vol. 10, no. 5, pp. 5186-5195, 2018.

[200] N. Karthikeyan, J. R. Pillai, B. Bak-Jensen, and J. W. Simpson-Porco, "Predictive control of flexible resources for demand response in active distribution networks," *IEEE Transactions on Power Systems,* vol. 34, no. 4, pp. 2957-2969, 2019.

[201] W. Zheng, W. Wu, B. Zhang, and W. Sheng, "Optimal residential demand response considering the operational constraints of unbalanced distribution networks," in *2017 IEEE Power & Energy Society General Meeting*, 2017: IEEE, pp. 1-5.

[202] A. S. Dobakhshari, M. Abdolmaleki, V. Terzija, and S. Azizi, "Robust hybrid linear state estimator utilizing SCADA and PMU measurements," *IEEE Transactions on Power Systems,* 2020.

[203] E. Manitsas, R. Singh, B. C. Pal, and G. Strbac, "Distribution system state estimation using an artificial neural network approach for pseudo measurement modeling," *IEEE Transactions on power systems,* vol. 27, no. 4, pp. 1888-1896, 2012.

[204] C. Ren and Y. Xu, "A fully data-driven method based on generative adversarial networks for power system dynamic security assessment with missing data," *IEEE Transactions on Power Systems,* vol. 34, no. 6, pp. 5044-5052, 2019.

[205] G. M. Gilbert, D. E. Bouchard, and A. Y. Chikhani, "A comparison of load flow analysis using DistFlow, Gauss-Seidel, and optimal load flow algorithms," 1998, vol. 2: IEEE, pp. 850-853.

[206] P. Liu, T. Ding, Z. Zou, and Y. Yang, "Integrated demand response for a load serving entity in multi-energy market considering network constraints," *Applied Energy,* vol. 250, pp. 512-529, 2019.

[207] Y. Liu, N. Zhang, Y. Wang, J. Yang, and C. Kang, "Data-driven power flow linearization: A regression approach," *IEEE Transactions on Smart Grid,* vol. 10, no. 3, pp. 2569-2580, 2018.

[208] Y. Liu, Y. Wang, N. Zhang, D. Lu, and C. Kang, "A data-driven approach to linearize power flow equations considering measurement noise," *IEEE Transactions on Smart Grid,* vol. 11, no. 3, pp. 2576 - 2587, 2019.

[209] A. Creswell, T. White, V. Dumoulin, K. Arulkumaran, B. Sengupta, and A. A. Bharath, "Generative adversarial networks: An overview," *IEEE Signal Processing Magazine,* vol. 35, no. 1, pp. 53-65, 2018.

[210] Y. Chen, Y. Wang, D. Kirschen, and B. Zhang, "Model-free renewable scenario generation using generative adversarial networks," *IEEE Transactions on Power Systems,* vol. 33, no. 3, pp. 3265-3275, 2018.

[211] I. Goodfellow *et al.*, "Generative adversarial nets," *Advances in Neural Information Processing Systems,* vol. 27, 2014.

[212] J. Yoon, J. Jordon, and M. Schaar, "Gain: Missing data imputation using generative adversarial nets," 2018: PMLR, pp. 5689-5698.

[213] J. Yosinski, J. Clune, Y. Bengio, and H. Lipson, "How transferable are features in deep neural networks?," in *Advances in Neural Information Processing Systems*, 2014 2014, pp. 3320-3328.

[214] T. Wan, Y. Tao, J. Qiu, and S. Lai, "Data-driven hierarchical optimal allocation of battery energy storage system," *IEEE Transactions on Sustainable Energy,* vol. 12, no. 4, pp. 2097 - 2109, 2021.

[215] J. Bedi and D. Toshniwal, "Empirical mode decomposition based deep learning for electricity demand forecasting," *IEEE Access,* vol. 6, pp. 49144-49156, 2018.

[216] M. Song, C. Gao, M. Shahidehpour, Z. Li, J. Yang, and H. Yan, "Impact of uncertain parameters on TCL power capacity calculation via HDMR for generating power pulses," *IEEE Transactions on Smart Grid,* vol. 10, no. 3, pp. 3112-3124, 2018.

[217] P. M. de Quevedo, G. Muñoz-Delgado, and J. Contreras, "Impact of electric vehicles on the expansion planning of distribution systems considering renewable energy, storage, and charging stations," *IEEE Transactions on Smart Grid,* vol. 10, no. 1, pp. 794-804, 2017.

[218] F. Tamp and P. Ciufo, "A sensitivity analysis toolkit for the simplification of MV distribution network voltage management," *IEEE Transactions on Smart Grid,* vol. 5, no. 2, pp. 559-568, 2014.

[219] S. Xu, W. Jiang, X. Deng, and Y. Shou, "A modified Physarum-inspired model for the user equilibrium traffic assignment problem," *Applied Mathematical Modelling,* vol. 55, pp. 340-353, 2018.

[220] S. Wang *et al.*, "A stochastic collaborative planning approach for electric vehicle charging stations and power distribution system," in *2016 IEEE Power and Energy Society General Meeting (PESGM)*, 2016: IEEE, pp. 1-5.

[221] S. Akram and Q. U. Ann, "Newton raphson method," *International Journal of Scientific & Engineering Research,* vol. 6, no. 7, pp. 1748-1752, 2015.

[222] S. Wang, S. Bi, Y.-J. A. Zhang, and J. Huang, "Electrical vehicle charging station profit maximization: Admission, pricing, and online scheduling," *IEEE Transactions on Sustainable Energy,* vol. 9, no. 4, pp. 1722-1731, 2018.

[223] Z. Wei, J. He, and L. Cai, "Admission control and scheduling for EV charging station considering time-of-use pricing," in *2016 IEEE 83rd Vehicular Technology Conference (VTC Spring)*, 2016: IEEE, pp. 1-5.

[224] H. C. Tijms, *A first course in stochastic models*. John Wiley and sons, 2003.

[225] H. Yang, Y. Deng, J. Qiu, M. Li, M. Lai, and Z. Y. Dong, "Electric vehicle route selection and charging navigation strategy based on crowd sensing," *IEEE Transactions on Industrial Informatics,* vol. 13, no. 5, pp. 2214-2226, 2017.

[226] Y.-F. Liu, J.-M. Guo, and J.-D. Lee, "Inverse halftoning based on the Bayesian theorem," *IEEE Transactions on Image Processing,* vol. 20, no. 4, pp. 1077-1084, 2010.

[227] S. Boyd, S. P. Boyd, and L. Vandenberghe, *Convex optimization*. Cambridge university press, 2004.

[228] K. P. Schneider *et al.*, "Analytic considerations and design basis for the IEEE distribution test feeders," *IEEE Transactions on power systems,* vol. 33, no. 3, pp. 3181-3188, 2017.

[229] S. Dey, S. Ali, and C. Park, "Weighted exponential distribution: properties and different methods of estimation," *Journal of Statistical Computation and Simulation,* vol. 85, no. 18, pp. 3641-3661, 2015.

[230] A. I. Nikolaidis, C. A. Charalambous, and P. Mancarella, "A graph-based loss allocation framework for transactive energy markets in unbalanced radial distribution networks," *IEEE Transactions on Power Systems,* vol. 34, no. 5, pp. 4109-4118, 2018.

[231] S. Cui, Y.-W. Wang, X.-K. Liu, Z. Wang, and J. Xiao, "An Economic Storage Sharing Framework: Asymmetric Bargaining Based Energy Cooperation," *IEEE Transactions on Industrial Informatics,* vol. 17, no. 11, pp. 7489-7500, 2021.

[232] Z. Wang, C. Gu, F. Li, P. Bale, and H. Sun, "Active demand response using shared energy storage for household energy management," *IEEE Transactions on Smart Grid,* vol. 4, no. 4, pp. 1888-1897, 2013.

[233] H. Zhu and K. Ouahada, "Credit-Based Distributed Real-Time Energy Storage Sharing Management," *IEEE Access,* vol. 7, pp. 185821-185838, 2019.

[234] J. Liu, N. Zhang, C. Kang, D. S. Kirschen, and Q. Xia, "Decision-making models for the participants in cloud energy storage," *IEEE Transactions on Smart Grid,* vol. 9, no. 6, pp. 5512-5521, 2017.

[235] C. P. Mediwaththe, M. Shaw, S. Halgamuge, D. B. Smith, and P. Scott, "An incentive-compatible energy trading framework for neighborhood area networks with shared energy storage," *IEEE Transactions on Sustainable Energy,* vol. 11, no. 1, pp. 467-476, 2019.

[236] N. Rahmah and I. S. Sitanggang, "Determination of optimal epsilon (eps) value on dbscan algorithm to clustering data on peatland hotspots in sumatra," in *IOP conference series: earth and environmental science*, 2016, vol. 31, no. 1: IOP Publishing, p. 012012.

[237] T. Wakui, H. Kawayoshi, and R. Yokoyama, "Optimal structural design of residential power and heat supply devices in consideration of operational and capital recovery constraints," *Applied Energy,* vol. 163, pp. 118-133, 2016.

[238] C. Li, X. Yu, W. Yu, G. Chen, and J. Wang, "Efficient computation for sparse load shifting in demand side management," *IEEE Transactions on Smart Grid,* vol. 8, no. 1, pp. 250-261, 2016.

[239] M. Tavakoli, F. Shokridehaki, M. F. Akorede, M. Marzband, I. Vechiu, and E. Pouresmaeil, "CVaR-based energy management scheme for optimal resilience and operational cost in commercial building microgrids," *International Journal of Electrical Power & Energy Systems,* vol. 100, pp. 1-9, 2018.

[240] "Smart-Grid Smart-City Customer Trial Data." Australian Government Department of the Environment and Energy. https://data.gov.au/data/dataset/smart-grid-smart-city-customer-trial-data (accessed Apr. 6, 2020).

[241] H. Du Nguyen, Q. T. Nguyen, K. P. Tran, and D. P. Ho, "On the performance of VSI Shewhart control chart for monitoring the coefficient of variation in the presence of measurement errors," *The International Journal of Advanced Manufacturing Technology,* vol. 104, no. 1-4, pp. 211-243, 2019.

[242] J.-H. Kim, J.-H. Choi, K.-H. Yoo, and A. Nasridinov, "AA-DBSCAN: an approximate adaptive DBSCAN for finding clusters with varying densities," *The Journal of Supercomputing,* vol. 75, no. 1, pp. 142-169, 2019.

[243] J. Qiu *et al.*, "A linear programming approach to expansion co-planning in gas and electricity markets," *IEEE Transactions on Power Systems,* vol. 31, no. 5, pp. 3594-3606, 2015.

[244] J. Shin, K. Sudhir, and D.-H. Yoon, "When to “fire” customers: Customer cost-based pricing," *Management Science,* vol. 58, no. 5, pp. 932-947, 2012.

[245] D. Srinivasan, S. Rajgarhia, B. M. Radhakrishnan, A. Sharma, and H. Khincha, "Game-Theory based dynamic pricing strategies for demand side management in smart grids," *Energy,* vol. 126, pp. 132-143, 2017.

[246] N. Liu, J. Wang, and L. Wang, "Hybrid energy sharing for multiple microgrids in an integrated

heat–electricity energy system," *IEEE Transactions on Sustainable Energy,* vol. 10, no. 3, pp. 1139-1151, 2018.

[247] A. Basnet and J. Zhong, "Integrating gas energy storage system in a peer-to-peer community energy market for enhanced operation," *International Journal of Electrical Power & Energy Systems,* vol. 118, p. 105789, 2020.

[248] N. Liu, X. Yu, C. Wang, C. Li, L. Ma, and J. Lei, "Energy-sharing model with price-based demand response for microgrids of peer-to-peer prosumers," *IEEE Transactions on Power Systems,* vol. 32, no. 5, pp. 3569-3583, 2017.

[249] C. Liu, M. Shahidehpour, Y. Fu, and Z. Li, "Security-constrained unit commitment with natural gas transmission constraints," *IEEE Transactions on Power Systems,* vol. 24, no. 3, pp. 1523-1536, 2009.

[250] J. Qiu, Z. Y. Dong, J. H. Zhao, K. Meng, Y. Zheng, and D. J. J. I. T. o. P. S. Hill, "Low carbon oriented expansion planning of integrated gas and power systems," *IEEE Transactions on Power Systems,* vol. 30, no. 2, pp. 1035-1046, 2014.

[251] K. Khan, S. U. Rehman, K. Aziz, S. Fong, and S. Sarasvady, "DBSCAN: Past, present and future," in *The fifth international conference on the applications of digital information and web technologies (ICADIWT 2014)*, 2014: IEEE, pp. 232-238.

[252] N. Wu, H. Wang, L. Yin, X. Yuan, and X. Leng, "Application Conditions of Bounded Rationality and a Microgrid Energy Management Control Strategy Combining Real-Time Power Price and Demand-Side Response," *IEEE Access,* vol. 8, pp. 227327-227339, 2020.

[253] J. Chen and Q. Zhu, "Interdependent strategic security risk management with bounded rationality in the internet of things," *IEEE Transactions on Information Forensics and Security,* vol. 14, no. 11, pp. 2958-2971, 2019.

[254] Q. Shao, M. H. Cheung, and J. Huang, "Multimedia crowdsourcing with bounded rationality: A cognitive hierarchy perspective," *IEEE Journal on Selected Areas in Communications,* vol. 37, no. 7, pp. 1478-1488, 2019.

[255] Q. Shao, M. H. Cheung, and J. Huang, "Crowdfunding with Cognitive Limitations," in *GLOBECOM 2020-2020 IEEE Global Communications Conference*, 2020: IEEE, pp. 1-6.

[256] K. Jhala, B. Natarajan, and A. Pahwa, "Prospect theory-based active consumer behavior under variable electricity pricing," *IEEE Transactions on Smart Grid,* vol. 10, no. 3, pp. 2809-2819, 2018.

[257] N. Zhao, B. Wang, L. Bai, and F. Li, "Quantitative Model of the Electricity-Shifting Curve in an Energy Hub based on Aggregated Utility Curve of Multi-Energy Demands," *IEEE Transactions on Smart Grid,* 2020.

[258] S. Zheng, Y. Sun, B. Qi, and B. Li, "Incentive-based Integrated Demand Response Considering S&C Effect in Demand Side With Incomplete Information," *IEEE Transactions on Smart Grid,* 2022.